Measurement and characterisation of atmospheric ice-nucleating particles

By
Michael Paul Adams

Submitted in accordance with the requirements for the degree of
Doctor of Philosophy

The University of Leeds
School of Earth and Environment
October 2020

The candidate confirms that the work submitted is his/her own, except where work which has formed part of jointly-authored publications has been included. The contribution of the candidate and the other authors to this work has been explicitly indicated below. The candidate confirms that appropriate credit has been given within the thesis where reference has been made to the work of others.

Ottmar Möhler , Michael Adams*, Larissa Lacher*, Franziska Vogel*, Jens Nadolny, Romy Ullrich, Cristian Boffo, Tatjana Pfeuffer, Achim Hobl, Maximilian Weiß, Hemanth S. K. Vepuri, Naruki Hiranuma, and Benjamin J. Murray: ***The portable ice nucleation experiment PINE: a new online instrument for laboratory studies and automated long-term field observations of ice-nucleating particles***
Chapter 2 is based upon a paper published in the journal Atmospheric Measurement Techniques (10.5194/amt-14-1143-2021) that details the technical workings and first validation experiments of the PINE chamber. I am joint first author on this manuscript, and lead the day-to-day development of the PINE chamber over a two year development phase. I led the PINE measurements in the EXTRA18 campaign (described in Chapter 2) which formed a core part of this manuscript. I assisted with the writing of the manuscript, with OM leading. All authors contributed to writing, LL led aspects of the development after the initial development phase, FV ran PINE on a day-to-day basis in the HyICE18 campaign along with myself.

M.P. Adams, F. Vogel, O. Möhler, L. Lacher, G.C.E Porter, B. Bertozzi, K. Höhler, J. Kaufmann, T. Schorr, N. Umo, J. Nadolny, J. Duplissy, T. Petäjä, E.S. Thompson and B.J. Murray: *Measurements of ice-nucleating particle concentrations with the Portable Ice Nucleation Experiment chamber (PINE) in a Finnish Boreal forest*
Chapter 3 is based upon a manuscript in preparation. The manuscript describes PINE measurements made during the HyICE18 campaign. I planned the PINE aspect of the field campaign along with OM and BJM, and supervised the operation of PINE throughout. FV was in charge of running PINE on a day-to-day basis. GCEP assisted with development of the PINE analysis scripts. I carried out all data analysis shown in the Chapter. All authors contributed to writing the manuscript.

M. P. Adams, M. D. Tarn, A. Sanchez-Marroquin, G. C. E. Porter, D. O'Sullivan, A. D. Harrison, Z. Cui, J. Vergara-Temprado, F. Carotenuto, M. A. Holden, M. I. Daily, T. F. Whale, S. N. F. Sikora, I. T. Burke, J.-u. Shim, J. B. McQuaid and B. J. Murray : *A major combustion aerosol event had a negligible impact on the atmospheric ice-nucleating particle population*
Chapter 4 is based on a paper published in the Journal of Geophysical Research: Atmospheres, entitled A major combustion aerosol event had a negligible impact on the atmospheric ice-nucleating particle population (10.1029/2020JD032938). The paper describes measurements made during the U.K. based celebration of Bonfire Night, and surrounding days, in 2016 and 2017. I am the lead author on this paper, conceptualising it with BJM. MPA, BJM, MDT, GCEP, DOS, ADH, FC, JBM and MID all made measurements during the Bonfire Night celebrations. ASM carried out the SEM analysis, assisted by ITB. SNFS gave technical assistance. JVT advised on comparisons to GLOMAP and literature data. ZC provided HySPLIT back trajectories. All authors assisted in the writing of the manuscript.

Michael P. Adams, Nina S. Atanasova, Svetlana Sofieva, Janne Ravantti, Aino Heikkinen, Zoé Brasseur, Jonathan Duplissy, Dennis H. Bamford & Benjamin J. Murray: ***Ice nucleation by viruses and their potential for cloud glaciation***
Chapter 5 is based upon a paper currently under review in *Biogeosciences* entitled *Viruses and their potential for cloud glaciation*. I am lead author of the study, with Dr Atanasova being a joint first author. I conceptualised the study along with NA, JD, DHB and BJM. MA, NA, SS, AH and ZB carried out ice nucleation experiments. All virus purification was carried out by NA, SS and AH. SS and JR lead the genomic sequencing work. All authors contributed to the writing of the paper, with NA explicitly writing the sections of virus purification methods and SS and JR writing the section of genomic sequencing.

M.P. Adams, J.U. Proske, G.C.E Porter, A.D. Harrison, M. Daily, S. Sikora, Z. Brasseur, J. Duplissy, T. Petäjä, K.S. Carslaw and B.J. Murray: ***Characteristics of ice-nucleating particles in a boreal forest environment***
Chapter 6 is based around an in preparation paper entitled *characteristics of ice-nucleating particles in a boreal forest environment*, on which I am the lead author. I planned the Leeds part of the HyICE field campaign, with assistance from BJM and JD. MPA, GCEP, ADH, MID, BJM, JUP and ZB made up the field work team in Hyytiälä. JUP led the modelling simulations, with MPA, KSC and BJM supervising. SS gave technical assistance. All authors contributed to writing the manuscript.

Acknowledgements

I'd like to thank my supervisor, Professor Ben Murray for his support and guidance throughout the course of this PhD, for encouraging me to develop from a post-graduate into a researcher, and for giving me the opportunity to take on a fantastic PhD project. I'd also like to thank Dr Jim McQuaid for all his help through the past 4 years (especially for putting an aethalometer out of an office window on Bonfire Night 2016) and Dr Ottmar Möhler for kindly hosting me at Karlsruhe Institute of Technology and for his leadership in the PINE project.

Throughout the course of this project I've been fortunate enough to work with some fantastic people. The friendship and guidance of Danny O'Sullivan and Mark Tarn, both within the University and without made transitioning to life in Leeds a much easier experience than it might have otherwise been. I'd like to thank the many members of the Murray group I've worked with, past and present: Jesus Vergara Temprado, Elena Maters, Mark Tarn, Grace Porter, Sarah Barr, Seb Sikora, Alberto-Sánchez Marroquin, Alex Harrison, Mark Holden, Rachel Hawker, Beth Wyld, Martin Daily, Daniel O'Sullivan, Thomas Whale, Leon King, Carys Puddephatt, Ulrike Proske, Sandy James and Tom Mangan. I'd also like to thank Emma Lonsdale, Jonny Lavery, Quentin Birkinshaw, Guillaume Evans and other members of the University of Leeds staff, who have many times helped me with last minute travel requests.

From outside the University of Leeds, I'd like to thank Jens Nadolny for his companionship on my many visits to Karlsruhe and hope there are more to come. I'd also like to thank Larissa Lacher, Franziska Vogel, Georg Scheurig, Stefan Vogt, Tobias Schorr, Evelyn Freney, Matt Salter, Paul Zieger, Zoé Brasseur, Jonathan Duplissy, Nina Atanasova, Sveta Svetlana, Dennis Bamford, Erik Thompson and many more.

To the friends I kept with me from before this project, to those I made along the way, I'm extremely lucky to maintain the company of such wonderful people. This PhD has allowed me to see so many places I've never been before, and even taken me to the top of the world. I'm grateful I was able to share it with some of you. To Stefan, Zöe, Jacob, Grace and Alex, I hope to see new places with you in the future. I'd like to thank Amber for her kindness, friendship and support and for buying me coffee every time it should have been my turn. To Mark, Jacob, Oli, and Grace, growing closer together as a group these past 4 years is one of my most happy memories, and I wish it to continue for many years to come. To Theo, Phil, Ali and Eddie, it brings me happiness to see you all happy and well in these new stages of your lives. To Jonathan, thank you for being my friend for all these years, for growing up with me and for everything we experienced together. To Jacob, it makes me happy to have you back nearby, but I hope you get to follow your dreams and leave again soon. To Grace, thank you for being so many things; a scientist I can look up to, a friend I can laugh with, and a partner I can rely on.

Finally to my loving and supportive family, without who I would not be the person I am today, thank you. It isn't always apparent how lucky I am to have been brought up by such kind, hard-working and supportive people, but reflecting at the end of this stage of my life, I see how fortunate I have been. I hope I make you proud.

Abstract

Ice-nucleating particles (INPs), a small fraction of the overall atmospheric burden, are responsible for heterogeneous ice nucleation in the atmosphere. INPs have the potential to catalyse ice formation in super-cooled cloud droplets, thus are able to influence cloud properties and radiative effects. Despite the importance of INPs, our knowledge of their spatial and temporal variation in the atmosphere is poor, limiting the predictive capacity of climate models. This thesis aimed to improve the knowledge surrounding atmospheric INPs through their measurements and characterization, but also through the development of instrumentation by which to do so.

The Portable Ice Nucleation Experiment (PINE) chamber was developed in order to meet the technical needs required to answer important questions about the abundance of INPs in our atmosphere. PINE is a portable INP counter capable of making measurements autonomously, with a high-time resolution across the entire temperature regime of mixed-phase clouds. Upon completion of the first PINE prototype, PINE was deployed to the Hyytiälä forestry research station with the goal of validating it in a field environment, and also quantifying the INP concentrations in a boreal environment.

A series of field and laboratory studies were carried out in order to improve our knowledge of the distribution and properties of INPs in the atmosphere. Combustion aerosol generated during Bonfire Night celebrations in the U.K. was shown to be an ineffective ice nucleator, unable to compete with ambient INPs. Viruses were shown to potentially play a role in atmospheric ice nucleation in marine environments, whilst the INPs responsible for greater than expected concentrations in a boreal forest environment were characterized through wet-dispersion experimental techniques.

Overall, this thesis serves to further our understanding of INP concentrations in the atmosphere through space and time, and elucidate the nature of the aerosol particles responsible. Further to that, the techniques and instrument development described here will aid in furthering this understanding through robust experimentation.

Table of Contents

List of Tables

List of Figures

List of Abbreviations

CCN	Cloud Condensation Nuclei
INP	Ice-Nucleating Particle
MPC	Mixed-phase cloud
CNT	Classical Nucleation Theory
HLD	High-Latitude Dust
LLD	Low-Latitude Dust
CFDC	Continuous Flow Diffusion Chambers
PINE	Portable Ice Nucleation Experiment
SEM	Scanning Electron Microscope
ODV	Optical Detection Volume
EDS	Energy Dispersive X-ray Spectroscopy

1. Introduction

1.1 The importance of clouds in the Earth's climate system

Clouds play a pivotal role in the Earth's climate and radiative budget, being first order considerations in the calculation of longwave and shortwave solar radiation reaching the Earth's surface and being trapped within the Earth's atmosphere (Matus & L'Ecuyer, 2017; Storelvmo, 2017; Tan, Storelvmo, & Zelinka, 2016). The 2013 Intergovernmental Panel on Climate Change (IPCC) estimated that clouds contribute a net cooling effect of up to −20 °C W m^{-3} (Boucher et al., 2013). Matus & L'Ecuyer (2017) give a specific breakdown for mixed-phase clouds (MPC), stating overall mixed-phase clouds exert a global net cloud radiative effect of −3.4 W m^{-2}, with contributions of −8.1 W m^{-2} and 4.7 W m^{-2} in the short-wave and long-range solar radiation forcing, respectively. Clouds also play a key role in the hydrological cycle through precipitation and water transport (Pruppacher & Klett, 1997). Boucher et al. (2013) stated in their executive summary '*Clouds and aerosols continue to contribute the largest uncertainty to estimates and interpretations of the Earth's changing energy budget*'.

The focus of this thesis is predominantly on ice-nucleating particles (INPs) relevant for mixed-phase clouds. Mixed-phase clouds form in the lower to mid troposphere and are comprised of both supercooled liquid droplets and ice crystals. They exist at temperatures in the range 0 to −38 °C (Hoose & Möhler, 2012; Kanji et al., 2017a; B. J. Murray, O'Sullivan, Atkinson, & Webb, 2012), with supercooled liquid droplets able to persist until the lower end of this range, although there is evidence that homogenous nucleation becomes an increasingly important factor below −33 °C (Herbert et al. 2015).

1.2 The influence of aerosol, cloud condensation nuclei and ice-nucleating particles on clouds

The phase of a cloud (liquid, ice or mixed) is of key importance to understanding the effect of that cloud on incoming and outgoing solar radiation and the hydrological cycle. The presence of a cloud is caused by the cloud particles it is composed of: liquid cloud droplets, ice crystals or both (Hoose & Möhler, 2012; Kanji et al., 2017a; B. J. Murray et al., 2012). Whilst it is possible for liquid cloud droplets to form homogeneously in extreme supersaturations, in the Earth's atmosphere all cloud particle formation in the troposphere occurs in the presence of a cloud condensation nuclei (CCN) (Storelvmo, 2017). The phase of the cloud is further influenced by the presence of ice-nucleating particles (INPs). Both of these particle types, CCN and INPs, are types of aerosol particles.

Aerosol particles can be primary or secondary. Primary aerosol particles are comprised of solid or liquid particulate matter that has been emitted directly into the atmosphere. Primary aerosol particles can be either natural (biogenic, sea salt, mineral dust, etc.) or anthropogenic (combustion aerosol, dust aerosolised via anthropogenic processes, emissions from human induced forest fires, etc.). Secondary aerosol products are a result of condensing gasses in the atmosphere. These aerosol particles potentially serve as CCN and INPs, if the atmospheric conditions are suitable for them to do so.

1.2.1 Cloud condensation nuclei

Cloud condensation nuclei play a vital role in the formation of clouds, providing a surface for water vapour to condense onto and form a cloud droplet, with larger aerosol particles

generally being better CCN than small ones (Köhler, 1936). The CCN fraction in an aerosol population, at a given supersaturation, is defined as the number of aerosol particles that can be activated to cloud droplets at this supersaturation or a higher one (Andreae & Rosenfeld, 2008), and play an important role in defining cloud properties. If a cloud forms in a CCN rich environment, then there will be a large number of cloud droplets that are small in size. Conversely, if a cloud forms in an environment deficient in CCN, there will be relatively few droplets but they will be large in size. This is an important consideration as clouds formed in the latter case (CCN deficient, few but large droplets) would be optically thinner than and cloud formed in the former case (CCN rich, many small droplets) and thus having a lower albedo; this is known as the Twomey effect (Twomey, 1977). It is hypothesised that the Twomey effect leads to a net cooling effect for thin to moderately thick clouds via the increased albedo from greater droplet number, but a warming effect for thick clouds through an increased absorption coefficient. This directly leads into the Albrecht effect; small cloud droplets have a lower collision rate, and thus do not coalesce as quickly. This leads to a reduction in the efficiency of precipitation, meaning the cloud will have a prolonged lifetime relative to a cloud with larger droplets. The ultimate effect of the Albrecht effect is a net cooling of the Earth's surface due to the increase in liquid clouds (Albrecht, 1989). The Twomey and Albrecht effect are known as the first and second indirect aerosol effect, respectively, and demonstrate the importance of CCN to cloud formation and properties.

1.2.2 Ice-nucleating particles

Ice-nucleating particles are particles that, under a certain set of conditions (primarily temperature and humidity), can catalyse the formation of an ice crystal. (Hoose & Möhler, 2012; Kanji et al., 2017a; B. J. Murray et al., 2012). Heterogeneous ice nucleation (i.e. as opposed to homogeneous nucleation, as discussed later) can have several effects on clouds, ranging from depletion of water vapour in the cloud and the triggering of precipitation, to changes in the cloud phase and composition.

The presence and morphology of ice crystals in clouds can influence important properties, such as cloud lifetime and optical thickness (D. L. Hartmann et al., 1992; U. Lohmann & Feichter, 2005). The importance of INPs for shallow, mixed-phase clouds was demonstrated in (Vergara-Temprado et al., 2018), wherein a low-level MPC cloud in the cloud sector of a tropical cyclone was modelled and subjected to different INP parameterisations from the literature. Hawker et al., (2020) demonstrated the controlling effect of INPs on the radiative properties of tropical convective cloud systems, noting that the INP concentration was important across the entire temperature range of mixed-phase clouds. This presents a challenge for the INP community, and will likely require the development of new instrumentation for measuring INPs.

1.3 Modes of ice nucleation

Ice nucleation can happen either homogenously or heterogeneously. Homogenous ice nucleation occurs in the absence of an INP. Supercooled water can remain in a metastable liquid state to temperature below − 36 °C (Hoose & Möhler, 2012; Kanji et al., 2017a; B. J. Murray et al., 2012), however there is evidence of homogeneous nucleation being important in mixed-phase clouds at – 33 °C and below (Herbert et al., 2015). Heterogeneous ice nucleation occurs in the presence of an INP, and can happen via a number of modes (Vali et al. 2015). Two main branches of heterogeneous ice nucleation can be considered, deposition nucleation and freezing nucleation (which has several modes therein).

Deposition nucleation is the only mode in which liquid water does not form in a macroscopic quantity, being a gas to solid process (Vali et al. 2015). Deposition mode occurs when water vapour deposits directly onto the surface of an ice-nucleating particle as ice, with the ice crystal then undergoing diffusional growth as more water vapour condenses onto the now present ice surface. Depositional mode nucleation occurs only when air is supersaturated with respected to ice, and in the atmosphere is thought to be of secondary importance in the MPC temperature regime, where freezing nucleation modes dominate (Albert Ansmann, 2005; Cui, Carslaw, Yin, & Davies, 2006; de Boer, Morrison, Shupe, & Hildner, 2011). Recently there has been discussion about whether deposition mode nucleation is an accurate description of the physical process by which nucleation may be occurring. Studies have shown the potential for freezing previously believed to be due to deposition mode nucleation to be explained via pore condensation freezing, where liquid water forms in pores and nanoscale features on particles (David et al., 2019; Marcolli, 2014; Wagner, Kiselev, Möhler, Saathoff, & Steinke, 2016). This is possible due to the concavity of the water surface in a pore resulting in a negative kelvin effect, where condensation can occur in water sub-saturated conditions (Wagner et al., 2016). This liquid water then goes on to freeze homogeneously, with water vapour then condensing onto the newly formed ice surface.

Freezing nucleation occurs in the presence of liquid water, and can be sub-divided into further modes; immersion freezing, condensation freezing and contact freezing. Immersion freezing occurs when a particle is completely immersed in a supercooled liquid droplet which is active as an INP at the droplet temperature. This can happen in the atmosphere as an aerosol particle reaches an environment at which it will form a CCN and become immersed in liquid water. Once that CCN reaches an altitude at which the droplet can become supercooled, immersion freezing can occur. Condensation freezing is hypothesised to occur simultaneously with the initial formation of liquid on a CCN. Like immersion freezing in the atmosphere, the particle must be at an altitude sufficiently high (and hence cold) for the liquid water condensing onto the aerosol particle to be supercooled. It is currently under debate as whether this can be considered truly distinct from either immersion or deposition nucleation (David et al., 2019; Marcolli, 2014). Contact freezing occurs when an INP comes into contact with a supercooled cloud droplet, with nucleation occurring at the air-water interface. Contact nucleation can also occur when, usually during evaporation, the particle immersed within a supercooled droplet interacts with the water-air interface. The measurements and discussion within this thesis nearly always pertains to immersion mode freezing. The atmospheric altitudes at which different nucleation processes are relevant is shown in Figure 1.

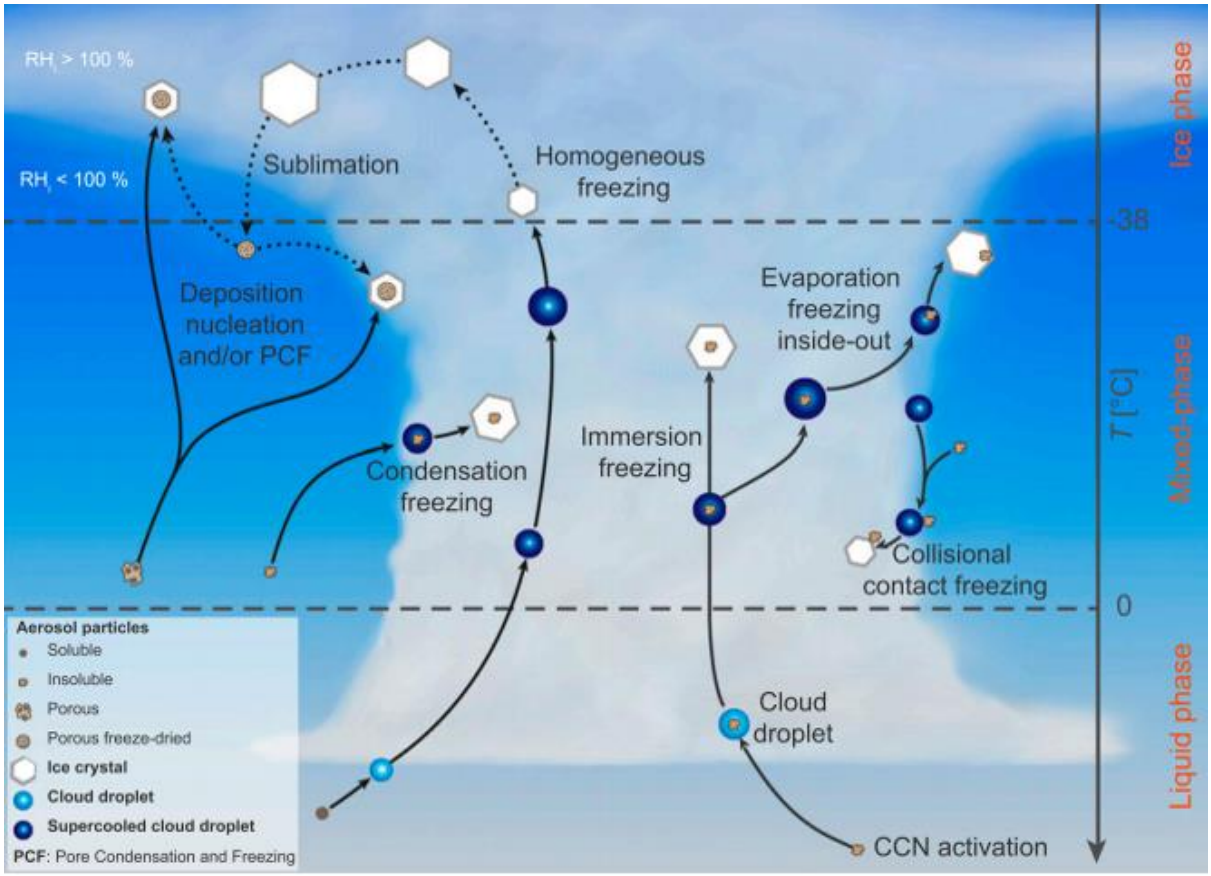

Figure 1: Schematic depicting known primary ice nucleation pathways possible in the atmosphere. Reproduced from (Kanji et al., 2017a)

1.3.1 Experimental methods

Experimental methods within the field of ice nucleation can take a number of forms, with subtly different aims. Often the aim of an experiment is simply to count the number if ice-nucleating particles in some system or environment, whereas at other times experiments can be focused on understanding the mechanisms behind ice nucleation. Most of these experiments are carried out with the aim of improving knowledge of the impact of atmospheric ice-nucleating particles, however other fields such as cryobiology have demonstrated an interest in conducting ice nucleation research to their own end (John Morris & Acton, 2013). Experiments designed to further understanding of ice nucleation for whatever reason will generally fall into one of two categories; dry dispersion or wet dispersion.

1.3.1.1 Wet dispersion

Wet dispersion experiments are used for the investigation of immersion mode nucleation, where liquid water is a pre-requisite. A commonality between wet dispersion methods involve dispersing ice-nucleating particles into pure water in some manner, making efforts to ensure that the nucleator is distributed homogeneously in the solution. Typical examples of this include making a defined weight percentage suspension with a given sample and pure liquid water (e.g. k-feldspar) (Atkinson et al., 2013), sampling air through a filter and then washing the particles of into pure liquid water (O'Sullivan et al., 2018), or directly measuring the ice-nucleation of a liquid samples (i.e. river water, precipitation or ocean water; Wilson et al. 2015; Irish et al. 2017). A sub-sample of this suspension is then tested for the presence of ice-nucleating particles, usually involving a drop freeze assay (Harrison et al., 2018; Kanji et

al., 2017; Murray et al., 2012; Whale et al., 2015). The presence of impurities in water leads to a limit of detection for many drop freeze assay systems, as these impurities can act as INPs. Thus a great deal of effort has been devoted to improving background signals in experimental setups (Polen, Brubaker, Somers, & Sullivan, 2018; Tobo, 2016). Once it can be robustly demonstrated that freezing is not observed in an experimental system at the temperature one wishes to make measurements when using pure liquid water, any freezing observed by droplets that have potential INPs suspended in them can be inferred to be due to the INPs (i.e. heterogonous freezing). An alternative method can be to pipette pure water directly on to a filter or substrate that potentially has ice-nucleating ability, and to lower the temperature of the droplet – filter/substrate system (Holden et al., 2019; Price et al., 2018; Alberto Sanchez-Marroquin et al., 2019a; Schnell & Tan-Schnell, 1982).

Droplets of different sizes can be used in drop freeze assays, ranging from those on the scale of pico-litres to millilitres (Bigg 1953; Whale et al. 2015; Tarn et al. 2018; Harrison et al. 2018; Beall et al. 2017; Daily et al. 2020). The larger a droplet in size, the more potential INPs it can have immersed within it, meaning it is more likely to have rarer INPs that are active at warmer temperatures. These larger droplets are also more likely to have impurities in them, meaning they will have a less sensitive limit of detection, thus a trade-off is found in the selection of droplet size (and thus experimental setup) depending on the experimental aims of the user. Detection of freezing in drop freeze assays can be observed using optical sensors (Budke & Koop, 2015; Demott et al., 2017; Tarn et al., 2018; Whale et al., 2015), infrared sensors (Harrison et al., 2018; Zaragotas, Liolios, & Anastassopoulos, 2016) and calorimetry (Marcolli, Gedamke, Peter, & Zobrist, 2007). In general, drop freeze assays are operated with a linear cooling rate (typical 1K min^{-1} for a 1 µL droplet)), however isothermal experiments have been carried out to investigate the time dependent nature of ice nucleation (Broadley et al., 2012; Herbert, Murray, Whale, Dobbie, & Atkinson, 2014; Sear, 2014). Other wet dispersion techniques include wind tunnels and free falling droplet systems.

Wind tunnels have been used to investigated the ice-nucleating ability of aerosol particles (Diehl & Mitra, 1998; Pitter & Pruppacher, 1973). In such experiments, supercooled droplets are suspending in a wind tunnel through the control of air flow. The relative humidity and temperature of wind tunnels can be controlled within a defined range, and for ice nucleation experiment the temperature is below 0°C. Supercooled droplets that freeze have a dramatically different velocity and path to that of supercooled liquid droplets, forming the basis for their detection and counting. Novel techniques involving the use of sugar solution and soap film were used to provide an environment in which collected ice crystals could grow to larger sizes that were easier to detect (Bigg et al., 1963).

Free falling droplet systems have been used for the investigation of both heterogeneous and homogeneous freezing (Wood, Baker, & Swanson, 2002). Droplets are generated and allow to free fall through a temperature controlled freezing tube, which has a temperature gradient along its vertical profile. The stream of droplets is illuminated by linearly polarized light, with the depolarisation of the back-scattered light measured. This technique allows for the distinguishing of liquid droplets from ice crystals.

1.3.1.2 Dry dispersion

Dry dispersion experiments are those which do not use pure water as an initial component of the experimental system. Generally, if immersion/condensation nucleation is to be

investigated, the supercooled liquid water required for freezing via this mechanism will originate from the vapour phase, forming on an aerosol particle once the temperature and humidity conditions make it thermodynamically favourable. Deposition freezing can also be measured using dry dispersion experiments.

Cloud expansion chambers work on the principle of simulating a parcel of air rising through the atmosphere into cooler altitudes, which allows for the investigation of both freezing and deposition nucleation (Connolly et al., 2009; Niemand et al., 2012; Ullrich et al., 2017). Cloud expansion chambers operated by pumping gas out of the chamber, leading to a reduction in pressure. This pressure decrease then leads to an adiabatic expansion of gas within the chamber, resulting in the temperature of the gas decrease. The starting conditions and pump rate determine the mode of ice nucleation that is investigated. For experiments investigating freezing modes (immersion, condensation, contact, etc.), the gas within the chamber becomes saturated with respect to water, leading to the activation of any aerosol particles suspended in the gas as cloud droplets. These cloud droplets will then freeze if the immersed particles are active as INPs at the droplet temperature, and grow at the expense of the supercooled liquid droplets. For experiments aimed at the deposition mode, conditions are set such that ice saturation is reached, but water saturation is not, leading to ice to deposit directly onto aerosol particles active as INPs under such conditions, forming ice crystals that experience diffusional growth.

Continuous Flow Diffusion Chambers (CFDCs) chambers are used to investigate the ice-nucleating ability of aerosol particles under a range of conditions, having the capability to vary temperature and humidity (many designs of CFDCs exist with specific features, but this principle holds true for any system that can be considered a CFDC) (Burkert-Kohn et al., 2017; Kanji & Abbatt, 2009; Lacher et al., 2017; Rogers et al., 2001; Stetzer, Baschek, Lüönd, & Lohmann, 2008). Aerosol particles are drawn into the chamber, where the supersaturation of air with respect to both ice and potentially water (water can be either super or sub-saturated) can be set by adjusting the temperature and humidity within the chamber. As the particles are drawn through the chamber, they pass through two independently temperature controlled walls that are coated with ice. The varying temperatures of the walls lead to a supersaturation with respect to ice (and possibly water) in the centre of the chamber leading to the growth of ice crystals. Depending on the CFDC, there may be an evaporation region at the bottom of the instrument for evaporating water droplets so that only ice crystals are detected in the sensor system used (Kanji & Abbatt, 2009). Whilst CFDCs have proved powerful instruments in lab studies and field campaigns, they have several limitations. The greatest of these limitations is a background count due to frost forming on the walls of the chamber, and the necessary downtime to remove the build-up of fragile frost on the cold wall. As the instrument is used over time, any frost that form on the walls can potential fragment and give false counts. These particles cannot be accounted for via the droplet evaporation section of the chamber or by the sensor system, as they are genuine ice crystals, they are just not produced by INPs.

Flow chambers invoke the principles of thermodynamics in a way not entirely dissimilar from CFDCs, albeit with some key experimental differences. Like CFDCs, flow chambers control the humidity and temperature that particles suspended in air experience, however they do so using a different mechanism. Whilst CFDCs use independently cooled walls to lead to a

temperature and humidity gradient across the chamber, flow chambers mix dry, sample air containing the aerosol particles to be studied with a humid, particle-free sheath flow to control the relative humidity of the mixture as desired, based upon experimental goals; flow chambers can be operated in the immersion, condensation or deposition mode. The temperature of the system is controlled by the chambers walls, and ice crystals are detected by an optical sensor.

Thermal diffusion chambers allow for the analysis of aerosol particle on filters or substrates via the cooling of the filter/substrate, and the resulting condensing of water vapour on to the aerosol particles to create liquid droplets. (Schrod et al., 2016; Stevenson, 1968). If the condensed droplets are supercooled, and the particle they are condensed onto active as an INP at the droplet temperature, then the supercooled water will freeze, which is detected by an optical sensor.

1.3.1.3 Inter-comparison of different INP counting instrumentation

Given the range of instrumentation and techniques employed in the field of ice nucleation research, comparison between methodologies is paramount to ensuring consistency between studies. To this end, a number of inter-comparison campaigns have been carried out in recent years, with varying conclusions. Emersic et al. (2015) made the argument that wet dispersion method inconsistencies with their own experiments was due to the issue of particle aggregation in suspended samples. Likewise, Hiranuma et al. (2015) carried out a comprehensive inter-comparison of 17 ice nucleation techniques using NX-illite, and also found a discrepancy of up to 8 °C or 3 orders of magnitude between wet and dry dispersion techniques. However, in contrast to Emersic et al. (2015), it was demonstrated that aggregation of particles is unlikely to be the cause of this discrepancy. Instead, it was proposed (although left open for interpretation) that the surface modification of the illite NX particles (e.g., due to ion dissolution effects in the aqueous suspension) could be a potential explanation (Hiranuma et al., 2015). The most recent example of an inter-comparison was the FIN-02 (Demott et al., 2018) workshop, an multi-national campaign with researchers and instrumentation from around the world gathered at Karlsruhe Institute of Technology's (KIT) Aerosol Interactions and Dynamics in the Atmosphere (AIDA) facility. The study noted greatly improved agreement between techniques when compared to previous campaigns, and did not observe a systematic discrepancy between wet and dry dispersion methods. This was in part attributed to each group sampling the same aerosol directly from the AIDA chamber, eliminating any potential heterogeneities in sampling.

Despite on the order of 50 teams around the world actively working on experimental ice nucleation, there is at present not a standard measurement technique for calibrating newly developed instrumentation to, nor a reference INP that is considered a reliable standard. Coupled with the divergence in sampling methodology for field measurements, there remains work to be done as a community in order to achieve robust, consistent measurement and reporting techniques.

1.4 Classical nucleation theory

Classical nucleation theory (CNT) describes the formation of a new phase from a parent metastable phase, such as the transition from supercooled water to ice. In pure water, clusters form and dissipate through the gain and loss of water molecules (B. J. Murray et al., 2012), with this process being thermodynamically unfavourable above 0 °C; the addition of a

water molecule is an endothermic process. Below 0 °C, when water is supercooled, ice can grow spontaneously once a cluster has reached a critical size and the addition of a water molecule is an exothermic process. For this to occur, the energy gain of adding a water molecule must be greater than the energy cost of forming a water-ice interface (Mullin, 2001). The Gibbs free energy for an ice cluster is Δ*G*, the Gibbs free energy for forming the liquid-ice interface is ΔG_s (this process has an energy cost making it thermodynamically unfavourable, giving it a positive value), whilst the Gibbs free energy required for forming bonds between water molecules within the cluster is ΔG_v (if the water is supercooled and the saturation ratio with respect to ice is ≥ 1, this process has an energy gain making it thermodynamically favourable, giving it a negative value). Thus, the Gibbs free energy of the system can be described as:

$$\Delta G = \Delta Gs + \Delta Gv \tag{1}$$

G_s can be expressed as:

$$Gs = 4\pi r^2 \gamma \tag{2}$$

where *r* is the radius of the cluster and γ is the interfacial energy per surface area (this form of the equation assumes a spherical cluster). Gv can be expressed as:

$$Gv = -\frac{4\pi r^3}{3v} K_B T \ln(S) \tag{3}$$

where *r* is the radius of the cluster, v is the volume of a water molecule in the condensed phase, K_B is the Boltzmann constant, *T* is the temperature of the system and *S* is the saturation ratio. Combining equations 2-3 gives:

$$\Delta G = -\frac{4\pi r^3}{3v} K_B T \ln(S) + 4\pi r^2 \gamma \tag{4}$$

The two terms in equation 4 are opposing, causing Δ*G* to reach a maximum value (and a turning point) when the cluster reaches critical size, r_{cl}, this is shown in Figure 2. The critical cluster size can be found by differentiating ΔG with respect to *r* and setting $d\Delta G_{cl}/dr = 0$. Equation 4 then becomes:

$$0 = 4\pi r_{cl}(2\gamma - \frac{r_{cl}}{v} K_B T \ln(S)) \tag{5}$$

Rearranging for the critical cluster size gives:

$$r_{cl} = \frac{2\gamma v}{K_B T \ln(S)} \tag{6}$$

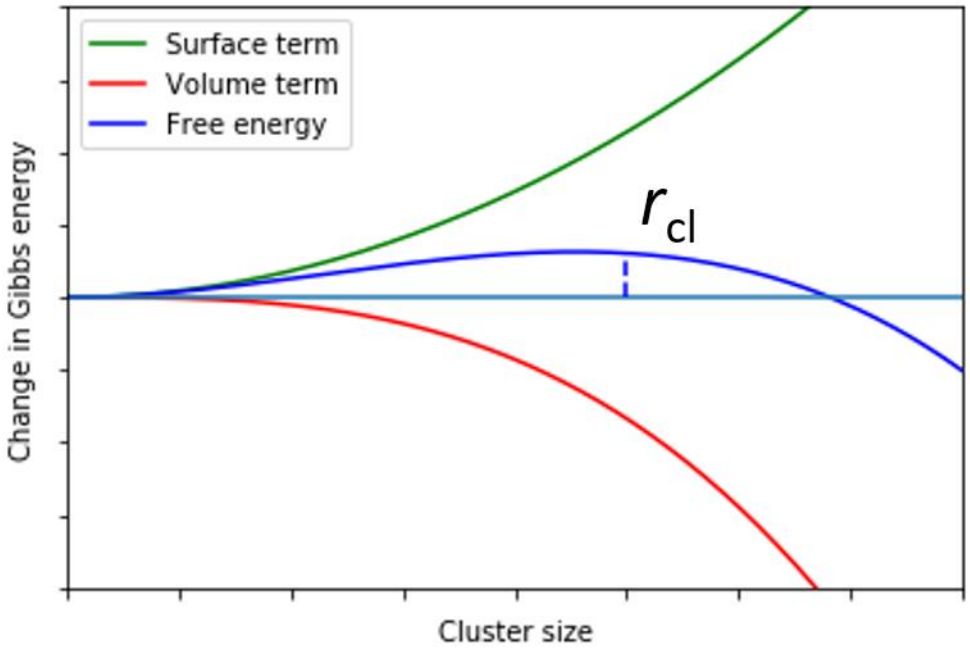

Figure 2: The change of the surface term (green), volume term (red) and Gibbs free energy (blue) as a function of cluster size.

The addition of new molecules to nuclei larger than r_{cl} is thermodynamically favourable as this decreases the Gibbs free energy. Finally, substituting r_{cl} into equation 5 yields:

$$\Delta G_{cl} = \frac{16\pi\gamma^3 v^2}{3(K_B T \ln(S))^2} \tag{7}$$

1.4.1 Homogeneous classical nucleation theory

The Gibbs free energy needed to form a critical cluster and initiate the spontaneous growth of ice can be used to determine the homogeneous rate coefficient J_{hom}, which is defined as nucleation events per unit volume per time at which ice crystals form in supercooled water. By substituting ΔG_{cl} into an Arrhenius style equation as the activation energy for the reaction we get:

$$J_{hom} = A_{hom} e^{-\frac{\Delta G_{cl}}{K_B T}} \tag{8}$$

where A_{hom} is the pre-exponential factor. Taking the natural logarithm, showing ΔG_{cl} explicitly and simplifying gives:

$$\ln(J_{hom}) = \ln(A_{hom}) - \frac{16\pi\gamma^3 v^2}{3K_B{}^3 T^3 \ln(S)^2} \tag{9}$$

This allows for the determining of J_{hom} through experimentation. As described above, J_{hom} is described as nucleation events per unit volume per time, and thus has units $cm^{-3}\ s^{-1}$. If a population of droplets is held at a constant temperature for a given time, a freezing rate $R\ (t)$ can be determined. Dividing the freezing rate by the total volume of the droplets (shown below in equation 10) gives J_{hom}:

$$J_{hom} = \frac{R\ (t)}{V} \tag{10}$$

1.4.2 Heterogeneous classical nucleation theory

The application of CNT to heterogeneous nucleation has many parallels with homogeneous freezing. An Arrhenius style equation is again used, with ΔG_{cl} being used as the activation energy, however in heterogeneous nucleation the surface in contact with supercooled liquid (water, in the case of ice nucleation) serves to reduce the energy barrier to the phase transition. This is accounted for by the addition of a coefficient to the activation energy term, ϕ, shown in equation 11:

$$J_{het} = A_{het} e^{-\frac{\Delta G_{cl} \phi}{K_B T}} \tag{11}$$

where A_{het} is the pre-exponential factor. ϕ can be expressed as:

$$\phi = \frac{(2 + cos\theta)(1 - cos\theta)^2}{4} \tag{12}$$

where θ is the contact angle between spherical ice nucleus and a flat surface. It can be seen that if θ is equal to 0° (i.e. the cluster is perfectly aligned with the surface), ϕ will become 0. This will result in the exponential term having a value of unity, and the heterogeneous reaction rate being equal to the pre-exponential term, A_{het}. Conversely, if θ is equal to 180°, ϕ will be equal to one, which results in the exponential term taking on its maximum possible value. Thus, a contact angle of 0° would describe a perfect ice nucleator, and a contact angle of 180° would describe a completely ineffective one. This is shown in Figure 3.

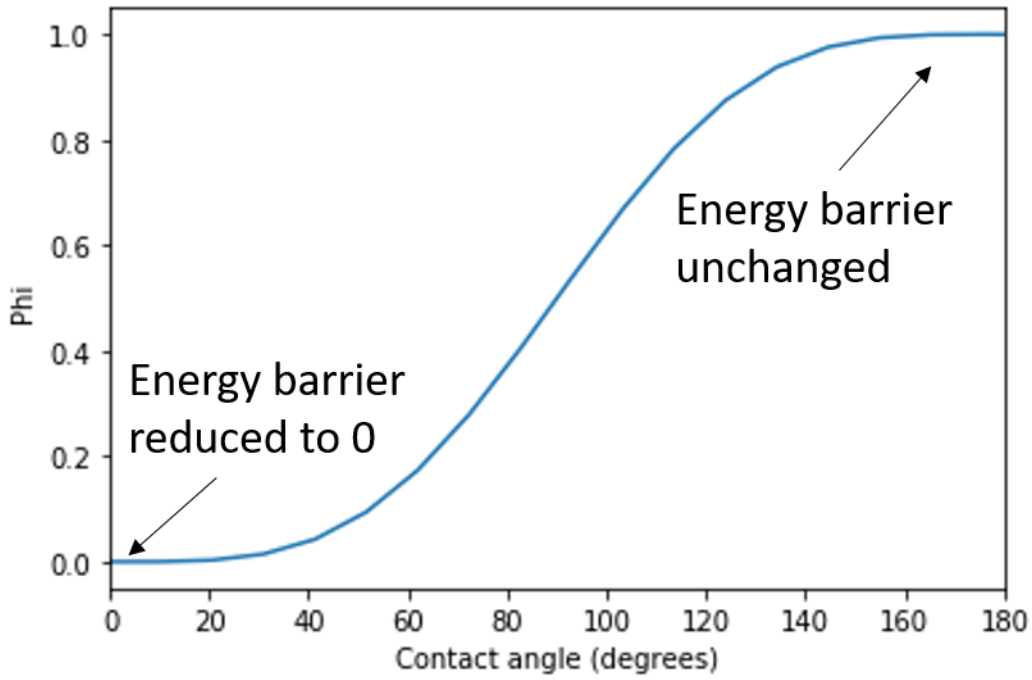

Figure 3: Phi as a function of contact angle, theta. A contact angle of 0 would represent a perfect ice nucleator, removing the energy barrier to nucleation. Conversely, a contact angle of 180 would be a completely ineffective ice nucleator and have no effective on the energy barrier to nucleation.

Substituting the equation of ϕ from equation 12 into equation 11 allows us to describe the rate of heterogeneous ice nucleation, factoring in the effect of the contact angle, as:

$$\ln(J_{het}) = \ln(A_{het}) - \frac{16\pi\gamma^3 v^2}{3{K_B}^3 T^3 \ln(S)^2} \frac{(2 + cos\theta)(1 - cos\theta)^2}{4} \tag{13}$$

Despite equation 13 appear to show a complete approach toward describing heterogeneous ice nucleation, unfortunately this is in reality not the case. The contact angle described is not well defined conceptually, and effectively serves as a means to account for the lowering of the energy barrier to phase transition, without providing any insight into what causes this reduction. Equation 13 assumes that particles that act as ice nucleators have a constant ice-nucleating effectiveness across their surface, which is demonstrably not the case, as recent studies have confirmed the existence of active sites as areas on a particle where ice preferentially nucleates (Holden et al. 2019; Kiselev et al. 2016; Whale et al. 2017).

1.5 Ice nucleation models and approximations

Ice nucleation is by nature a stochastic process, the probability of a nucleation event occurring is influenced by both time and the amount of nucleator present. This leads to a difficulty in describing observations related to ice nucleation, as it is not clear how to disentangle the two dependencies. In general two different approaches can be taken to describe heterogeneous ice nucleation. One can either approach from the basis of forming a fundamental understanding, with the intention to use CNT to craft a 'bottom-up' methodology to describing ice nucleation observations. Alternatively, one can attempt to represent observed ice nucleation characteristics using the most important parameters in an effort to best represent complex ice-nucleating systems (i.e. mixed atmospheric aerosol). Single Component Stochastic (SCM) models and Multiple Component Stochastic (MSC) models fall under the former approach, with the singular description being a methodology adopted when using the latter approach. This contrast in approaches has implications for both freezing and deposition nucleation modes, however as all the work in this thesis is related to freezing nucleation, implications for deposition nucleation are not discussed.

1.5.1 Single component stochastic models

SCS models use CNT to determine a single nucleation rate of a heterogeneous nucleator, J_{het} as described in section 1.4.2. SCS models make the assumption that the nucleating material in each droplet is homogenous and thus all droplets freeze at the same rate, allowing for J_{het} to be calculate based on contact angle of a nucleator as described in equation 13. This holds true for some materials, such as KGa-1b kaolinite, which was demonstrated to be best described by a SCS model (B J Murray, Broadley, Wilson, Atkinson, & Wills, 2011), however for a great many materials this not the case (Herbert et al., 2014; Vali, 2008, 2014).

1.5.2 Multiple component stochastic models

In an effort to account for the variation in droplet to droplet nucleation rate, MSC models treat each droplet has having its own single component rate (Broadley et al., 2012; Marcolli et al., 2007). A nucleation rate at any given temperature is then determined by summing the individual nucleation rates of each droplet. MCS models have more degrees of freedom than SCS models whilst still accounting for both the time dependence and the variation in nucleation rate between droplets. This means that MCS models will provide a more accurate fit to experimental data, however they are still dependant on a contact angle value, which is simply a scaling factor to describe the reduction in activation energy when compared to homogeneous freezing.

1.5.3 Singular description

To reduce the complexity in involved with droplet to droplet variation, the singular description was developed. In the singular description, droplet to droplet variability is thought to be driven by individual INPs having active sites on their surface, which will trigger

nucleation once a critical droplet temperature, T_c is reached, and not before (i.e. at temperatures warmer than T_c) (Murray et al. 2012; Holden et al. 2019; Whale et al. 2017; Connolly et al. 2009; Vali 2014). Whilst nucleation is a time dependent process, it is neglected in the singular description; within this framework a droplet held at a temperature above the T_c of the INP in question would never nucleate.

An array of droplets cooled at a constant rate would then nucleate at a distribution of temperatures according to the active site with the highest T_c in a given droplet, and thus a temperature spectrum could be plotted. At any temperature in a given spectrum, a fraction of frozen droplets can be calculated and related to the number of active sites per unit surface area, n_s:

$$f_{ice}(T) = \frac{n_{ice}(T)}{N_{Tot}} = 1 - \exp(-n_s(T)A) \quad (14)$$

where $f_{ice}(T)$ is the fraction of droplets frozen at a given temperature, $n_{ice}(T)$ is the number of droplets frozen at a given temperature, N_{Tot} is the total number of droplets in the experiment (i.e. at the start of the experiment when they were all liquid). *A* is the surface area of the nucleating material per droplet, whilst $n_s(T)$ is the number of active sites per unit surface area for an ice-nucleating material at a given temperature. Equation 14 can also be expressed in terms of density of active sites per unit volume, *K* as opposed to surface area, as done in Vali, 1971:

$$f_{ice}(T) = \frac{n_{ice}(T)}{N_{Tot}} = 1 - \exp(-K(T)V) \quad (15)$$

where *V* is the volume of an individual droplet. The validity of disregarding time dependence has been tested by repeating freezing experiments in a freeze/thaw manner and by varying the cooling rate of an experiment (Vali & Stansbury, 1966; Vali, 2008). It was found this whilst the time dependence caused a much smaller variation in freezing temperature than the droplet to droplet variation, it was not negligible. Thus, a modified version of the singular description was proposed (Vali, 1994):

$$f_{ice}(T) = \frac{n_{ice}(T)}{N_{Tot}} = 1 - \exp(-n_s(T - \alpha)A) \quad (16)$$

where α serves as the temperature offset compared to an experiment with a cooling rate of 1 K min^{-1} and α is defined as:

$$\alpha = \beta \log(|r|) \quad (17)$$

where *r* is the cooling rate of the experiment and β is a coefficient that appears to be variable between ice-nucleating materials (Herbert et al., 2014; Murray et al., 2012).
As ice nucleation is a surface driven process, n_s is a useful tool for quantifying the ice-nucleating activity of a material or sample and has a tangible physical meaning as opposed to describing ice-nucleating activity using contact angles. The singular description is used throughout this thesis when describing ice nucleation.

1.6 Sources of atmospheric ice-nucleating particles

Ice-nucleating particles in the atmosphere are poorly understood, in both their variation temporally and spatially, their nature and their sources (Kanji et al., 2017a; B. J. Murray et al.,

2012). INPs that are dominant in one region of the Earth may be a negligible contributor somewhere else or at some other time, and vice versa. The picture is further complicated by the temperature range at which mixed-phase clouds can exist, as through the temperature spectrum different INPs may dominate at different temperatures. Understanding of fundamental properties of INPs can be investigated in a laboratory environment, with the knowledge gained in this way then being applied and extrapolated to the atmosphere. A complete atmospheric picture cannot, however, be discerned entirely from laboratory experiments, as it is not possible to recreate the entirety of the processes INPs may experience in nature, such as chemical weathering, saltation processes, UV exposure etc. (although effort can be made to simulate at least some of these).

Despite these significant knowledge gaps, a great deal is known about INPs in the atmosphere; there is simply a great deal more to yet learn. Known and important source of atmospheric INPs include mineral dust from both high and low latitude sources (Atkinson et al., 2013; Boose et al., 2016; DeMott et al., 2003; Sanchez-Marroquin et al., 2020), marine organics (DeMott et al., 2016; Irish et al., 2017; McCluskey et al., 2018; McCluskey et al., 2018; Wilson et al., 2015), terrestrial biology (Tom C J Hill et al., 2016; Huffman et al., 2013; O'Sullivan et al., 2018; Tobo et al., 2013), volcanic ash (Mangan et al., 2017; Maters et al., 2019; Steinke et al., 2011) and to a lesser extent, anthropogenic combustion aerosol (Chen et al., 2018; Kanji, Welti, Corbin, & Mensah, 2020; Vergara-Temprado et al., 2018). The sources of atmospheric INPs are discussed in further detail below.

1.6.1 Mineral dusts

Ice-nucleating particles of mineral dust origin have traditionally been thought of as being synonymous with desert dust (Atkinson et al., 2013; Boose et al., 2016; DeMott et al., 2003) originating from low-latitude deserts such as the Gobi or Sahara, however more recent work has shown that high latitude dust of glacial origin is also a potentially important regional source of dust INPs (Sanchez-Marroquin et al. 2020; Tobo et al. 2019). A great deal has been learned about the ice-nucleating mechanisms and ability of mineral dusts in the laboratory, and it is worth reviewing this before considering the complexities of atmospheric ice nucleation by mineral dusts.

The ice-nucleating ability of mineral dust is controlled primarily by its size and mineralogy. The most effective mineral dust INP typically contains Feldspar (Boose., 2016; Harrison et al., 2016, 2019), which is an aluminosilicate mineral with charge balancing cations. The cations associated with the framework are most commonly K^+ and Na^+, or Na^+ and Ca^{2+}, defined as alkali Feldspar and plagioclase feldspar respectively). Alkali Feldspars are typically better at nucleating ice than plagioclase, and despite being a minor component, K-feldspar is the most effective at nucleating ice and parameterisations considering only this component have been developed (Atkinson et al., 2013; Harrison et al., 2016; Vergara-Temprado et al., 2017). A number of factors have been suggested as the cause for the exceptional ice-nucleating ability of alkali Feldspars. Kiselev et al., (2016) proposed that ice nucleates preferentially on high energy crystallographic faces at steps, cracks and cavities. In the case of highly active alkali feldspars, topographical features driven by phase separation between Na^+ and K^+ rich regions were shown to be responsible for the enhanced ice-nucleating ability, relative to samples that do not have such surface features (Whale et al. 2017). Holden et al., (2019) went further in probing the effect of surface heterogeneity on ice nucleation, by using a high-speed camera to identify the sites at which ice nucleates, demonstrating the existence of active sites. K-

feldspar is not the only driver of dust as atmospheric INPs, with quartz and clay particles also demonstrating ice-nucleating ability (Boose et al., 2016; Broadley et al., 2012; Harrison et al., 2019; Holden et al., 2019; Niemand et al., 2012; Ullrich et al., 2017).

1.6.1.1 Desert dust

Desert dust, or low-latitude dust (LLD) originating from the equatorial regions is a dominant source of ice-nucleating particles in many regions of the world, especially at temperatures below −15 °C (Paul J. DeMott et al., 2003; Price et al., 2018; Vergara-Temprado et al., 2017). This dominance is due to a combination of quantity of desert dust present in the atmosphere and its effectiveness as an INP. Dust from North African deserts has been observed to act as INPs in regions far from their source (Paul J. DeMott et al., 2003; O'Sullivan et al., 2018), with Vergara-Temprado et al., (2017) simulating global INP concentrations using a global aerosol model and including a parameterisation for feldspar INP concentrations based on laboratory studies, to demonstrate the dominance of K-feldspar dust in most regions of the world, especially at temperatures < − 20°C.

1.6.1.2 High latitude dust

High latitude dust (HLD) sources are estimated to contribute approximately 5% of the global dust budget (Bullard et al., 2016). Despite HLD only contributing a small fraction of the global dust budget, at high latitudes they comprise a larger proportion of the total mineral dust concentration because there are significantly lower desert dust concentrations at high latitudes. This means that they may be important INPs in the atmosphere (Vergara-Temprado et al., 2017). Dust in this region is also emitted into an area where it can directly affect shallow, mixed-phase clouds in the boundary layer (Fu, Deng, Shupe, & Xue, 2019; U. Lohmann, Diehl, Lohmann, & Diehl, 2006; Vergara-Temprado et al., 2018). Recent studies have investigated the ice-nucleating ability of HLD dust from different regions, Iceland and Svalbard (Sanchez-Marroquin et al. 2020; Tobo et al. 2019). Sanchez-Marroquin et al., (2020)showed that glaciofluvial dust of volcanic origin in Iceland can have comparable ice-nucleating ability to that of LLD at temperatures relevant to mixed-phase clouds (i.e. > −30 °C), whilst Tobo et al., (2019) demonstrated a proxy for glacially sourced dusts in the form of glacial outwash sediments in Svalbard also has comparable ice-nucleating ability to LLD, concluding that the high ice-nucleating ability observed is likely due to small amounts of organic material associated with the dust. Both studies conclude that HLD may be a potentially important source of INPs in the high-latitudes, emphasising that as climate change takes further effect snow cover and glacier retreat are likely to mean the emission of HLD is likely to increase in the future.

1.6.2 Volcanic ash

Volcanic ash emissions into the atmosphere are on the order of 176-256 Tg year^{-1}, which is considerably lower than the 2 Pg year−1 of mineral dust that is emitted into the atmosphere, however single eruptions can release huge quantities of ash at one time (Bullard et al., 2016; Dentener et al., 2006; Durant et al., 2010). Despite this major imbalance, volcanic eruptions effectively act as point sources of high quantities of ash, and thus can be important on a regional scale. For example, ash lofted from a high-latitude volcano (i.e. Eyjafjallajokull at 63° N) will be extremely concentrated in a region where mineral dust from deserts is much less numerous due to the distance from its origin. This is a similar argument for why HLD dust may be an important source of atmospheric INPs in high-latitude regions, but ash is emitted well above ground level so is more likely to be abundant at altitudes where mixed-phase clouds occur.

There have been a number of laboratory and field studies investigating the ice-nucleating ability of volcanic ash, which have so far illustrated a mixed picture on the effectiveness and importance of ash as INPs. In the laboratory, ash has been observed to nucleate ice across a wide range of temperatures (>-5 to <−30 °C; Fornea et al. 2009; Durant et al. 2008; Mangan et al. 2017; Genareau et al. 2018; Jahn et al. 2019; Maters et al. 2019), with a similar ice active site density, ns to that of certain mineral dust species (Hoyle et al., 2011; Steinke et al., 2011). Other studies have observed volcanic ash acting only as a weak INP, at temperatures just a few degrees above homogenous freezing (Gibbs, Charman, Schwarzacher, & Rust, 2015; Zolles et al., 2015). Field based measurements on volcanic ash INPs are limited, but indicate that ash emissions may act as a source of atmospheric INPs (Hobbs, Fullerton, & Bluhm, 1971; Isono, Komabayasi, & Ono, 1959; Seifert et al., 2011). Aircraft measurements made by Prenni et al., (2009) observed enhanced INP concentrations in an aircraft sample that had a back-trajectory intersecting with Shiveluch volcano in Kamchatka. Overall, these studies indicate that volcanic ash can nucleate ice, but its ice nucleating ability is massively variable, meaning its importance as an atmospheric INP is uncertain.

One explanation for the range of reported ice-nucleating ability of volcanic ash may be provided by Maters et al., (2019). They used tephra and glass pair equivalents to show that the presence of crystalline phases are key to the ice-nucleating ability of volcanic ash, observing the presence of K-feldspar in the most active samples as for mineral dust, but with Na/Ca-feldspar or pyroxene potentially driving a high ice-nucleating activity of some ash. A key conclusion of the study was that glass-dominated ash typically emitted from the larger, more explosive, eruptions may be an inferior INP when compared to crystalline ash that is more commonly emitted from smaller, more frequent eruptions. Most recently, Maters et al., (2020) demonstrated that high temperature ash-gas interaction can modify the ice-nucleating ability of ash (in some cases enhancing it), such that the variability observed in natural samples may also relate to different conditions of chemical processing in the volcanic eruption plume. More work is needed to understand the ice-nucleating ability of volcanic ash generated from different eruption conditions and different times after eruptions.

1.6.3 Combustion aerosol

Combustion aerosol, either natural (forest fires not caused by human activity) or anthropogenic (domestic wood burning, combustion engines, fossil fuel burning, etc.) in origin contribute significantly to the atmospheric aerosol burden. Due to the broad definition of combustion aerosol and the range of starting conditions (fuel, combustion conditions), the particles that fall under this definition vary significantly in chemical composition, morphology and size (Elsasser et al., 2013; Lighty, Veranth, & Sarofim, 2000). Particle types that may be emitted into the atmosphere range from combustion burning vary from soot (black carbon and elemental carbon) (Petzold et al., 2013), which has a fractal morphology and is usually on the 10-100 nm scale in terms of diameter, to ash particles that may be on the order of microns in diameter and have a chemical composition not entirely dissimilar to mineral dust (Paul J. DeMott et al., 2003; Kumai, 1961). Given that these varying properties of combustion aerosol are known to affect a particle's ice-nucleating ability, it's clear that there will not be a straightforward answer to the question of how effective an atmospheric INP it may be. Chapter 3 presents further detailed discussion of the wider literature on combustion aerosol

and its potential to act as an atmospheric INP, so they are not discussed here in any more detail.

1.6.4 Bioaerosol

There are many sources of biological INPs that have been studied, with varying relevance for the atmosphere. Biological ice nucleation is also of interest to fields such as environmental modification (Boudenne et al., 2010), cryopreservation (Daily et al., 2020) and agricultural/botanical sciences (Lindow, Arny, and Upper 1982). Atmospheric bioaerosols that might potentially act as atmospheric INPs include bacteria, fungi, pollen, viruses and fragments of any of these. Bioaerosols in the terrestrial environment are produced from flora, fauna and anthropogenic sources (i.e. from fossil fuel burning), whereas in marine environments they may be emitted as sea-spray aerosol from bubble bursting or wave-breaking processes. Bio-INPs in marine environments are typically referred to as marine organics and are emitted into the atmosphere through bubble bursting and wave breaking processes (Vergara-Temprado et al., 2017; T. W. Wilson et al., 2015).

Biological INPs have been shown to be active at very warm temperatures (as high as −2 °C) for heterogeneous freezing (Morris, Georgakopoulos, and Sands 2004; Morris, Monteil, and Berge 2013). Whilst these INPs are extremely effective at inducing freezing at warmer temperatures, their relevance in the atmosphere has been questioned due to their low number concentration in the atmosphere. (Hoose, Kristjánsson, & Burrows, 2010). There is an ongoing debate as to the importance of bioaerosols as a source of INPs in the atmosphere, especially terrestrial bioaerosols (Hoose et al., 2010; Hummel et al., 2018; Sahyoun et al., 2016; Sesartic, Lohmann, & Storelvmo, 2013). Hoose, Kristjánsson, and Burrows (2010) ran simulations of immersion mode freezing in the atmosphere, showing that when integrated over the MPC temperature regime, bioaerosol contributed less than 1% of INPs. Spracklen and Heald (2014) reached a similar conclusion, but stating that at temperatures above −15 °C bioaerosols may dominate the INP population. Neither of these studies considered bioaerosols as whole cells or spores, without considering Nano-INP fragments or ice-nucleating macromolecules (O'Sullivan et al., 2015; Pummer et al., 2015). Field based observations of bio-INPs have been made in both terrestrial (Hill et al., 2016; Huffman et al., 2013; McCluskey et al., 2014; O'Sullivan et al., 2018; Tobo et al., 2013) and marine environments (Irish et al., 2017, 2019; C. S. McCluskey et al., 2018; T. W. Wilson et al., 2015). Sources and potential atmospheric implications of bio-INPs are discussed in further detail in Chapter 4 and 6.

1.7 Project objectives

This thesis is focussed on two areas of atmospheric ice nucleation. The first was to develop and deploy a new ice-nucleating particle counter, the Portable Ice nucleation Experiment (PINE) chamber (represented by Chapters 2 & 3 of this thesis). The second was to use existing techniques to investigate potential sources of atmospheric ice-nucleating particles (represented by Chapters 3,4 & 5 of this thesis).

1.7.1 Developing the PINE chamber

The first objective of this research project was to develop a new ice-nucleating particle counter for autonomous use in the field and laboratory, which improves upon existing

instrumentation. This chapter is based upon a paper (in online review with positive responses at the time of submitting, doi 10.5194/amt-2020-307) that details the technical workings and first validation experiments of the PINE chamber. PINE is a novel new instrument that utilises the principles of adiabatic expansion to simulate a cloud and quantify INP concentration in either a laboratory or field environment, based on the principles of the AIDA chamber at Karlsruhe Institute of Technology. This project was conceptualised by Benjamin Murray and Ottmar Möhler in January 2016, after which Murray created a PhD position based around the development of the PINE chamber, which I started in August 2016. Overall, this strongly collaborative project was led by Möhler, with myself playing a key role in the development of PINE over the next two years (I was the only PhD student assigned to the project during the development phase and was tasked with leading the day-to-day development of the chamber, with Murray and Möhler providing conceptual and technical guidance). In order to achieve this I spend a total of 8 months working at KIT over the course of my PhD. This is reflected by myself, Murray and Möhler being listed as inventors on the related patent (https://patents.google.com/patent/US20200003671A1/en). I am listed as joint first author on this paper, with Möhler listed as lead. I have adapted the submitted paper *The portable ice nucleation experiment PINE: a new online instrument for laboratory studies and automated long-term field observations of ice-nucleating particles* into a thesis chapter by removing any part that I did not either lead or contribute significantly to. This effectively means the removal of section 6 in the paper, which related to field measurements with the new, commercially available PINE-c chamber.

1.7.2 Deploying and validating PINE in the field

The second objective of this research project was to deploy the PINE chamber in a field environment to demonstrate its capability as a field instrument and validate it against other field instruments. This was done by deploying the PINE chamber on the HyICE18 campaign, a multi-national field campaign to the Hyytiälä forestry research station in Finland. The University of Leeds was involved in two aspects of this campaign; PINE chamber measurements and filter sampling for cold stage experiments (discussed in 1.7.5). PINE chamber measurements were a joint effort between Leeds and KIT, with Franziska Vogel (a KIT Masters student at the time) being responsible for the day-to-day operation of the PINE chamber, with myself taking a supervising role and being responsible for the post measurement data analysis and manuscript writing.

This chapter is based on a manuscript draft entitled Measurements of ice-nucleating particle concentrations with the Portable Ice Nucleation Experiment chamber (PINE) in a Finnish Boreal forest. It details the principles of the PINE chamber with particular focus on field measurement specifics, validation against simultaneously deployed field instruments, and a preliminary analysis of the data obtained during the field campaign.

1.7.3 Quantifying the importance of combustion aerosol as an atmospheric ice-nucleating particle

The third objective of this research project was to quantify the importance of combustion aerosol as an atmospheric INP. This objective spanned the length of my PhD, with the first measurements being made within 3 months of my starting. As the PINE chamber was still in development at this point, existing techniques were used to carry out measurements.

This chapter is based upon an accepted paper entitled A major combustion aerosol event had a negligible impact on the atmospheric ice-nucleating particle population, to be published in the Journal of Geophysical Research: Atmospheres. The paper describes measurements made during the U.K. based celebration of Bonfire Night, and surrounding days, in 2016 and 2017. I am the lead author on this paper, conceptualising it with Murray and being kindly assisted by a team of co-authors (listed in Chapter 4).

1.7.4 Investigating the potential for viruses to nucleate ice

The fourth objective of this research project was borne out of a chance meeting with Dr Nina Atanasova and Professor Dennis Bamford in April 2018, on my final day at the HyICE field campaign. We first discussed the potential for measuring the ice-nucleating ability of bacteria and fungi captured from the air in Hyytiälä as part of the HyICE18 campaign, but after a visit to their research labs and learning more about their expertise, I initiated a new project to investigate the ice-nucleating ability of viruses. Viruses present a largely uninvestigated candidate for ice-nucleating particles, often being eschewed by the research community as being too small to be effective ice nucleators, but also proving extremely difficult to test for their ice-nucleating ability. It was upon seeing the expertise of the Bamford group at isolating and purifying virus samples that I initiated this study into the ice-nucleating ability of viruses. This chapter is based upon a paper currently in submission entitled *Viruses and their potential for cloud glaciation*. I am lead author of the study, with Dr Atanasova being a joint first author. Dr Atanasova and the Bamford group provided the expertise and technical ability to provide the virus samples, with myself leading the investigation into their ice-nucleating ability. All methods within this chapter that pertain to the isolating and purifying of virus particles were conducted and written by the Bamford group, in collaboration with myself and Murray.

1.7.5 Measuring the concentrations and characteristics of ice-nucleating particles in a boreal forest

The final objective of this research project was to use existing cold stage and filter measurement techniques to measure the concentrations of ice-nucleating particles in Hyytiälä, Finland. This was done as part of the wider HyICE campaign, with the Leeds contingent led by myself. This chapter is based around an in preparation paper entitled *characteristics of ice-nucleating particles in a boreal forest environment*, on which I am the lead author.

This study shows filter based INP measurements over a 6 week period from Hyytiälä, Finland, and uses an array of experimental techniques to elucidate further information about the INPs such as their size and whether they are biological aerosols. I led a team of 6 (including myself), making systematic measurements for the duration of the 6 week campaign. After the campaign, a Masters student (Ulrike Proske, University of Frankfurt) visiting our group undertook a project based on modelling INP concentrations at Hyytiälä for the time period of the HyICE18 field campaign, which was supervised in part by myself. The measured data and simulation predictions are brought together in this chapter to present the case that the boreal forest is a source of atmospheric INPs that dominate the INP population in the region at temperatures warmer than −25 °C.

1.8 Other work completed during the course of my PhD

Throughout the course of my PhD I have had the opportunity to take part in a number of field campaigns and laboratory based studies, many of which have led to, or will lead to, publications. I have listed a selection of these and my involvement below.

1.8.1 O'Sullivan et al., (2018) is a paper based upon a 6 week field campaign at a rural site near the University of Leeds I contributed significantly to the preparation of the field campaign and the experimental work taken on during it, reflected by my status as 2nd author on the paper. This was my first field campaign, and was effectively the first project I worked on during my PhD. I served as an excellent learning experience and I remain extremely grateful to have been given a leading role in this study so early in my PhD.

O'Sullivan, D., Adams, M.P., Tarn, M.D. et al. Contributions of biogenic material to the atmospheric ice-nucleating particle population in North Western Europe. Sci Rep 8, 13821 (2018). https://doi.org/10.1038/s41598-018-31981-7

1.8.2 Tarn et al., (2018) is a techniques paper describing a new microfluidic platform for the measuring of ice-nucleating particles. I provided experimental samples and data which contributed to the paper.

Tarn, M. D., Sikora, S. N. F., Grace, ·, Porter, C. E., O 'Sullivan, D., Adams, M., et al. (2018). The study of atmospheric ice-nucleating particles via microfluidically generated droplets. Microfluidics and Nanofluidics, 22(22). https://doi.org/10.1007/s10404-018-2069-x

1.8.3 Harrison et al., (2018) describes a new instrument and technique for immersion mode ice nucleation experiments. I provided experimental samples and data which contributed to the paper.

Harrison, A. D., Whale, T. F., Rutledge, R., Lamb, S., Tarn, M. D., Porter, G. C. E., Adams, M. P., McQuaid, J. B., Morris, G. J., and Murray, B. J.: An instrument for quantifying heterogeneous ice nucleation in multiwell plates using infrared emissions to detect freezing, Atmos. Meas. Tech., 11, 5629–5641, https://doi.org/10.5194/amt-11-5629-2018, 2018.

1.8.4 Ickes et al., (2020) investigated the ice-nucleating ability of sea surf ace microlayer samples and algae cultures. I was involved in a 4 week experimental campaign at the AIDA lab in Karlsruhe Institute of Technology and the manuscript writing.

Ickes, L., Porter, G. C. E., Wagner, R., Adams, M. P., Bierbauer, S., Bertram, A. K., Bilde, M., Christiansen, S., Ekman, A. M. L., Gorokhova, E., Höhler, K., Kiselev, A. A., Leck, C., Möhler, O., Murray, B. J., Schiebel, T., Ullrich, R., and Salter, M. E.: The ice-nucleating activity of Arctic sea surface microlayer samples and marine algal cultures, Atmos. Chem. Phys., 20, 11089–11117, https://doi.org/10.5194/acp-20-11089-2020, 2020.

1.8.5 Porter et al., (2020) is a techniques paper that detail the development and deployment of the Selective Height Aerosol Research Kit (SHARK). The SHARK was designed with intent to be used to make size-resolved, balloon-borne measurements of INPs at the North Pole, and is now an established field instrument.

Porter, G. C. E., Sikora, S. N. F., Adams, M. P., Proske, U., Harrison, A. D., Tarn, M. D., Brooks, I. M., and Murray, B. J.: Resolving the size of ice-nucleating particles with a balloon deployable aerosol sampler: the SHARK, Atmos. Meas. Tech., 13, 2905–2921, https://doi.org/10.5194/amt-13-2905-2020, 2020.

1.8.6 Harrison et al., (In prep) is a manuscript based on a 6 week field campaign to Barbados, to make measurements of dust transported across the Atlantic Ocean from African Deserts. I took part in the entirety of the campaign.

A. D. Harrison, D. O'Sullivan, M. P. Adams, G. C. E. Porter, C. Brathwaite, R. Chewitt-Lucas, R. Hawker, O. O. Krüger, L. Neve, M. L. Pöhlker, C. Pöhlker, U. Poschl, J. M. Prospero, A. Sanchez-Marroquin, 2A. Sealy, P. Sealy, M. D. Tarn, S. Whitehall, J. B. McQuaid , K. S. Carslaw, and B.

J. Murray. Ice-nucleating activity of African desert dust in the Caribbean boundary layer is lower than expected. In prep

1.8.7 Porter et al., (In prep) is a manuscript based on a 2 month expedition to the High Arctic. This campaign involved ship and balloon based filter measurements of INPs, with some of the measurements being size resolved. I was involved in the campaign preparation and the entire field campaign.

Grace Porter, Michael Adams, Paul Zieger, Matthew Salter, Ian Brooks, Jutta Vullers, Julika Zinke, Julia Schmale, Sebastien Sikora, Mark Tarn, Caroline Leck, Benjamin Murray. Sources and variability of Ice-Nucleating Particles at the North Pole. In prep

1.9 References

Albrecht, B. A. (1989). Aerosols, cloud microphysics, and fractional cloudiness. Science, 245(4923), 1227–1230. https://doi.org/10.1126/science.245.4923.1227

Andreae, M. O., & Rosenfeld, D. (2008). Aerosol-cloud-precipitation interactions. Part 1. The nature and sources of cloud-active aerosols. Earth-Science Reviews, 89(1–2), 13–41. https://doi.org/10.1016/j.earscirev.2008.03.001

Ansmann, A. (2005). Ice formation in Saharan dust over central Europe observed with temperature/humidity/aerosol Raman lidar. Journal of Geophysical Research, 110(D18), D18S12. https://doi.org/10.1029/2004JD005000

Atkinson, J. D., Murray, B. J., Woodhouse, M. T., Whale, T. F., Baustian, K. J., Carslaw, K. S., et al. (2013). The importance of feldspar for ice nucleation by mineral dust in mixed-phase clouds. Nature, 498(7454), 355–358. https://doi.org/10.1038/nature12278

Beall, C. M., Stokes, M. D., Hill, T. C., Demott, P. J., Dewald, J. T., & Prather, K. A. (2017). Automation and heat transfer characterization of immersion mode spectroscopy for analysis of ice nucleating particles. Atmos. Meas. Tech, 10, 2613–2626. https://doi.org/10.5194/amt-10-2613-2017

Bigg, E. K. (1953). The formation of atmospheric ice crystals by the freezing of droplets. Quarterly Journal of the Royal Meteorological Society, 79(342), 510–519. https://doi.org/10.1002/qj.49707934207

Bigg, E. K., Mossop, S. C., Meade, R. T., Thorndike, N. S. C., Bigg, E. K., Mossop, S. C., et al. (1963). The Measurement of Ice Nucleus Concentrations by Means of Millipore Filters. Http://Dx.Doi.Org/10.1175/1520-0450(1963)002<0266:TMOINC>2.0.CO;2. https://doi.org/10.1175/1520-0450(1963)002<0266:TMOINC>2.0.CO;2

de Boer, G., Morrison, H., Shupe, M. D., & Hildner, R. (2011). Evidence of liquid dependent ice nucleation in high-latitude stratiform clouds from surface remote sensors. Geophysical Research Letters, 38(1), n/a-n/a. https://doi.org/10.1029/2010GL046016

Boose, Y., Welti, A., Atkinson, J., Ramelli, F., Danielczok, A., Bingemer, H. G., et al. (2016). Heterogeneous ice nucleation on dust particles sourced from nine deserts worldwide - Part 1: Immersion freezing. Atmospheric Chemistry and Physics, 16(23), 15075–15095. https://doi.org/10.5194/acp-16-15075-2016

Boose, Y., Sierau, B., García, M. I., Rodríguez, S., Alastuey, A., Linke, C., et al. (2016). Ice nucleating particles in the Saharan Air Layer. Atmospheric Chemistry and Physics, 16(14), 9067–9087. https://doi.org/10.5194/acp-16-9067-2016

Boucher, O., Randall, D., Artaxo, P., Bretherton, C., Feingold, G., Forster, P., et al. (2013). Clouds and Aerosols. In: Climate Change 2013: The Physical Science Basis. Contribution of Working Group I to the Fifth Assessment Report of the Intergovernmental Panel on Climate Change Coordinating Lead Authors: Lead Authors.

Boudenne, J.-L., Absi, R., Berjeaud, J.-M., Chevalier, S., Creppy, E. E., Gilli, E., et al. (2010). Bacterial-based additives for the production of artificial snow: What are the risks to human health? 2 3 4 Arnaud LAGRIFFOUL. Science of the Total Environment (Vol. 408).

Broadley, S. L., Murray, B. J., Herbert, R. J., Atkinson, J. D., Dobbie, S., Malkin, T. L., et al. (2012). Immersion mode heterogeneous ice nucleation by an illite rich powder representative of atmospheric mineral dust. Atmospheric Chemistry and Physics, 12(1), 287–307. https://doi.org/10.5194/acp-12-287-2012

Budke, C., & Koop, T. (2015). BINARY: an optical freezing array for assessing temperature and time dependence of heterogeneous ice nucleation. Atmospheric Measurement Techniques, 8(2), 689–703. https://doi.org/10.5194/amt-8-689-2015

Bullard, J. E., Baddock, M., Bradwell, T., Crusius, J., Darlington, E., Gaiero, D., et al. (2016, June 1). High-latitude dust in the Earth system. Reviews of Geophysics. Blackwell Publishing Ltd. https://doi.org/10.1002/2016RG000518

Burkert-Kohn, M., Wex, H., Welti, A., Hartmann, S., Grawe, S., Hellner, L., et al. (2017). Leipzig Ice Nucleation chamber Comparison (LINC): intercomparison of four online ice nucleation counters. Atmospheric Chemistry and Physics, 17(18), 11683–11705. https://doi.org/10.5194/acp-17-11683-2017

Chen, Wu, Z., Augustin-Bauditz, S., Grawe, S., Hartmann, M., Pei, X., et al. (2018). Ice-nucleating particle concentrations unaffected by urban air pollution in Beijing, China. Atmospheric Chemistry and Physics, 18(5), 3523–3539. https://doi.org/10.5194/acp-18-3523-2018

Connolly, P. J., Möhler, O., Field, P. R., Saathoff, H., Burgess, R., Choularton, T., & Gallagher, M. (2009). Studies of heterogeneous freezing by three different desert dust samples. Atmos. Chem. Phys. Atmospheric Chemistry and Physics, 9, 2805–2824. Retrieved from www.atmos-chem-phys.net/9/2805/2009/

Cui, Z., Carslaw, K. S., Yin, Y., & Davies, S. (2006). A numerical study of aerosol effects on the dynamics and microphysics of a deep convective cloud in a continental environment. Journal of Geophysical Research, 111(D5), D05201. https://doi.org/10.1029/2005JD005981

Daily, M. I., Whale, T. F., Partanen, R., Harrison, A. D., Kilbride, P., Lamb, S., et al. (2020). Cryopreservation of primary cultures of mammalian somatic cells in 96-well plates benefits from control of ice nucleation. Cryobiology, 93, 62–69. https://doi.org/10.1016/j.cryobiol.2020.02.008

David, R. O., Marcolli, C., Fahrni, J., Qiu, Y., Perez Sirkin, Y. A., Molinero, V., et al. (2019). Pore condensation and freezing is responsible for ice formation below water saturation for porous particles. Proceedings of the National Academy of Sciences of the United States of America, 116(17), 8184–8189. https://doi.org/10.1073/pnas.1813647116

Demott, P. J. ;, Möhler, O. ;, Cziczo, D. J. ;, Hiranuma, N. ;, Petters, M. D. ;, Petters, S. S. ;, et al. (2018). The Fifth InternationalWorkshop on Ice Nucleation phase 2 (FIN-02): laboratory intercomparison of ice nucleation measurements ETH Library. Atmospheric Measurement Techniques, 11(11). https://doi.org/10.3929/ethz-b-000306690

Demott, P. J., Hill, T. C. J., Petters, M. D., Bertram, A. K., Tobo, Y., Mason, R. H., et al. (2017). Comparative measurements of ambient atmospheric concentrations of ice nucleating particles using multiple immersion freezing methods and a continuous flow diffusion chamber. Atmos. Chem. Phys, 17, 11227–11245. https://doi.org/10.5194/acp-17-11227-2017

DeMott, P. J., Sassen, K., Poellot, M. R., Baumgardner, D., Rogers, D. C., Brooks, S. D., et al. (2003). African dust aerosols as atmospheric ice nuclei. Geophysical Research Letters, 30(14). https://doi.org/10.1029/2003GL017410

DeMott, P. J., Hill, T. C. J., McCluskey, C. S., Prather, K. A., Collins, D. B., Sullivan, R. C., et al. (2016). Sea spray aerosol as a unique source of ice nucleating particles. Proceedings of the National Academy of Sciences of the United States of America, 113(21), 5797–803. https://doi.org/10.1073/pnas.1514034112

Dentener, F., Kinne, S., Bond, T., Boucher, O., Cofala, J., Generoso, S., et al. (2006). Emissions of primary aerosol and precursor gases in the years 2000 and 1750 prescribed data-sets for AeroCom. Atmospheric Chemistry and Physics, 6(12), 4321–4344. https://doi.org/10.5194/acp-6-4321-2006

Diehl, K., & Mitra, S. K. (1998). A laboratory study of the effects of a kerosene-burner exhaust on ice nucleation and the evaporation rate of ice crystals. Atmospheric Environment, 32(18), 3145–3151. https://doi.org/10.1016/S1352-2310(97)00467-6

Durant, A. J., Shaw, R. A., Rose, W. I., Mi, Y., & Ernst, G. G. J. (2008). Ice nucleation and overseeding of ice in volcanic clouds. Journal of Geophysical Research Atmospheres, 113(9). https://doi.org/10.1029/2007JD009064

Durant, Adam J., Bonadonna, C., & Horwell, C. J. (2010). Atmospheric and environmental impacts of volcanic particulates. Elements, 6(4), 235–240. https://doi.org/10.2113/gselements.6.4.235

Elsasser, M., Busch, C., Orasche, J., Schön, C., Hartmann, H., Schnelle-Kreis, J., & Zimmermann, R. (2013). Dynamic Changes of the Aerosol Composition and Concentration during Different Burning Phases of Wood Combustion. Energy & Fuels, 27(8), 4959–4968. https://doi.org/10.1021/ef400684f

Emersic, C., Connolly, P. J., Boult, S., Campana, M., & Li, Z. (2015). Investigating the discrepancy between wet-suspension- and dry-dispersion-derived ice nucleation efficiency of mineral particles. Atmospheric Chemistry and Physics, 15(19), 11311–11326. https://doi.org/10.5194/acp-15-11311-2015

Fornea, A. P., Brooks, S. D., Dooley, J. B., & Saha, A. (2009). Heterogeneous freezing of ice on atmospheric aerosols containing ash, soot, and soil. Journal of Geophysical Research, 114(D13), D13201. https://doi.org/10.1029/2009JD011958

Fu, S., Deng, X., Shupe, M. D., & Xue, H. (2019). A modelling study of the continuous ice formation in an autumnal Arctic mixed-phase cloud case. Atmospheric Research, 228, 77–85. https://doi.org/10.1016/j.atmosres.2019.05.021

G. Vali, & Stansbury, E. . (1966). Time dependent characteristics of the heterogeneous nucleation of ice. Canadian Journal of Physics, (44), 477–502.

Genareau, K., Cloer, S., Primm, K., Tolbert, M., & Woods, T. (2018). Compositional and Mineralogical Effects on Ice Nucleation Activity of Volcanic Ash. Atmosphere, 9(7), 238. https://doi.org/10.3390/atmos9070238

Gibbs, A., Charman, M., Schwarzacher, W., & Rust, A. C. (2015). Immersion freezing of supercooled water drops containing glassy volcanic ash particles. GeoResJ, 7, 66–69. https://doi.org/10.1016/j.grj.2015.06.002

Harrison, A. D., Whale, T. F., Carpenter, M. A., Holden, M. A., Neve, L., O'Sullivan, D., et al. (2016). Not all feldspars are equal: a survey of ice nucleating properties across the feldspar group of minerals. Atmospheric Chemistry and Physics, 16(17), 10927–10940. https://doi.org/10.5194/acp-16-10927-2016

Harrison, A. D., Whale, T. F., Rutledge, R., Lamb, S., Tarn, M. D., Porter, G. C. E., et al. (2018). An instrument for quantifying heterogeneous ice nucleation in multiwell plates using infrared emissions to detect freezing. Atmospheric Measurement Techniques, 11(10), 5629–5641. https://doi.org/10.5194/amt-11-5629-2018

Harrison, A. D., Lever, K., Sanchez-Marroquin, A., Holden, M. A., Whale, T. F., Tarn, M. D., et al. (2019). The ice-nucleating ability of quartz immersed in water and its atmospheric importance compared to K-feldspar. Atmospheric Chemistry and Physics, 19(17), 11343–11361. https://doi.org/10.5194/acp-19-11343-2019

Hartmann, D. L., Ockert-Bell, M. E., Michelsen, M. L., Hartmann, D. L., Ockert-Bell, M. E., & Michelsen, M. L. (1992). The Effect of Cloud Type on Earth's Energy Balance: Global Analysis. Journal of Climate, 5(11), 1281–1304. https://doi.org/10.1175/1520-0442(1992)005<1281:TEOCTO>2.0.CO;2

Hawker, R., Miltenberger, A., Wilkinson, J., Hill, A., Shipway, B., Cui, Z., et al. (2020). The nature of ice-nucleating particles affects the radiative properties of tropical convective cloud systems. Atmospheric Chemistry and Physics Discussions, 1–39. https://doi.org/10.5194/acp-2020-571

Herbert, R. J., Murray, B. J., Whale, T. F., Dobbie, S. J., & Atkinson, J. D. (2014). Representing time-dependent freezing behaviour in immersion mode ice nucleation. Atmospheric Chemistry and Physics, 14(16), 8501–8520. https://doi.org/10.5194/acp-14-8501-2014

Herbert, R. J., Murray, B. J., Dobbie, S. J., & Koop, T. (2015). Sensitivity of liquid clouds to homogenous freezing parameterizations. Geophysical Research Letters, 42(5), 1599–1605. https://doi.org/10.1002/2014GL062729

Hill, T. C. J., Demott, P. J., Tobo, Y., Fröhlich-Nowoisky, J., Moffett, B. F., Franc, G. D., & Kreidenweis, S. M. (2016). Sources of organic ice nucleating particles in soils. Atmos. Chem. Phys, 16, 7195–7211. https://doi.org/10.5194/acp-16-7195-2016

Hiranuma, N., Augustin-Bauditz, S., Bingemer, H., Budke, C., Curtius, J., Danielczok, A., et al. (2015). A comprehensive laboratory study on the immersion freezing behavior of illite NX particles: a comparison of 17 ice nucleation measurement techniques. Atmospheric Chemistry and Physics, 15(5), 2489–2518. https://doi.org/10.5194/acp-15-2489-2015

Hobbs, P. V., Fullerton, C. M., & Bluhm, G. C. (1971). Ice Nucleus Storms in Hawaii. Nature Physical Science, 230(12), 90–91. https://doi.org/10.1038/physci230090a0

Holden, M. A., Whale, T. F., Tarn, M. D., O'Sullivan, D., Walshaw, R. D., Murray, B. J., et al. (2019). High-speed imaging of ice nucleation in water proves the existence of active sites. Science Advances, 5(2). https://doi.org/10.1126/sciadv.aav4316

Hoose, C., & Möhler, O. (2012). Heterogeneous ice nucleation on atmospheric aerosols: a review of results from laboratory experiments. Atmospheric Chemistry and Physics, 12(20), 9817–9854. https://doi.org/10.5194/acp-12-9817-2012

Hoose, C., Kristjánsson, J. E., & Burrows, S. M. (2010). How important is biological ice nucleation in clouds on a global scale? Environmental Research Letters, 5(2). https://doi.org/10.1088/1748-9326/5/2/024009

Hoyle, C. R., Pinti, V., Welti, A., Zobrist, B., Marcolli, C., Luo, B., et al. (2011). Ice nucleation properties of volcanic ash from Eyjafjallajökull. Atmospheric Chemistry and Physics, 11(18), 9911–9926. https://doi.org/10.5194/acp-11-9911-2011

Huffman, J. A., Prenni, A. J., Demott, P. J., Mason, R. H., Huffman, J. A., Prenni, A. J., et al. (2013). High concentrations of biological aerosol particles and ice nuclei during and after rain CERN CLOUDy Project View project IAGOS In-service Aircraft for a Global Observing System View project Sciences ess Atmospheric Chemistry and Physics Climate of the Pa. Atmos. Chem. Phys, 13, 6151–6164. https://doi.org/10.5194/acp-13-6151-2013

Hummel, M., Hoose, C., Pummer, B., Schaupp, C., Fröhlich-Nowoisky, J., & Möhler, O. (2018). Simulating the influence of primary biological aerosol particles on clouds by heterogeneous ice nucleation. Atmospheric Chemistry and Physics, 18(20), 15437–15450. https://doi.org/10.5194/acp-18-15437-2018

Ickes, L., Porter, G. C. E., Wagner, R., Adams, M. P., Bierbauer, S., Bertram, A. K., et al. (2020). The ice-nucleating activity of Arctic sea surface microlayer samples and marine algal cultures. Atmospheric Chemistry and Physics, 20(18), 11089–11117. https://doi.org/10.5194/acp-20-11089-2020

Irish, V. E., Elizondo, P., Chen, J., Chou, C., Charette, J., Lizotte, M., et al. (2017). Ice-nucleating particles in Canadian Arctic sea-surface microlayer and bulk seawater. Atmospheric Chemistry and Physics, 17(17), 10583–10595. https://doi.org/10.5194/acp-17-10583-2017

Irish, V. E., Hanna, S. J., Xi, Y., Boyer, M., Polishchuk, E., Ahmed, M., et al. (2019). Revisiting properties and concentrations of ice-nucleating particles in the sea surface microlayer and bulk seawater in the Canadian Arctic during summer. Atmospheric Chemistry and Physics, 19(11), 7775–7787. https://doi.org/10.5194/acp-19-7775-2019

Isono, K., Komabayasi, M., & Ono, A. (1959). Volcanoes as a source of atmospheric ice nuclei. Nature. Nature Publishing Group. https://doi.org/10.1038/183317a0

Jahn, L. G., Fahy, W. D., Williams, D. B., & Sullivan, R. C. (2019). Role of Feldspar and Pyroxene Minerals in the Ice Nucleating Ability of Three Volcanic Ashes. ACS Earth and Space Chemistry, 3(4), 626–636. https://doi.org/10.1021/acsearthspacechem.9b00004

John Morris, G., & Acton, E. (2013, April). Controlled ice nucleation in cryopreservation - A review. Cryobiology. Cryobiology. https://doi.org/10.1016/j.cryobiol.2012.11.007

Kanji, Z. A., & Abbatt, J. P. D. (2009). The University of Toronto Continuous Flow Diffusion Chamber (UT-CFDC): A Simple Design for Ice Nucleation Studies. Aerosol Science and Technology, 43(7), 730–738. https://doi.org/10.1080/02786820902889861

Kanji, Z. A., Ladino, L. A., Wex, H., Boose, Y., Burkert-Kohn, M., Cziczo, D. J., et al. (2017). Overview of Ice Nucleating Particles. Meteorological Monographs, 58, 1.1-1.33. https://doi.org/10.1175/amsmonographs-d-16-0006.1

Kanji, Z. A., Welti, A., Corbin, J. C., & Mensah, A. A. (2020). Black Carbon Particles Do Not Matter for Immersion Mode Ice Nucleation. Geophysical Research Letters. https://doi.org/10.1029/2019gl086764

Kiselev, A., Bachmann, F., Pedevilla, P., Cox, S. J., Michaelides, A., Gerthsen, D., & Leisner, T. (2016). Active sites in heterogeneous ice nucleation-the example of K-rich feldspars. Science, 355(6323), 367–371. https://doi.org/10.1126/science.aai8034

Köhler, H. (1936). The nucleus in and the growth of hygroscopic droplets. Transactions of the Faraday Society, 32(0), 1152–1161. https://doi.org/10.1039/TF9363201152

Kumai, M. (1961). SNOW CRYSTALS AND THE IDENTIFICATION OF THE NUCLEI IN THE NORTHERN UNITED STATES OF AMERICA. Http://Dx.Doi.Org/10.1175/1520-0469(1961)018<0139:SCATIO>2.0.CO;2. https://doi.org/10.1175/1520-0469(1961)018<0139:SCATIO>2.0.CO;2

Lacher, L., Lohmann, U., Boose, Y., Zipori, A., Herrmann, E., Bukowiecki, N., et al. (2017). The Horizontal Ice Nucleation Chamber (HINC): INP measurements at conditions relevant for mixed-phase clouds at the High Altitude Research Station Jungfraujoch. Atmospheric Chemistry and Physics, 17(24), 15199–15224. https://doi.org/10.5194/acp-17-15199-2017

Lighty, J. A. S., Veranth, J. M., & Sarofim, A. F. (2000). Combustion aerosols: Factors governing their size and composition and implications to human health. Journal of the Air and Waste Management Association, 50(9), 1565–1618. https://doi.org/10.1080/10473289.2000.10464197

Lindow', S. E., Arny, D. C., & Upper, C. D. (1982). Bacterial Ice Nucleation: A Factor in Frost Injury to Plants'. Plant Physiol (Vol. 70). Retrieved from www.plantphysiol.org

Lohmann, U., & Feichter, J. (2005). Global indirect aerosol effects: a review. Atmospheric Chemistry and Physics, 5(3), 715–737. https://doi.org/10.5194/acp-5-715-2005

Lohmann, U., Diehl, K., Lohmann, U., & Diehl, K. (2006). Sensitivity Studies of the Importance of Dust Ice Nuclei for the Indirect Aerosol Effect on Stratiform Mixed-Phase Clouds. Journal of the Atmospheric Sciences, 63(3), 968–982. https://doi.org/10.1175/JAS3662.1

Mangan, T. P., Atkinson, J. D., Neuberg, J. W., O'Sullivan, D., Wilson, T. W., Whale, T. F., et al. (2017). Heterogeneous Ice Nucleation by Soufriere Hills Volcanic Ash Immersed in Water Droplets. PLOS ONE, 12(1), e0169720. https://doi.org/10.1371/journal.pone.0169720

Marcolli, C. (2014). Deposition nucleation viewed as homogeneous or immersion freezing in pores and cavities. Atmospheric Chemistry and Physics, 14(4), 2071–2104. https://doi.org/10.5194/acp-14-2071-2014

Marcolli, C., Gedamke, S., Peter, T., & Zobrist, B. (2007). Efficiency of immersion mode ice nucleation on surrogates of mineral dust. Atmospheric Chemistry and Physics, 7(19), 5081–5091. https://doi.org/10.5194/acp-7-5081-2007

Maters, E. C., Dingwell, D. B., Cimarelli, C., Müller, D., Whale, T. F., & Murray, B. J. (2019). The importance of crystalline phases in ice nucleation by volcanic ash. Atmospheric Chemistry and Physics, 19(8), 5451–5465. https://doi.org/10.5194/acp-19-5451-2019

Maters, E. C., Cimarelli, C., Casas, A. S., Dingwell, D. B., & Murray, B. J. (2020). Volcanic ash ice-nucleating activity can be enhanced or depressed by ash-gas interaction in the eruption plume. Earth and Planetary Science Letters, 551, 116587. https://doi.org/10.1016/j.epsl.2020.116587

Matus, A. V., & L'Ecuyer, T. S. (2017). The role of cloud phase in Earth's radiation budget. Journal of Geophysical Research: Atmospheres, 122(5), 2559–2578. https://doi.org/10.1002/2016JD025951

McCluskey, C. S., Hill, T. C. J., Humphries, R. S., Rauker, A. M., Moreau, S., Strutton, P. G., et al. (2018). Observations of Ice Nucleating Particles Over Southern Ocean Waters. Geophysical Research Letters, 45(21), 11,989-11,997. https://doi.org/10.1029/2018GL079981

McCluskey, Christina S., DeMott, P. J., Prenni, A. J., Levin, E. J. T., McMeeking, G. R., Sullivan, A. P., et al. (2014). Characteristics of atmospheric ice nucleating particles associated with biomass burning in the US: Prescribed burns and wildfires. Journal of Geophysical Research: Atmospheres, 119(17), 10458–10470. https://doi.org/10.1002/2014JD021980

McCluskey, Christina S., Ovadnevaite, J., Rinaldi, M., Atkinson, J., Belosi, F., Ceburnis, D., et al. (2018). Marine and Terrestrial Organic Ice-Nucleating Particles in Pristine Marine to Continentally Influenced Northeast Atlantic Air Masses. Journal of Geophysical Research: Atmospheres, 123(11), 6196–6212. https://doi.org/10.1029/2017JD028033

Morris, C. E., Georgakopoulos, D. G., & Sands, D. C. (2004). Ice nucleation active bacteria and their potential role in precipitation. Journal de Physique IV (Proceedings), 121, 87–103. https://doi.org/10.1051/jp4:2004121004

Morris, Cindy E., Monteil, C. L., & Berge, O. (2013). The Life History of Pseudomonas syringae : Linking Agriculture to Earth System Processes . Annual Review of Phytopathology, 51(1), 85–104. https://doi.org/10.1146/annurev-phyto-082712-102402

Mullin, J. W. (2001). Crystallization: Chpater 5- Nucleation. In Crystallization (pp. 181–215). https://doi.org/10.1016/B978-075064833-2/50007-3

Murray, B. J., Broadley, S. L., Wilson, T. W., Atkinson, J. D., & Wills, R. H. (2011). Heterogeneous freezing of water droplets containing kaolinite particles. Atmos. Chem. Phys, 11, 4191–4207. https://doi.org/10.5194/acp-11-4191-2011

Murray, B. J., O'Sullivan, D., Atkinson, J. D., & Webb, M. E. (2012). Ice nucleation by particles immersed in supercooled cloud droplets. Chemical Society Reviews, 41(19), 6519. https://doi.org/10.1039/c2cs35200a

Niemand, M., Möhler, O., Vogel, B., Vogel, H., Hoose, C., Connolly, P., et al. (2012). A Particle-Surface-Area-Based Parameterization of Immersion Freezing on Desert Dust Particles. Journal of the Atmospheric Sciences, 69(10), 3077–3092. https://doi.org/10.1175/JAS-D-11-0249.1

O'Sullivan, D., Murray, B. J., Ross, J. F., Whale, T. F., Price, H. C., Atkinson, J. D., et al. (2015). The relevance of nanoscale biological fragments for ice nucleation in clouds. Scientific Reports, 5, 8082. https://doi.org/10.1038/srep08082

O'Sullivan, D., Adams, M. P., Tarn, M. D., Harrison, A. D., Vergara-Temprado, J., Porter, G. C. E., et al. (2018). Contributions of biogenic material to the atmospheric ice-nucleating particle population in North Western Europe. Scientific Reports, 8(1), 13821. https://doi.org/10.1038/s41598-018-31981-7

Petzold, A., Ogren, J. A., Fiebig, M., Laj, P., Li, S.-M., Baltensperger, U., et al. (2013). Geoscientific Instrumentation Methods and Data Systems Recommendations for reporting " black carbon " measurements. Atmos. Chem. Phys, 13, 8365–8379. https://doi.org/10.5194/acp-13-8365-2013

Pitter, R. L., & Pruppacher, H. R. (1973). A wind tunnel investigation of freezing of small water drops falling at terminal velocity in air. Quarterly Journal of the Royal Meteorological Society, 99(421), 540–550. https://doi.org/10.1002/qj.49709942111

Polen, M., Brubaker, T., Somers, J., & Sullivan, R. C. (2018). Cleaning up our water: reducing interferences from nonhomogeneous freezing of "pure" water in droplet freezing assays of ice-nucleating particles. Atmos. Meas. Tech, 11, 5315–5334. https://doi.org/10.5194/amt-11-5315-2018

Porter, G. C. E., Sikora, S. N. F., Adams, M. P., Proske, U., Harrison, A. D., Tarn, M. D., et al. (2020). Resolving the size of ice-nucleating particles with a balloon deployable aerosol sampler: the SHARK. Atmospheric Measurement Techniques, 13(6), 2905–2921. https://doi.org/10.5194/amt-13-2905-2020

Prenni, A. J., Demott, P. J., Rogers, D. C., Kreidenweis, S. M., Mcfarquhar, G. M., Zhang, G., & Poellot, M. R. (2009). Ice nuclei characteristics from M-PACE and their relation to ice formation in clouds. Tellus, Series B: Chemical and Physical Meteorology, 61 B(2), 436–448. https://doi.org/10.1111/j.1600-0889.2009.00415.x

Price, H. C., Baustian, K. J., Mcquaid, J. B., Blyth, A., Bower, K. N., Choularton, T., et al. (2018). Atmospheric Ice-Nucleating Particles in the Dusty Tropical Atlantic. https://doi.org/10.1002/2017JD027560

Pruppacher, H. R., & Klett, J. . (1997). Microphysics of Clouds and Precipitation,. Dordrecht : Springer Netherlands : Imprint: Springer.

Pummer, B. G., Budke, C., Augustin-Bauditz, S., Niedermeier, D., Felgitsch, L., Kampf, C. J., et al. (2015). Ice nucleation by water-soluble macromolecules. Atmospheric Chemistry and Physics, 15(8), 4077–4091. https://doi.org/10.5194/acp-15-4077-2015

Rogers, D. C., DeMott, P. J., Kreidenweis, S. M., Chen, Y., Rogers, D. C., DeMott, P. J., et al. (2001). A Continuous-Flow Diffusion Chamber for Airborne Measurements of Ice Nuclei. Http://Dx.Doi.Org/10.1175/1520-0426(2001)018<0725:ACFDCF>2.0.CO;2. https://doi.org/10.1175/1520-0426(2001)018<0725:ACFDCF>2.0.CO;2

Sahyoun, M., Wex, H., Gosewinkel, U., Šantl-Temkiv, T., Nielsen, N. W., Finster, K., et al. (2016). On the usage of classical nucleation theory in quantification of the impact of bacterial INP on weather and climate. Atmospheric Environment, 139, 230–240. https://doi.org/10.1016/j.atmosenv.2016.05.034

Sanchez-Marroquin, A., Arnalds, O., Baustian-Dorsi, K. J., Browse, J., Dagsson-Waldhauserova, P., Harrison, A. D., et al. (2020). Iceland is an episodic source of atmospheric ice-nucleating particles relevant for mixed-phase clouds. Science Advances, 6(26), eaba8137. https://doi.org/10.1126/sciadv.aba8137

Sanchez-Marroquin, Alberto, Hedges, D. H. P., Hiscock, M., Parker, S. T., Rosenberg, P. D., Trembath, J., et al. (2019). Characterisation of the filter inlet system on the BAE-146 research aircraft and its use for size resolved aerosol composition measurements. Atmospheric Measurement Techniques Discussions, 1–35. https://doi.org/10.5194/amt-2019-196

Schnell, R. C., & Tan-Schnell, S. . (1982). Kenyan tea litter: A source of ice nuclei. Tellus, 34(1), 92–95. https://doi.org/10.1111/j.2153-3490.1982.tb01796.x

Schrod, J., Danielczok, A., Weber, D., Ebert, M., Thomson, E. S., & Bingemer, H. G. (2016). Re-evaluating the Frankfurt isothermal static diffusion chamber for ice nucleation. Atmos. Meas. Tech, 9, 1313–1324. https://doi.org/10.5194/amt-9-1313-2016

Sear, R. P. (2014). Quantitative studies of crystal nucleation at constant supersaturation: Experimental data and models. CrystEngComm, 16(29), 6506–6522. https://doi.org/10.1039/c4ce00344f

Seifert, P., Ansmann, A., Groß, S., Freudenthaler, V., Heinold, B., Hiebsch, A., et al. (2011). Ice formation in ash-influenced clouds after the eruption of the Eyjafjallajkull volcano in April 2010. Journal of Geophysical Research Atmospheres, 116(18), D00U04. https://doi.org/10.1029/2011JD015702

Sesartic, A., Lohmann, U., & Storelvmo, T. (2013). Modelling the impact of fungal spore ice nuclei on clouds and precipitation. Environmental Research Letters, 8(1), 014029. https://doi.org/10.1088/1748-9326/8/1/014029

Spracklen, D. V., & Heald, C. L. (2014). The contribution of fungal spores and bacteria to regional and global aerosol number and ice nucleation immersion freezing rates. Atmospheric Chemistry and Physics, 14(17), 9051–9059. https://doi.org/10.5194/acp-14-9051-2014

Steinke, I., Möhler, O., Kiselev, A., Niemand, M., Saathoff, H., Schnaiter, M., et al. (2011). Ice nucleation properties of fine ash particles from the Eyjafjallajökull eruption in April 2010. Atmospheric Chemistry and Physics, 11(24), 12945–12958. https://doi.org/10.5194/acp-11-12945-2011

Stetzer, O., Baschek, B., Lüönd, F., & Lohmann, U. (2008). The Zurich Ice Nucleation Chamber (ZINC)-A New Instrument to Investigate Atmospheric Ice Formation. Aerosol Science and Technology, 42(1), 64–74. https://doi.org/10.1080/02786820701787944

Stevenson, C. M. (1968). An improved Millipore filter technique for measuring the concentrations of freezing nuclei in the atmosphere. Quarterly Journal of the Royal Meteorological Society, 94(399), 35–43. https://doi.org/10.1002/qj.49709439905

Storelvmo, T. (2017). Aerosol Effects on Climate via Mixed-Phase and Ice Clouds. Annual Review of Earth and Planetary Sciences, 45(1), 199–222. https://doi.org/10.1146/annurev-earth-060115-012240

Tan, I., Storelvmo, T., & Zelinka, M. D. (2016). Observational constraints on mixed-phase clouds imply higher climate sensitivity. Science (New York, N.Y.), 352(6282), 224–7. https://doi.org/10.1126/science.aad5300

Tarn, M. D., Sikora, S. N. F., Grace, ·, Porter, C. E., O 'sullivan, D., Adams, M., et al. (2018). The study of atmospheric ice-nucleating particles via microfluidically generated droplets. Microfluidics and Nanofluidics, 22(22). https://doi.org/10.1007/s10404-018-2069-x

Tobo, Y. (2016). An improved approach for measuring immersion freezing in large droplets over a wide temperature range. Scientific Reports, 6(1), 1–9. https://doi.org/10.1038/srep32930

Tobo, Y., Prenni, A. J., Demott, P. J., Huffman, J. A., McCluskey, C. S., Tian, G., et al. (2013). Biological aerosol particles as a key determinant of ice nuclei populations in a forest ecosystem. Journal of Geophysical Research Atmospheres, 118(17), 10100–10110. https://doi.org/10.1002/jgrd.50801

Tobo, Y., Adachi, K., DeMott, P. J., Hill, T. C. J., Hamilton, D. S., Mahowald, N. M., et al. (2019). Glacially sourced dust as a potentially significant source of ice nucleating particles. Nature Geoscience, 12(April). https://doi.org/10.1038/s41561-019-0314-x

Twomey, S. (1977). The Influence of Pollution on the Shortwave Albedo of Clouds. American Meteorological Society Jounral. https://doi.org/10.1175/1520-0469(1977)034<1149:TIOPOT>2.0.CO;2

Ullrich, R., Hoose, C., Möhler, O., Niemand, M., Wagner, R., Höhler, K., et al. (2017). A New Ice Nucleation Active Site Parameterization for Desert Dust and Soot. Journal of the Atmospheric Sciences, 74(3), 699–717. https://doi.org/10.1175/JAS-D-16-0074.1

Vali, G. (2008). Repeatability and randomness in heterogeneous freezing nucleation. Atmospheric Chemistry and Physics, 8(16), 5017–5031. https://doi.org/10.5194/acp-8-5017-2008

Vali, G. (2014). Interpretation of freezing nucleation experiments: singular and stochastic; sites and surfaces. Atmospheric Chemistry and Physics, 14(11), 5271–5294. https://doi.org/10.5194/acp-14-5271-2014

Vali, G., DeMott, P. J., Möhler, O., & Whale, T. F. (2015). Technical Note: A proposal for ice nucleation terminology. Atmospheric Chemistry and Physics, 15(18). https://doi.org/10.5194/acp-15-10263-2015

Vali, Gabor. (1971). Quantitative Evaluation of Experimental Results an the Heterogeneous Freezing Nucleation of Supercooled Liquids. Journal of the Atmospheric Sciences, 28(3), 402–409. https://doi.org/10.1175/1520-0469(1971)028<0402:QEOERA>2.0.CO;2

Vali, Gabor, & Vali, G. (1994). Freezing Rate Due to Heterogeneous Nucleation. Http://Dx.Doi.Org/10.1175/1520-0469(1994)051<1843:FRDTHN>2.0.CO;2. https://doi.org/10.1175/1520-0469(1994)051<1843:FRDTHN>2.0.CO;2

Vergara-Temprado, J., Murray, B. J., Wilson, T. W., O'sullivan, D., Browse, J., Pringle, K. J., et al. (2017). Contribution of feldspar and marine organic aerosols to global ice nucleating particle concentrations. Atmospheric Chemistry and Physics, 17(5), 3637–3658. https://doi.org/10.5194/acp-17-3637-2017

Vergara-Temprado, J., Miltenberger, A. K., Furtado, K., Grosvenor, D. P., Shipway, B. J., Hill, A. A., et al. (2018). Strong control of Southern Ocean cloud reflectivity by ice-nucleating particles. Proceedings of the National Academy of Sciences of the United States of America, 115(11), 2687–2692. https://doi.org/10.1073/pnas.1721627115

Vergara-Temprado, J., Holden, M. A., Orton, T. R., O'Sullivan, D., Umo, N. S., Browse, J., et al. (2018). Is Black Carbon an Unimportant Ice-Nucleating Particle in Mixed-Phase Clouds? Journal of Geophysical Research: Atmospheres, 123(8), 4273–4283. https://doi.org/10.1002/2017JD027831

Wagner, R., Kiselev, A., Möhler, O., Saathoff, H., & Steinke, I. (2016). Pre-activation of ice-nucleating particles by the pore condensation and freezing mechanism. Atmos. Chem. Phys, 16. https://doi.org/10.5194/acp-16-2025-2016

Whale, T. F., Murray, B. J., O'Sullivan, D., Wilson, T. W., Umo, N. S., Baustian, K. J., et al. (2015). A technique for quantifying heterogeneous ice nucleation in microlitre supercooled water droplets. Atmospheric Measurement Techniques, 8(6), 2437–2447. https://doi.org/10.5194/amt-8-2437-2015

Whale, Thomas F., Holden, M. A., Kulak, A. N., Kim, Y. Y., Meldrum, F. C., Christenson, H. K., & Murray, B. J. (2017). The role of phase separation and related topography in the exceptional ice-nucleating ability of alkali feldspars. Physical Chemistry Chemical Physics, 19(46), 31186–31193. https://doi.org/10.1039/c7cp04898j

Wilson, T. W., Ladino, L. A., Alpert, P. A., Breckels, M. N., Brooks, I. M., Browse, J., et al. (2015). A marine biogenic source of atmospheric ice-nucleating particles. Nature, 525(7568), 234–238. https://doi.org/10.1038/nature14986

Wood, S. E., Baker, M. B., & Swanson, B. D. (2002). Instrument for studies of homogeneous and heterogeneous ice nucleation in free-falling supercooled water droplets. Review of Scientific Instruments, 73(11), 3988. https://doi.org/10.1063/1.1511796

Zaragotas, D., Liolios, N. T., & Anastassopoulos, E. (2016). Supercooling, ice nucleation and crystal growth: A systematic study in plant samples. Cryobiology, 72(3), 239–243. https://doi.org/10.1016/j.cryobiol.2016.03.012

Zolles, T., Burkart, J., Häusler, T., Pummer, B., Hitzenberger, R., & Grothe, H. (2015). Identification of ice nucleation active sites on feldspar dust particles. Journal of Physical Chemistry A, 119(11), 2692–2700. https://doi.org/10.1021/jp509839x

Chapter 2

The portable ice nucleation experiment PINE: a new online instrument for laboratory studies and automated long-term field observations of ice-nucleating particles

Ottmar Möhler[1] , Michael Adams[2],*, Larissa Lacher[1],*, Franziska Vogel[1],*, Jens Nadolny[1] , Romy Ullrich[1] , Cristian Boffo[3,4], Tatjana Pfeuffer[3] , Achim Hobl[3] , Maximilian Weiß[5] , Hemanth S. K. Vepuri[6] , Naruki Hiranuma[6] , and Benjamin J. Murray[2]

1 Institute of Meteorology and Climate Research, Karlsruhe Institute of Technology, Karlsruhe, Germany

2 School of Earth and Environment, University of Leeds, Leeds, UK

3 Bilfinger Noell GmbH, Würzburg, Germany

4 Fermi National Accelerator Laboratory, IL, USA.

5 Palas GmbH, Karlsruhe, Germany

6 Department of Life, Earth and Environmental Sciences, West Texas A&M University, TX, USA

Chapter 2 is based upon a paper published in the journal Atmospheric Measurement Techniques (10.5194/amt-14-1143-2021) that details the technical workings and first validation experiments of the PINE chamber. I am joint first author on this manuscript, and lead the day-to-day development of the PINE chamber over a two year development phase. I led the PINE measurements in the EXTRA18 campaign (described in Chapter 2) which formed a core part of this manuscript. I assisted with the writing of the manuscript, with OM leading. All authors contributed to writing, LL led aspects of the development after the initial development phase, FV ran PINE on a day-to-day basis in the HyICE18 campaign along with myself.

I contributed to the writing of each section, but made the most contribution to sections 2.4 (PINE operating principle) and 2.5 (Laboratory tests of the prototype version PINE-1A). In section 2.5 I analysed the data behind and produced Figures 11-14 which demonstrate the good agreement between PINE and the AIDA chamber, which makes up the core of the results presented in this chapter. I also produced Figure 19 which demonstrates that the liquid cloud produced during an expansion has the same characteristic size distribution regardless of whether ice crystals were formed (and thus if INP were present). I led the measurements that are shown in Figures 7-9, and was involved in the development and testing that are shown in Figures 4-6. I was also heavily involved with the testing of the drying system and background measurements shown in Figures 15-17.

Abstract

Atmospheric ice-nucleating particles (INP) play an important role in determining the phase of clouds, which affects their albedo and lifetime. A lack of data on the spatial and temporal variation of INPs around the globe limits our predictive capacity and understanding of clouds containing ice. Automated instrumentation that can robustly measure INP concentrations across the full range of tropospheric temperatures is needed in order to address this knowledge gap. In this study, we demonstrate the functionality and capacity of the new Portable Ice Nucleation Experiment (PINE) to study ice nucleation processes and to measure INP concentrations under conditions pertinent for mixed-phase clouds, with temperatures from about −10°C to about −38°C. PINE is a cloud expansion chamber which avoids frost formation on the cold walls, and thereby omits frost fragmentation and related background

ice signals during the operation. The development, working principle, and treatment of data for the PINE instrument is discussed in detail. We present extensive laboratory based tests where PINE measurements were compared with those from the established AIDA (Aerosol Interaction and Dynamics in the Atmosphere) cloud chamber. The results show good agreement of PINE with AIDA for homogeneous freezing of pure water droplets and the immersion freezing activity of mineral aerosols.

2.1 Introduction

Atmospheric ice-nucleating particles (INP) induce ice formation in atmospheric clouds, and by that are important for initiating precipitation in mixed-phase clouds and determining the phase of clouds, their albedo, lifetime and other important properties (DeMott et al. 2010). However, the details of these aerosol-cloud-climate interactions remains highly uncertain (Boucher et al., 2013; Fan, Leung, Rosenfeld, & DeMott, 2017; Ulrike Lohmann, 2017). This is partly due to the fact that such clouds are rather complex systems, and that the knowledge on the formation, the concentration and the fate of ice crystals is still uncertain (Heymsfield et al., 2017; Korolev et al., 2017). In the absence of homogeneous freezing, the cloud ice phase is initiated in various ways by a very small fraction of atmospheric aerosol particles (INPs) (G. Vali et al., 2015). In mixed-phase clouds, immersion freezing is thought to be the dominating freezing mechanism (de Boer et al., 2011; Hande & Hoose, 2017; Hoose et al., 2010).

Vergara-Temprado et al., (2018) showed INPs to have a strong control of cloud reflectivity over the Southern Ocean. Mülmenstädt et al., (2015) and Field and Heymsfield (2015) showed the ice or snow phase to exist in a large fraction of precipitating clouds, in particular over the continents. This underlines the importance of INPs for cloud radiative properties and precipitation formation, but it should be noted here that the cloud ice phase not only depends on the primary ice formation by INPs, but is also largely influenced by a cascade of secondary ice formation and interaction processes, in particular at temperatures above −15°C (Field et al., 2016). Increased ice crystal concentrations can lead to rapid cloud glaciation and associated dissipation (Campbell & Shiobara, 2008; Paukert & Hoose, 2014), as also observed recently in a laboratory cloud chamber experiment (Desai, Chandrakar, Kinney, Cantrell, & Shaw, 2019). At higher altitudes with temperatures below about −35°C, cirrus cloud ice crystals can either be formed by homogeneous freezing of aqueous aerosol particles at relatively high ice supersaturations (Kärcher & Lohmann, 2002; Koop, Luo, Tsias, & Peter, 2000), or by heterogeneous ice nucleation processes at lower ice supersaturations (Hoose & Möhler, 2012; Kärcher & Lohmann, 2003; Krämer et al., 2016; Murray et al., 2010).

As in the mixed-phase cloud regimes, the heterogeneous pathways of cirrus ice crystal formation are limited and controlled by the abundance of INPs in the upper troposphere, in addition to other factors like dynamic, thermodynamic or kinetic processes (Heymsfield et al., 2017). Throughout the troposphere, INPs are difficult to identify and to quantify due to their low and largely variable number fraction to the total aerosol concentration (DeMott et al., 2010; Kanji et al., 2017). This fraction strongly depends not only on temperature and relative humidity conditions, but also on the particle type, size, and surface properties (Holden et al., 2019; Pruppacher & Klett, 2010). Nevertheless, cloud, weather and climate models need to formulate and quantify primary ice formation as accurately as possible (Vergara-Temprado et al., 2018; Waliser et al., 2009). This is achieved by calculating the abundance of INPs with parameterizations based on either laboratory ice-nucleation experiments (Hoose & Möhler, 2012; Murray et al., 2012; Sesartic et al., 2013; Spracklen & Heald, 2014; Vergara-Temprado et al., 2018) or field measurements (DeMott et al., 2010; McCluskey et al., 2018; Tobo et al., 2013; Wilson et al., 2015). A number of different parameterizations for the various pathways of atmospheric ice nucleation in supercooled liquid and cirrus clouds have been developed under different assumptions, based on either temperature and time dependent ice formation rates according to classical nucleation rate formulations (Barahona & Nenes, 2009; Kärcher & Lohmann, 2002, 2003), the number concentration of larger aerosol particles (DeMott et al.

2015; DeMott et al. 2010), or the temperature-dependent ice nucleation active site (INAS) density on the surface of aerosol particles (Connolly et al., 2009; Harrison et al., 2019; Niemand et al., 2012; Ullrich et al., 2017). The proper use of aerosol particle specific INP parameterizations, however, requires aerosol type specific knowledge of parameters like number concentration and size distribution, needed as input to the calculation and prediction of INP concentrations.

The application of these ice nucleation parameterizations can be challenging, because of limitations in aerosol characterization in field campaigns and modelling studies. In particular, information on the types, chemical nature, and mixing state of aerosol particles is often missing, but may have a strong impact on the ice nucleation activity or INP abundance (Möhler et al., 2008). At present, the atmospheric INP data that we can compare with global fields of INP concentrations are extremely limited in spatial, temporal and concentration ranges (Burrows, Hoose, Pöschl, & Lawrence, 2013; Vergara-Temprado et al., 2017). Hence, there is an urgent need for more INP observation and monitoring, not only for constraining INP predictions by models and representing a fuller range of INP sources in those models, but also to extend the data base for a better understanding of temperature dependent INP concentrations throughout the atmosphere and the year. Existing measurements of ambient INP concentrations at mixed-phase cloud temperatures (Kanji et al., 2017a) show a great variability not only across the temperature range from about −5°C to −35°C (10 orders of magnitudes), but also at a single temperature (∼ 4 orders of magnitude). Different aerosol types were found to dominate the INP population at specific temperatures. While high temperature INPs are typically associated with biological particles (DeMott et al. 2010; Creamean et al. 2013; Prenni et al. 2013; Mason et al. 2015; Després et al. 2012; Hummel et al. 2018), their atmospheric implication remains uncertain (Després et al., 2012; Hummel et al., 2018). Marine aerosol particles were identified to be ice active at T > −30°C (Alpert et al., 2011; Brier & Kline, 1959; DeMott et al., 2015; Mason, Chou, et al., 2015; McCluskey et al., 2018; Wilson et al., 2015). They might be an important source for INPs in the absence of more ice active aerosol particles (Burrows et al., 2013; Vergara-Temprado et al., 2017; T. W. Wilson et al., 2015). Mineral dust particles are very efficient INPs at T < −20°C 75 (Boose et al., 2016; Harrison et al., 2019; Ullrich et al., 2017) and may dominate the INP number concentrations in many locations (Atkinson et al., 2013; A. Sanchez-Marroquin et al., 2020; Tobo et al., 2019). Most of these measurements were only sensitive for immersion freezing INPs in the temperature range of mixed-phase clouds, and were carried out at boundary layer field sites which were considered to be predominantly influenced by different aerosol types. Measurements in the free troposphere were either performed at high altitude mountain stations (Boose et al., 2016; Boose., 2016; Conen et al., 2015; DeMott et al., 2003; Lacher et al., 2018; Lacher, Steinbacher, et al., 2018) or with aircraft-based measurements (DeMott et al., 2003; Eidhammer et al., 2010; Field et al., 2012; Pratt et al., 2010; Prenni et al., 2009; Rogers et al., 2001) , but most of them were also limited to measure immersion freezing INPs at higher temperatures. DeMott et al., (2003) also measured the concentration of INPs active in the deposition mode at temperatures below −40°C.

The identification of INP types in ambient air remains challenging. Most ambient studies focus on sampling INPs in campaigns over a limited time period and focused on specific air masses like Saharan dust events (Boose et al., 2016),biogenic source regions (O'Sullivan et al., 2018) or marine environments (Mason, Chou, et al., 2015), or use back trajectories to identify source

regions (Wex et al. 2019; Lacher et al. 2017). Such approaches are not only in need of high-time resolution INP measurements to characterize changing air masses, but also long-term monitoring of INPs to capture the bigger picture and not only short-term periods of the atmosphere. An increasing number of new methods and instruments for INP measurements have been developed and compared to each other during the previous years (DeMott et al. 2011; Demott et al. 2018; Hiranuma et al. 2015; H. Wex et al. 2015). The most recent and comprehensive INP instrument and method inter-comparison study was the Fifth International Workshop on Ice Nucleation Research (FIN-02), and many of the latest developments for atmospheric INP measurements are included and described with respective references in the overview paper by Demott et al., (2018). Most of the INP methods showed reasonable agreement with each other, but most of them are time and operator intensive. A general feature is that available online instruments can only be operated periodically, and offline methods based on aerosol samples have poor time resolution depending on required aerosol sampling time of hours to days. All existing methods require intensive man-power and time for operation or offline analysis. The low time resolution of offline techniques challenges the comparison to potential driving factors for ice nucleation, as e.g. the size and chemistry of the aerosol population. For such measurements, online INP instruments are desirable, having a high-time resolution of minutes.

This paper presents the development, technical description, working principle, as well as first laboratory and field applications of the new Portable Ice Nucleation Experiment PINE. PINE is the first fully automated instrument for laboratory ice nucleation studies and long-term field observations of INPs in a wide temperature range from −10°C to about −60°C, including mixed-phase cloud and cirrus cloud regimes and related primary ice formation processes. Similar to the AIDA (Aerosol Interaction and Dynamics in the Atmosphere) cloud simulation chamber, PINE is based on a pumped expansion principle to induce ice and water supersaturated conditions for aerosol particles sampled either from laboratory setups or natural environments. The instrument is operated in repeated cycles of sampling the aerosol into a pre-cooled cloud chamber, activating the aerosol particles as supercooled droplets and ice crystals by expanding the air inside the cloud chamber, and refilling the cloud chamber with fresh aerosol for the next cycle (see section 4).

2.2 Basic principles and milestones of the PINE development

The idea for PINE resulted from almost 20 years of experience operating the AIDA facility for cloud experiments at simulated conditions of up-drafting atmospheric air parcels. Cloud formation in the rigid but large AIDA chamber with a volume of 84 m^3 is induced in a controlled way by lowering the pressure at different rates, starting from well controlled thermodynamic conditions (Möhler et al., 2005, 2003). With a volume of only about 10 L, the PINE cloud simulation chamber is much smaller, transportable, and operated in a fully automated sequence. Similar to the AIDA cloud chamber, PINE also uses the principle of pressure reduction by controlled pumping of air out of the cloud chamber. By that, the temperature in the chamber decreases due to expansion cooling, while the relative humidity increases. This causes the aerosol particles, which are present in the chamber prior to the expansion, to act as Cloud Condensation Nuclei (CCN) and/or INPs to form liquid cloud droplets and ice crystals, depending on the temperature, ice supersaturation and the type of aerosol. The starting temperature of each expansion run, and thereby the temperature range of ice formation and INP detection, can be set in a wide range from about −10°C to −60°C,

depending on the capacity of the cooling system. Large aerosol particles, droplets and ice crystals are measured and counted with an optical particle counter (OPC) mounted directly to the vertically oriented pump tube below the cloud chamber. PINE can be operated both for ice nucleation research in the laboratory, and for INP measurements in field campaigns or long term monitoring activities. The first version of PINE was successfully tested in January 2016. It consisted of a simple Perspex chamber of 10 L volume with manual valve and flow control, and a Welas 2300 single particle optical detector from Palas GmbH, Karlsruhe, Germany. This setup was operated in a cold room at temperatures around −10°C and sampled Snomax© aerosol particles for first proof-of-concept studies of immersion freezing in the small cloud expansion chamber. The critical development idea for PINE was to pass the total pump flow during the cloud expansion cycle through the optical particle counter directly attached to the pump line (see patent applications DE 10 2018 210 643 A1 and US2020/0003671 A1). Another prototype chamber of about 7L volume was then built of stainless steel and also operated in a cold room for further proof-of-concept experiments. Based on the development and operational experience with the prototype versions, we developed the first mobile versions PINE-1A and PINE-1B with their own cooling systems and a control system for semi-autonomous operation during laboratory ice nucleation measurements and field INP observations. Because both systems are almost identical, we only refer to PINE-1A in the following sections, for simplicity. PINE-1A can be operated in a temperature range from −10°C to about −40°C, was characterized in a series of laboratory experiments, and was used in a first field campaign (Chapter 3.). As a next step, the version PINE-c was developed, which is now commercially available from Bilfinger Noell GmbH in Germany (see https://www.noell.bilfinger.com/pine/#c167514). PINE-c is operated in the same way as PINE-1A, but received a few new components and features making it more compact and autonomous for operation in both field and lab studies. This will be detailed in Sect. 3, together with a general technical description of the new PINE instrument. The typical working principle and operation of PINE will be explained in Sect. 4. In Sect. 5 we summarize and discuss some first results from laboratory test and characterization experiments of PINE-1A in comparison with the AIDA cloud chamber.

2.3 PINE instrument setup

As illustrated in Figure 4, PINE consists of 5 major parts, (I) an inlet system, (II) a cloud chamber, (III) a cooling system, (IV) a particle detection system, and (V) a control and data acquisition system. Figure 5 shows a simplified schematics of the PINE setup in the different operational flow configurations. The inlet system (Figure 4, part I) is composed of an inlet or sampling tube, a diffusion dryer, a humidity sensor and a bypass flow section with aerosol particle filter for background measurements. The relative humidity, measured with a dew point sensor (Vaisala DRYCAP® DMT143) has to be high enough to allow cloud droplet formation upon expansion cooling, and at the same time low enough to avoid frost formation on the chamber walls. Both the prototype version PINE-1A and the commercial version PINE-c (see Table 1), are equipped with two nafion membrane diffusion dryers (Permapure, MD-700-24S-1, length 62 cm) in parallel, in order to reduce the flow through one single dryer and by that enhance the drying efficiency. Figure 15 shows the PINE sample flow dryer setup with two nafion diffusion dryers and other major components. The sample flow passes the straight nafion tube of 1.7 cm diameter and 62 cm length from top to bottom. The nafion tube is located inside an airtight stainless steel tube of 2.5 cm diameter. A second air flow is passing the annular gap between the coaxial nafion and stainless steel tubes from bottom to top

(counter flow arrangement). For simplicity, the PINE system uses ambient air for this counter flow, but at reduced absolute pressure. The absolute pressure reduction also reduces the water vapour partial pressure compared the sample flow inside the nafion tube at ambient pressure. This water vapour partial pressure difference across the nafion membrane, which is permeable for water molecules, drives a diffusional flow of water molecules from the sample flow to the counter flow. The molar flux of water molecules increases with the pressure difference across the membrane and the residence time of the sample air inside the nafion tube. As seen in Figure 16, the drying efficiency increases with pressure reduction. The pressure of the counter flow air is controlled with a pressure controller (Wagner-MSR type P-702), located between the dryer and the vacuum pump, and the volumetric flow rate of the counter flow air is controlled with a critical orifice at the inlet side. In comparison to conventionally used diffusion dryers with water adsorption material, the membrane dryers used in the PINE setup have the great advantage that they can be operated for long-term without decreasing their drying efficiency. Because the current PINE instrument versions are typically operated with a sample flow rate of up to 4 L min^{-1} , two nafion dryers are used in parallel operation, in order to limit the sample flow through each dryer to 2 L min^{-1} . If needed, the dryers can then be operated with a maximum pressure difference of about 800 hPa to achieve a high drying efficiency with a drop in the sample flow dew point temperature of at least 10 °C. As mentioned above, the frost point temperature of the sample air should be close to the wall temperature of the PINE cloud chamber. If the sampled air is too humid, frost may form at the coldest wall sections, potentially causing and an increasing ice background due to frost artefacts. However, this was not the case when operating PINE-1A during a first field application (Chapter 3) for several weeks at temperatures below −25°C and sample air frost point temperatures around −15°C. This was tested by passing the sample flow through the particle filter (see Figure 5) resulting in zero particle counts after about 5 consecutive runs (Figure 17; see also Chapter 3). This means that when the sample air is passing through the bypass particle filter, the system detects neither aerosol particles, nor activated droplets nor ice crystals. The heart of a PINE instrument is a temperature controlled cloud chamber (Part II in Figure 4). The PINE-1A cloud chamber has a volume of about 7 L and is made of stainless steel, with a central cylindrical part and two cones at the top and the bottom (Table 1). With the cooling system (part III in Figure 4), the wall temperature of the cloud chamber can either be precisely controlled at a constant value, or changed at constant cooling or heating rates of up to 0.3°C min−1 . The PINE-1A cloud chamber is temperature-controlled with an ethanol bath chiller (Lauda RP 855; Lauda-Königshofen, Germany). The wall temperature of the chamber is measured with three thermocouples attached to the outer chamber walls at three different locations. The gas temperature inside the cloud chamber is also measured with three thermocouples located in the bottom, middle and upper section of the chamber about 5 cm off the wall (see Figure 18). All thermocouples have been calibrated to a reference sensor (Lake Shore, Model PT-103, Sensor Typ Platinum Resistor) with an accuracy of ±0.1°C. A minimum wall temperature of about −33°C can be reached with PINE-1A. With additional expansion cooling of the chamber volume (see Sect. 4), a minimum gas temperature of about −33°C is then reached for ice activation of the aerosol particles. PINE-c is equipped with a thin-walled aluminium cloud chamber with a slightly larger volume of 10 L as compared to PINE-1A (see Table 1). Mainly for thermal insulation, the cloud chamber is located in an evacuated stainless steel container and is cooled with a Stirling cooler (Thales, LPT9310). The combination of the low mass and heat capacity of the thin-walled cloud chamber and the high cooling power of the Stirling cooler allows to cool the PINE-c cloud chamber at a rate of up to

approximately 0.6 °C min^{-1} without any notable effects of measurement disturbance. The heating rate of the chamber can also automatically be set to a value up to 0.6 °C min^{-1}. By that, faster temperature scans than with PINE-1A can be achieved for temperature-dependent ice nucleation and INP measurements. PINE-c can also be cooled to a lower wall temperature of − 60°C and can therefore be operated for ice nucleation experiments and INP measurements at cirrus cloud temperatures. The PINE particle detection system (part IV in Figure 4) consists of an OPC connected to the control and data acquisition system (part V in Figure 4). Depending on the OPC type, aerosol particles, activated cloud droplets and ice crystals are detected during the different run modes as described in Chapter 3. The OPC is mounted to the pump tube, with a minimum distance to the cloud chamber in order to minimize warming of the cold air flow from the cloud chamber and by that avoid evaporation of supercooled cloud droplets and sublimation or melting of ice crystals. PINE-1A is equipped with a Welas 2500 sensor connected to a Promo© 2000 system (Palas GmbH, Karlsruhe, Germany). The same sensor has been operated for many years at the AIDA cloud chamber for cloud droplet and ice crystal detection (Möhler et al., 2006; Wagner & Möhler, 2013). It measures aerosol particles, water droplets and ice crystals with optical sizes between 0.7 and 220µm diameter, depending on the sensitivity setting of the photomultiplier measuring the intensity of light scattered by single particles when passing the optical detection volume (ODV). The Welas sensor records for each detected particle the time of detection, the transit time through the ODV, and the intensity of light scattered into a range of scattering angles around 90° (sideward scattering). This optical arrangement is favourable for the selective detection of a-spherical ice crystals, which are measured at a larger optical size than spherical droplets of the same volume and can therefore more easily be distinguished from droplets by setting a simple threshold for the optical size. The Welas 2500 sensor has a well confined ODV with a sample flow cross section area Aw = 0.24mm2 and a length l_w = 0.31mm. Because the transect time τ_w of particles through the ODV is also measured, the sample flow rate through the ODV can be calculated as

$$F_w = \frac{A_w l_w}{\tau_w} \tag{18}$$

With the count rate c_p of detected particles, one can then calculate the particle number concentration

$$n_p = \frac{c_p}{F_w} \tag{19}$$

On average, the ratio of the volume flow through the ODV to the total volume flow through the Welas 2500 sensor is about 0.105. This means that the sensor detects only about 10% of the particles sampled from the cloud chamber. The PINE-c version uses a new OPC called Fidas-pine (Palas GmbH, Karlsruhe, Germany). This new OPC was developed especially for the PINE-c instrument and analyses the full sample flow of up to 5 L min^{-1} for particles in a size range similar to the Welas 2500 sensor. For PINE-c, the particle number concentration can still be calculated with Eq.2, just by replacing the flow rate through the ODV of the Welas 2500 sensor by the total sample flow rate F_{em} during the expanion mode. Therefore, Fidas-pine has a 10 times higher detection rate of particles, and by that a 10 times lower INP concentration detection threshold than PINE-1A. PINE is controlled via a bespoke LabVIEW program, which sets the respective measurement condition, displays the parameters such as particle size, temperature, pressure, and flows, and saves the data internally. Metadata

describing the experiment are saved automatically using LabVIEW, such as date and time, type of OPC used and its configuration, temperature and pressure conditions.

2.4 PINE operating principle

The PINE instrument can either be used in an individual operator controlled mode for laboratory ice nucleation experiments and measurements, or in a fully automated mode for long-term field measurements and observations of INPs. The instrument's settings during a laboratory or field campaign and the data storage systems of PINE are organized in a well-defined sequence of operations and runs. All data and metadata are saved automatically using the LabVIEW program. An operation is defined as a specific series of runs, which can be, for example, performed at one temperature, and during a specific sampling time. Each run is composed of a sequence of three modes called "flush", "expansion", and "refill". The flow settings of PINE in these three run modes are illustrated in Figure 5. In the flush mode (Figure 5a), the sample flow is passed through the cloud chamber to fill it with the aerosol under investigation. This can either be ambient air at a field station where PINE measures INP concentrations, or an aerosol generated in a laboratory for ice nucleation studies. For PINE-1A and PINE-c, the sample flow rate is limited to about 4 L min^{-1}. In the flush mode, the sample flow can also be passed through an aerosol filter for background, particle-free measurements. In the expansion mode (Figure 5b), the sample flow is kept constant, but switched to a bypass line around the cloud chamber. At the same time, a valve at the chamber inlet is closed and the OPC flow rate is set to a value between 2 and 5 L min^{-1}, such that the pressure in the cloud chamber is lowered at a constant rate and to a pre-defined minimum pressure. This forced gas expansion in the cloud chamber causes an adiabatic cooling and thereby an increase of the relative humidity. When the relative humidity exceeds ice or water saturation, the aerosol particles in the cloud chamber, which were sampled during the flush mode, are then activated to form ice crystals and/or liquid cloud droplets, depending on the temperature and the type of aerosols.

The number of ice crystals is measured with the OPC downstream of the chamber, and equals the number of INPs in the same sampling volume. The expansion mode flow rate F_{em} is limited to 2 and 5 L min^{-1}, because both the Welas 2500 and Fidas-pine OPCs can only be operated to a maximum sample flow rate of 5 L min^{-1}. Smaller flow rates can cause cloud droplet evaporation or ice crystal sublimation in the tube connection between the cloud chamber and the OPC. The end pressure is typically 200 to 300 hPa lower than the start pressure that is given by the pressure of the aerosol sampled during the flush mode. The refill mode (Figure 5c) is the final run mode and is carried out to safely re-pressurize the PINE chamber to the start pressure. Once this pressure is reached, the sample flow is immediately switched back to pass the cloud chamber, starting the next run with the same series of flush, expansion and refill modes.

A full run takes about 4 to 6 minutes, depending on the flush time, the pump flow rate during the expansion mode and the end pressure. The higher the sample flow rate, the faster the air in the cloud chamber is replenished and renewed for the next run, and the shorter the flush time can be chosen. The lower the minimum pressure during expansion, the longer the refill mode time. Figures 6-9 show results from a PINE-1A operation on March 25, 2018 during the HyICE field campaign, which includes a series of 59 identical runs. Each run took about 6 minutes, so the whole operation lasted almost 6 hours. During this time, the ambient total

aerosol concentration varied between about 900 and 2300 cm^{-3}, and PINE-1A sampled ambient air at a flow rate of 3 L min^{-1}. The flush time was set to 4 minutes. Each expansion was started at a wall temperature of about −26 °C with pump flow rate of 4 L min^{-1} , and took about 40 seconds. An example of these 59 runs is depicted in Figure 6, which shows the end of the flush mode, the expansion mode and the refill mode. The data time series are plotted as a function of the time in seconds relative to the start of the expansion mode. A temperature and pressure decrease of about 6 °C and 300 hPa, respectively, is observed during the expansion (Figure 6a). Here, only the data from the lowest of the three gas temperature sensors (see Figure 18) is plotted, which reaches a minimum value of about −32 °C at the end of the expansion after about 40 seconds. The relative humidity is not directly measured in the PINE cloud chamber, but can be calculated from the change of the temperature dependent water saturation pressure, assuming ice saturated conditions at the start of the expansion and omitting water vapour sources and sinks during the expansion. As mentioned above, we assumed ice saturated conditions so that the water vapour partial pressure at the start of expansion equals the ice saturation pressure calculated as function of the wall temperature at start of expansion ($p_{w,0} = p_{sat,\,ice}(T_{g,0})$, and the corresponding saturation ratio with respect to liquid water is $S_w = 0.79$ at the same start temperature $T_{g,0} = -26$ °C. During the expansion mode, the liquid water saturation ratio was then calculated as

$$S_w = \frac{p_w}{p_{sat,liq}(T_g)} \tag{20}$$

with

$$p_w = p_{w,0}\frac{p}{p_0} \tag{21}$$

where p_0 is the pressure at start of expansion and p the pressure during the expansion. It can be seen that after about 10 seconds, the so calculated S_w exceeds 1 (Figure 6b). Note that S will in reality be limited by the growth of cloud droplets, but that conditions of $S > 1$ indicate conditions where a liquid cloud could form. This roughly corresponds with the start of cloud droplet activation as shown in panel (c) of Figure 6, shown by the sudden occurrence of a large number of particles with diameters up to 10 µm. This panel shows each single particle detected by the OPC plotted as a single blue dot at the time of occurrence and with its measured optical diameter. With ongoing pressure reduction and related cooling, a small number of particles is detected at larger optical size, with diameters larger as the dense "cloud" of liquid droplets (Figure 6c). Those particles are identified as ice crystals formed by immersion freezing of only a minor droplet fraction. The expansion mode stops after about 40 seconds and the chamber is refilled to ambient pressure within about 1 minute. The next run is started with the flush mode, filling the cloud chamber again with ambient aerosol particles for the next expansion run. Refilling causes compression of the chamber air and related warming (see upper panel of Figure 6). This also leads to the evaporation of the droplets and ice crystals after some time, however, the abrupt stop of particle recording is related to the fact that the pump flow rate through the OPC is stopped at the end of expansion, so that only a few particles are moving through the OPC detection volume during the refill mode. For the same PINE-1A operation during the HyICE field campaign, there is little run-to-run variation for the total OPC counts per second of run time (Figure 7). This means that PINE is able to reproduce aerosol CCN activation and super-cooled droplet formation in repeated runs at constant sampling and operation conditions, which provides a good basis for

conducting series of immersion mode INP and freezing measurements at high precision. The small grey dots in this figure show the OPC count rates of individual runs, the bigger black circle the mean over all 59 runs of this operation. The variation can partly be explained by the natural variability of the ambient aerosol concentration which also causes a variation of the droplet number concentration. As mentioned above, the aerosol number concentration varied by about a factor of two between 900 and 2300 cm^{-3}. Not only cloud droplets but also ice crystals were detected during the same operation as shown by the occurrence of particles larger than ~ 10 µm (Figure 6c). The whole size distribution of both cloud droplet and ice crystals (Figure 8) reveals that there is only little variation from run to run, at least for the droplet mode with maximum diameters of ~ 10 µm. Larger particles are identified as ice crystals, and can be distinguished from the droplets by setting a size threshold close to the end (the "right edge") of the sharp droplet mode. Based on Eq. 1, the immersion mode INP number concentration measured in one run of the PINE-1A system can then be calculated by dividing the total number ΔN_{ice} of ice crystals detected by the total volume ΔV_w of air passing the ODV of the Welas OPC during the expansion mode after the formation of the supercooled liquid cloud

$$n_{INP,w} = \frac{\Delta N_{ice}}{\Delta V_w} = \frac{\Delta N_{ice}}{F_w \Delta t_{em}} \tag{22}$$

where F_w is the volumetric flow rate through the optical detection volume of the Welas sensor, and Δt_{em} the duration of the expansion mode from the start of liquid cloud formation (Eq. 2). For the Welas 2500 sensor, ΔV_w is about 10% of the total volume ΔV_{em} passing the OPC during the same time. For the PINE-c system equipped with a Fidas-pine (fp) sensor analysing the total pump flow $F_{em} = \Delta V_{em}/\Delta t_{em}$ for particles, the INP number concentration results from

$$n_{INP,fp} = \frac{\Delta N_{ice}}{\Delta V_{em}} = \frac{\Delta N_{ice}}{F_{em} \Delta t_{em}} \tag{23}$$

Examples from PINE-1A at higher temperatures without ice crystal formation prove that this "right edge" of the activated droplet size distribution is indeed rather sharp in typical expansion runs (Figure 19). For data interpretation, the size threshold to distinguish between droplets and ice crystals can be set manually, however it varies with operation temperature and droplet number concentration. Therefore, in Chapter 3 an automated procedure for setting this threshold was developed. Setting this size threshold and counting all larger particles as ice crystals is a simple straightforward procedure, but neglects smaller ice particles which may also be present in the overlapping size range with the droplets and may cause an underestimation of the ice crystal number concentration. Therefore, the PINE instrument was also operated next to the AIDA cloud chamber for homogeneous droplet freezing and immersion freezing experiments in order to identify and quantify potential systematic uncertainties and biases. In addition to detecting the accurate number of ice crystals, the quality of ice nucleation and INP measurements also depends on measuring the precise temperature, at which the ice crystals are actually nucleated, either homogeneously or at the surface of an INP. The variability of the gas temperature in the PINE cloud chamber during 59 expansions is illustrated in Figure 9. Here, all ice crystals detected during the 59 expansions are plotted for the relative time after start of the run in which they were measured, and the respective gas temperature measured with three sensors located in the lower (blue), the middle (green) and the upper (red) part of the chamber (see Figure 18). First

of all, one can see that the number of ice crystals, and thereby also the number of immersion freezing INPs that caused the ice formation in these expansions, increases with decreasing temperature, which reflects the temperature dependent INP number concentration in ambient air. For individual sensors, the temperature variability from run to run is less than about 0.5°C, clearly underlining that PINE is able to detect the temperature dependent ice crystal formation from run to run at well controlled conditions. However, there is an increasing deviation of the temperature readings at the different locations in the PINE cloud chamber, with the lowest temperature measured at the bottom and the largest at the top. This inhomogeneity of the temperature across the chamber arises from the fact that there is an increasing temperature difference between the expanding gas and the almost constant wall temperature. This causes an increasing heat flux into the chamber volume and by that an increasing temperature distortion and deviation from the adiabatic temperature profile. The hereby formed warm air tends to be collected in the top part of the chamber. The related temperature variability inside the cloud chamber impacts the temperature uncertainty for the INP and ice nucleation detection. However, it can be assumed that most of the ice crystals detected in the PINE expansion mode are formed at the lowest temperature in the bottom part of the chamber, where all the air flowing to the OPC passes through. Since ice nucleation is a strong function of temperature, it is a good first order approximation to assume the coldest temperature in the chamber to guide the ice nucleation. This assumption will be solidified by the results of experiments presented and discussed in the following section. An important part of PINE operations are the background runs, during which the sampled air is guided through a filter, while the operation runs are ongoing. After typically 5 to 10 runs, the chamber becomes particle free, as such any remaining particle counts indicate the presence of frost formation on the walls or a leak in the chamber or pipework. A typical background measurement, where almost no particles are present after 5 cycles, is presented in Figure 17.

Regular background run series are performed with PINE at least during longer measurement phases at low temperatures. A frost-free chamber is a prerequisite for operating PINE with highest sensitivity. In case of zero background conditions, the detection limit for INP number concentrations can be calculated by dividing the minimum number of ice crystals detected in a certain volume of air. In one expansion with PINE-1A and PINE-c analysing about 0.2 and 2 litres of air per run, respectively, the resulting one count detection threshold is 5 L^{-1} and 0.5L^{-1}, respectively (see also Table 1). Note that the detection limit of PINE-1A is a factor of 10 lower because only about 10% of the pump flow during the expansion is analysed, whereas the OPC of PINE-c detects all ice crystals in the pump flow. If 10 consecutive runs are conducted and summed up in one hour, assuming the total run time is set to 6min, about 10 times more volume of air is analysed, and all ice crystals detected can be summed-up, so that the INP detection limits are reduced by a factor of 10 to 0.5L^{-1} and 0.05L^{-1} for PINE-1A and PINE-c, respectively, with a time resolution of one hour. When summing-up over a whole day of subsequent runs, the detection limits are further reduced to 0.02L^{-1} and 0.002L^{-1}, respectively.

2.5 Laboratory tests of the prototype version PINE-1A

During several test series, immersion freezing and cloud droplet freezing measurements with PINE-1A were compared to the AIDA cloud camber results. For these inter-comparison studies, PINE-1A sampled aerosols directly from the AIDA chamber and was operated at similar wall temperatures as the AIDA cloud chamber. By that, the cloud expansion runs

covered a similar temperature range, and as such allowed the inter-comparison of temperature-dependent INP concentrations. Figure 10 shows the results for homogeneous freezing of supercooled water droplets, which are known to start freezing in a typical AIDA cloud expansion run at about −36 °C, in good agreement with other experimental results and formulations for classical nucleation theory (Benz et al., 2005), however there is a single anomalous data point from the PINE chamber that shows a freezing event at a temperature warmer than expected based on both AIDA and the remainder of the PINE measurements. This data point falls outside of the experimental uncertainty and we do not presently have an explanation for it, however we include it for transparency. As in the experiments by Benz et al., (2005), aqueous sulphuric acid particles were first added to the AIDA chamber. Then, the aerosol particles with a diameter around 0.8 µm and a number concentration of about 200 cm^{-3} were sampled into the PINE-1A chamber for its homogeneous freezing experiments, followed by an AIDA cloud expansion experiment with the same aerosol.

Figure 10 shows good agreement for the onset temperature of the homogeneous freezing in PINE-1A and the AIDA cloud expansion experiment. The PINE-1A data is plotted as a function of the temperature measured with the bottom temperature sensor, which always measures the lowest temperature during a run (see Figure 9). This result underlines the assumption, that the ice formation measured with PINE is mainly controlled by the minimum temperature in the cloud chamber. PINE-1A was also operated next to the AIDA cloud chamber during the EXTRA18 campaign in February 2018. This campaign was mainly organized to test and calibrate the newly constructed PINE-1A in preparation to the first field campaign, which will be described in more detail in a follow-up paper. During this campaign, PINE-1A sampled aerosol particles directly from the AIDA chamber again, and measured their ice nucleation activity in the same temperature range covered by AIDA cloud expansion runs with the same aerosols. Arizona test dust (ATD) and illite NX aerosols where used during this campaign. These aerosols are well studied for their ice nucleation activities and were also used in previous inter-comparison experiments for INP instruments (DeMott et al. 2011; Demott et al. 2018; Hiranuma et al. 2015). We used the same aerosol sources as Steinke et al., (2015) for ATD and Hiranuma et al., (2015) for illite NX, and the methods for generating and characterizing these aerosols are described in these papers. The supercooling or minimum temperature reached in a PINE expansion can be controlled by two parameters, the pump flow rate and the end pressure. This allows for a quick scan through a certain temperature range of ice nucleation activity. Both higher pump flow rates and lower end pressure cause a larger supercooling of the air in the cloud chamber, means a lower minimum temperature at the end of expansion. An example is shown in Figure 11.

In this operation, PINE-1A sampled ATD aerosol directly from the AIDA chamber and measured the number fraction f_{ice} of ice-active ATD particles in a series of runs starting from a temperature of about −18 °C. The expansion flow rate was 5 L min^{-1} in all runs, but the end pressure was stepwise reduced every 5 runs from about 800 hPa at the beginning to about 500 hPa at the end of this operation (see panel (a) of Figure 11). This caused a stepwise decrease of the minimum gas temperature in the cloud chamber, as also shown in panel (a). The Welas 2500 single particle data (Figure 11, panel (b)) indicates an increasing amount of ice formation with decreasing minimum temperature. This stepwise increase in the number concentration of ice crystals or INPs is shown in panel (c) of Figure 11, which depicts the time series of the ice crystal number concentrations measured at the end of each expansion. Figure

12 depicts the ice crystal number fraction calculated with Eq. 5 divided by the aerosol number concentration for each individual run as function of gas temperature measured with the sensor in the bottom of the PINE-1A cloud chamber. The measured number concentration of ice crystals equals the number concentration of ice-active ATD particles measured in an AIDA cloud chamber experiment with the same aerosol (Figure 12). For the PINE measurements, we estimate a temperature uncertainty of ±1 °C, mainly caused by the inhomogeneous temperature distribution in the PINE cloud chamber during the expansion run (see Figure 9). The temperature uncertainty during AIDA cloud expansion experiments is ±1 °C. The estimated uncertainty for the ice number concentration is ±20% for both PINE and AIDA, mainly due to the uncertainty in the dimension of the ODV of the Welas sensor and the measured transect time of particles passing the ODV (see Eq. 1). The same measurements as for ATD were also performed with illite NX aerosol (Figure 13 and Figure 14), but with both AIDA and PINE-1A starting their cloud expansions at a slightly lower temperature of about −22 °C because of the somewhat lower ice nucleation activity of illite NX compared to ATD. Within the given uncertainty ranges, the PINE-1A data is in excellent agreement with the AIDA data for both ATD (Figure 11 and Figure 12) and illite NX (Figure 13 and Figure 14). This also underlines the assumption, that the ice formation in PINE is mainly controlled by the coldest temperature in the bottom part of the chamber and that the number concentration of ice crystals, and by that the number concentration of ice-active aerosol particles in laboratory experiments and of INPs during field measurements can correctly be calculated with Eqs. 5 and 6.

2.6 Summary and conclusions

We present a new instrument called PINE (Portable Ice Nucleation Experiment) for laboratory studies of ice nucleation and field measurement of ice-nucleating particles (INPs). Inspired by the large AIDA cloud chamber (Möhler et al., 2005, 2003), the PINE instrument also uses the principle of expansion to expose aerosols from different sources to cloud-relevant conditions. By that, the sampled aerosol particles are activated to form both supercooled water droplets and ice crystals, which are detected with an optical particle counter (OPC). However, with a volume of only about 10 L, PINE is much smaller than the AIDA cloud chamber. The instrument is sensitive to detect ice formation and INPs in the immersion freezing, pore condensation freezing and deposition nucleation modes in a wide temperature range from −10 °C to −65 °C. Equipped with a LabVIEW control system, PINE can be operated autonomously over longer time periods and is therefore also suitable for INP monitoring at atmospheric field sites and observatories.

The operation of PINE is organized in a well-defined sequence of runs. Each run is composed of three modes called “flush”, “expansion”, and “refill”. During the flush mode, the aerosol under investigation is sampled into the pre-cooled cloud chamber. The sampled aerosol particles are activated as supercooled cloud droplets and ice crystals during the expansion mode, depending on the pre-set wall temperature, the expansion rate and the minimum pressure reached at the end of the expansion mode. Droplets and ice crystals are detected with the OPC, and the fraction of ice-active aerosol particles or the number concentration of INPs in the sample can be calculated from the total number of ice crystals detected during the expansion mode and the volume of air that has passed the detection volume of the OPC. During the refill mode, the cloud chamber is just refilled to the ambient pressure to immediately start the next run. In the current PINE versions, one run takes about 4 to 6

minutes, which defines the largest time resolution that can be achieved with PINE when e.g. measuring time series of atmospheric INP concentration. Here we presented and discussed the construction and performance of both the prototype version of the new instrument, called PINE-1A, and the more advanced and commercially available version PINE-c (Bilfinger Noell GmbH). PINE-1A has a stainless steel cloud chamber of 7 L volume that is cooled with a chiller to measure immersion freezing INPs at temperatures between about −10 °C to −40 °C.

This instrument was tested and characterized in a series of laboratory measurements in comparison with the benchmarked AIDA chamber. PINE-1A results for both homogeneous freezing of cloud water droplets and immersion freezing of ATD and illite NX aerosols were in excellent agreement with AIDA results. The first operation of PINE-1A during the HyICE field campaign in Hyytiälä, Finland, also demonstrated that there is only little variability of the measured droplet and ice size distribution from run to run. The INP concentration is measured with a high precision and repeatability. The temperature uncertainty is estimated to be about ±1 °C, mainly influenced by an increasing temperature inhomogeneity during the expansion mode. The field operation also showed that the Welas 2000 OPC can well distinguish between ice crystals and droplets by setting an optical size threshold, and that PINE-1A was operated over longer time periods at almost zero background conditions without any detectable frost formation on the cold cloud chamber walls. Chapter 3 will present more results from the HyICE field activity and will discuss in more detail the performance of PINE-1A during long-term field operation. The advanced instrument version PINE-c has a somewhat larger cloud chamber of 10 L volume which is made of thin-walled aluminium and located in an evacuated chamber for thermal insulation. The cooling system is based on a Stirling cooler and allows cooling the chamber to temperatures as low as −60 °C. One of the unique features of PINE, in contrast to flow diffusion or mixing devices, is its operation under dry and frost-free wall conditions. Therefore, long-term continuous operation over days and weeks can be performed without the occurrence of increasing background from frost artefacts. This is achieved by drying the sampled aerosol to a frost point temperature close to the minimum wall temperature.

This was proven in a series of measurements during a field campaign in Hyytiälä, Finland. The PINE-1A results from this campaign will be discussed in more detail in Chapter 3. The sampled air needs to be humidified when its frost point temperature is clearly below the lowest chamber wall temperature. This may only be the case when sampling from extremely cold or dry environments, like polar regions or desert areas, or when sampling laboratory aerosols generated in extremely dry air. In most surface-based atmospheric sampling locations, the sample includes sufficient humidity and needs to be dried before entering the PINE chamber. Future versions of PINE may therefore also include an optional air humidification system in addition to the diffusion dryers. In addition, the newest version PINE-c is operated with a novel and liquid-free cooling system, which makes it suitable to be even operated autonomously at remote measurement sites. Given the dearth of atmospheric INP measurements with which to challenge and inform our aerosol, cloud and climate models, an instrument, such as PINE, capable of making measurements on a routine and autonomous basis is needed. The development of PINE is timely, since INP control the radiative properties of clouds around the globe and are first order for defining cloud feedbacks (Tan et al., 2016; Vergara-Temprado et al., 2018). We anticipate that PINE will become a standard autonomous

instrument at atmospheric observatories around the globe as well as a versatile laboratory and research tool.

Appendix A: Membrane diffusion dryer: The PINE instruments are equipped with a dual membrane dryer system (Figure 15) to reduce the humidity of the aerosol sampled into the cold cloud chamber and by that to avoid frost formation on the cold cloud chamber walls. The drying efficiency of the Nafion tube was measured as a function of the pressure difference Δp between the sample flow and the counter flow and also as 490 a function of the volumetric sample flow rate. The drying efficiency is plotted in Figure 16 as the difference ΔTd of the sample air dew point temperatures measured with a chilled mirror dew point sensor (MBW type 393) before and after the dryer. The measurements shown in Figure 16 were conducted with the dew point temperature of the sample air ranging from about 6 to 7°C. The drying efficiency is increasing with the pressure difference and decreasing with the sample flow rate. High drying efficiency with a drop in dew point temperature of more than 10°C is achieved when operating the dryers with a sample flow rate below 2 to 3L min−1 495 and at the maximum pressure difference of about 800 hPa across the membrane.

Appendix B: Background measurements: Operating PINE with high sensitivity for INP detection requires low or even zero background conditions. Therefore, the control system allows for regular background checks, where the instrument is set to flush mode and passing the sample flow through the bypass line with particle filter (via dashed line in Figure 5a). A typical background run sequence (operation) from the HyICE field measurements with PINE-1A (Figure 17) shows that the particle counts approach or drop to zero after about 4 to 5 runs. More details about background behaviour of PINE will be presented and discussed in a follow-up paper.

Appendix C: PINE construction and operation: Figure 18 shows the construction of the PINE-1A cloud chamber with the location of the three gas temperature sensors. For PINE measurements, a size threshold is used in order to distinguish larger ice crystals from smaller liquid water droplets in the OPC single particle data (see discussion in Sects. 3 and 4). In the absence of INPs, the droplet size distribution measured with the OPC has a sharp edge to larger particle diameters (Figure 19), which is favourable for setting the size threshold.

Table 1: Configuration and operational parameters of PINE prototype version 1A as well as the currently available commercial version PINE-c.

	PINE-1A	PINE-c
Chamber type	Stainless steel, single walled	Aluminium, thin-walled
Thermal insulation	2 cm thick armaflex layer	Vacuum chamber
Chamber length	75 cm	57 cm
Chamber diameter	15 cm	18 cm
Chamber volume	7 L	10 L
Cooling system	Chiller Lauda (RP855)	Stirling (Thales, LPT9310)
Wall temperature range	0 °C to −33 °C	0 °C to −60 °C
Measurement temperature range	−10 °C to −40 °C	−10 °C to −65 °C
Temperature uncertainty	±1 °C	±1 °C
Wall cooling rates	0.3 °C min^{-1}	0.6 °C min^{-1}
Wall heating rates	0.3 °C min^{-1}	0.6 °C min^{-1}
Particle detector	welas 2500	fidas-pine
Inlet dryer	Permapure, MD-700-24S-1	Permapure, MD-700-24S-1
Detection limit at 6 minute time resolution (single run)	5 L^{-1}	0.5 L^{-1}
Detection limit at 1 hour time resolution (10 runs)	0.5 L^{-1}	0.05 L^{-1}
Detection limit at 24 hour time resolution (240 runs)	0.02 L^{-1}	0.002 L^{-1}

2.7 Figures and tables

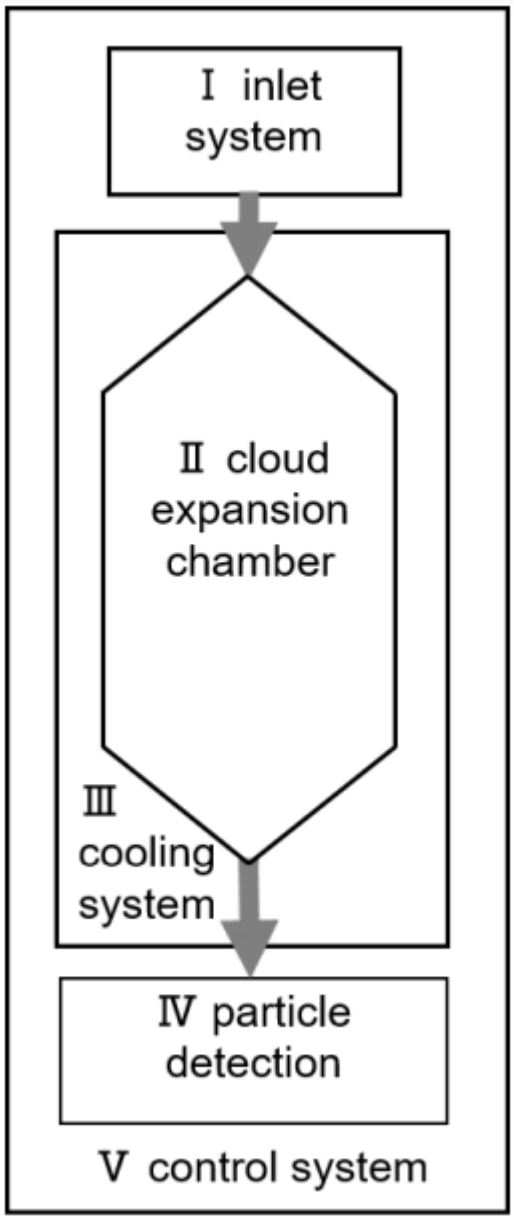

Figure 4: Scheme of a PINE instrument with its five basic components.

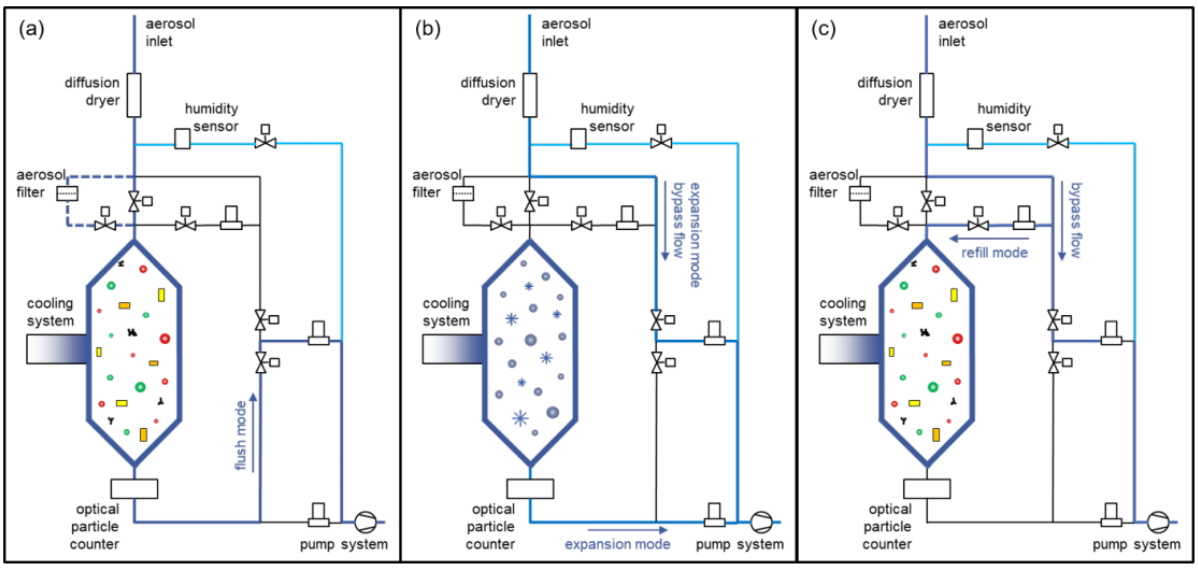

Figure 5: Schematic setup of the PINE-1A. The three figures show the same instrument, but in the different run modes (a) flush, (b) expansion, and (c) refill. The thick blue lines indicate which parts of the flow setup are active in the respective modes. The sampling gas flow through the humidity sensor (light blue line) is active all the time in a bypass line to the sampling pump. A background measurement can be done by passing the sample flow over an aerosol filter (dashed line, panel a). In the flush mode (a), aerosol particles are sampled (coloured various symbols), and activate into cloud droplets and ice crystals during the expansion mode (panel b, blue circles and stars, respectively). During the refill mode, aerosol particles are entering the chamber again (panel c, coloured various symbols).

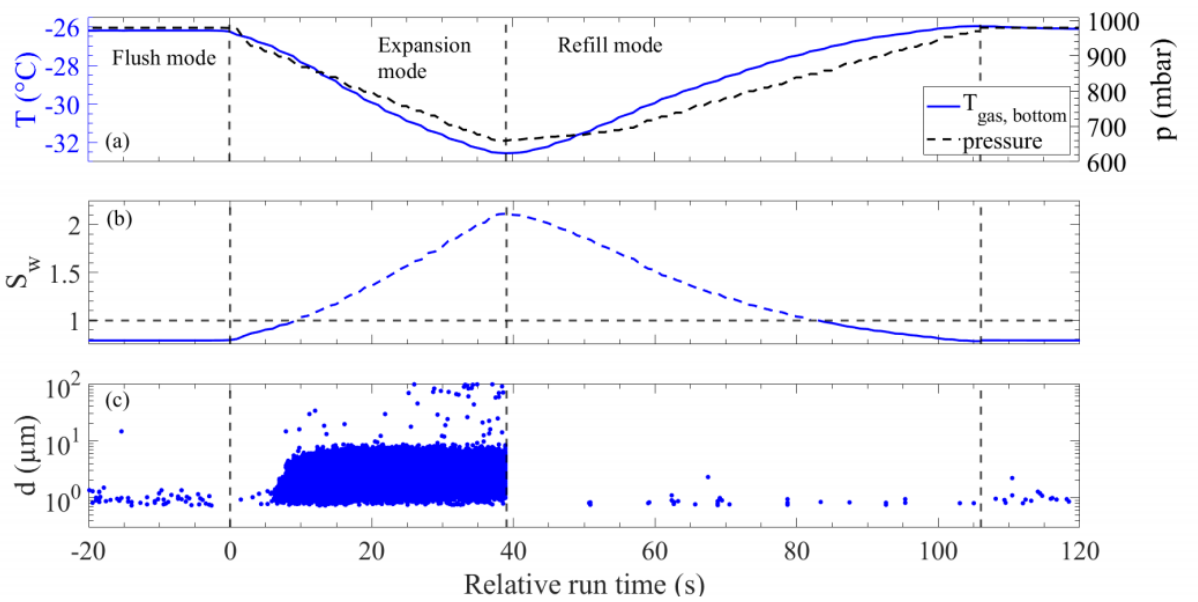

Figure 6: A typical run of PINE-1A showing both cloud droplet formation and ice formation during the cloud expansion mode. Upper panel: Temperature (T; blue line) and pressure (p; black line). Middle panel: Liquid water saturation ratio (Sw). Lower panel: Optical particle diameter (d) detected in the OPC. This panel shows each single particle detected by the OPC plotted as a single blue dot at the time of occurrence and with its measured optical diameter.

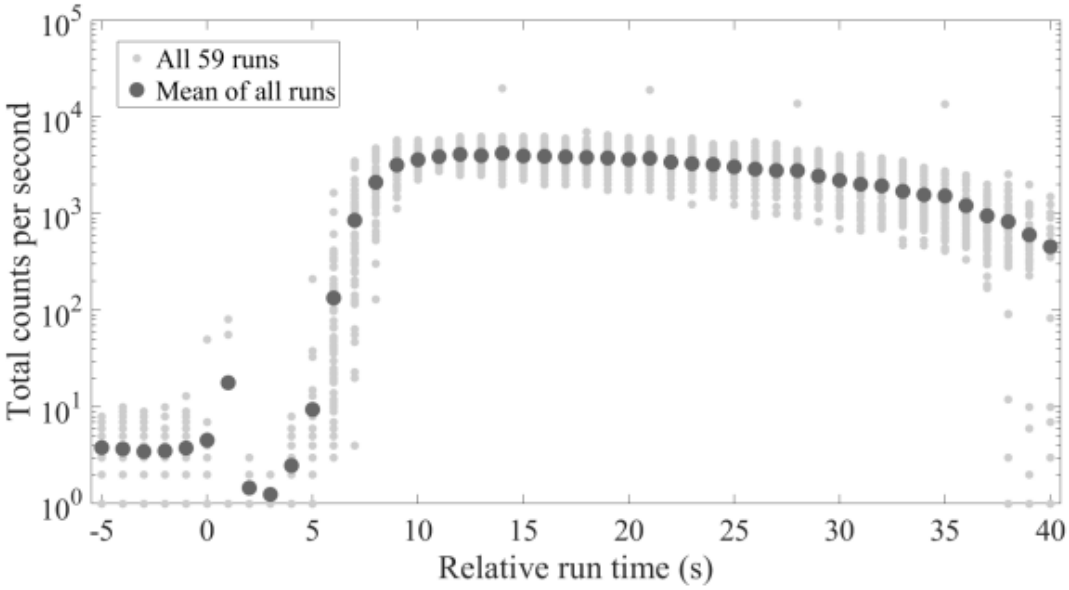

Figure 7: Total number counts measured with PINE-1A in 1 sec time intervals of 59 consecutive runs during the HyICE field campaign (operation 64 on 25th March 2018). The measured count rates are plotted as a function of time relative to the start of expansion. The small grey dots in this figure show the OPC count rates of individual runs, the bigger black circle the mean over all 59 runs of this operation. The sharp increase after about 6 s of expansion is due to CCN activation of the aerosol particles in the chamber and the growth of droplets.

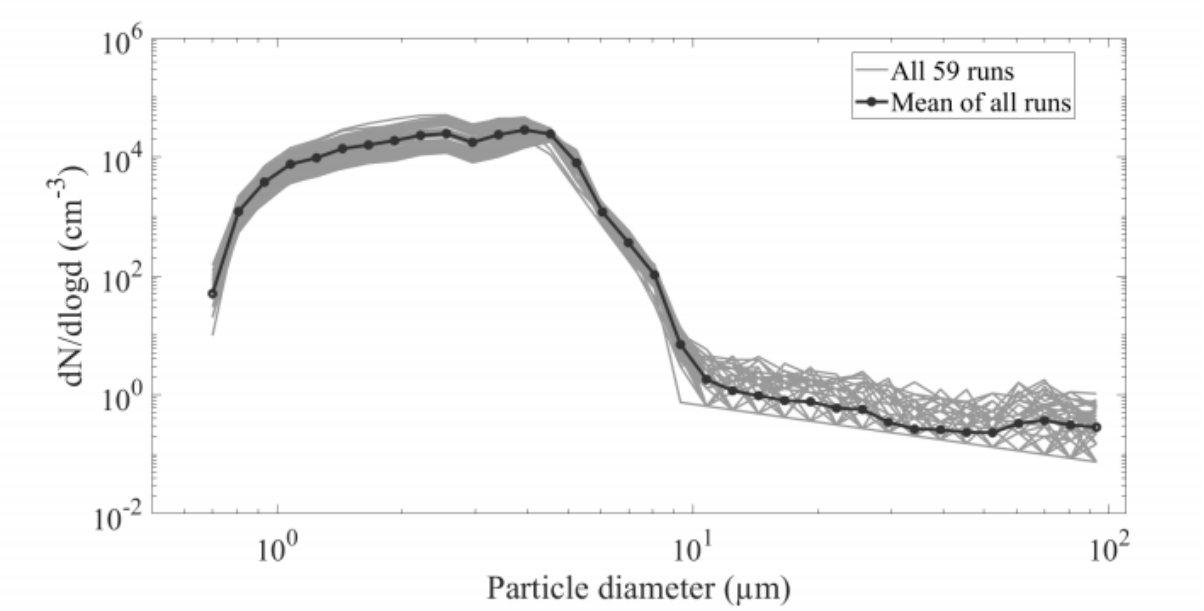

Figure 8: Particle size distribution for the same series of runs shown in Figure 7.

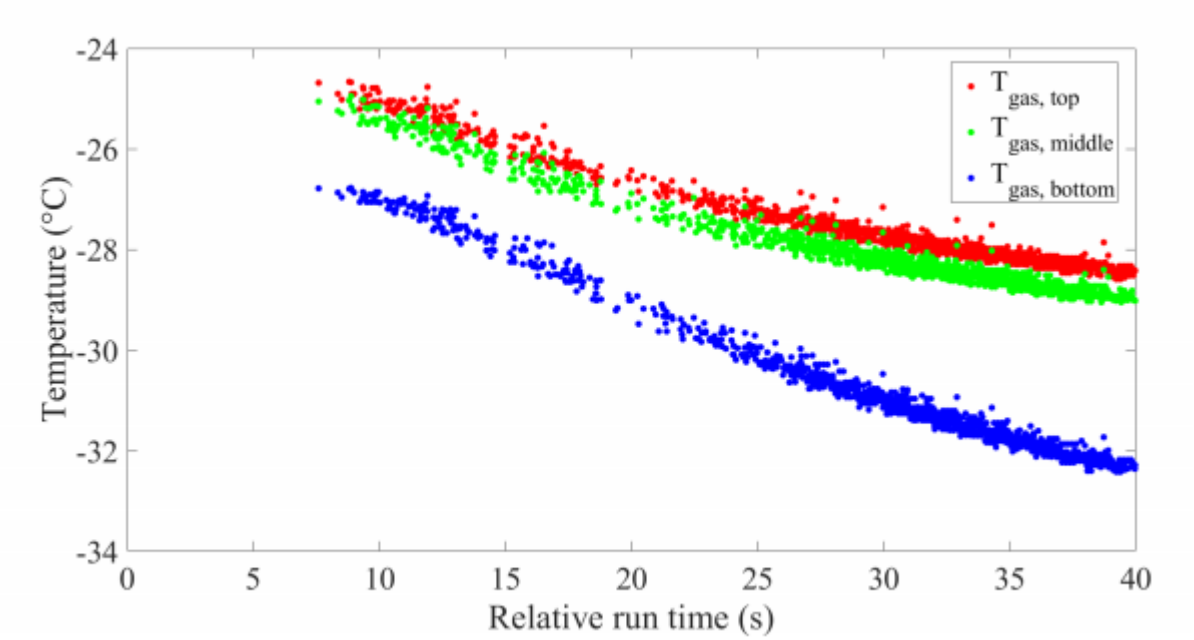

Figure 9: All single ice crystals measured with PINE-1A during the same operation of 59 runs shown in Figures 7 and 8. The ice crystals are plotted for the relative time after start of the run they were measured, and the respective gas temperature measured with three sensors located in the lower (blue), the middle (green) and the upper (red) part of the chamber.

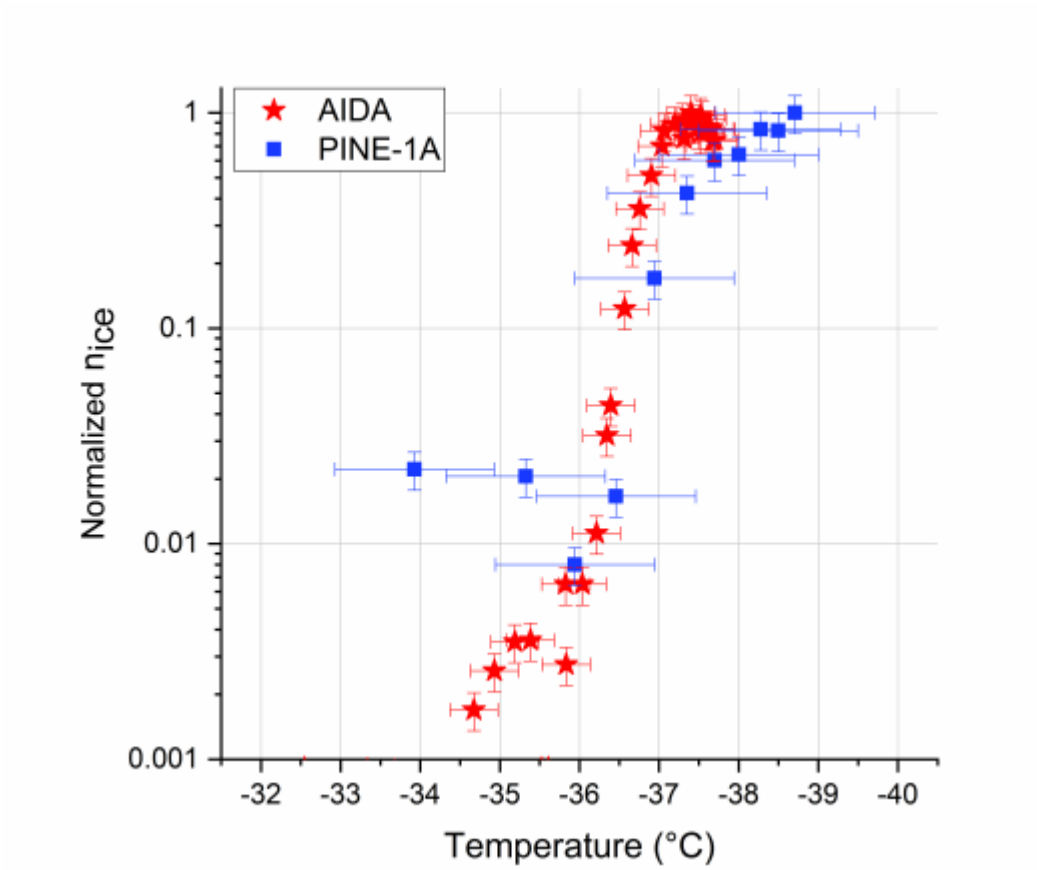

Figure 10: Homogeneous freezing of supercooled water droplets measured with PINE-1A and with AIDA during a PINE characterisation campaign in December 2018. For this measurement, the PINE-1A was equipped with a Welas 2500 OPC and sampled sulphuric acid aerosol directly from the AIDA chamber. PINE-1A was operated at a wall temperature of about −32.5°C, the expansion run was done with a flow rate of 5 L min^{-1}, and reached a minimum gas temperature of −39°C. The AIDA expansion was started at a temperature of about -31°C and reached a minimum temperature of about −38°C.

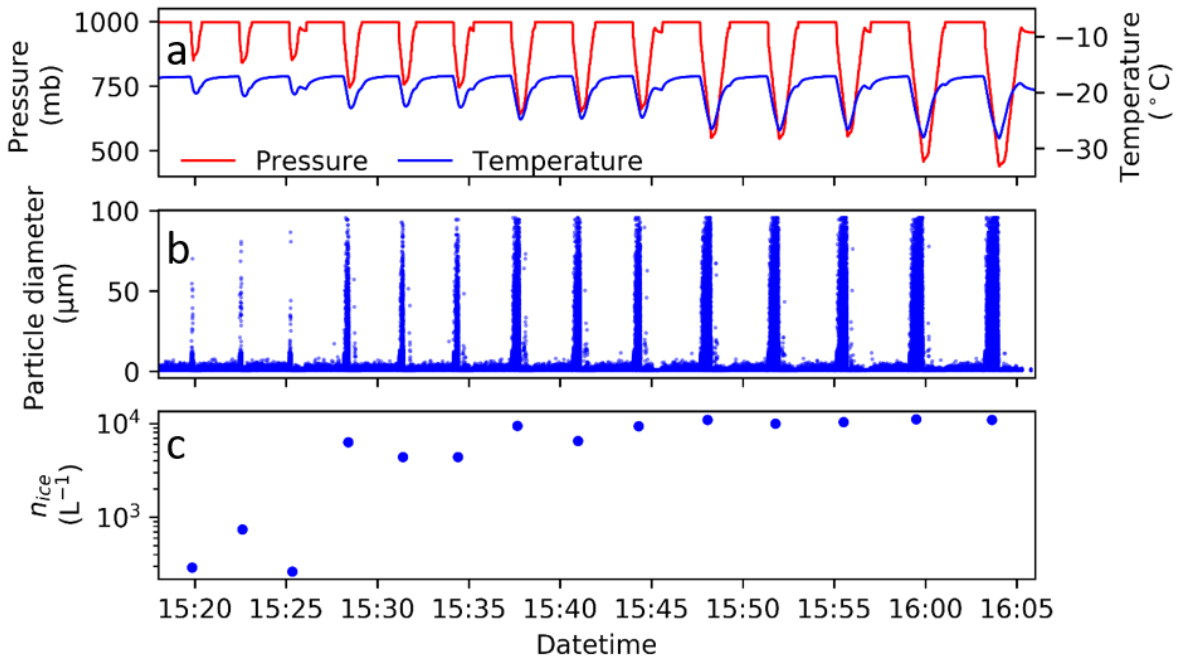

Figure 11: Repeated runs of PINE-1A sampling ATD aerosol from the AIDA cloud chamber during the EXTRA18 laboratory test campaign in preparation of the HyICE field campaign. The runs were started at the same temperature of about −18°C (blue line), but the minimum expansion pressure (red line) and by that also the minimum gas temperature in the PINE cloud chamber was stepwise changed every 5th run (upper panel). Therefore, the number of ice crystals formed by immersion freezing also stepwise increased, as shown in the single particle plot from the Welas 2500 OPC data (middle panel) and the ice crystal concentration measured at the end of each expansion (lower panel).

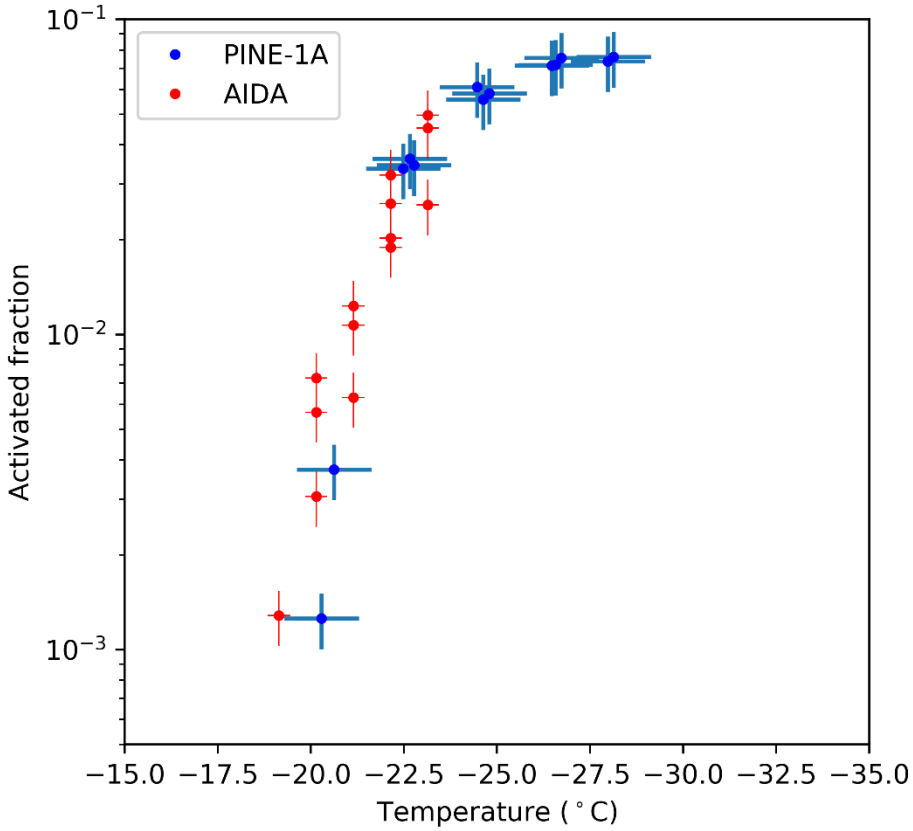

Figure 12: Ice-active particle fraction f_{ice} measured with PINE-1A for ATD as a function of temperature (see also Figure 11), in comparison to f_{ice} measured in an AIDA cloud expansion experiment with the same aerosol, right after the PINE-1A runs were finished.

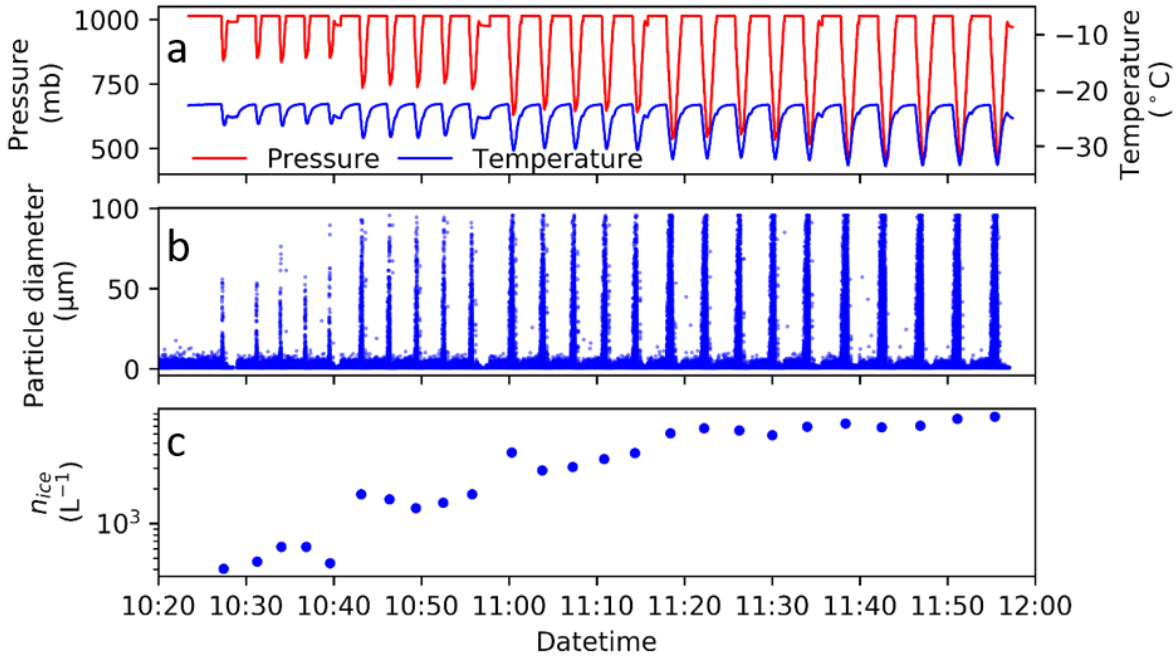

Figure 13: Same plot as shown in Figure 11, but with PINE-1A sampling illite NX aerosol from the AIDA cloud chamber, and with a lower start temperature of about -22°C (see upper panel, blue line). As for ATD runs, the minimum expansion pressure (red line) and by that also the minimum gas temperature in the PINE cloud chamber was stepwise changed every 5th run (upper panel). Therefore, the number of ice crystals formed by immersion freezing also stepwise increased, as shown in the single particle plot from the Welas OPC data (middle panel) and the ice crystal concentration measured at the end of each expansion (lower panel).

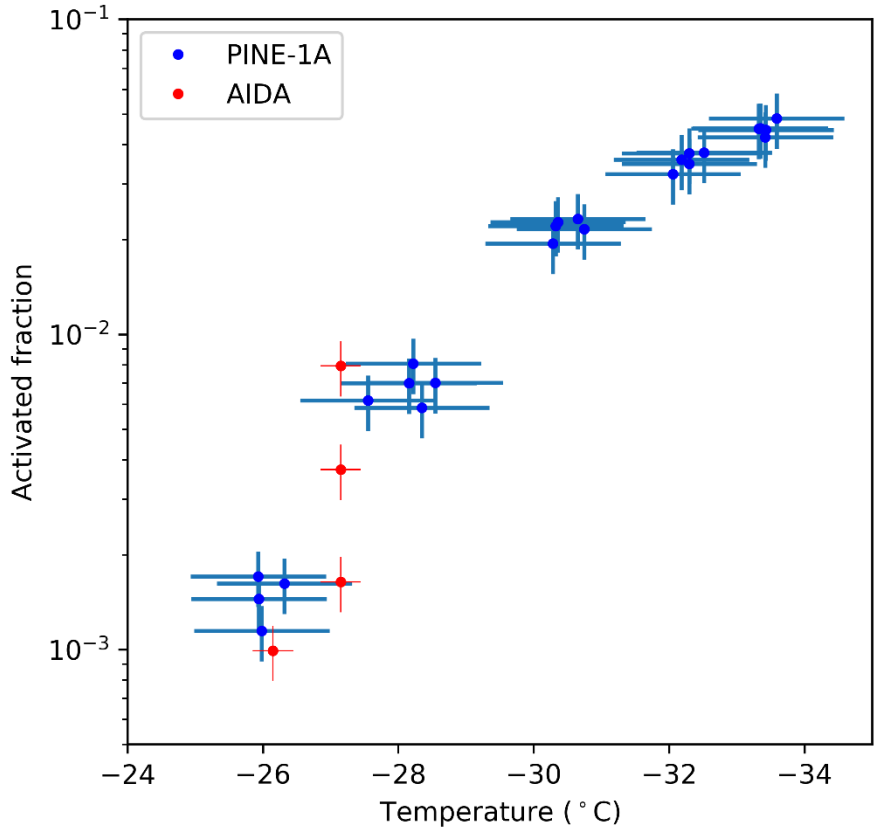

Figure 14: Ice-active particle fraction f_{ice} measured with PINE-1A (blue dots) for illite NX as a function of temperature (see also Fig. 13), in comparison to f_{ice} measured in an AIDA (red dots) cloud expansion experiment with the same aerosol, right after the PINE-1A runs were finished.

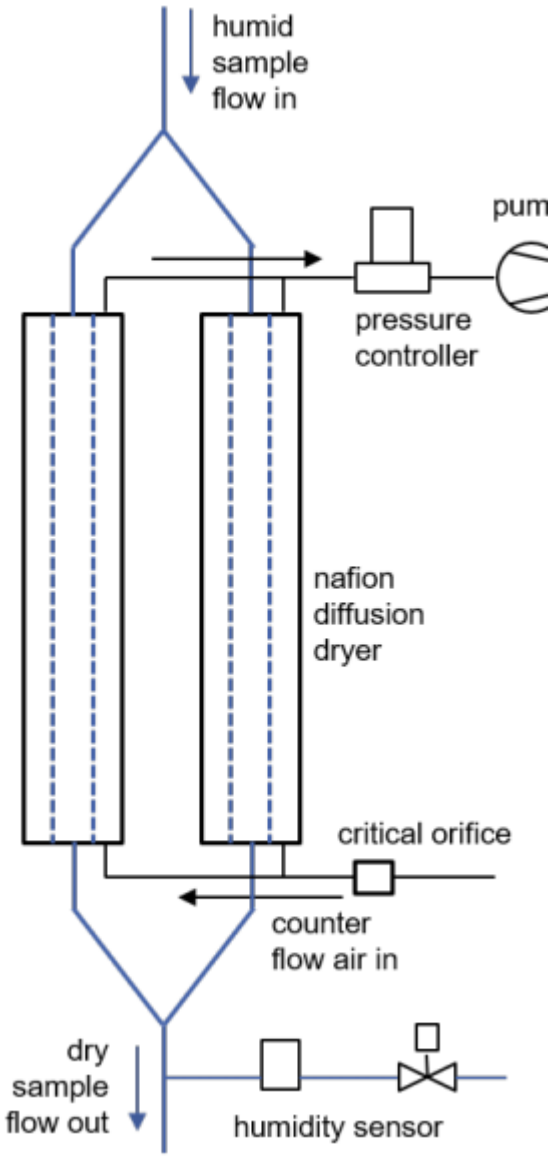

Figure 15: Schematic setup of the dual Nafion dryer setup as part of the PINE inlet system.

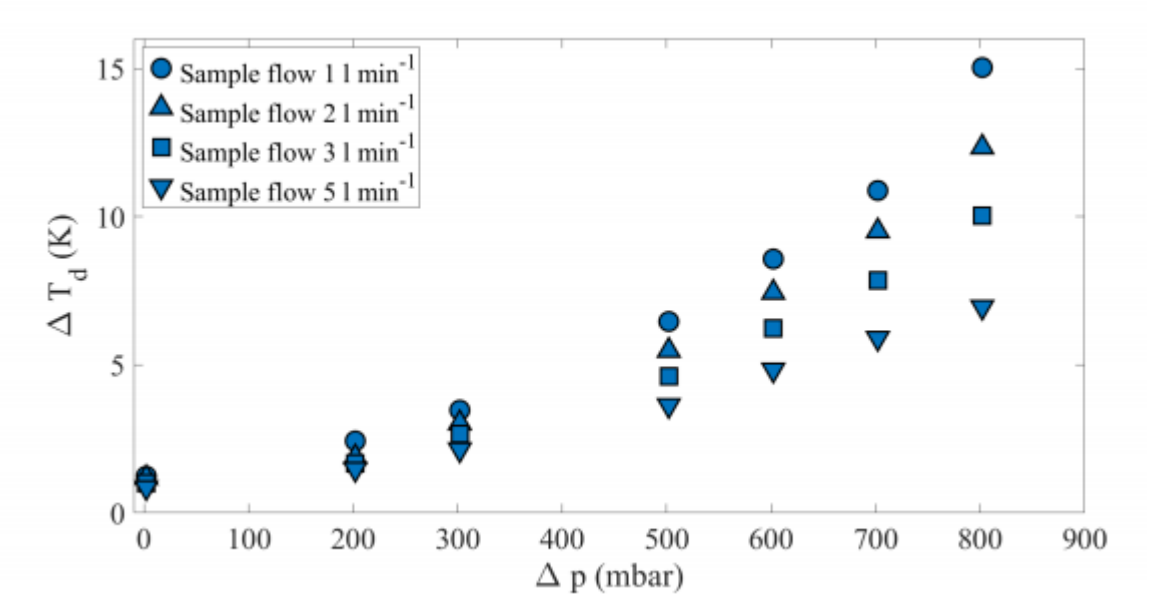

Figure 16: Drying efficiency of one Nafion diffusion dryer, plotted as the difference ΔTd of the dew point temperatures measured in the sample air before and after the Nafion tube. The drying efficiency is increasing with the pressure difference Δp between the sample air and the counter flow air, and decreasing with the sample flow.

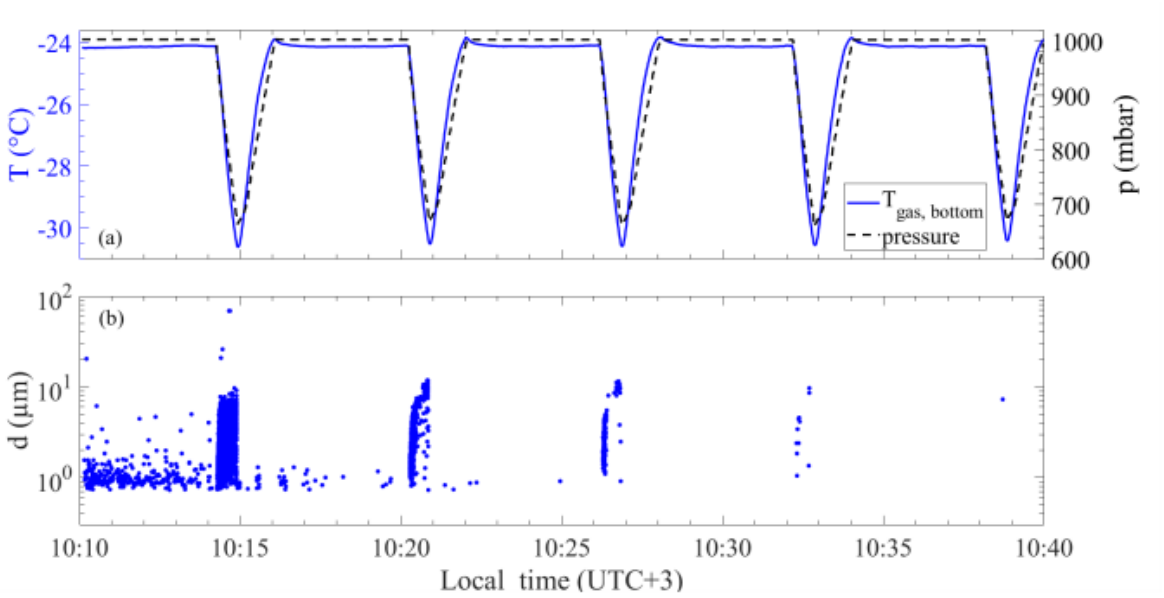

Figure 17: Background test run showing that after 4 consecutive expansion runs the total particle count is almost zero (only one droplet count detected in expansion no. 5).

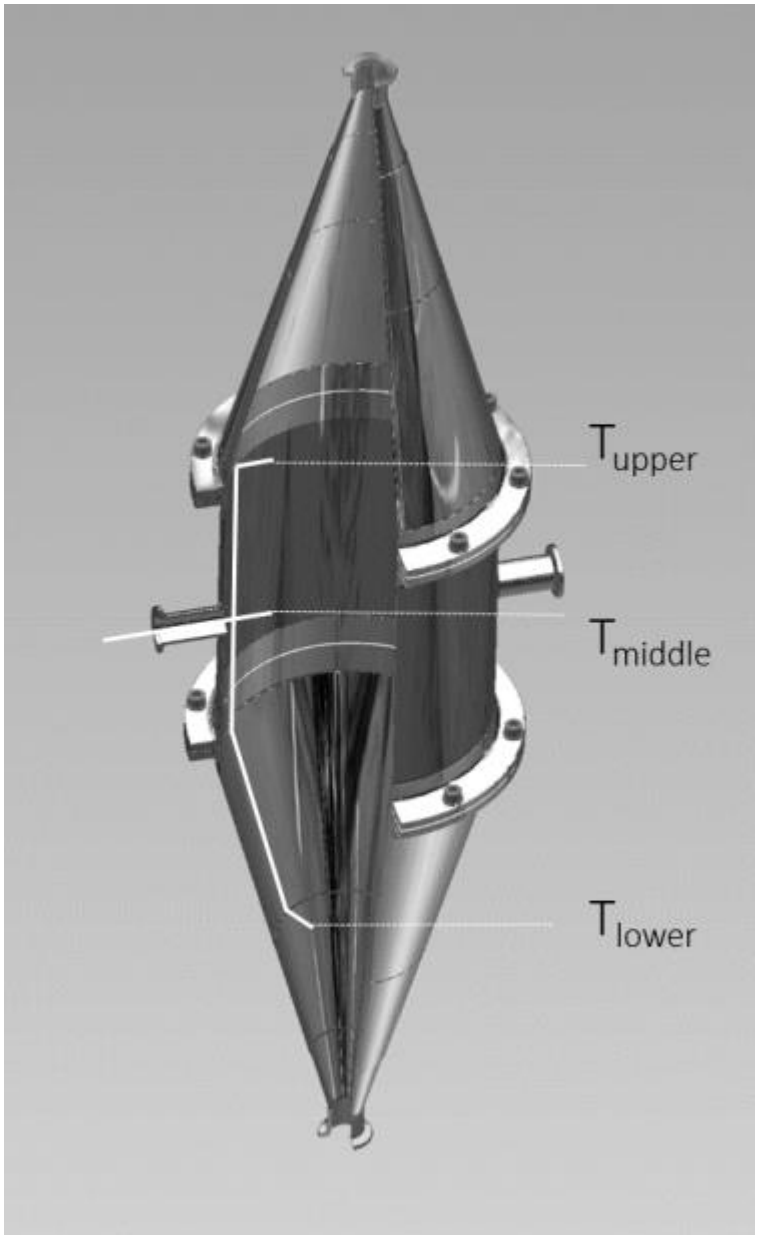

Figure 18: Construction of the PINE-1A stainless steel cloud chamber, without cooling and thermal insulation. The white lines indicate the location of the three thermocouples measuring the gas temperature inside the cloud chamber.

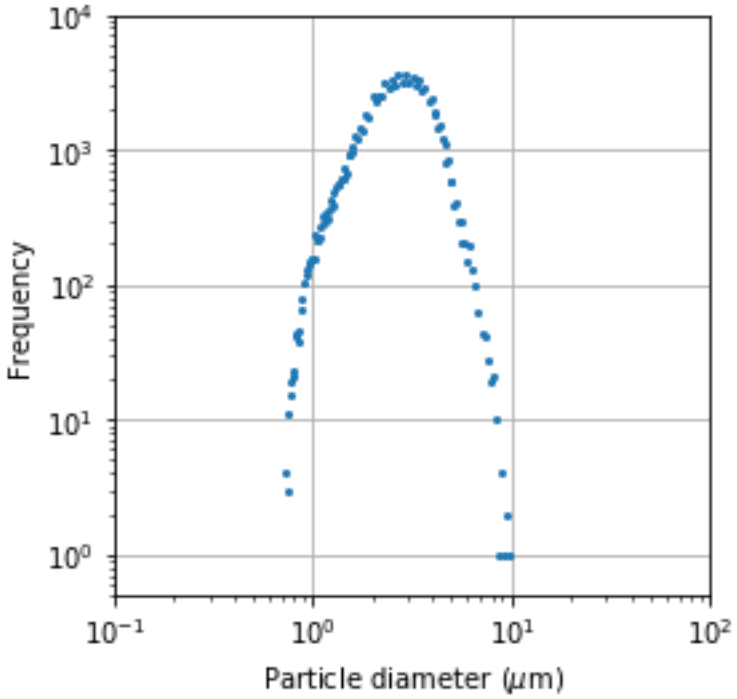

Figure 19: Size distribution of activated droplets measured with PINE-1A at high temperature conditions where no active INPs were present.

2.8 References

Alpert, P. A., Aller, J. Y., & Knopf, D. A. (2011). Ice nucleation from aqueous NaCl droplets with and without marine diatoms. Atmospheric Chemistry and Physics, 11(12), 5539–5555. https://doi.org/10.5194/acp-11-5539-2011

Atkinson, J. D., Murray, B. J., Woodhouse, M. T., Whale, T. F., Baustian, K. J., Carslaw, K. S., et al. (2013). The importance of feldspar for ice nucleation by mineral dust in mixed-phase clouds. Nature, 498(7454), 355–358. https://doi.org/10.1038/nature12278

Barahona, D., & Nenes, A. (2009). Parameterizing the competition between homogeneous and heterogeneous freezing in cirrus cloud formation – monodisperse ice nuclei. Atmospheric Chemistry and Physics, 9(2), 369–381. https://doi.org/10.5194/acp-9-369-2009

Benz, S., Megahed, K., Möhler, O., Saathoff, H., Wagner, R., & Schurath, U. (2005). T-dependent rate measurements of homogeneous ice nucleation in cloud droplets using a large atmospheric simulation chamber. Journal of Photochemistry and Photobiology A: Chemistry, 176(1-3 SPEC. ISS.), 208–217. https://doi.org/10.1016/j.jphotochem.2005.08.026

de Boer, G., Morrison, H., Shupe, M. D., & Hildner, R. (2011). Evidence of liquid dependent ice nucleation in high-latitude stratiform clouds from surface remote sensors. Geophysical Research Letters, 38(1), n/a-n/a. https://doi.org/10.1029/2010GL046016

Boose, Y., Welti, A., Atkinson, J., Ramelli, F., Danielczok, A., Bingemer, H. G., et al. (2016). Heterogeneous ice nucleation on dust particles sourced from nine deserts worldwide - Part 1: Immersion freezing. Atmospheric Chemistry and Physics, 16(23), 15075–15095. https://doi.org/10.5194/acp-16-15075-2016

Boose, Y., Kanji, Z. A., Kohn, M., Sierau, B., Zipori, A., Crawford, I., et al. (2016). Ice nucleating particle measurements at 241K during winter months at 3580m MSL in the swiss alps. Journal of the Atmospheric Sciences, 73(5), 2203–2228. https://doi.org/10.1175/JAS-D-15-0236.1

Boose, Y., Sierau, B., García, M. I., Rodríguez, S., Alastuey, A., Linke, C., et al. (2016). Ice nucleating particles in the Saharan Air Layer. Atmospheric Chemistry and Physics, 16(14), 9067–9087. https://doi.org/10.5194/acp-16-9067-2016

Boucher, O., Randall, D., Artaxo, P., Bretherton, C., Feingold, G., Forster, P., et al. (2013). Clouds and Aerosols. In: Climate Change 2013: The Physical Science Basis. Contribution of Working Group I to the Fifth Assessment Report of the Intergovernmental Panel on Climate Change Coordinating Lead Authors: Lead Authors.

Brier, G. W., & Kline, D. B. (1959). Ocean water as a source of ice nuclei. Science, 130(3377), 717–718. https://doi.org/10.1126/science.130.3377.717

Burrows, S. M., Hoose, C., Pöschl, U., & Lawrence, M. G. (2013). Ice nuclei in marine air: Biogenic particles or dust? Atmospheric Chemistry and Physics, 13(1), 245–267. https://doi.org/10.5194/acp-13-245-2013

Campbell, J. R., & Shiobara, M. (2008). Glaciation of a mixed-phase boundary layer cloud at a coastal arctic site as depicted in continuous lidar measurements. Polar Science, 2(2), 121–127. https://doi.org/10.1016/j.polar.2008.04.004

Conen, F., Rodríguez, S., Hülin, C., Henne, S., Herrmann, E., Bukowiecki, N., & Alewell, C. (2015). Atmospheric ice nuclei at the high-altitude observatory Jungfraujoch, Switzerland. Tellus B: Chemical and Physical Meteorology, 67(1), 25014. https://doi.org/10.3402/tellusb.v67.25014

Connolly, P. J., Möhler, O., Field, P. R., Saathoff, H., Burgess, R., Choularton, T., & Gallagher, M. (2009). Studies of heterogeneous freezing by three different desert dust samples. Atmos. Chem. Phys. Atmospheric Chemistry and Physics, 9, 2805–2824. Retrieved from www.atmos-chem-phys.net/9/2805/2009/

Creamean, J. M., Suski, K. J., Rosenfeld, D., Cazorla, A., DeMott, P. J., Sullivan, R. C., et al. (2013). Dust and biological aerosols from the Sahara and Asia influence precipitation in the Western U.S. Science, 340(6127), 1572–1578. https://doi.org/10.1126/science.1227279

Demott, P. J. ;, Möhler, O. ;, Cziczo, D. J. ;, Hiranuma, N. ;, Petters, M. D. ;, Petters, S. S. ;, et al. (2018). The Fifth InternationalWorkshop on Ice Nucleation phase 2 (FIN-02): laboratory intercomparison of ice nucleation measurements ETH Library. Atmospheric Measurement Techniques, 11(11). https://doi.org/10.3929/ethz-b-000306690

DeMott, P. J., Cziczo, D. J., Prenni, A. J., Murphy, D. M., Kreidenweis, S. M., Thomson, D. S., et al. (2003). Measurements of the concentration and composition of nuclei for cirrus formation. Proceedings of the National Academy of Sciences of the United States of America, 100(25), 14655–14660. https://doi.org/10.1073/pnas.2532677100

DeMott, P. J., Prenni, A. J., Liu, X., Kreidenweis, S. M., Petters, M. D., Twohy, C. H., et al. (2010). Predicting global atmospheric ice nuclei distributions and their impacts on climate. Proceedings of the National Academy of Sciences of the United States of America, 107(25), 11217–11222. https://doi.org/10.1073/pnas.0910818107

DeMott, Paul J., Sassen, K., Poellot, M. R., Baumgardner, D., Rogers, D. C., Brooks, S. D., et al. (2003). African dust aerosols as atmospheric ice nuclei. Geophysical Research Letters, 30(14). https://doi.org/10.1029/2003GL017410

DeMott, Paul J., Möhler, O., Stetzer, O., Vali, G., Levin, Z., Petters, M. D., et al. (2011). Resurgence in ice nuclei measurement research. Bulletin of the American Meteorological Society, 92(12), 1623–1635. https://doi.org/10.1175/2011BAMS3119.1

DeMott, Paul J., Hill, T. C. J., McCluskey, C. S., Prather, K. A., Collins, D. B., Sullivan, R. C., et al. (2015). Sea spray aerosol as a unique source of ice nucleating particles. Proceedings of the National Academy of Sciences of the United States of America, 113(21), 5797–5803. https://doi.org/10.1073/pnas.1514034112

Desai, N., Chandrakar, K. K., Kinney, G., Cantrell, W., & Shaw, R. A. (2019). Aerosol-Mediated Glaciation of Mixed-Phase Clouds: Steady-State Laboratory Measurements. Geophysical Research Letters, 46(15), 9154–9162. https://doi.org/10.1029/2019GL083503

Després, V. R., Alex Huffman, J., Burrows, S. M., Hoose, C., Safatov, A. S., Buryak, G., et al. (2012). Primary biological aerosol particles in the atmosphere: A review. Tellus, Series B: Chemical and Physical Meteorology, 64(1). https://doi.org/10.3402/tellusb.v64i0.15598

Eidhammer, T., DeMott, P. J., Prenni, A. J., Petters, M. D., Twohy, C. H., Rogers, D. C., et al. (2010). Ice initiation by aerosol particles: Measured and predicted ice nuclei concentrations versus measured ice crystal concentrations in an orographic wave cloud. Journal of the Atmospheric Sciences, 67(8), 2417–2436. https://doi.org/10.1175/2010JAS3266.1

Fan, J., Leung, L. R., Rosenfeld, D., & DeMott, P. J. (2017). Effects of cloud condensation nuclei and ice nucleating particles on precipitation processes and supercooled liquid in mixed-phase orographic clouds. Atmospheric Chemistry and Physics, 17(2), 1017–1035. https://doi.org/10.5194/acp-17-1017-2017

Field, P. R., & Heymsfield, A. J. (2015). Importance of snow to global precipitation. Geophysical Research Letters, 42(21), 9512–9520. https://doi.org/10.1002/2015GL065497

Field, P. R., Heymsfield, A. J., Shipway, B. J., Demott, P. J., Pratt, K. A., Rogers, D. C., et al. (2012). Ice in clouds experiment-layer clouds. Part II: Testing characteristics of heterogeneous ice formation in lee wave clouds. Journal of the Atmospheric Sciences, 69(3), 1066–1079. https://doi.org/10.1175/JAS-D-11-026.1

Field, P. R., Lawson, R. P., Brown, P. R. A., Lloyd, G., Westbrook, C., Moisseev, D., et al. (2016). Chapter 7. Secondary Ice Production - current state of the science and recommendations for

the future. Meteorological Monographs, 58, 7.1-7.20. https://doi.org/10.1175/amsmonographs-d-16-0014.1

Hande, L. B., & Hoose, C. (2017). Partitioning the primary ice formation modes in large eddy simulations of mixed-phase clouds. Atmospheric Chemistry and Physics, 17(22), 14105–14118. https://doi.org/10.5194/acp-17-14105-2017

Harrison, A. D., Lever, K., Sanchez-Marroquin, A., Holden, M. A., Whale, T. F., Tarn, M. D., et al. (2019). The ice-nucleating ability of quartz immersed in water and its atmospheric importance compared to K-feldspar. Atmospheric Chemistry and Physics, 19(17), 11343–11361. https://doi.org/10.5194/acp-19-11343-2019

Heymsfield, A. J., Krämer, M., Luebke, A., Brown, P., Cziczo, D. J., Franklin, C., et al. (2017). Cirrus Clouds. Meteorological Monographs, 58, 2.1-2.26. https://doi.org/10.1175/amsmonographs-d-16-0010.1

Hiranuma, N., Augustin-Bauditz, S., Bingemer, H., Budke, C., Curtius, J., Danielczok, A., et al. (2015). A comprehensive laboratory study on the immersion freezing behavior of illite NX particles: a comparison of 17 ice nucleation measurement techniques. Atmospheric Chemistry and Physics, 15(5), 2489–2518. https://doi.org/10.5194/acp-15-2489-2015

Holden, M. A., Whale, T. F., Tarn, M. D., O'Sullivan, D., Walshaw, R. D., Murray, B. J., et al. (2019). High-speed imaging of ice nucleation in water proves the existence of active sites. Science Advances, 5(2). https://doi.org/10.1126/sciadv.aav4316

Hoose, C., & Möhler, O. (2012). Heterogeneous ice nucleation on atmospheric aerosols: a review of results from laboratory experiments. Atmospheric Chemistry and Physics, 12(20), 9817–9854. https://doi.org/10.5194/acp-12-9817-2012

Hoose, C., Kristjánsson, J. E., & Burrows, S. M. (2010). How important is biological ice nucleation in clouds on a global scale? Environmental Research Letters, 5(2). https://doi.org/10.1088/1748-9326/5/2/024009

Hummel, M., Hoose, C., Pummer, B., Schaupp, C., Fröhlich-Nowoisky, J., & Möhler, O. (2018). Simulating the influence of primary biological aerosol particles on clouds by heterogeneous ice nucleation. Atmospheric Chemistry and Physics, 18(20), 15437–15450. https://doi.org/10.5194/acp-18-15437-2018

Kanji, Z. A., Ladino, L. A., Wex, H., Boose, Y., Burkert-Kohn, M., Cziczo, D. J., et al. (2017). Overview of Ice Nucleating Particles. Meteorological Monographs, 58, 1.1-1.33. https://doi.org/10.1175/amsmonographs-d-16-0006.1

Kärcher, B., & Lohmann, U. (2002). A Parameterization of cirrus cloud formation: Homogeneous freezing including effects of aerosol size. Journal of Geophysical Research Atmospheres, 107(23), AAC 9-1-AAC 9-10. https://doi.org/10.1029/2001JD001429

Kärcher, B., & Lohmann, U. (2003). A parameterization of cirrus cloud formation: Heterogeneous freezing. Journal of Geophysical Research: Atmospheres, 108(14). https://doi.org/10.1029/2002jd003220

Koop, T., Luo, B., Tsias, A., & Peter, T. (2000). Water activity as the determinant for homogeneous ice nucleation in aqueous solutions. Nature, 406(6796), 611–614. https://doi.org/10.1038/35020537

Korolev, A., McFarquhar, G., Field, P. R., Franklin, C., Lawson, P., Wang, Z., et al. (2017). Mixed-Phase Clouds: Progress and Challenges. Meteorological Monographs, 58, 5.1-5.50. https://doi.org/10.1175/amsmonographs-d-17-0001.1

Krämer, M., Rolf, C., Luebke, A., Afchine, A., Spelten, N., Costa, A., et al. (2016). A microphysics guide to cirrus clouds – Part 1: Cirrus types. Atmospheric Chemistry and Physics, 16(5), 3463–3483. https://doi.org/10.5194/acp-16-3463-2016

Lacher, L., Lohmann, U., Boose, Y., Zipori, A., Herrmann, E., Bukowiecki, N., et al. (2017). The Horizontal Ice Nucleation Chamber (HINC): INP measurements at conditions relevant for mixed-phase clouds at the High Altitude Research Station Jungfraujoch. Atmospheric Chemistry and Physics, 17(24), 15199–15224. https://doi.org/10.5194/acp-17-15199-2017

Lacher, L., DeMott, P. J., Levin, E. J. T., Suski, K. J., Boose, Y., Zipori, A., et al. (2018). Background Free-Tropospheric Ice Nucleating Particle Concentrations at Mixed-Phase Cloud Conditions. Journal of Geophysical Research: Atmospheres, 123(18), 10,506-10,525. https://doi.org/10.1029/2018JD028338

Lacher, L., Steinbacher, M., Bukowiecki, N., Herrmann, E., Zipori, A., & Kanji, Z. (2018). Impact of Air Mass Conditions and Aerosol Properties on Ice Nucleating Particle Concentrations at the High Altitude Research Station Jungfraujoch. Atmosphere, 9(9), 363. https://doi.org/10.3390/atmos9090363

Lohmann, U. (2017). Anthropogenic Aerosol Influences on Mixed-Phase Clouds. Curr Clim Change Rep, 3, 32–44. https://doi.org/10.1007/s40641-017-0059-9

Mason, R. H., Si, M., Li, J., Chou, C., Dickie, R., Toom-Sauntry, D., et al. (2015). Ice nucleating particles at a coastal marine boundary layer site: Correlations with aerosol type and meteorological conditions. Atmospheric Chemistry and Physics, 15(21), 12547–12566. https://doi.org/10.5194/acp-15-12547-2015

Mason, R. H., Chou, C., McCluskey, C. S., Levin, E. J. T., Schiller, C. L., Hill, T. C. J., et al. (2015). The micro-orifice uniform deposit impactor–droplet freezing technique (MOUDI-DFT) for measuring concentrations of ice nucleating particles as a function of size: improvements and initial validation. Atmospheric Measurement Techniques, 8(6), 2449–2462. https://doi.org/10.5194/amt-8-2449-2015

McCluskey, C. S., Ovadnevaite, J., Rinaldi, M., Atkinson, J., Belosi, F., Ceburnis, D., et al. (2018). Marine and Terrestrial Organic Ice-Nucleating Particles in Pristine Marine to Continentally Influenced Northeast Atlantic Air Masses. Journal of Geophysical Research: Atmospheres, 123(11), 6196–6212. https://doi.org/10.1029/2017JD028033

Möhler, O., Stetzer, O., Schaefers, S., Linke, C., Schnaiter, M., Tiede, R., et al. (2003). Experimental investigation of homogeneous freezing of sulphuric acid particles in the aerosol chamber AIDA. Atmospheric Chemistry and Physics, 3(1), 211–223. https://doi.org/10.5194/acp-3-211-2003

Möhler, O., Büttner, S., Linke, C., Schnaiter, M., Saathoff, H., Stetzer, O., et al. (2005). Effect of sulfuric acid coating on heterogeneous ice nucleation by soot aerosol particles. Journal of Geophysical Research, 110(D11), D11210. https://doi.org/10.1029/2004JD005169

Möhler, O., Field, P. R., Connolly, P., Benz, S., Saathoff, H., Schnaiter, M., et al. (2006). Efficiency of the deposition mode ice nucleation on mineral dust particles. Atmospheric Chemistry and Physics, 6(10), 3007–3021. https://doi.org/10.5194/acp-6-3007-2006

Möhler, O., Benz, S., Saathoff, H., Schnaiter, M., Wagner, R., Schneider, J., et al. (2008). The effect of organic coating on the heterogeneous ice nucleation efficiency of mineral dust aerosols. Environmental Research Letters, 3(2), 025007. https://doi.org/10.1088/1748-9326/3/2/025007

Mülmenstädt, J., Sourdeval, O., Delanoë, J., & Quaas, J. (2015). Frequency of occurrence of rain from liquid-, mixed-, and ice-phase clouds derived from A-Train satellite retrievals. Geophysical Research Letters, 42(15), 6502–6509. https://doi.org/10.1002/2015GL064604

Murray, B. J., O'Sullivan, D., Atkinson, J. D., & Webb, M. E. (2012). Ice nucleation by particles immersed in supercooled cloud droplets. Chemical Society Reviews, 41(19), 6519. https://doi.org/10.1039/c2cs35200a

Murray, Benjamin J., Wilson, T. W., Dobbie, S., Cui, Z., Al-Jumur, S. M. R. K., Möhler, O., et al. (2010). Heterogeneous nucleation of ice particles on glassy aerosols under cirrus conditions. Nature Geoscience, 3(4), 233–237. https://doi.org/10.1038/ngeo817

Niemand, M., Möhler, O., Vogel, B., Vogel, H., Hoose, C., Connolly, P., et al. (2012). A Particle-Surface-Area-Based Parameterization of Immersion Freezing on Desert Dust Particles. Journal of the Atmospheric Sciences, 69(10), 3077–3092. https://doi.org/10.1175/JAS-D-11-0249.1

O'Sullivan, D., Adams, M. P., Tarn, M. D., Harrison, A. D., Vergara-Temprado, J., Porter, G. C. E., et al. (2018). Contributions of biogenic material to the atmospheric ice-nucleating particle population in North Western Europe. Scientific Reports, 8(1), 13821. https://doi.org/10.1038/s41598-018-31981-7

Paukert, M., & Hoose, C. (2014). Modeling immersion freezing with aerosol-dependent prognostic ice nuclei in Arctic mixed-phase clouds. Journal of Geophysical Research, 119(14), 9073–9092. https://doi.org/10.1002/2014JD021917

Pratt, K. A., Twohy, C. H., Murphy, S. M., Moffet, R. C., Heymsfield, A. J., Gaston, C. J., et al. (2010). Observation of playa salts as nuclei in orographic wave clouds. Journal of Geophysical Research Atmospheres, 115(15). https://doi.org/10.1029/2009JD013606

Prenni, A. J., Tobo, Y., Garcia, E., DeMott, P. J., Huffman, J. A., McCluskey, C. S., et al. (2013). The impact of rain on ice nuclei populations at a forested site in Colorado. Geophysical Research Letters, 40(1), 227–231. https://doi.org/10.1029/2012GL053953

Prenni, Anthony J., Demott, P. J., Rogers, D. C., Kreidenweis, S. M., Mcfarquhar, G. M., Zhang, G., & Poellot, M. R. (2009). Ice nuclei characteristics from M-PACE and their relation to ice formation in clouds. Tellus, Series B: Chemical and Physical Meteorology, 61 B(2), 436–448. https://doi.org/10.1111/j.1600-0889.2009.00415.x

Pruppacher, H. R., & Klett, J. D. (2010). Microstructure of Atmospheric Clouds and Precipitation (pp. 10–73). https://doi.org/10.1007/978-0-306-48100-0_2

Rogers, D. C., DeMott, P. J., Kreidenweis, S. M., Chen, Y., Rogers, D. C., DeMott, P. J., et al. (2001). A Continuous-Flow Diffusion Chamber for Airborne Measurements of Ice Nuclei. Http://Dx.Doi.Org/10.1175/1520-0426(2001)018<0725:ACFDCF>2.0.CO;2.

Sanchez-Marroquin, A., Arnalds, O., Baustian-Dorsi, K. J., Browse, J., Dagsson-Waldhauserova, P., Harrison, A. D., et al. (2020). Iceland is an episodic source of atmospheric ice-nucleating particles relevant for mixed-phase clouds. Science Advances, 6(26), eaba8137. https://doi.org/10.1126/sciadv.aba8137

Sesartic, A., Lohmann, U., & Storelvmo, T. (2013). Modelling the impact of fungal spore ice nuclei on clouds and precipitation. Environmental Research Letters, 8(1), 014029. https://doi.org/10.1088/1748-9326/8/1/014029

Spracklen, D. V., & Heald, C. L. (2014). The contribution of fungal spores and bacteria to regional and global aerosol number and ice nucleation immersion freezing rates. Atmospheric Chemistry and Physics, 14(17), 9051–9059. https://doi.org/10.5194/acp-14-9051-2014

Steinke, I., Hoose, C., Möhler, O., Connolly, P., & Leisner, T. (2015). A new temperature- and humidity-dependent surface site density approach for deposition ice nucleation. Atmospheric Chemistry and Physics, 15(7), 3703–3717. https://doi.org/10.5194/acp-15-3703-2015

Tan, I., Storelvmo, T., & Zelinka, M. D. (2016). Observational constraints on mixed-phase clouds imply higher climate sensitivity. Science (New York, N.Y.), 352(6282), 224–7. https://doi.org/10.1126/science.aad5300

Tobo, Y., Prenni, A. J., Demott, P. J., Huffman, J. A., McCluskey, C. S., Tian, G., et al. (2013). Biological aerosol particles as a key determinant of ice nuclei populations in a forest

ecosystem. Journal of Geophysical Research Atmospheres, 118(17), 10100–10110. https://doi.org/10.1002/jgrd.50801

Tobo, Y., Adachi, K., DeMott, P. J., Hill, T. C. J., Hamilton, D. S., Mahowald, N. M., et al. (2019). Glacially sourced dust as a potentially significant source of ice nucleating particles. Nature Geoscience, 12(April). https://doi.org/10.1038/s41561-019-0314-x

Ullrich, R., Hoose, C., Möhler, O., Niemand, M., Wagner, R., Höhler, K., et al. (2017). A New Ice Nucleation Active Site Parameterization for Desert Dust and Soot. Journal of the Atmospheric Sciences, 74(3), 699–717. https://doi.org/10.1175/JAS-D-16-0074.1

Vali, G., DeMott, P. J., Möhler, O., & Whale, T. F. (2015). Technical Note: A proposal for ice nucleation terminology. Atmospheric Chemistry and Physics, 15(18). https://doi.org/10.5194/acp-15-10263-2015

Vergara-Temprado, J., Murray, B. J., Wilson, T. W., O'sullivan, D., Browse, J., Pringle, K. J., et al. (2017). Contribution of feldspar and marine organic aerosols to global ice nucleating particle concentrations. Atmospheric Chemistry and Physics, 17(5), 3637–3658. https://doi.org/10.5194/acp-17-3637-2017

Vergara-Temprado, J., Miltenberger, A. K., Furtado, K., Grosvenor, D. P., Shipway, B. J., Hill, A. A., et al. (2018). Strong control of Southern Ocean cloud reflectivity by ice-nucleating particles. Proceedings of the National Academy of Sciences of the United States of America, 115(11), 2687–2692. https://doi.org/10.1073/pnas.1721627115

Vergara-Temprado, J., Holden, M. A., Orton, T. R., O'Sullivan, D., Umo, N. S., Browse, J., et al. (2018). Is Black Carbon an Unimportant Ice-Nucleating Particle in Mixed-Phase Clouds? Journal of Geophysical Research: Atmospheres, 123(8), 4273–4283. https://doi.org/10.1002/2017JD027831

Wagner, R., & Möhler, O. (2013). Heterogeneous ice nucleation ability of crystalline sodium chloride dihydrate particles. Journal of Geophysical Research: Atmospheres, 118(10), 4610–4622. https://doi.org/10.1002/jgrd.50325

Waliser, D. E., Li, J. L. F., Woods, C. P., Austin, R. T., Bacmeister, J., Chern, J., et al. (2009). Cloud ice: A climate model challenge with signs and expectations of progress. Journal of Geophysical Research Atmospheres, 114(8). https://doi.org/10.1029/2008JD010015

Wex, H., Augustin-Bauditz, S., Boose, Y., Budke, C., Curtius, J., Diehl, K., et al. (2015). Intercomparing different devices for the investigation of ice nucleating particles using Snomax as test substance. Atmospheric Chemistry and Physics, 15(3), 1463–1485. https://doi.org/10.5194/acp-15-1463-2015

Wex, Heike, Huang, L., Zhang, W., Hung, H., Traversi, R., Becagli, S., et al. (2019). Annual variability of ice-nucleating particle concentrations at different Arctic locations. Atmospheric Chemistry and Physics, 19(7), 5293–5311. https://doi.org/10.5194/acp-19-5293-2019

Wilson, T. W., Ladino, L. A., Alpert, P. A., Breckels, M. N., Brooks, I. M., Browse, J., et al. (2015). A marine biogenic source of atmospheric ice-nucleating particles. Nature, 525(7568), 234–238. https://doi.org/10.1038/nature14986

Chapter 3

Measurements of ice-nucleating particle concentrations with the Portable Ice Nucleation Experiment chamber (PINE) in a Finnish Boreal forest

M.P. Adams[1, #], F. Vogel[2, #], O. Möhler[2, #], L. Lacher[2], G.C.E Porter[1], B. Bertozzi[2], K. Höhler[2], J. Kaufmann[2], T. Schorr[2], N. Umo[2], J. Nadolny[2]J. Duplissy[3], T. Petäjä[3], E.S. Thompson[4] and B.J. Murray[1]

[1]Institute of Climate and Atmospheric Science, School of Earth and Environment, University of Leeds, Leeds, United Kingdom

[2]Institute of Meteorology and Climate Research, Karlsruhe Institute of Technology, Karlsruhe, Germany

[3]Institute for Atmospheric and Earth System Research/Physics, Faculty of Science, University of Helsinki, Helsinki, Finland

[4] Department of Chemistry and Molecular Biology, Atmospheric Science, University of Gothenburg, Gothenburg, Sweden

# - Authors contributed equally to this work

Corresponding author – Michael Adams, M.P.Adams@leeds.ac.uk

Chapter 3 is based upon a manuscript in preparation. The manuscript describes PINE measurements made during the HyICE18 campaign. I planned the PINE aspect of the field campaign along with OM and BJM, and supervised the operation of PINE throughout. FV was in charge of running PINE on a day-to-day basis. GCEP assisted with development of the PINE analysis scripts. I carried out all data analysis shown in the Chapter. All authors contributed to writing the manuscript.

I led the writing of each section of this chapter, and made every Figure except Figure 20 which was kindly made by LL for a previous conference presentation. I carried out all the data analysis presented within this chapter. The methods laid out within this chapter have formed the basis for future field measurements using PINE.

Abstract

The formation of ice in clouds strongly influences their properties, but our knowledge of the global distribution of particles that trigger ice formation is poor. Part of the reason for the paucity of data for ice-nucleating particle (INP) concentrations is the lack of simple to use, automated instruments for quantifying atmospheric INP that can be operated over extended time periods. In this study, we demonstrate the utility of the Portable Ice Nucleation Experiment (PINE), an INP counter based on an expansion chamber with an optical particle system to quantify the size distribution of the cloud which forms on each expansion. We report a new dataset of expansion measurements, from which we derive INP concentrations, in the boreal forest site of Hyytiälä, Finland, between 05.03.2018 and 05.05.2018 with a time resolution of up to 6 minutes. We present a methodology for automating the analysis of the hydrometeor size distributions to determine ice particle concentrations, which are assumed equal to the INP concentration. Measurements of the INP concentration made by PINE are compared to those made by other INP measurements in the same location at concurrent times, demonstrating its consistency with established measurement techniques. The high time resolution dataset allows us to capture the variability of INP and aerosol concentrations on a short (≈ 5 minute) timescale. At –32 °C, INP concentrations vary by over two orders of

magnitude on the scale of hours, whilst total aerosol concentration appears to be decoupled from INP concentration. We present several case studies where the INP concentration changes as air mass changes, illustrating the benefit of having high time resolution measurements.

3.1 Introduction

Clouds interact strongly with incoming and outgoing solar radiation, thus changes in cloud properties with a changing climate and changing aerosol emissions can cause a climate feedback (Boucher et al., 2013; Matus & L'Ecuyer, 2017). Clouds in the temperature range where water can persist in a supercooled state are susceptible to the formation of ice (Hoose & Möhler, 2012; Kanji et al., 2017a; B. J. Murray et al., 2012). These clouds are thought to represent a significant uncertainty in climate projections since the amount of ice in these clouds and their response to a changing climate is highly uncertain (B J Murray, Carslaw, & Field, 2020; Storelvmo, 2017; Tan et al., 2016). Hence, we need to improve our understanding of the population of aerosol particles which trigger ice formation under conditions pertinent to mixed phase clouds.

INPs trigger the heterogeneous nucleation of ice in supercooled liquid cloud droplets, that can otherwise supercool down to below ~-33 °C before freezing homogenously (Herbert et al., 2015; Pruppacher & Klett, 2010). This process has demonstrable relevance in the atmosphere; Choi et al. (2010) showed that over the course of a year at an ambient temperature of −20 °C, about 50% of the total cloud population was supercooled, thus the remaining 50% were to some extent glaciated. As −20 °C is substantially warmer than the temperature at which homogenous freezing would be expect to become important in supercooled cloud droplet (Herbert et al., 2015), it can be inferred that atmospheric ice nucleation plays a role in determining the phase of these clouds. Complexity is added to the picture by the further observation that this supercooled cloud fraction varies both spatially and temporally for different regions and at different times of year (Kanitz et al., 2011; Storelvmo, Tan, & Korolev, 2015).

The predictive capacity of global climate models is dependent on accurately representing cloud phase, and therefore is tied to our ability to accurately predict ice-nucleating particle concentrations in the atmosphere, including their variability both spatially and temporally. As there is presently no robust theoretical approach for determining what makes an aerosol particle a good ice nucleator, we must rely on empirical measurements to determine what aerosol particles in the atmosphere serve as INPs. There is a body of literature reporting INP concentrations, but the majority of this data is for single locations over relatively short periods of time (weeks- few months), or has poor time resolution. Hence, we lack an understanding of how INP concentrations vary with time and location for much of the globe. This limits our ability to define INP sources and to define the impact of INP on clouds and their impact on climate.

There are several well-established sources of INPs discussed in the literature, such as (but not limited to) mineral dust from both desert dust (Atkinson et al., 2013; Boose et al., 2016; DeMott et al., 2003) and from high-latitude sources (A. Sanchez-Marroquin et al., 2020; Tobo et al., 2019), marine organics/sea spray aerosol (Paul J DeMott et al., 2016; Irish et al., 2017, 2019; T. W. Wilson et al., 2015), volcanic ash (Jahn et al., 2019; Mangan et al., 2017; Maters et al., 2019; Steinke et al., 2011) and anthropogenic emissions (Bi et al. 2019; McCluskey et al. 2014; Korhonen et al. 2020; Chapter 4). In addition, there is potential for terrestrial biological aerosols to serve as INPs (Tom C J Hill et al., 2016; O'Sullivan et al., 2018; Tobo et al., 2013), however there is not a clear picture of how important they may be as a source on both a regional and global scale (Hoose et al., 2010; Spracklen and Heald 2014; Phillips et al.

2009; Sesartic, Lohmann, and Storelvmo 2013). More field measurements are required in a range of environments to understand what role different species of aerosol may play in atmospheric ice nucleation.

In order to address the gap in instrumentation capability to measure INP on an autonomous basis we have developed an instrument capable of making long-term, automated measurements of INP concentrations with a high time resolution; the Portable Ice Nucleation Experiment (PINE) chamber. A technical description of PINE can be found in Möhler et al., (2020) (referred to as PINE-1A), whilst in this study we focus on describing aspects related to field operation. In order to both test PINE in a field environment and also demonstrate its utility for making multi-month measurements of INP concentrations with high time resolution we made use of the well-established Hyytiälä forestry research station in Southern Finland. The station has been making operating since 1995, making numerous atmospheric, aerosol and ecological measurements (among others), and is notable for its new particle formation events (M. Kulmala et al., 2001).

The HyICE18 campaign was started in February 2018 and continuing until June 2018, a collaboration between 13 universities and institutions across 5 countries, with the aim of making the first ice nucleation measurements at the Hyytiälä research station. The forest is a known source of bio aerosols (Spracklen, Bonn, and Carslaw 2008; Kulmala et al. 2001; Tunved et al. 2006); however prior to this campaign no ice nucleation research from the station had been published. The objectives of this paper are to demonstrate that PINE can be used in a field environment, compare to established INP counting techniques, and demonstrate the utility of PINE in terms of high-time resolution and to describe the development of methods for measuring and processing field data from this new instrument. The novel data from PINE presented here will be incorporated into other papers making use of the broader dataset from the HyICE18 campaign where we will discuss the nature and sources of INP in this boreal forest environment.

3.2 The PINE chamber – description and working principle

The PINE chamber is a new instrument, designed to measure INP concentrations in a novel way, based on the AIDA chamber at Karlsruhe Institute of Technology (Möhler et al., 2005, 2003). The PINE chamber was described in detail in (Möhler et al., 2020), but will be discussed in brief here, with specific attention paid to field specific considerations. A schematic of PINE is shown in Figure 20. The PINE chamber consists of five principle parts; the inlet system (I), the cloud expansion chamber (II), the cooling system (III), the optical particle counter (IV) and the control system (V). The working principle of PINE is based on the theory of adiabatic expansion, and simulates a cloud forming in the atmosphere when a parcel of air rises, cools and forms a cloud upon reaching water saturation. This process is simulated by the PINE chamber being flushed with ambient air until it is considered representative of the ambient sampling environment; this is known as the flush phase. The sample inlet is then sealed, whilst air continues to be pumped out of the expansion chamber, leading to a decrease in pressure and gas temperature. This decrease in temperature leads to an increase in relative humidity with respect to water, until water saturation is reached and aerosol particles within the chamber are activated as cloud droplets. This is referred to as the expansion phase. Once a target pressure, P_{target}, has been reached, the evacuation of the chamber ceases and dryer,

filtered air is allowed to flow into the chamber through the inlet system in order to refill the chamber. The recommencing of the flush phase then begins the start of a new cycle.

The starting temperature of the expansion chamber at the beginning of the expansion phase, T_{set}, is set by the user and controlled by the cooling system. If the temperature during the expansion reaches below 0 °C, then there is the potential for the cloud droplets formed within the chamber to freeze if the aerosol particle immersed within the supercooled droplet is active as an ice-nucleating particle at the temperature of the droplet. (Hoose & Möhler, 2012; Kanji et al., 2017a; B. J. Murray et al., 2012). Of key importance to this process is the humidity of the air within the chamber. It may not be suitable to carry out the expansion phase with air of the same humidity as the ambient environment. If the air is too humid, frost may form on the walls, potentially leading to the false detection of INPs if frost falls off the walls. If the air is too dry, water saturation will not be reached during the expansion, and a liquid cloud will not form. Temperatures during the field campaign ranged between –15 °C and 25 °C, with relative humidity typically around 75%. As such, the air sampled by PINE needed to be dried and its relative humidity monitored to ensure the chamber walls did not become frost covered. Gas sample dryers (Permapure, MD-700) were used to dry the incoming sample air, with the post-drying sample air relative humidity and frost point was monitored using a dew point mirror (MBS 573). Originally, it was believed that to avoid frost formation on the walls, the frost point of the sampled air would need to be kept below the coldest wall temperature. This proved not to be the case, as the PINE chamber operated continuously for several days at a time with sample air that had a frost point around 10 °C above the coldest wall temperature. This is potentially due to the adiabatic heating of the gas within the expansion chamber during the refill phase; the gas temperature rises above the wall temperature, hindering the build-up of frost over time on the walls. Another potential reason could be that the absolute amount of water vapour within the chamber available to deposit onto the walls as frost is not enough to lead to an appreciable build-up of frost.

With our goal of testing and validating PINE as a field instrument in mind, PINE was operated over a range of temperatures throughout the campaign. Sometimes PINE was operated for a significant period at one fixed temperature (static mode) whereas in other instances the cooling system was programmed in order that PINE would operate at a variable temperature (temperature cycling mode). PINE was situated in the Main cottage for the duration of the campaign (Figure 21).

3.3 Aerosol and hydrometeor size distribution measurements

The Welas sensor used on the PINE chamber records each particle it measures, listing for each measured particle the time of observation, the transit time through the detection volume, and the particle diameter (indirectly, using a signal amplitude and a pre-defined calibration table). Combing these values with the dimensions of the Welas sensor, one can determine the number of particles in the sample flow. This differs from the number of measured particles, as the Welas sensor does not have a 100% detection rate. The total number of particles measured in the expansion, N_{mes} is

$$N_{mes} = \sum n \tag{24}$$

The next step is to calculate the *sensor ratio,* or S_R. The ratio of detection flow rate (F_{dv}) to total flow rate (F_T) is explicitly calculated as follows

$$S_R = \frac{F_{dv}}{F_T} \tag{25}$$

With the detection volume flow (F_{dv}) being calculated with

$$F_{dv} = \frac{L_w}{\tau_w} A_w \tag{26}$$

Where A_w is the cross-sectional area of the detection volume, L_w is the length of the detection volume and τ_w is the mean transit time of particle through the detection volume. Thus, S_R can be written explicitly as

$$S_R = \frac{L_w A_w}{F_\tau \tau_w} \tag{27}$$

Dividing N_{mes} by the S_R will yield the total number of particles to have passed through the sensor during that expansion

$$N_{Tot} = \frac{N_{mes}}{S_R} \tag{28}$$

Now that the total number of particles to pass through the sensor in an expansion has been calculated, all that to remains is to divide this by the total volume of air to pass through the sensor during the expansion to calculate the particle concentration. This can be calculated with

$$V_e = F_\tau T_e \tag{29}$$

where V_e is the volume of gas evacuated in an expansion and T_e is the expansion duration. This culminates in

$$N = \frac{N_{Tot}}{V_e} \tag{30}$$

This can be written explicitly as

$$N = \frac{N_{mes} \tau_w}{T_e L_w A_w} \tag{31}$$

For results shown in this study, the sensor ratio is calculated explicitly for each expansion, as this value depends on the properties of the particles measured, which can change over time. This leads to a more accurate value of total concentration compared to simply setting a sensor ratio for an entire measurement period (which might be appropriate in a lab setting where the aerosol might be more uniform).

3.4 Distinguishing ice crystals from cloud droplets

In order to distinguish ice crystals from supercooled clouds droplets we use the fact that ice crystals in a cloud of supercooled droplets will grow much more rapidly than the cloud

droplets. This occurs because the supersaturation in the cloud during an expansion will only become marginally supersaturated with respect to liquid water, but becomes substantially supersaturated with respect to ice. Since growth rate is proportional to supersaturation, the growth of ice crystals is much more rapid than water droplets. Hence, by applying a suitable size threshold defining the boundary between ice crystals and water droplets we can quantify the concentration of ice crystals produced in each expansion. This section describes how we define this threshold.

During an expansion a liquid cloud will form, the droplets of which are detected by the PINE OPC. These size distributions are influenced by several factors including aerosol particle concentration, humidity, temperature and critically the concentration of INP. Dependent on whether any of the immersed aerosol particles are active as INPs at the temperature of the droplets, ice crystals will form. Whilst the presence of INPs, and hence ice crystals, does affect the profile of the size distribution, it does not affect the profile of the liquid cloud (Figure 22). Figure 22a shows size distributions from multiple expansions overlaid, with each expansion having single colour dots, with these dots representing the frequency of measurements in a given size bin. Indicated in Figure 22a are the different size modes present during the expansion; aerosol particles, liquid cloud and ice crystals. Figure 22b shows a single expansion (one of the many composite expansions in Figure 22a) in which no ice crystals form. Whilst the is no characteristic 'tail' of particles in the larger size bins, the profile of the liquid cloud remains similar to those shown in Figure 22a. The factors that govern the profile of the size distributions varied throughout the campaign, leading to the liquid portion of the cloud having substantially different size distributions (Figure 23). In laboratory work, it is feasible to hold conditions more constant and therefore apply a constant threshold (Möhler et al. 2020), however in the field a constant threshold would clearly lead to substantial errors.

The two different time periods containing multiple expansions shown in Figure 23demonstrate setting a single ice threshold for an entire campaign could lead to substantial errors in the ice particle count. Figure 23a shows an example where an ice threshold of 10 µm would cause cloud droplets to be misrepresented as ice crystals. This effect is made severe by the steepness of the droplet size distributions; setting the ice threshold too small by even a micron can cause a substantial over counting of ice crystals. Given the clear danger of setting the ice threshold too low, it is tempting to set a conservative ice threshold, well above where the liquid cloud influence could end. Unfortunately, throughout the course of this campaign, the liquid cloud profile differed significantly (having an influence in certain instances at > 25 µm), and thus any such pre-set ice threshold would lead to an inaccurate representation of the number of ice crystals. This is demonstrated in Figure 23b, where an accurately placed ice threshold at 10 µm would give an ice crystal count a factor of two higher than a conservative threshold at 30 µm. Whilst this is less of an issue than the potential for over counting discussed previously, it is still unsatisfactory, especially in conditions with low ice crystal counts. One possibility is for a user to inspect the size distribution of each expansion and then set an appropriate threshold. Whilst this is likely the most accurate method, it is highly time consuming and not appropriate for an automated instrument. The HyICE18 campaign resulted in 7571 individual expansions over a two-month period. Hence, a solution was devised in order to obtain an ice threshold on an expansion-by-expansion basis that gave results comparable to that of manual inspection, but in an automated fashion.

To realise this, for each expansion criteria were defined to indicate the location of an ice threshold. First, the mode of the size distribution was found (i.e. the highest point on the y-axis) and all data points in a size bin smaller than the size bin of the mode were disregarded. Next, the change in count frequency from one bin to the next was divided by the log of each bin subtracted from one another (which is approximately constant), $dy/d(\ln(x_i)-\ln(x_{i-1}))$, which transforms to $dy/d(\ln(x_i/x_{i-1})$. Then, $dy/d(\ln(x_i/x_{i-1})$, was evaluated at each remaining increment on the x-axis (post the removal of all data to the left of the mode) and once the condition $1 > dy/d(\ln(x_i/x_{i-1}), > -1$ was met in three consecutive bins, the ice threshold was placed at the following size bin. The ice threshold detection process also has a number of built in 'flags' – situations in which the user will be alerted to a potential inaccurate ice threshold being set. These include if moving the ice threshold to the next largest bin causes a decrease in particle count by a factor of two (implying the liquid cloud is still influencing the ice crystal count under the current ice threshold) or if the mode of the entire size distribution is above 10 µm (this would indicate an extremely unusual size distribution for the expansion). The flags do not stop the analysis from taking place, but a warning is given to the user to manually inspect these instances upon completion of the analysis. A minimum value for the ice threshold based on background measurements is described below.

3.5 Background measurements

Since we use hydrometeor size to distinguish between ice crystals and liquid droplets there is potential for large aerosol particles or ice crystals from frost to be erroneously counted as ice crystals resulting from heterogeneous nucleation. Hence we need to examine the possibility of false counts from large aerosol particles from the ambient atmosphere, frost on the walls that breaks off and falls through the detector, or some fault in the system that allows aerosol particles not related to the ambient environment into the system. We first address the issue of large aerosol particles in the ambient atmosphere as a source of error.

The size dependent inlet transmission efficiency for the inlet system used by PINE in HyICE18 is shown in Figure 24. This was derived using ambient number concentrations and then comparing them to number concentrations measured at the entrance of PINE (i.e. at the inlet-PINE interface; both measurements made using an Aerodynamic Particle Sizer (APS, TSI model 3321) in the Main cottage, see Figure 21). Number concentrations for particles greater than 10 µm in diameter were analysed for the entire campaign, shown in Figure 25. Particle with diameter >10 µm concentration never exceeded 0.5 L^{-1} even at peak times, with a mean concentration of 0.037 L^{-1}. Coupling these ambient values with the transmission efficiency of the PINE inlet yields the result that we could expect to never have more than 0.05 L^{-1}, and on average less than 0.01 L^{-1}, in the chamber. At the maximum observed concentration of 0.05 L^{-1} we would expect to observe a false count in every 50 expansions, whereas at the average observed concentration we would expect a false count every 250 expansions. Hence, we conclude that large aerosol particles would not be a significant background artefact in the measurements during the HyICE18 campaign. In the future, a size cut in the inlet could be used to reduce this artefact if necessary.

The cleanliness of the system can be tested by inserting a HEPA filter between the PINE chamber and the ambient environment (Figure 20) and running a series of expansions. If there is no source of contamination in PINE, then we expect to observe no cloud after several expansion cycles. A set of such expansions are shown in Figure 26, where there were a

significant number of residual aerosol particles in the first and second expansion, but after several cycles the chamber was deemed particle free. At this point, the chamber would be considered clean and ready for sampling. This was done systematically throughout the campaign, with nearly every measurement day having a background run to ensure PINE was ready for operation. Figure 26d shows the final expansion of each background run prior to a measurement period. In none of these expansions was a particle greater than 11 microns observed. In order to ensure no background counts from particles not related to the ambient environment, a minimum size of 11 microns was set for all ice thresholds.

To test for frost build up on the walls, background tests for three consecutive days were analysed. Figure 27 shows a temperature and pressure profile within the chamber overlaid with OPC data showing particle sizes. If frost had accumulated on the wall over the course of these three days, an increasing amount of ice crystals should be seen during the flush mode and the expansion. As can be seen, the final expansion on each day shows no particles. In order to prevent frost formation on the walls of the chamber over long time periods of operation, the chamber has to be warmed up periodically. For the HyICE18 campaign, PINE was warmed up every third day to a temperature of approximately −3 °C for at least one hour.

3.6 Time averaging and limit of detection

As described previously, PINE can be shown to effectively have a zero background measurement throughout the campaign when setting an ice threshold of 11 microns. This leads to PINE's limit of detection (LoD) being defined not by background measurements, but a combination of experimental and measurement variables. Equations 27 & 29 can be combined and adjusted for detection of ice crystals to form equation 32

$$N_{ice} = \frac{N_{mes>threshold}}{V_e \, S_R} \tag{32}$$

It can be seen from equation 10 that the concentration of ice crystals in an expansion is dependent on the number of ice crystals measured that have a diameter above the ice threshold, the volume of air evacuated in an expansion and the SR for that expansion. To calculate PINE's LoD for a single expansion under given parameters, the number of ice crystals measured is defined as unity, the total evacuated volume measured and S_R values entered as per expansion conditions. For a typical expansion during the HyICE18 campaign, the volume evacuated would be around 4 L, with the S_R around 0.1. This gives a value of 2.5 ice crystals L^{-1}, which we take as the limit of detection for a single expansion during the campaign. This value can vary slightly, due to variation in the volume of air evacuated or the sensor ratio (which is directly proportional to the mean transit time of particles through the OPC during an expansion), but for the duration of the HyICE campaign this value is within a factor of 1.5. When averaging measurements over time, and thus multiple expansions, the LoD decreases in magnitude (thus the instrument becomes more sensitive) due to the increase in the value of the denominator in equation 10. This increase is due to the total evacuated volume being the sum of several expansions, whilst the number of measured ice crystals remains at 1. Repeating the calculation above for a period of 1 hour consisting of 8 expansions gives a LoD value of approximately 0.3 ice crystals L^{-1}. This is illustrated in Figure 28. Uncertainties on the measurement of INPs is dominated by Poisson counting error. In the instance of a single ice

crystal being measured, the Poisson error is 100%, decrease fractionally as the number of measured ice crystals increase (as the Poisson error is equal to 1/√N). Increasing the time averaging, and thus the number of observed ice crystals, decreases the uncertainty on the measurement as a proportion of the measurement value.

3.7 Comparison to other INP instruments

To validate PINE as a field instrument, we compare results from PINE to other field based instruments that made measurements at the same time. We first compare filter based samples analysed by the µL-NIPI (O'Sullivan et al., 2018; T. F. Whale et al., 2015) to measurements made by PINE in an equivalent time period (we set a criteria of the filter sample start and end times being within 10 minutes of the start and end of a PINE cycle). As described previously, PINE was sometimes operated in a temperature-cycling mode, and thus expansions carried out during the duration of the filter sample will have different T_{target} values. For the purpose of comparison with other instruments, we show a selection of measurements where PINE was operated at a single temperature for the duration of the measurements period. If >95% of the expansions T_{exp_min} carried out within the comparison period are within the temperature uncertainty of the mean T_{exp_min} for the duration, then it is suitable for comparison. A mean INP concentration is calculated for the comparison period and plotted against the mean T_{exp_min}; this is visualized in Figure 29. The temperature uncertainty of ± 1 °C is shown on the x-axis, along with the standard deviation of the INP concentration from all the expansions in the comparison period. Data from individual expansion is shown as translucent markers, demonstrating that >95% of expansions in this time were within the quoted temperature uncertainty from the mean temperature. Values outside of the temperature uncertainty do not contribute to the INP concentration mean.

There were 8 examples from the HyICE18 campaign that fitted the criteria discussed, from which PINE INP concentration mean values are plotted alongside spectra from corresponding µL-NIPI experiments in Figure 30. As the µL-NIPI mostly made measurements at warmer temperatures than PINE, consistency in this case is defined as the INP concentration measured at the coldest temperature by the µL-NIPI being not greater than the INP concentration as measured by PINE. INP concentrations calculated from µL-NIPI measurements are derived from the cumulative nucleus spectrum (Gabor Vali, 1971), and thus cannot decrease due to their cumulative nature. We define this as 'consistent' rather than 'agreement' as we cannot know where the µL-NIPI spectra would lie if measured at colder temperatures, expect that we can say it would not decrease. Hence we do not know if it would 'agree' with the PINE data (i.e. overlap within uncertainties), but we can (or cannot, in some instances) say that the µL-NIPI spectra could agree with the PINE data and is therefore consistent with it. As can be seen in Figure 30 five out of the eight cases show consistency between the µL-NIPI and PINE, with the µL-NIPI data plausibly being able to pass through the vertical error bars on the PINE data point (this error bar was calculated using the standard deviation of the measurements from all the individual expansions that were averaged to produce the single PINE data point shown, as described above). A potential explanation for the discrepancy observed in three of the comparisons is the use of different inlet sizes. Figure 24 shows that PINE is effectively sampling PM_5 aerosol, albeit with a shallow cut-off compared to a dedicated impactor. The µL-NIPI experiments were conducted using filter samples collected from a PM_{10} sampling unit (described in Chapter 6). Thus any INPs that were between 5 - 10 µm would have been present in the µL-NIPI analysis but not the PINE analysis.

Size-resolved INP measurements made in Chapter 6 show that the majority of INPs in Hyytiälä are found in the coarse mode (>2.5 µm), with (Porter et al., 2020) observing INPs in the size range 2.5 - 10 µm from a single experiment made during the HyICE18 campaign.
.
A second instrument comparison was done between PINE and the Portable Ice Nucleation Chamber (PINC) (Boose et al., 2016), which was measuring in the Winter/Spring period in the main cottage with PINE. PINE and PINC were operating at the same time for 16 days, during which time PINC was operating at −31 °C and PINE was operating between −24 °C and −32 °C (at either −30 °C or −32 °C) in the temperature cycling mode described previously (Paramonov et al., 2020). Figure 31 shows a time series of the instrument overlap period, whilst in Figure 32 a comparison of daily average INP concentration measured by PINE and PINC is shown, for the 5 days in which PINE measured at equivalent temperature to PINC for at least some time during the day. These measurements demonstrate the good agreement between the two instruments, with 4 out of 5 of the comparable days showing agreement within approximately a factor and all within a factor of 5 and the general trends being consistent.

3.8 INP time series and correlations

INP concentrations were measured throughout the campaign, spanning approximately 5 – 500 INP L^{-1} in the temperature range −24 °C to −32 °C (Figure 33). The greatest data density is found when averaging over a period of 10 minutes for measurements made at −32 °C (1846 data points). None of the data at any temperature shows a trend throughout the duration of the campaign, although given the changing seasons this is perhaps to be expected. Despite there being no trend throughout the campaign duration, there is considerable variation in INP concentration throughout the measurement period. At −32 °C 2 orders of magnitude variation was observed in INP concentrations on the timescale of hours, highlighting the need for high-time resolution instrumentation. The variability in INP concentration decreases as the time averaging is increasing, suggesting the variability in INP concentration is happening on short time scales (i.e. 60 minutes), as opposed to over days and weeks. This could indicate that INP concentrations are controlled on short time scales by local variables (aerosol concentrations/species), as demonstrated in the case studies below, but that long-term synoptic scale variables control the INP concentrations over longer time frames.

A correlation table of INP concentrations at different temperatures with different aerosol parameters using different time averaging is shown in Table 2. Cells are coloured to indicate the strength and direction of a correlation (-1 is red, 1 is green), with Pearson correlation coefficient values being explicitly shown also. Colder temperature measurements (−30 °C and below) have a much higher data density during the course of the campaign, so we show only correlation from measurements at −30 °C and −32 °C. Of note is the increasingly positive correlation between INP concentration at −30 °C and aerosol particles greater than 500 nm, although this is not observed at the slightly colder temperature of − 32 °C. This seems extremely unlikely given the cumulative nature of INP measurements made by PINE, but it is important to note that if PINE was making INP concentrations at −30 °C, it was not making them at − 32 °C. Figure 33 shows that PINE measured at − 32 °C most frequently throughout the campaign, operating at this temperature frequently throughout (except for a 2 week period between 07.04.2018 – 21.04.2018). Conversely, most of the measurements made at −30 °C came in the latter half of the campaign (i.e. spring time). Thus the difference in correlation between INP concentration and aerosol should not necessarily be similar between

different temperature measurements. In future campaigns, a more systematic temperature cycling strategy will be employed to avoid this. For the case of INP concentrations at −30 °C and aerosol concentrations greater than 500 nm, whilst INP and aerosol concentration are decoupled on short-time scales, they are coupled on longer timescales. A potential explanation for this could be that synoptic scale trends may be more important for determining INP concentrations than short time variations in aerosol concentration. However, there are examples were INP and aerosol concentrations are well correlated on shorter timescales, as discussed below in a series of case studies.

3.9 Case studies

To illustrate the value of deploying PINE in a field environment, we now focus on three case studies in some more detail. These case studies feature events that influenced the INP population in some manner that PINE was able to measure and quantify using its unique capabilities.

3.9.1 Case study 1: 25/03/2018

The first example is from 25/03/2018 between 10:00 – 22:00, and covers a period where there was a change in air mass origin and is illustrated in Figure 34. PINE measurements are made at −32 °C and have a time averaging of 15 minutes (on the order of two expansions). Paramonov et al., (2020) also looked in detail at this event using PINC, so this case study serves to both demonstrate the capability of PINE and also further validate PINE against an existing field instrument, this time on a shorter timescale. Temperature increases for the first half of the measurement period, before decreasing with the changing air mass at 14:30. Pressure is approximately constant until 14:30 before increasing slightly by 10 mb through until 21:00. Wind speed throughout the period varies between 2 - 4 ms^{-1}, whilst wind direction is South Westerly from 10:00 – 14:30 before dramatically turning Northerly after 14:30. Little precipitation is observed throughout the measurement period, with relative humidity decreasing proportionally to an increase in temperature before increasing abruptly with the air mass change, however relative humidity never reaches 100%. Fluorescent particle concentration is approximately constant during the first half of the period, increases by a factor of 3 when the air mass origin changes, and then remains constant.

INP concentrations range from 10 - 300 INP L^{-1}, with the trend changing multiple times in the measurement period. Initially INP concentrations decrease around 80 INP L^{-1} to 15 INP L^{-1} from 10 10:00 – 12:00, before increasing to a maximum value of 300 INP L^{-1} until the change in air mass origin at 14:30, from which point it steadily decreases back to 100 INP L^{-1} at the end of the measurement period. Aerosol concentrations vary between 500 – 2200 cm^{-3} and are generally more consistent throughout, increasing to a maximum at 14:30 before decreasing for the rest of the period. The fraction of aerosol particles active as INPs followed a similar profile as the INP concentrations, varying an order of magnitude throughout the course of the period.

There are two distinct periods in the day, before and after the air mass/wind direction changes. The first period sees both increasing and decreasing INP concentrations, whilst the second seems INP concentration steadily decrease. The correlation between INP and total aerosol concentration (Pearson correlation coefficient = 0.65) appears to be driven primarily by particles below 100 nm in diameter. Particle in this size range increase by over a factor of

4 in concentration from 12:00 - 14:30 (Figure 35), corresponding with the increase in INP concentration, and also decrease in concentration after the air mass origin change. Particle concentration below 100 nm have a Pearson correlation coefficient value almost the same as that of the total aerosol concentration with INP concentration (Pearson correlation coefficient = 0.65).

The fraction of particle active as INPs shows a similar profile to that of INP concentration. This implies that there are different aerosol species acting as INPs throughout the course of the day, before and after the air mass change. For the period before the air mass change, it implies that if the increase in INP concentration is due to particles smaller than 100 nm (this is suggested by the strong correlation, but is by no means certain) then those aerosol particles are more effective INPs than whatever was dominating the INP population prior to their increase at 12:00. Paramonov et al. (2020) made similar measurements using PINC at −31 °C from a concentrator from the same measurement cottage at PINE. They observed INP concentrations in the range 52 and 416 L^{-1} which followed the same profile as the time series measured by PINE in Figure 34e.

3.9.2 Case study 2: 03/04/2018 – 06/04/2020

The second case study is for the dates 03/04/2018 – 06/04/2018, for a total of 72 hours (Figure 36). PINE made measurements at −32 °C, and data as averaged on an hourly basis. Temperature ranged between −8 to 5 °C following the day/night cycle, with pressure varying only slightly between 975 - 990 mb. Wind direction was Westerly for the first 12 hours of measurement, and then predominantly Southerly, whilst wind speed ranged from 0 – 4 ms^{-1} at an average of 1.72 ms^{-1}. Precipitation was low throughout the measurement period, but during the latter half of the measurement relative humidity was consistently at 100%. As the relative humidity was at 100% during the measurement period, there was the potential for fog to develop, which could cause aerosol particles to swell or become enveloped in liquid water. Both of these occurrences would serve to increase size of the aerosol particle/droplet in which the particle was immersed which could prevent it from making it through the inlet system to the PINE chamber (Figure 24). This would artificially reduce the INP concentration measured by PINE, especially if the INPs in the ambient environment were more susceptible to swelling/becoming immersed. INP and aerosol concentrations ranged between 2 – 200 L^{-1} and 800 – 2000 cm^{-3} throughout the period, respectively. The fraction of aerosol particles active as INPs generally trended downward throughout the duration of the measurement period, however it did increase at approximately 15:00 on 04/04/2018 from a minimum value of 2 x 10^{-6} to 2 x 10^{-5} over the course of 3 hours, before again decreasing. This corresponded with a peak in fluorescent particles (FPs), as measured by the WIBS, in all size ranges and also for FPs over 2.5 µm.

During this period there is a strong correlation (Pearson correlation coefficient of 0.81) between INP concentration and aerosol concentration for particles > 1 µm (Figure 37). The profile of the INP time series also correlates well with fluorescent particle concentration for both particles 0.5 - 10 µm and 2.5 – 10 µm. This could indicate that there was a source of super micron, biological particles active at – 32 °C during the measurement period.

3.9.3 Case study 3: 19/04/2018 – 21/04/2020

The third study was chosen for the period 19/04/2020 – 21/04/2020 (Figure 38). PINE's operating temperature during this measurement period was 4 °C warmer than the previous case, at −28 °C, with a time averaging of 30 minutes (approximately 4 expansion cycles). This period was characterised by variable local temperature, rising and falling with the day-night cycle in the range of 5 - 15 °C. Pressure decreased throughout the measurement period from approximately 1000 mb to 980 mb. Wind direction (North-Westerly) and speed was approximately constant for the first 36 hours, changing to an erratic directionality for the next 6 hours, before becoming Northerly for the final 6 hours. Relative humidity varied between 40 – 100 %, following the inverse profile of the temperature, whilst some precipitation was observed in the final 12 hours of the measurement period, coinciding with the period of variable wind direction. As described in case study 2, there was the potential for fog to form during this measurement period and reduce the INP concentration measured by PINE through the swelling of aerosol/forming of CCN that could not make it through the inlet system due to their size. Fluorescent particle concentration (all size ranges and coarse mode) decreased by around a factor of 5 during the period. INP concentrations ranged from 1 – 70 INP L^{-1}, with the majority of this variation being captured in the 12 hours between 06:00 – 18:00 hrs on 20/04/2020. As temperatures rise and relative humidity decreases through the morning and into the afternoon, both aerosol and INP concentrations increase. After 12:00 on 20/04/2018 until the end of the measurement period, both aerosol and INP concentrations decrease, however the magnitude in change is not equal for both variables; aerosol concentration experiences approximately a factor of 2 decrease whereas INP concentration decreases by approximately an order of magnitude. The fraction of particle active as INPs decreases by just under two orders of magnitude during the measurement period, following a similar profile to that of INP concentration.

This rise and subsequent fall in INP concentration does not directly correlate with aerosol total concentration of any particle size bin (Pearson correlation coefficient all below 0.3), as can be seen in Figure 39. The fraction of aerosol particles activated as INPs over time (shown in Figure 38f) has a similar profile to the INP time series, indicating that the number of aerosol particle present does not control the number of INPs present and hence that the INP population is changing. It is not at present clear what is driving this variation in INP concentration.

3.10 Conclusion

The PINE chamber is a new, automated ice-nucleating particle counter developed with the aim of providing high time resolution measurements in both a laboratory and field environment. In this study, we discuss the working principle of PINE and focus on aspects that are specifically related to field measurements. The basis for liquid cloud/ice crystal discrimination is detailed, along with a discussion of the treatment of background measurements in the PINE chamber and a justification for why PINE can be considered to have no background during the HyICE18 campaign. We also show the potential of PINE to make automated measurements at a range of temperatures relevant to mixed-phase clouds over a two-month period and compared results from PINE to other established field INP counters in this time period with PINE measurements shown to be consistent with those of the µL-NIPI and PINC (Paramonov et al., 2020; T. F. Whale et al., 2015). INP concentrations are observed to vary by 2 orders of magnitude at a fixed temperature on the time scale of hours. We also look at specific case studies on a short time-scale (hours) to investigate the

relationship between INP concentrations at different temperatures to variables such as local meteorology and aerosol concentration. This preliminary data analysis suggests there may be competing sources of INPs at any given temperature, and demonstrates the need for a more thorough analysis of the data (which is beyond the scope of this techniques paper). The PINE chamber has the potential to dramatically improve the data collection of INP measurements in the field and bring us closer to answering key questions about the spatial and temporal distribution of atmospheric INPs through high time resolution measurements across the INP_T spectrum.

3.11 Figures and tables

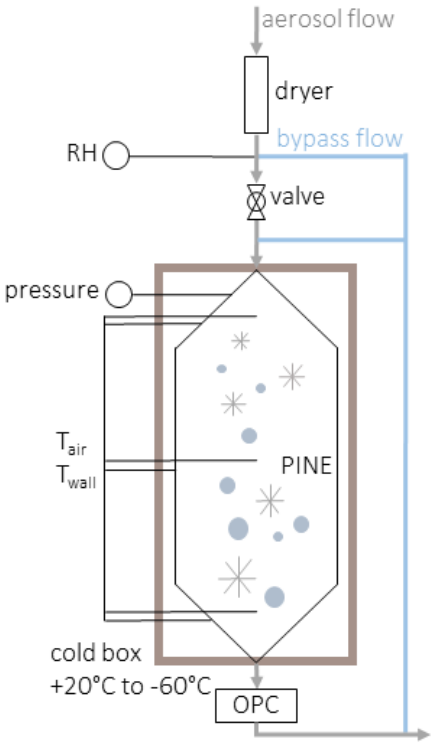

Figure 20: A schematic of the PINE chamber configuration when it was deployed in Hyytiälä. For cleanliness experiments, a HEPA filter could be placed above the dryer.

Figure 21: A map of the Hyytiälä forestry research station. Key points are noted on the map to aid in understanding the sampling location and instrument location.

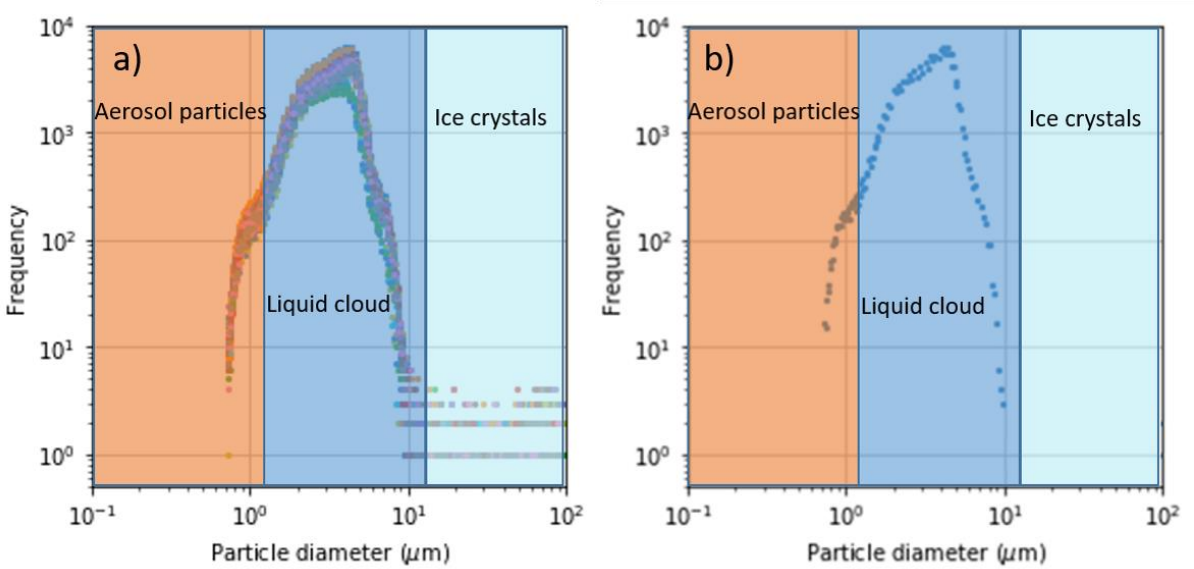

Figure 22: Size distribution as measured by the OPC during an expansion. a) Multiple expansions showing the liquid cloud and ice crystals b) a single expansion in which no ice crystals formed. Orange, blue and turquoise represent aerosol particle, liquid clouds droplets and ice crystals respectively.

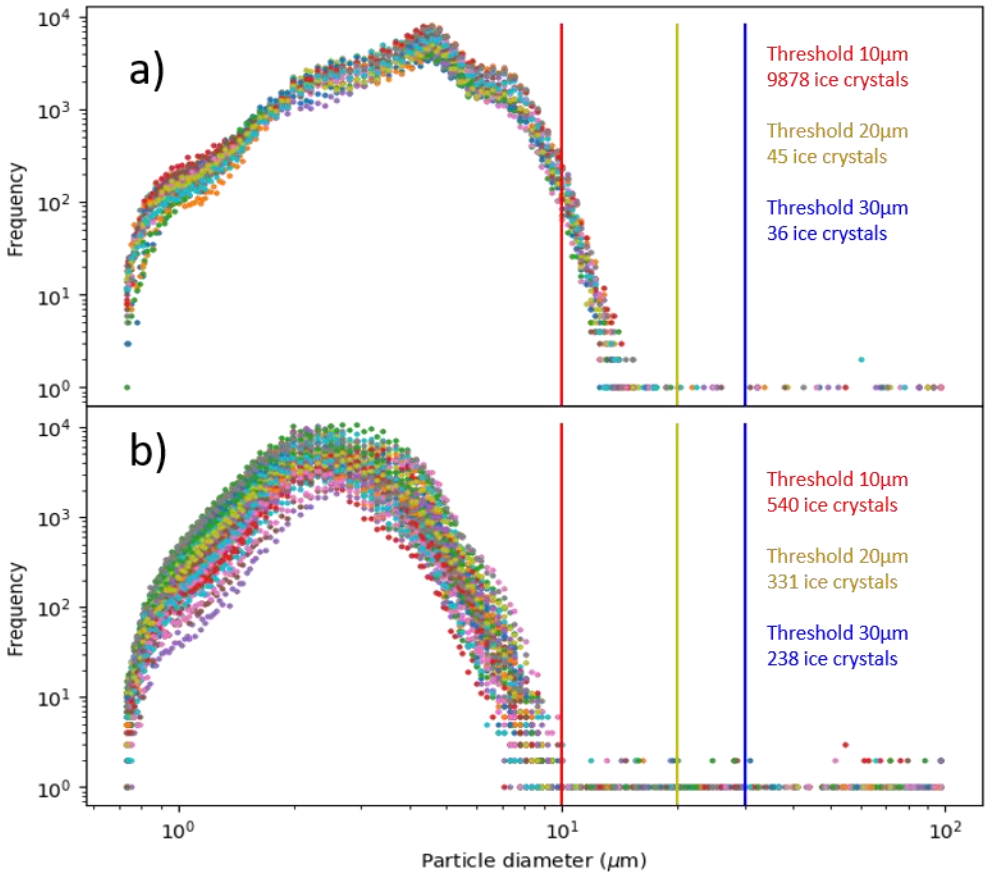

Figure 23: Multiple size distributions during different measurement periods. a) An example of when setting an ice threshold too low leads to orders of magnitude over counting. b) An example of setting an ice threshold too high leading to undercounting back around a factor of two. Size distributions from multiple expansions are shown as different colours.

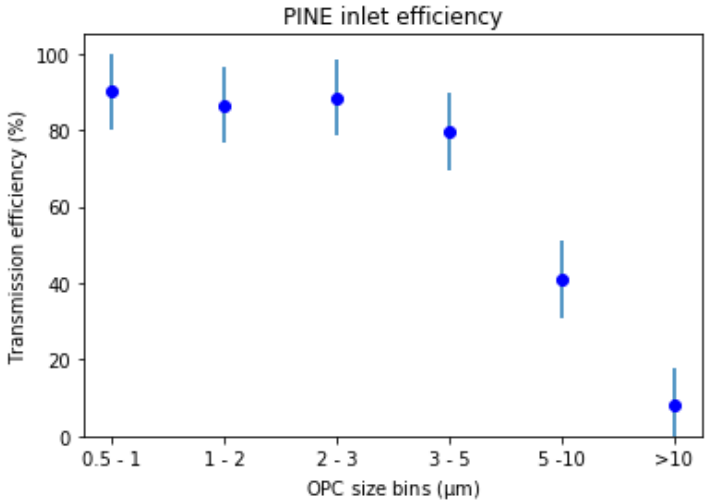

Figure 24: The transmission efficiency of the inlet PINE sampled from during the HyICE18 campaign.

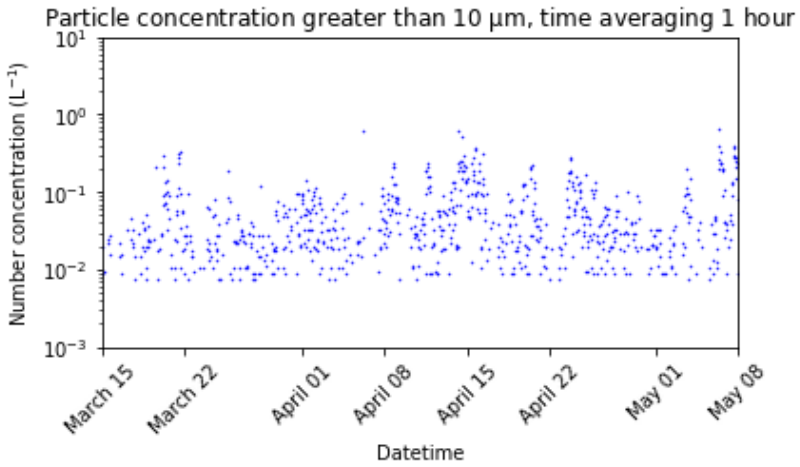

Figure 25: Ambient particle concentrations for particles greater than 10 µm in diameter during the HyICE18 campaign.

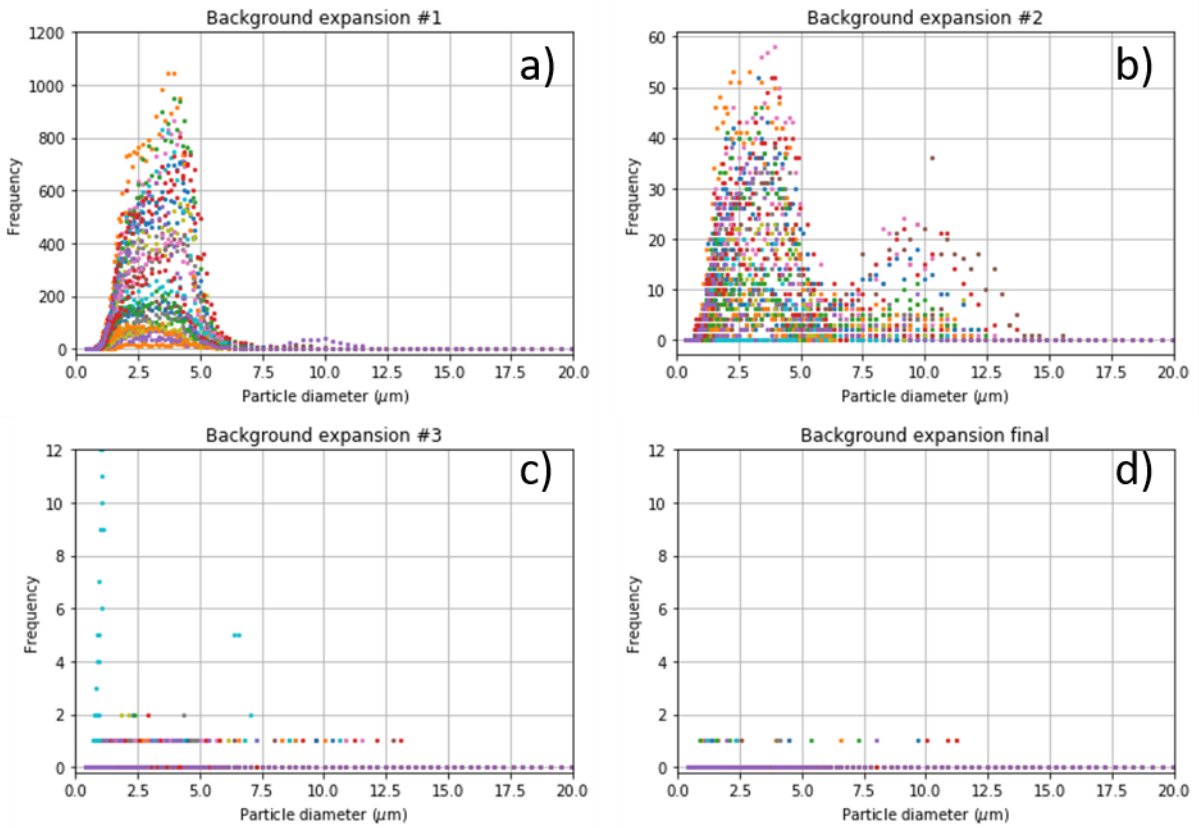

Figure 26: Size distributions for background expansions. Background expansions occur when PINE is being cleaned of aerosol prior to the beginning of a measurement period. A HEPA filter is placed between PINE and the inlet, and repeated expansions are carried out to remove any aerosol particles from the chamber, until no particles (or none over a certain size threshold) remain: a) First expansion in a cleaning cycle b) Second expansion c) Third expansion d) Final expansion.

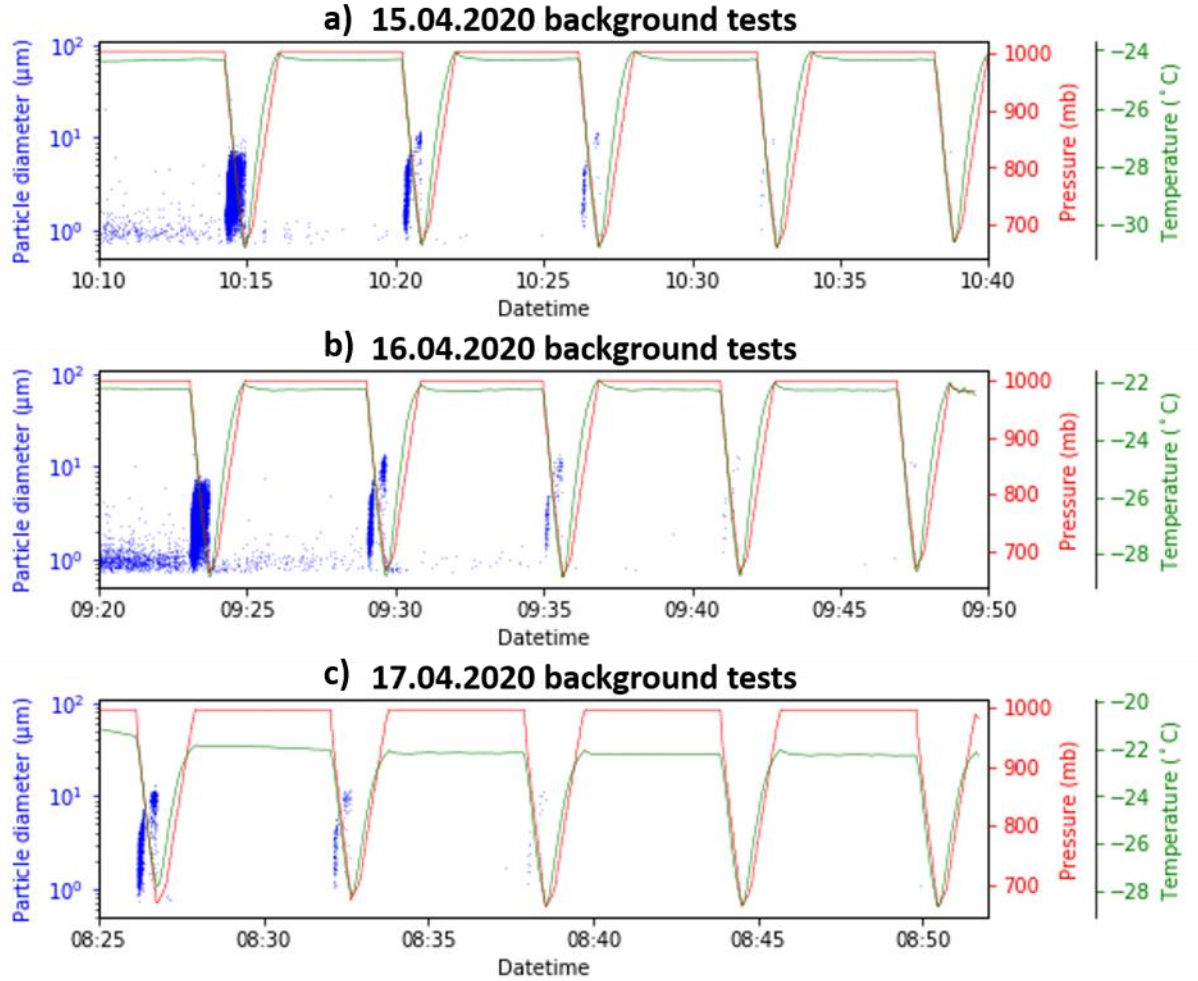

Figure 27: Background measurements for 3 consecutive days showing PINE being cleaned of aerosol prior to a measurement period.

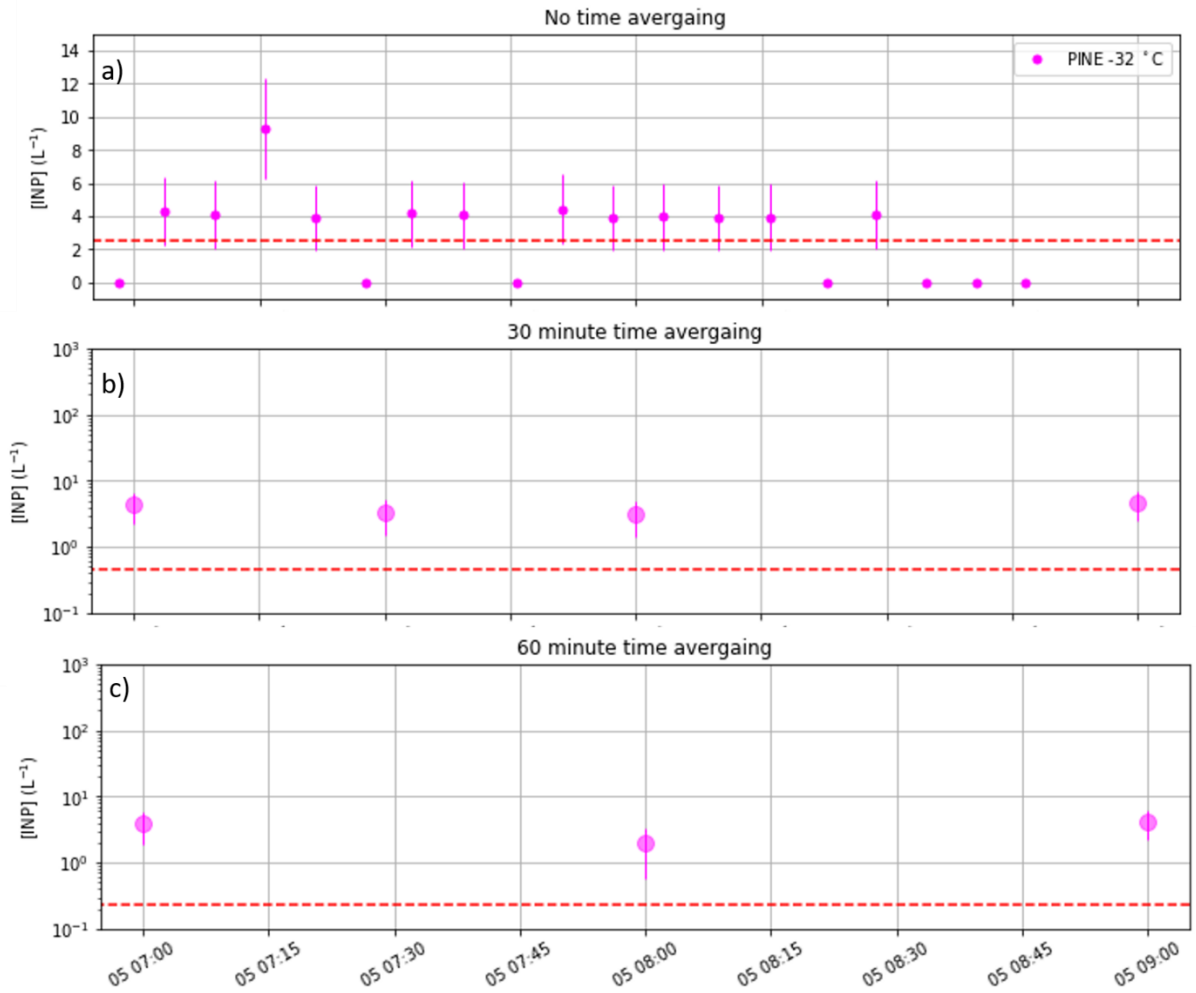

Figure 28: An example case of how PINE's limit of detection changes based upon the time averaging of data. a) No time averaging b) 30 minute time averaging c) 60 minute time averaging. This example has been chosen to emphasis the Poisson counting uncertainty, specifically in which cases of only 1 ice crystal being measured, the lower limit of the uncertainty is equal to zero.

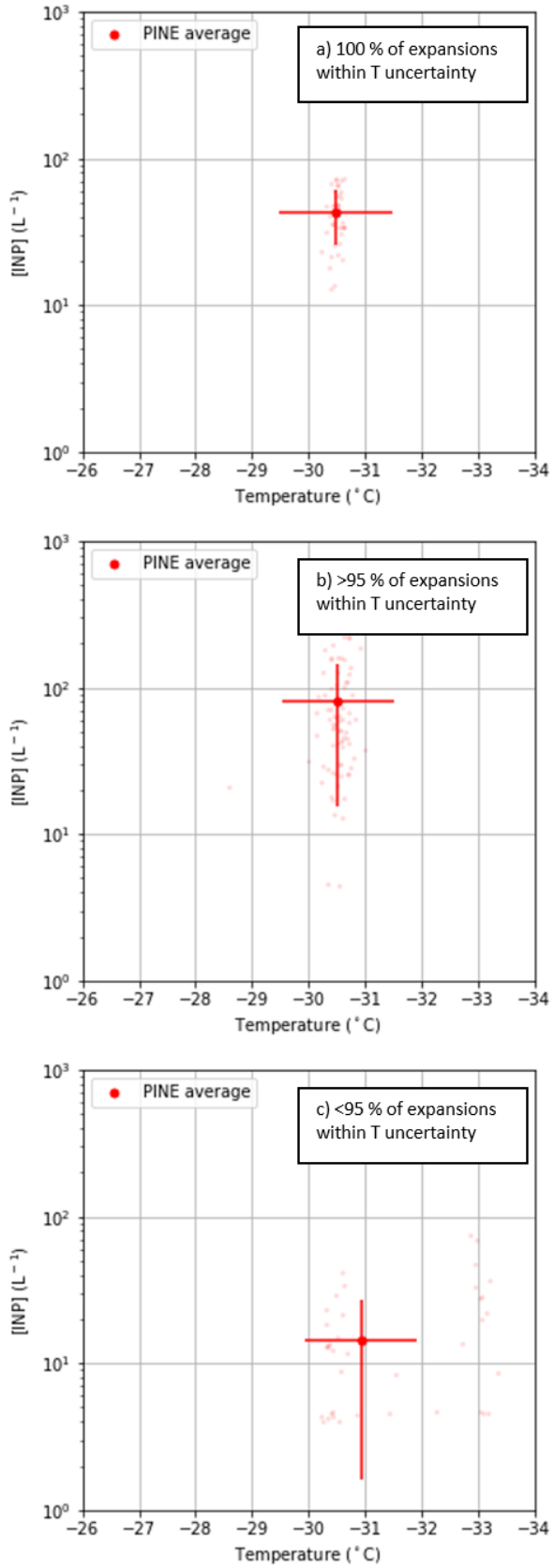

Figure 29: Examples cases for when PINE can be compared to other instrumentation. PINE can only be compared to other instrumentation when measurement times are concurrent and PINE was operating at a single set temperature for the duration of the comparison period. a) 100% of cases within temperature range b) >95 % of cases within temperature

range c) < 95 % of cases within temperature range. In this example, only cases a and b would be acceptable.

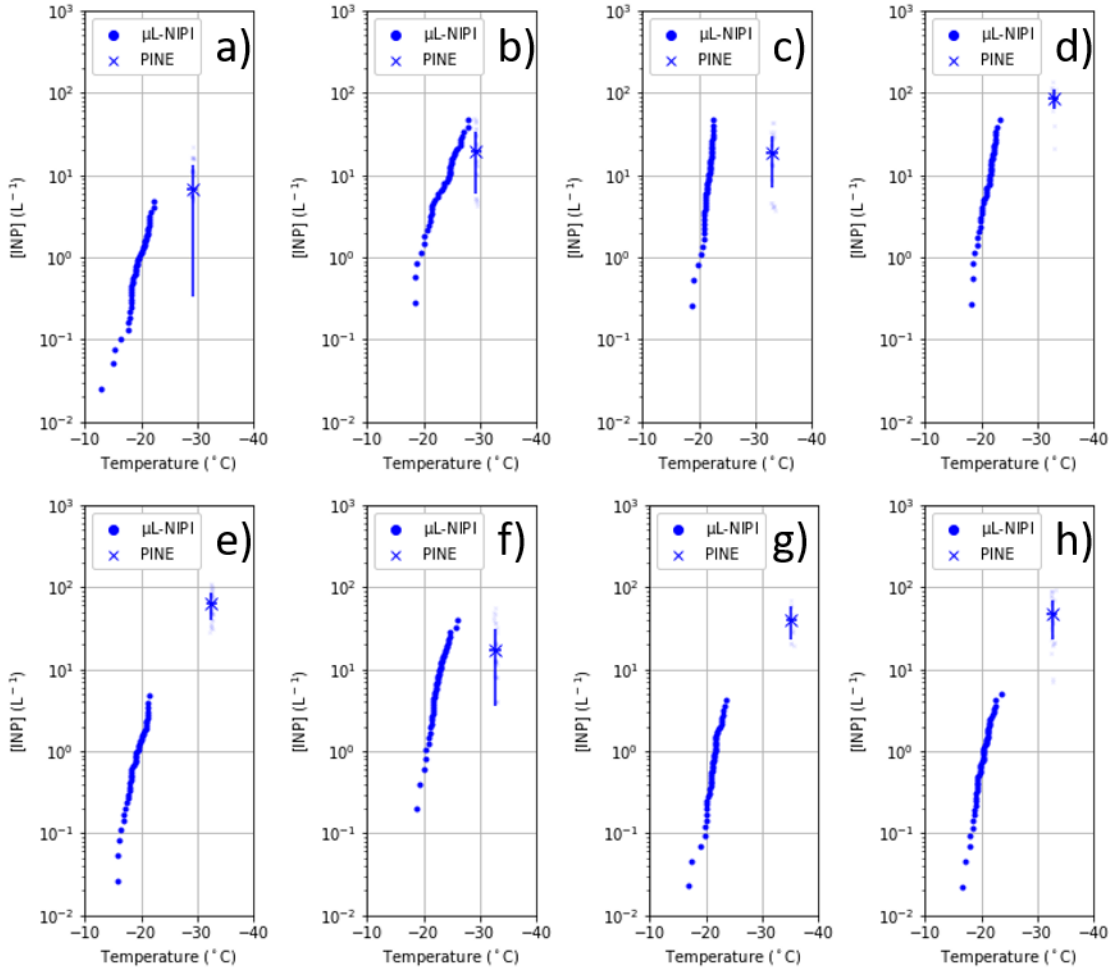

Figure 30: The eight cases during which PINE and µL-NIPI could be compared, as according to the criteria described. In the majority of cases PINE and µL-NIPI measurements are consistent with one another.

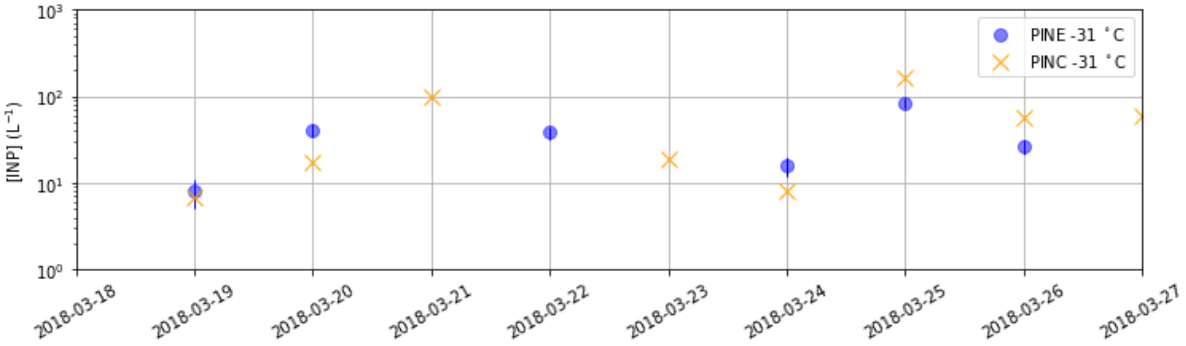

Figure 31: A time series showing PINE and PINC measurements at -31 C during the HyICE18 campaign. Error bars on PINE data points are calculated according to the Poisson counting uncertainty. Data is time averaged over 24 hours.

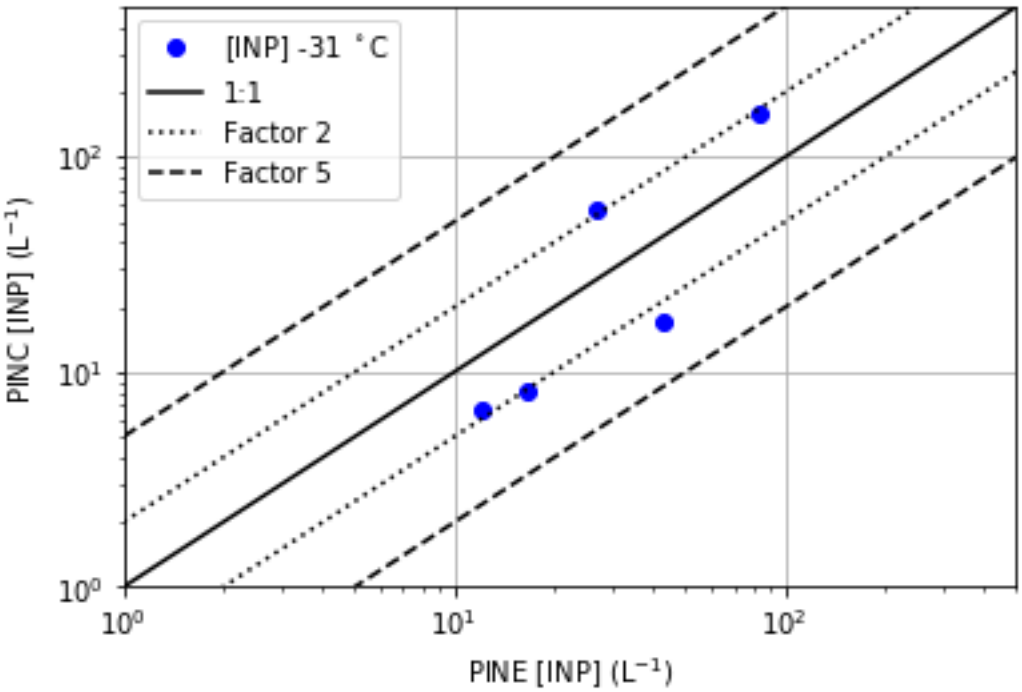

Figure 32: A plot comparing INP concentrations measured by PINE and PINC for equivalent time periods.

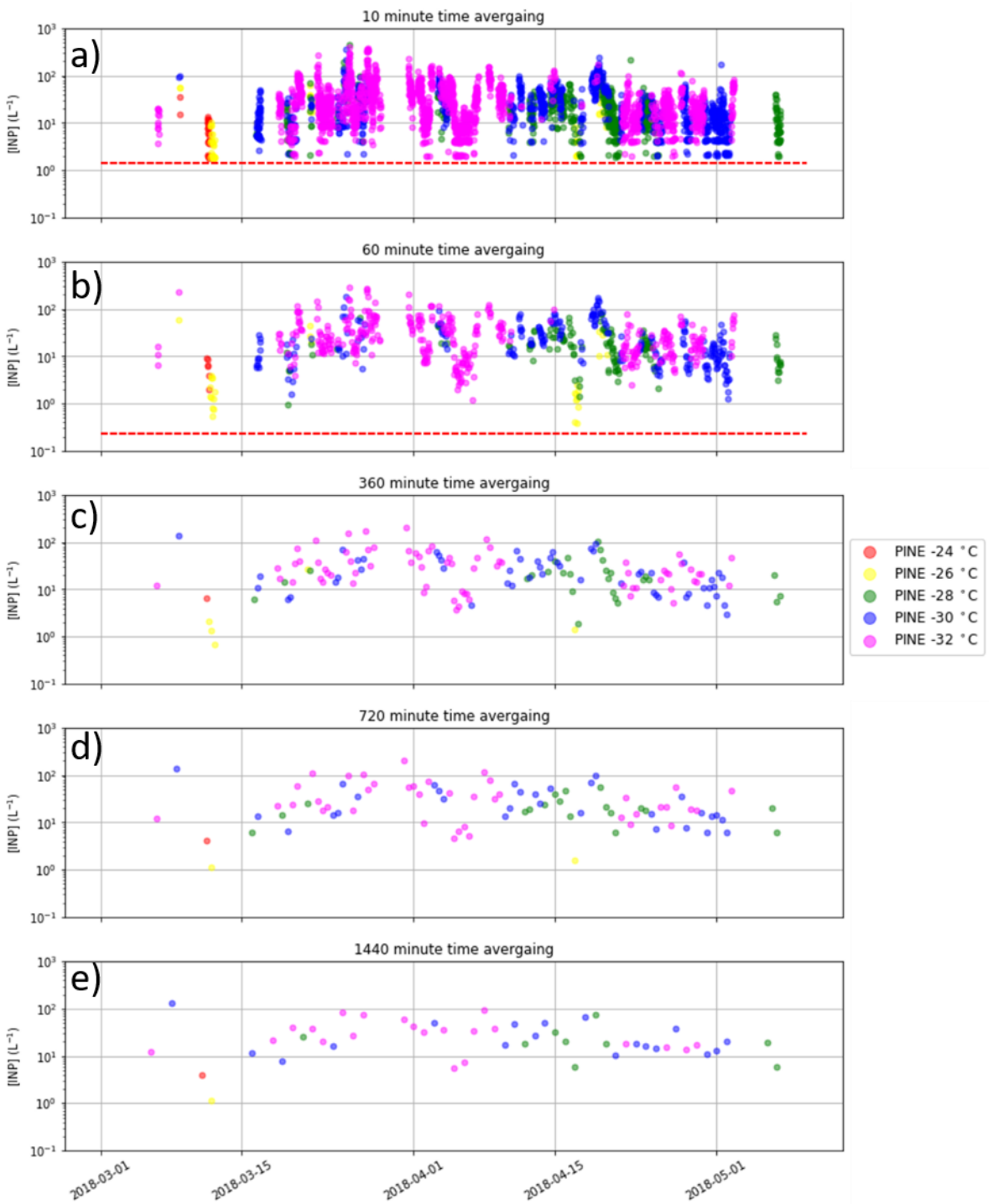

Figure 33: INP concentrations at a series of temperatures throughout the HyICE18 campaign. a) 10 minute time averaging b) 60 minute time averaging c) 360 minute time averaging d) 720 minute time averaging e) 1440 minute time averaging.

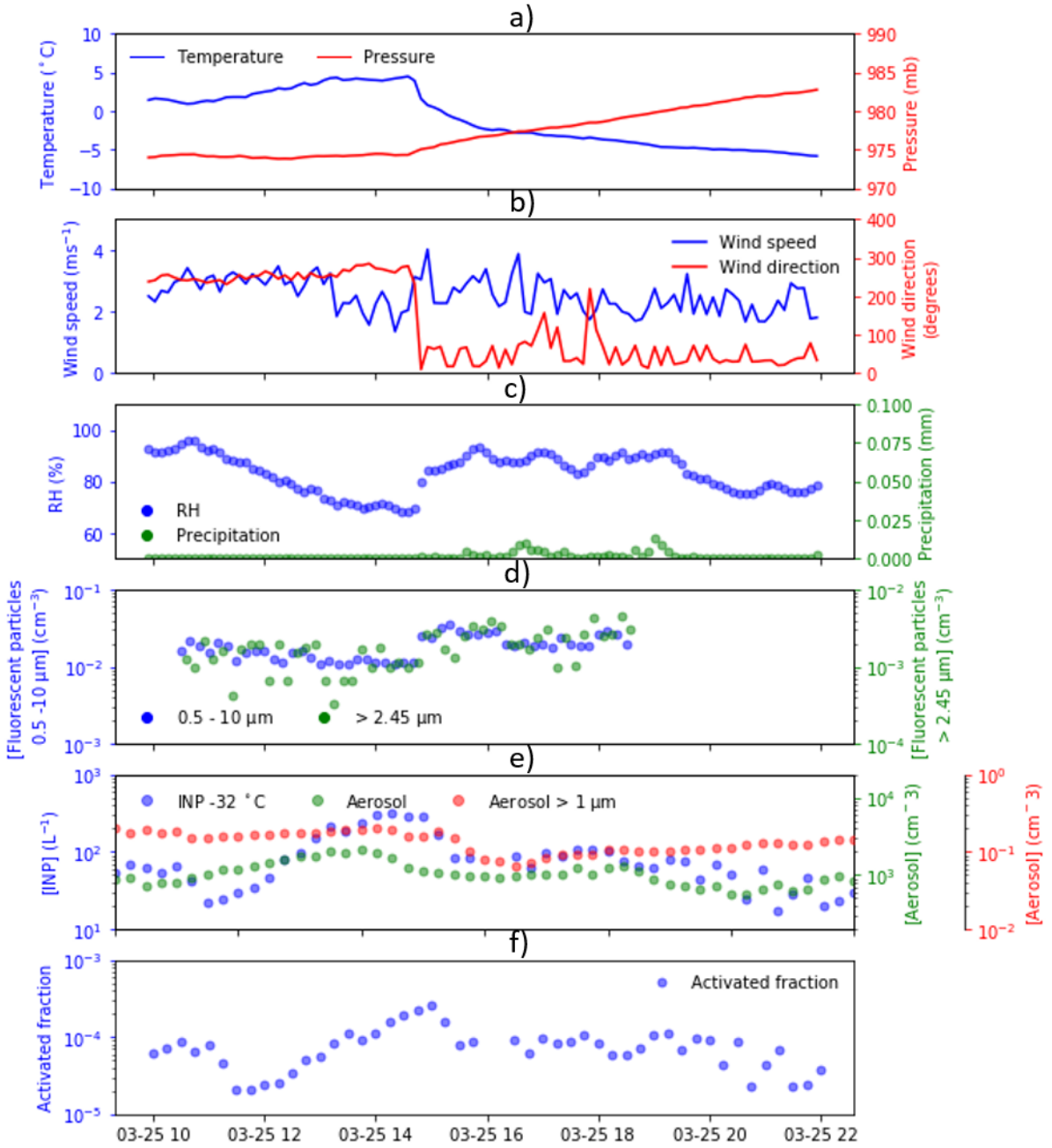

Figure 34: Data for case study 1 from 25/03/2018. a) INP concentration at −32 °C as measured by the PINE chamber (blue), total aerosol concentration as measured by a DMPS (green). Data is average into 8 minute intervals b) Temperature (blue) measured 4.2 m above ground, pressure (red) measured at ground level c) Wind speed (blue) and direction (red) measured 16.8 m above ground. d) Relative humdity measured 16.8 m above ground e) Fraction of aerosol particles active as INPs at −32 °C.

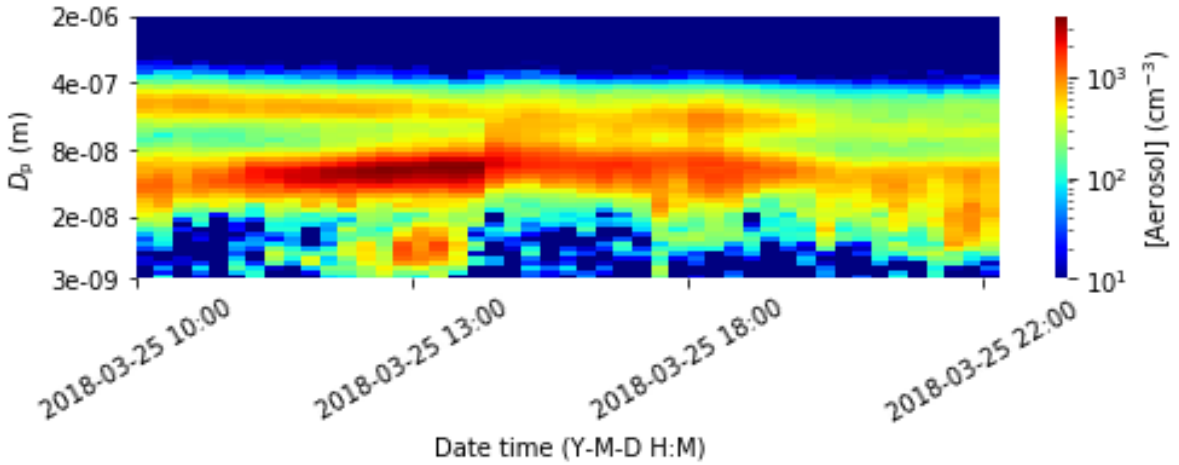

Figure 35: Size distribution of aerosol particle over time during case study 1on the 25/03/2020 between 10:00 - 22:00.

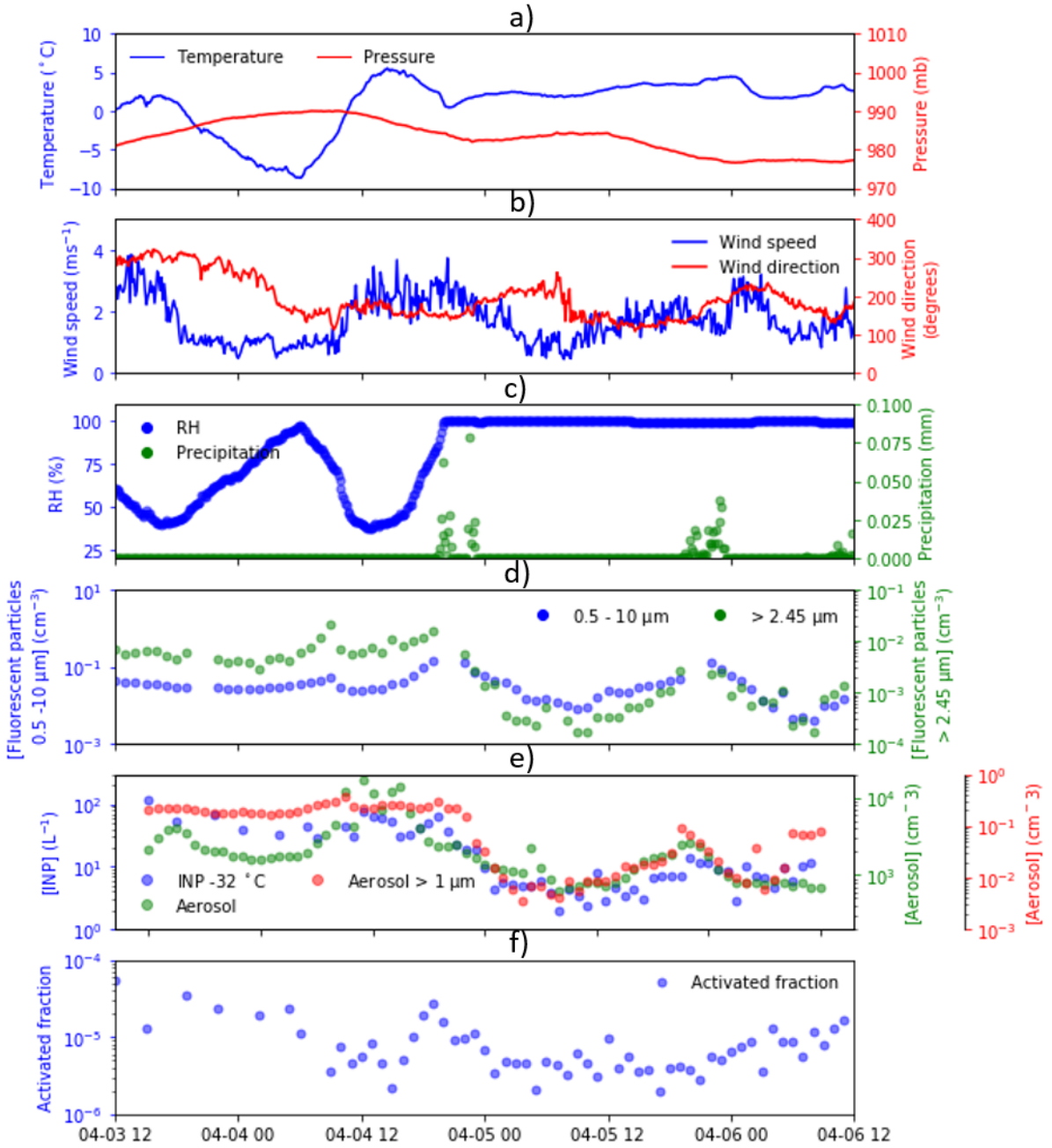

Figure 36: Data for case study 2 from 03/04/2018 – 06/04/2018. a) INP concentration at −32 °C as measured by the PINE chamber (blue), total aerosol concentration as measured by a DMPS (green), aerosol concentration of particles > 1 µm (red). Data is average into 60 minute intervals b) Temperature (blue) measured 4.2 m above ground, pressure (red) measured at ground level c) Wind speed (blue) and direction (red) measured 16.8 m above ground. d) Relative humdity measured 16.8 m above ground (blue) Precipitation measured (green) e) Fraction of aerosol particles active as INPs at −28 °C f) Fluorescent particle concentration > 0.5 µm (blue) > 2.4 µm (green).

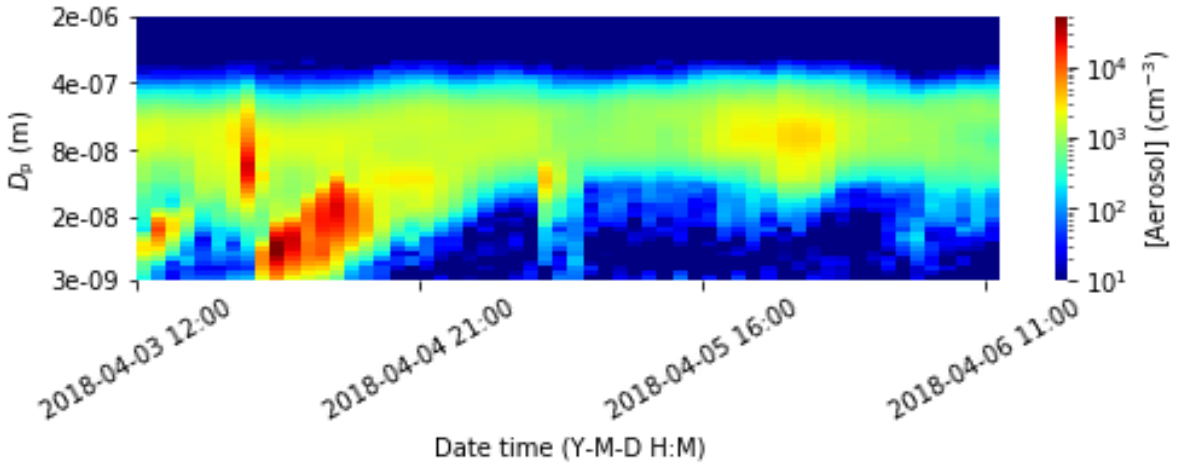

Figure 37: Size distribution of aerosol particle over time during the measurement period on 03/04/2020 12:00 - 06/04/2020 12:00.

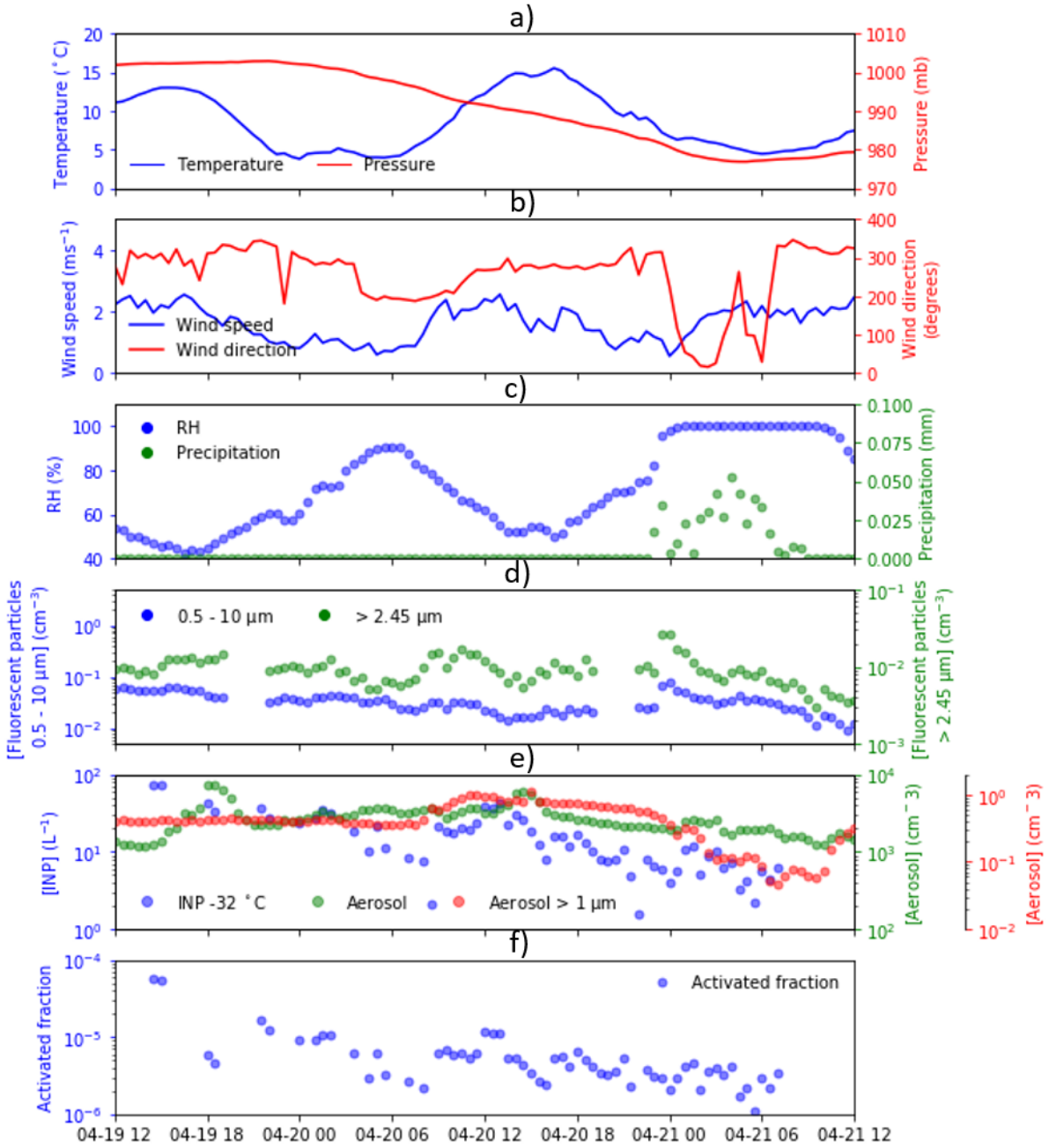

Figure 38: Data for case study 3 from 19/04/2018 – 21/04/2018. a) INP concentration at −28 °C as measured by the PINE chamber (blue), total aerosol concentration as measured by a DMPS (green). Data is average into 60 minute intervals b) Temperature (blue) measured 4.2 m above ground, pressure (red) measured at ground level c) Wind speed (blue) and direction (red) measured 16.8 m above ground. d) Relative humdity measured 16.8 m above ground e) Fraction of aerosol particles active as INPs at −28 °C.

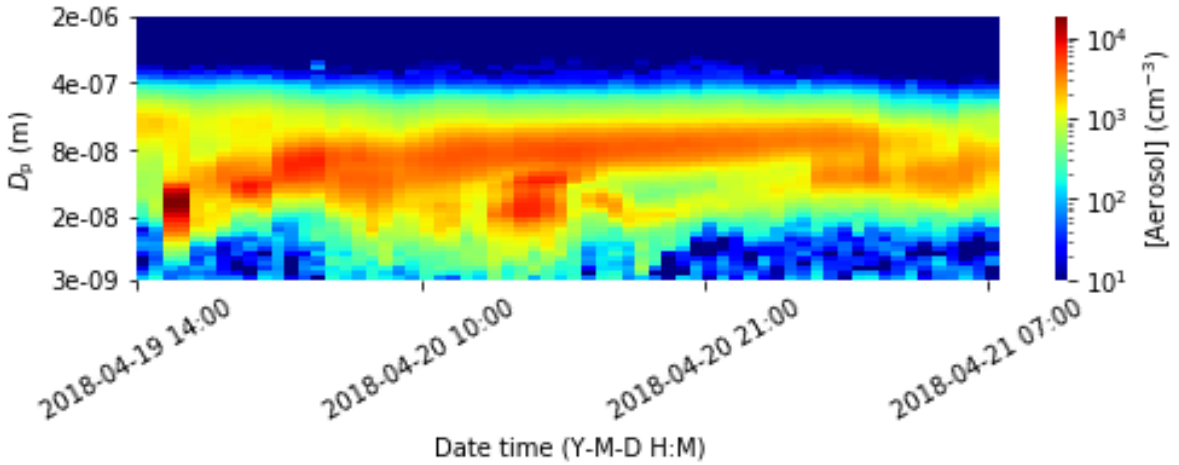

Figure 39: Size distribution of aerosol particle over time during the measurement period on 19/04/2020 12:00 - 21/04/2020 12:00.

Table 2: A R correlation analysis of INP concentrations at different temperatures with aerosol parameters.

Temp (°C)	−30	−32	Time averaging
R Total Conc.	0.047869	0.09658	10 minutes
R >500 nm	0.338015	-0.05734	
R >1000 nm	0.30359	0.201118	
R >2500 nm	0.3855	0.221841	
R <500 nm	0.047552	0.096638	
R <100 nm	0.047851	0.096569	
R <20 nm	0.047868	0.09658	
No. samples	909	1846	
R Total Conc.	0.064094	0.091991	60 minutes
R >500 nm	0.424807	-0.02752	
R >1000 nm	0.339885	0.237755	
R >2500 nm	0.449112	0.237384	
R <500 nm	0.063733	0.092017	
R <100 nm	0.064074	0.091977	
R <20 nm	0.064095	0.091991	
No. samples	230	386	
R Total Conc.	0.173311	0.093495	360 minutes
R >500 nm	0.585821	-0.00498	
R >1000 nm	0.406724	0.263267	
R >2500 nm	0.501946	0.256769	
R <500 nm	0.172781	0.093498	
R <100 nm	0.173287	0.093476	
R <20 nm	0.173311	0.093495	
No. samples	53	71	
R Total Conc.	0.214076	0.126692	720 minutes
R >500 nm	0.727917	-0.01647	
R >1000 nm	0.421702	0.27026	
R >2500 nm	0.53046	0.292029	
R <500 nm	0.213317	0.126734	
R <100 nm	0.214044	0.126669	
R <20 nm	0.214076	0.126692	
No. samples	30	40	
R Total Conc.	0.243602	0.18517	1440 minutes
R >500 nm	0.808212	-0.00408	
R >1000 nm	0.557746	0.36091	
R >2500 nm	0.520355	0.424227	
R <500 nm	0.242643	0.185189	
R <100 nm	0.243562	0.185136	
R <20 nm	0.243602	0.18517	
No. samples	18	21	

3.12 References

Atkinson, J. D., Murray, B. J., Woodhouse, M. T., Whale, T. F., Baustian, K. J., Carslaw, K. S., et al. (2013). The importance of feldspar for ice nucleation by mineral dust in mixed-phase clouds. Nature, 498(7454), 355–358. https://doi.org/10.1038/nature12278

Bi, K., McMeeking, G. R., Ding, D. P., Levin, E. J. T., DeMott, P. J., Zhao, D. L., et al. (2019). Measurements of Ice Nucleating Particles in Beijing, China. Journal of Geophysical Research: Atmospheres, 124(14), 8065–8075. https://doi.org/10.1029/2019JD030609

Boose, Y., Welti, A., Atkinson, J., Ramelli, F., Danielczok, A., Bingemer, H. G., et al. (2016). Heterogeneous ice nucleation on dust particles sourced from nine deserts worldwide - Part 1: Immersion freezing. Atmospheric Chemistry and Physics, 16(23), 15075–15095. https://doi.org/10.5194/acp-16-15075-2016

Boose, Y., Kanji, Z. A., Kohn, M., Sierau, B., Zipori, A., Crawford, I., et al. (2016). Ice nucleating particle measurements at 241K during winter months at 3580m MSL in the swiss alps. Journal of the Atmospheric Sciences, 73(5), 2203–2228. https://doi.org/10.1175/JAS-D-15-0236.1

Boucher, O., Randall, D., Artaxo, P., Bretherton, C., Feingold, G., Forster, P., et al. (2013). Clouds and Aerosols. In: Climate Change 2013: The Physical Science Basis. Contribution of Working Group I to the Fifth Assessment Report of the Intergovernmental Panel on Climate Change Coordinating Lead Authors: Lead Authors.

Choi, Y. S., Lindzen, R. S., Ho, C. H., & Kim, J. (2010). Space observations of cold-cloud phase change. Proceedings of the National Academy of Sciences of the United States of America, 107(25), 11211–11216. https://doi.org/10.1073/pnas.1006241107

DeMott, P. J., Sassen, K., Poellot, M. R., Baumgardner, D., Rogers, D. C., Brooks, S. D., et al. (2003). African dust aerosols as atmospheric ice nuclei. Geophysical Research Letters, 30(14). https://doi.org/10.1029/2003GL017410

DeMott, P. J., Hill, T. C. J., McCluskey, C. S., Prather, K. A., Collins, D. B., Sullivan, R. C., et al. (2016). Sea spray aerosol as a unique source of ice nucleating particles. Proceedings of the National Academy of Sciences of the United States of America, 113(21), 5797–803. https://doi.org/10.1073/pnas.1514034112

Herbert, R. J., Murray, B. J., Dobbie, S. J., & Koop, T. (2015). Sensitivity of liquid clouds to homogenous freezing parameterizations. Geophysical Research Letters, 42(5), 1599–1605. https://doi.org/10.1002/2014GL062729

Hill, T. C. J., Demott, P. J., Tobo, Y., Fröhlich-Nowoisky, J., Moffett, B. F., Franc, G. D., & Kreidenweis, S. M. (2016). Sources of organic ice nucleating particles in soils. Atmos. Chem. Phys, 16, 7195–7211. https://doi.org/10.5194/acp-16-7195-2016

Hoose, C., & Möhler, O. (2012). Heterogeneous ice nucleation on atmospheric aerosols: a review of results from laboratory experiments. Atmospheric Chemistry and Physics, 12(20), 9817–9854. https://doi.org/10.5194/acp-12-9817-2012

Hoose, C., Kristjánsson, J. E., & Burrows, S. M. (2010). How important is biological ice nucleation in clouds on a global scale? Environmental Research Letters, 5(2). https://doi.org/10.1088/1748-9326/5/2/024009

Irish, V. E., Elizondo, P., Chen, J., Chou, C., Charette, J., Lizotte, M., et al. (2017). Ice-nucleating particles in Canadian Arctic sea-surface microlayer and bulk seawater. Atmospheric Chemistry and Physics, 17(17), 10583–10595. https://doi.org/10.5194/acp-17-10583-2017

Irish, V. E., Hanna, S. J., Xi, Y., Boyer, M., Polishchuk, E., Ahmed, M., et al. (2019). Revisiting properties and concentrations of ice-nucleating particles in the sea surface microlayer and bulk seawater in the Canadian Arctic during summer. Atmospheric Chemistry and Physics, 19(11), 7775–7787. https://doi.org/10.5194/acp-19-7775-2019

Jahn, L. G., Fahy, W. D., Williams, D. B., & Sullivan, R. C. (2019). Role of Feldspar and Pyroxene Minerals in the Ice Nucleating Ability of Three Volcanic Ashes. ACS Earth and Space Chemistry, 3(4), 626–636. https://doi.org/10.1021/acsearthspacechem.9b00004

Kanitz, T., Seifert, P., Ansmann, A., Engelmann, R., Althausen, D., Casiccia, C., & Rohwer, E. G. (2011). Contrasting the impact of aerosols at northern and southern midlatitudes on heterogeneous ice formation. Geophysical Research Letters, 38(17), n/a-n/a. https://doi.org/10.1029/2011GL048532

Kanji, Z. A., Ladino, L. A., Wex, H., Boose, Y., Burkert-Kohn, M., Cziczo, D. J., et al. (2017). Overview of Ice Nucleating Particles. Meteorological Monographs, 58, 1.1-1.33. https://doi.org/10.1175/amsmonographs-d-16-0006.1

Korhonen, K., Kristensen, T. B., Falk, J., Lindgren, R., Andersen, C., Carvalho, R. L., et al. (2020). Ice-nucleating ability of particulate emissions from solid-biomass-fired cookstoves: an experimental study. Atmospheric Chemistry and Physics, 20(8), 4951–4968. https://doi.org/10.5194/acp-20-4951-2020

Kulmala, M., Hameri, K., Aalto, p. P., Makela, j. M., Pirjola, L., Nilsson, e. D., et al. (2001). Overview of the international project on biogenic aerosol formation in the boreal forest (BIOFOR). Tellus B, 53(4), 324–343. https://doi.org/10.1034/j.1600-0889.2001.530402.x

Mangan, T. P., Atkinson, J. D., Neuberg, J. W., O'Sullivan, D., Wilson, T. W., Whale, T. F., et al. (2017). Heterogeneous Ice Nucleation by Soufriere Hills Volcanic Ash Immersed in Water Droplets. PLOS ONE, 12(1), e0169720. https://doi.org/10.1371/journal.pone.0169720

Maters, E. C., Dingwell, D. B., Cimarelli, C., Müller, D., Whale, T. F., & Murray, B. J. (2019). The importance of crystalline phases in ice nucleation by volcanic ash. Atmospheric Chemistry and Physics, 19(8), 5451–5465. https://doi.org/10.5194/acp-19-5451-2019

Matus, A. V., & L'Ecuyer, T. S. (2017). The role of cloud phase in Earth's radiation budget. Journal of Geophysical Research: Atmospheres, 122(5), 2559–2578. https://doi.org/10.1002/2016JD025951

McCluskey, C. S., DeMott, P. J., Prenni, A. J., Levin, E. J. T., McMeeking, G. R., Sullivan, A. P., et al. (2014). Characteristics of atmospheric ice nucleating particles associated with biomass burning in the US: Prescribed burns and wildfires. Journal of Geophysical Research: Atmospheres, 119(17), 10458–10470. https://doi.org/10.1002/2014JD021980

Möhler, O., Stetzer, O., Schaefers, S., Linke, C., Schnaiter, M., Tiede, R., et al. (2003). Experimental investigation of homogeneous freezing of sulphuric acid particles in the aerosol chamber AIDA. Atmospheric Chemistry and Physics, 3(1), 211–223. https://doi.org/10.5194/acp-3-211-2003

Möhler, O., Büttner, S., Linke, C., Schnaiter, M., Saathoff, H., Stetzer, O., et al. (2005). Effect of sulfuric acid coating on heterogeneous ice nucleation by soot aerosol particles. Journal of Geophysical Research, 110(D11), D11210. https://doi.org/10.1029/2004JD005169

Murray, B. J., O'Sullivan, D., Atkinson, J. D., & Webb, M. E. (2012). Ice nucleation by particles immersed in supercooled cloud droplets. Chemical Society Reviews, 41(19), 6519. https://doi.org/10.1039/c2cs35200a

Murray, B. J., Carslaw, K. S., & Field, P. R. (2020). Opinion: Cloud-phase climate feedback and the importance of ice-nucleating particles. Atmospheric Chemistry and Physics. https://doi.org/10.5194/acp-2020-852

O'Sullivan, D., Adams, M. P., Tarn, M. D., Harrison, A. D., Vergara-Temprado, J., Porter, G. C. E., et al. (2018). Contributions of biogenic material to the atmospheric ice-nucleating particle population in North Western Europe. Scientific Reports, 8(1), 13821. https://doi.org/10.1038/s41598-018-31981-7

Ottmar Möhler, Adams, M. P., Lacher, L., Vogel, F., Nadolny, J., Ullrich, R., et al. (2020). AMTD - The portable ice nucleation experiment PINE: a new online instrument for laboratory studies and automated long-term field observations of ice-nucleating particles. Retrieved September 8, 2020, from https://amt.copernicus.org/preprints/amt-2020-307/

Paramonov, M., Drossaart van Dusseldorp, S., Gute, E., Abbatt, J. P. D., Heikkilä, P., Keskinen, J., et al. (2020). Condensation/immersion mode ice-nucleating particles in a boreal environment. Atmospheric Chemistry and Physics, 20(11), 6687–6706. https://doi.org/10.5194/acp-20-6687-2020

Phillips, V. T. J., Andronache, C., Christner, B., Morris, C. E., Sands, D. C., Bansemer, A., et al. (2009). Potential impacts from biological aerosols on ensembles of continental clouds simulated numerically. Biogeosciences, 6(6), 987–1014. https://doi.org/10.5194/bg-6-987-2009

Porter, G. C. E., Sikora, S. N. F., Adams, M. P., Proske, U., Harrison, A. D., Tarn, M. D., et al. (2020). Resolving the size of ice-nucleating particles with a balloon deployable aerosol sampler: the SHARK. Atmospheric Measurement Techniques, 13(6), 2905–2921. https://doi.org/10.5194/amt-13-2905-2020

Pruppacher, H. R., & Klett, J. D. (2010). Microstructure of Atmospheric Clouds and Precipitation (pp. 10–73). https://doi.org/10.1007/978-0-306-48100-0_2

Sanchez-Marroquin, A., Arnalds, O., Baustian-Dorsi, K. J., Browse, J., Dagsson-Waldhauserova, P., Harrison, A. D., et al. (2020). Iceland is an episodic source of atmospheric ice-nucleating particles relevant for mixed-phase clouds. Science Advances, 6(26), eaba8137. https://doi.org/10.1126/sciadv.aba8137

Sesartic, A., Lohmann, U., & Storelvmo, T. (2013). Modelling the impact of fungal spore ice nuclei on clouds and precipitation. Environmental Research Letters, 8(1), 014029. https://doi.org/10.1088/1748-9326/8/1/014029

Spracklen, D. V., & Heald, C. L. (2014). The contribution of fungal spores and bacteria to regional and global aerosol number and ice nucleation immersion freezing rates. Atmospheric Chemistry and Physics, 14(17), 9051–9059. https://doi.org/10.5194/acp-14-9051-2014

Spracklen, Dominick V., Bonn, B., & Carslaw, K. S. (2008). Boreal forests, aerosols and the impacts on clouds and climate. Philosophical Transactions of the Royal Society A: Mathematical, Physical and Engineering Sciences, 366(1885), 4613–4626. https://doi.org/10.1098/rsta.2008.0201

Steinke, I., Möhler, O., Kiselev, A., Niemand, M., Saathoff, H., Schnaiter, M., et al. (2011). Ice nucleation properties of fine ash particles from the Eyjafjallajökull eruption in April 2010. Atmospheric Chemistry and Physics, 11(24), 12945–12958. https://doi.org/10.5194/acp-11-12945-2011

Storelvmo, T. (2017). Aerosol Effects on Climate via Mixed-Phase and Ice Clouds. Annual Review of Earth and Planetary Sciences, 45(1), 199–222. https://doi.org/10.1146/annurev-earth-060115-012240

Storelvmo, T., Tan, I., & Korolev, A. V. (2015, December 1). Cloud Phase Changes Induced by CO2 Warming—a Powerful yet Poorly Constrained Cloud-Climate Feedback. Current Climate Change Reports. Springer. https://doi.org/10.1007/s40641-015-0026-2

Tan, I., Storelvmo, T., & Zelinka, M. D. (2016). Observational constraints on mixed-phase clouds imply higher climate sensitivity. Science (New York, N.Y.), 352(6282), 224–7. https://doi.org/10.1126/science.aad5300

Tobo, Y., Prenni, A. J., Demott, P. J., Huffman, J. A., McCluskey, C. S., Tian, G., et al. (2013). Biological aerosol particles as a key determinant of ice nuclei populations in a forest

ecosystem. Journal of Geophysical Research Atmospheres, 118(17), 10100–10110. https://doi.org/10.1002/jgrd.50801

Tobo, Y., Adachi, K., DeMott, P. J., Hill, T. C. J., Hamilton, D. S., Mahowald, N. M., et al. (2019). Glacially sourced dust as a potentially significant source of ice nucleating particles. Nature Geoscience, 12(April). https://doi.org/10.1038/s41561-019-0314-x

Tunved, P., Hansson, H. C., Kerminen, V. M., Ström, J., Dal Maso, M., Lihavainen, H., et al. (2006). High natural aerosol loading over boreal forests. Science, 312(5771), 261–263. https://doi.org/10.1126/science.1123052

Vali, G. (1971). Quantitative Evaluation of Experimental Results an the Heterogeneous Freezing Nucleation of Supercooled Liquids. Journal of the Atmospheric Sciences, 28(3), 402–409. https://doi.org/10.1175/1520-0469(1971)028<0402:QEOERA>2.0.CO;2

Whale, T. F., Murray, B. J., O'Sullivan, D., Wilson, T. W., Umo, N. S., Baustian, K. J., et al. (2015). A technique for quantifying heterogeneous ice nucleation in microlitre supercooled water droplets. Atmospheric Measurement Techniques, 8(6), 2437–2447. https://doi.org/10.5194/amt-8-2437-2015

Wilson, T. W., Ladino, L. A., Alpert, P. A., Breckels, M. N., Brooks, I. M., Browse, J., et al. (2015). A marine biogenic source of atmospheric ice-nucleating particles. Nature, 525(7568), 234–238. https://doi.org/10.1038/nature14986

Chapter 4
A major combustion aerosol event had a negligible impact on the atmospheric ice-nucleating particle population

M. P. Adams[1], M. D. Tarn[1,2], A. Sanchez-Marroquin[1], G. C. E. Porter[1,2], D. O'Sullivan[1,*], A. D. Harrison[1], Z. Cui[1], J. Vergara-Temprado[1,+], F. Carotenuto[3,4,^], M. A. Holden[1,2,5,~], M. I. Daily[1], T. F. Whale[1,5,>], S. N. F. Sikora[1], I. T. Burke[6], J.-u. Shim[2], J. B. McQuaid[1] and B. J. Murray[1]
1 – Institute of Climate and Atmospheric Science, School of Earth and Environment, University of Leeds, Woodhouse Lane, LS2 9JT, UK
2 –School of Physics and Astronomy, University of Leeds, Woodhouse Lane, LS2 9JT, UK
3 – University of Innsbruck, 6020, Austria
4 – CNR Institute of BioMeteorology, Florence, 50019, Italy
5 – School of Chemistry, University of Leeds, Woodhouse Lane, LS2 9JT, UK

6 – Earth Science Institute, School of Earth and Environment, University of Leeds, Woodhouse Lane, LS2 9JT, UK

* Now at The Stars Group, Wellington place, Leeds, West Yorkshire, UK

+ Now at Institute for Atmospheric and Climate Science, ETH Zürich, Zurich, Switzerland

^ Now at CNR Institute of BioEconomy, Florence, 50019, Italy

~ Now at School of Physical Sciences and Computing, University of Central Lancashire, Fylde Road, Preston, PR1 2HE, UK

> Now at Department of Chemistry, University of Warwick, Gibbet Hill Road, Coventry, CV4 7AL, UK

A manuscript that forms the basis for this chapter has been published in JGR: Atmospheres with the author list stated above. The main manuscript and Supplementary Information (SI) from the accepted version have been merged for completeness in the forming of this chapter.

Chapter 4 is based on a paper published in the Journal of Geophysical Research: Atmospheres, entitled A major combustion aerosol event had a negligible impact on the atmospheric ice-nucleating particle population (10.1029/2020JD032938). The paper describes measurements made during the U.K. based celebration of Bonfire Night, and surrounding days, in 2016 and 2017. I am the lead author on this paper, conceptualising it with BJM. MPA, BJM, MDT, GCEP, DOS, ADH, FC, JBM and MID all made measurements during the Bonfire Night celebrations. ASM carried out the SEM analysis, assisted by ITB. SNFS gave technical assistance. JVT advised on comparisons to GLOMAP and literature data. ZC provided HySPLIT back trajectories. All authors assisted in the writing of the manuscript.

I led every section of this chapter, however MDT contributed much of the discussion on the pico-litre Nucleation by Immersed Particle Instrument (pL-NIPI) technique in section 4.2.3

(INP analysis), and ASM contributed heavily to section 4.2.5 (Scanning electron microscopy). ZC made Figures 41-44, ASM made Figure 51. I made all other Figures.

Abstract

Clouds containing supercooled water are important for both climate and weather, but our knowledge of which aerosol particle types nucleate ice in these clouds is far from complete. Combustion aerosols have strong anthropogenic sources and if these aerosol types were to nucleate ice in clouds they might exert a climate forcing. Here, we quantified the atmospheric ice-nucleating particle (INP) concentrations during the UK's annual Bonfire Night celebrations, which are characterised by large amounts of combustion aerosol from bonfires and fireworks. We used three immersion mode techniques covering more than six orders of magnitude in INP concentration over the temperature range from −10 °C to homogeneous freezing. We found no observable systematic change in the INP concentration on three separate nights, despite more than a factor of 10 increase in aerosol number concentrations, up to a factor of 10 increase in PM10 concentration and more than a factor of 100 increase in black carbon (BC) mass concentration relative to pre-event levels. This implies that BC and other combustion aerosol such as ash did not compete with the INPs present in the background air. Furthermore, the upper limit of the ice-active site surface density, ns(T), of BC generated in these events was shown to be consistent with several other recent laboratory studies, showing a very low ice-nucleating activity of BC. We conclude that combustion aerosol particles similar to those emitted on Bonfire Night are at most of secondary importance for the INP population relevant for mixed-phase clouds in typical mid-latitude terrestrial locations.

4.1 Introduction

The formation of ice in supercooled water droplets plays a central role in regulating cloud properties, such as radiative forcing and lifetime, as well as the generation of precipitation (Hoose & Möhler, 2012; Kanji et al., 2017b; U. Lohmann et al., 2006; B. J. Murray et al., 2012; Rosenfeld et al., 2011). While ice nucleation only occurs spontaneously in supercooled clouds at temperatures below around −33 °C (Herbert et al., 2015), ice-nucleating particles (INPs) can catalyse the freezing process at higher temperatures. Clouds composed of supercooled water or mixtures of supercooled water and ice, which are referred to as mixed-phase clouds, exist in the lower to mid-troposphere and are susceptible to the presence of INPs. The formation of ice in shallow clouds tends to reduce the amount of liquid water in them and decrease their albedo (Vergara-Temprado et al., 2018). Representing the contribution and evolution of cloud ice processes in both the present day and a future warmer climate is important for obtaining accurate climate predictions (Storelvmo, 2017; Tan et al., 2016). Hence, it is essential that we identify and quantify all relevant sources of INPs to understand their impact on mixed-phase clouds.

In general, it is thought that, in the mixed-phase regime (~ −38 °C to 0 °C), ice formation only becomes significant once a liquid cloud exists, hence the pathways involving liquid water are thought to be most relevant (A. Ansmann et al., 2009; de Boer et al., 2011; B. J. Murray et al., 2012; Westbrook & Illingworth, 2011). INPs are also important for upper tropospheric ice

clouds (Cziczo et al., 2013; Paul J. DeMott et al., 2003), but the pathways of ice formation are distinct under those colder conditions and we do not consider INPs relevant for in situ-formed cirrus type clouds here (Vali et al., 2015). What makes certain aerosol particles effective at nucleating ice under mixed phase conditions is complex and poorly understood. Recent work indicates that ice-active sites on mineral nucleators require a specific combination of chemistry and topography (Holden et al., 2019), whereas some biological materials, like specific bacteria, have evolved the capacity to produce proteins that nucleate ice (Šantl-Temkiv et al., 2015). As a result of both our limited understanding and also the fact that different materials nucleate ice through different mechanisms, we have no a priori means of establishing if a particular material is an effective ice nucleator. There has been much discussion over whether aerosol from combustion processes are important as INPs, with mixed conclusions (Ardon-Dryer & Levin, 2014; Chen et al., 2018; DeMott, 1990; Grawe et al., 2018; Kanji et al., 2020; Mahrt et al., 2018; McCluskey et al., 2014; Schill et al., 2016; Umo et al., 2015; Vergara-Temprado et al., 2018). This is significant because carbonaceous combustion aerosol, and presumably other aerosol associated with combustion such as ash, have increased in concentration dramatically since pre-industrial times and therefore have the potential to exert a significant anthropogenic impact on clouds and climate (Bond et al., 2013; Lavanchy, Gäggeler, Schotterer, Schwikowski, & Baltensperger, 1999; D. V. Spracklen, Carslaw, Pöschl, Rap, & Forster, 2011).

The composition of combustion aerosol is massively variable, depending on fuel types and combustion conditions (Elsasser et al., 2013; Lighty et al., 2000). Soot particles, with characteristic fractal morphologies, are synonymous with incomplete combustion. Once emitted, soot aerosol then evolve through the uptake of other chemical species, undergoing heterogeneous reactions and aggregating with other aerosol types; it is then referred to with the more general term, black carbon (BC) (Petzold et al., 2013). Lower temperature combustion can result in the formation of organic rich particles, termed tar balls (Adachi & Buseck, 2011; Pósfai et al., 2004). In addition, inorganic components of the fuels can form ash particles that can also be lofted into the atmosphere (DeMott, 2003; Kumai, 1961). Clearly, laboratory studies of ice nucleation by combustion products are valuable, but real-world combustion aerosol is likely to have much more varied compositions and therefore could conceivably have very different ice-nucleating properties.

Previous studies in the field have been carried out to investigate the relationship between combustion and INP concentrations relevant for mixed-phase clouds, with conflicting results. During a field campaign, Twohy et al. (2010) observed that, in mixed-phase clouds, there was a strong correlation between BC and ice crystal concentration, implying that aerosol containing BC may act as INPs. However, ice crystal residues from the same campaign were not obviously enhanced in BC or other combustion aerosol (Pratt et al., 2009). McCluskey et al. (2014) found that a substantial number of INPs (up to 64 % for some of the samples) from wildfires and prescribed burns were identified as BC particles via analysis with a scanning electron microscope (SEM), while Petters et al. (2009) conducted laboratory burns with controlled fuel types and found that some fuels created aerosols that nucleated ice whilst others did not. Others have measured INPs emitted from forest fires and shown that aerosol particles produced from biomass burning can act as a source of INPs (Prenni et al., 2012; Hobbs and Locatelli, 1969). For example, Prenni et al. (2012) suggested that whilst the fraction of aerosol able to nucleate ice is relatively small, the high concentration of particles emitted

from a forest fire means that these aerosol could be an important source of INPs. Levin et al. (2016) investigated contributions of BC from biomass burning to the atmospheric INP burden, finding a positive relationship between BC and INP concentrations. Furthermore, observations of ice crystal residues sampled at mountain top sites revealed that there are instances in which they were composed of BC (Cozic et al., 2008), while in other cases BC was not observed (Baustian et al., 2012; Kamphus et al., 2010).

In addition to the above studies on the activity of wildfires or controlled burns of natural fuels, there have also been studies of aerosol produced by bonfire burning and more general human-related pollution aerosol in which combustion aerosol plays a major role. Ardon-Dryer and Levin (2014) investigated the effect of the Lag BaOmer festival, when bonfires are lit across Israel, on local INP concentrations. They found INP concentrations to be higher before the festival began, despite a clear rise in total aerosol concentration after the start of the festival. Chen et al. (2018) took measurements in Beijing, China, where combustion aerosol are in abundance, over a 30-day field campaign. In this study, no relationship was found between INP concentrations and either total particle number or BC concentration. More recently in Beijing, Bi et al. (2019) also observed no clear relation between INP concentrations and pollution events (defined by the increase in fine mode aerosol along with back trajectories that passed over heavily industrialised areas). A study investigating the potential of a steel mill as a source of INPs found that air influenced by emissions from the steel mill did have higher INP concentrations than ambient air at temperatures above −12 °C, but concluded that the mill was unlikely to have any effect on the synoptic scale as the INPs were not detectable at distances greater than 15 km (Schnell, Pueschel, Weickmann, & Wellman, 1980). Hartmann et al. (2019) measured historic INP concentrations in the European Arctic using ice cores from up to 500 years ago. They found no correlation between increasing anthropogenic aerosol (with BC being specifically measured) reaching the Arctic and INP concentrations, which were found to be similar to present day concentrations and without a long-term trend (i.e. INP concentrations did not increase with increasing anthropogenic emissions). A study combining observational data with model simulations in an effort to understand the potential importance of anthropogenic aerosols as INPs indicated that polluted continental aerosols contain a significant fraction of INPs (Zhao et al., 2019). Whether these INP were associated with combustion aerosol or other terrestrial INP types is unclear. Overall, the evidence from observations and field campaigns is mixed, without a clear resolution as to whether combustion aerosol is an important source of INPs.

There have also been a number of laboratory studies carried out to investigate the ice-nucleating potential of BC and other combustion aerosol types produced in a variety of ways, again with contrasting results. There is evidence that BC nucleates ice when immersed in (or at least in the presence of) supercooled droplets (DeMott, 1990; Diehl & Mitra, 1998; Fornea et al., 2009; Gorbunov et al., 2001; Kireeva et al., 2009; Popovicheva et al., 2008; Wright et al., 2013). In addition, carbon-based materials including graphene oxides and carbon nanotubes nucleate ice, which shows that carbon-rich materials have the potential to nucleate ice (Alstadt, Dawson, Losey, Sihvonen, & Freedman, 2017; Bai et al., 2019; Whale et al., 2015). Murray et al. (2012) parameterised data from DeMott (1990), who used soot from an oxygen deficient acetylene burner, and Diehl and Mitra (1998), who used a kerosene burner, by calculating the ice-active site surface density, $n_s(T)$, of BC, and concluded that BC may be a very important INP type globally. However, more recent work strongly contradicts

this conclusion. Schill et al. (2016) found that the concentration of immersion mode INPs produced by an off-road diesel engine was below their limit of detection at −30 °C, thus reporting upper limits for the ice-nucleating activity of BC, and suggested that previous literature parameterisations were likely overestimating the importance of BC-based INPs, especially in the Northern Hemisphere. Similarly, measurements reported by Ullrich et al. (2017) showed that droplets containing BC particles in the AIDA (Aerosol Interaction and Dynamics in the Atmosphere) cloud simulation chamber did not exhibit heterogeneous freezing in sufficient quantity (i.e. a low number of ice crystals was observed) to constitute a signal, and hence their results were also presented as upper limits. Mahrt et al. (2018) observed no evidence of immersion/condensation freezing above water saturation using a continuous flow diffusion chamber (CFDC), regardless of particle size or physiochemical properties, based on measurements of commercially available soots and laboratory-generated propane-based soots. Kanji et al. (2020) made similar measurements to that of Mahrt et al., (2018), demonstrating that different soot/BC types generated from synthetic and fossil fuels at atmospherically relevant size do not effectively nucleate ice in their system. Vergara-Temprado et al. (2018a) investigated the relationship between INP concentrations and BC produced from two different fuel sources, *n*-decane and eugenol, by immersing particles in microlitre volume droplets. No freezing was observed at temperatures above those in the control experiments. The authors were able to derive limiting values of the effectiveness of BC's ability to nucleate ice and suggested that, even given the copious amounts of BC in the atmosphere, BC does not compete with other INP types, such as mineral dust.
Far fewer studies of ice nucleation by combustion ashes have been performed, but it has been shown that ashes from multiple fuels nucleate ice with varying effectiveness. However, the amounts of ash in the atmosphere are poorly constrained and it is therefore difficult to determine their importance (Grawe et al., 2016; Grawe et al., 2018; Umo et al., 2015; Umo et al., 2019).

Overall, the picture of whether combustion aerosol is important for ice nucleation is far from clear. The fuel burned and the combustion conditions play important roles in controlling the properties of the ash and aerosol produced, hence it might be expected that the ice nucleating properties are also variable (Levin et al., 2016; Christina S. McCluskey et al., 2014; Markus D. Petters et al., 2009). Hence, a fruitful approach may be to target real-world combustion events that produce combustion aerosol from a range of fuels and combustion conditions in order to assess whether these events yield elevated (or reduced) INP concentrations.

In this study, we made measurements during a combustion aerosol event associated with the Bonfire Night, or Guy Fawkes Night, festivities that are widely celebrated annually on and around the 5th November across the United Kingdom and involve the burning of bonfires and setting off of fireworks. Measurements were made over one day and night in 2016 (during the day on 05/11/2016 (dd/mm/yyyy) and into the early hours of the following morning), and over two days and nights in 2017 (04/11/2017 and 05/11/2017). During these events, the bonfires consist of a range of combustible materials. These fuels include: waste wood, some of which is untreated while some is treated with a range of preservatives and paints; garden waste, including branches, leaves, stems of plants etc, with varying water content; and household waste from old newspapers and cardboard to plastic and rubber items. These bonfires produce large quantities of combustion aerosol that can be observed from space

(Pope, Marshall, & O'Kane, 2016). Fireworks also produce combustion aerosol, and potentially release aerosol containing trace metals into the atmosphere (Lin, 2016). Previous studies have shown increases in aerosol concentration during cultural celebrations of a similar nature (Ardon-Dryer & Levin, 2014; Moreno et al., 2007; Singh, Bloss, & Pope, 2015), with the aerosol produced during these events containing a mixture of BC, unburnt hydrocarbons, combustion ashes, and aerosols composed of metals and sulphates that are associated with fireworks (Jiang, Sun, Wang, & Yin, 2015) (Jiang et al., 2015; Reyes-Villegas et al., 2018). Another factor that can affect the aerosol produced is the temperature of the bonfires, with typical bonfires being between 600 - 1100 °C when lit. Given that atmospheric aerosol and BC concentrations are well known to be significantly enhanced during Bonfire Night, we would therefore anticipate an enhancement in ambient INP concentrations if the combustion aerosols produced were effective INPs.

4.2 Methods

4.2.1 Sampling site, meteorological conditions and air mass origins

Aerosol sampling was performed on the balcony of the School of Earth and Environment building which is approximately 15 m above surface level. This measuring site was chosen in part because it is some distance from any point sources of combustion aerosol. The site was more than ~0.5 km from any specific bonfires or firework displays in order to provide a representative overview of combustion aerosol emitted across the city during Bonfire Night, and also being situated in the centre of the Campus it is around 0.3 km from any major roads, suburban areas and other typical urban combustion sources. Bonfire Night is typically celebrated with small fires and fireworks in private gardens as well as more significant fires and firework displays at organised events at designated sites in, for example, suburban parks. The vast majority of the festivities are in the suburbs and less densely built up areas, hence the University of Leeds campus (53.8067° N, 1.5550° W), which is located close to Leeds city centre, was chosen a sampling location. A map indicating the sampling point and the surrounding urban location can be seen in Figure 40a and Figure 40 1b respectively.

Air mass back trajectories corresponding to the INP sampling periods, determined using HYSPLIT (Stein et al., 2015), are in Figures 43-46. The evening of 05/11/2016 (16:00-01:00) was characterised with moderately strong northerly winds (2.9 m s^{-1} average speed), a lack of precipitation, and temperatures ranging from 3.3-7.3 °C. The air masses uniformly came from the North of the UK, the North Sea and Scandinavia. The sampling period of 04/11/2017 (15:30-23:30) saw north-westerly winds (1.3 m s^{-1} average speed), no precipitation, and temperatures ranging between 6.1-10.3 °C. The air masses uniformly came across the North Atlantic Ocean, having been in the Canadian Arctic 120 h previously. The sampling period of 05/11/2017 (16:00-02:30) had similar characteristics to that of the previous evening, with the air masses having travelled uniformly over the North Atlantic Ocean from the Canadian Arctic. Wind speed was at an average of 0.9 m s^{-1}, no precipitation was observed, and temperatures ranged between 2.3-8.6 °C.

The fact that the air mass back trajectories were uniform in origin during each of the sampling periods, were all free from precipitation, and saw similar temperature variation, allowed for comparison between sampling periods. Hence any changes in the INP concentration might be more readily attributed to Bonfire Night combustion aerosol. Given that the majority of the combustion aerosol we sampled would have come from the suburbs of the city of Leeds, i.e.

from about 0.5 to ~10 km away, this corresponds to a time between emission and sampling of between 3 and 60 minutes for the 05/11/2016 and 15 to 180 minutes for the lower wind day of 05/11/2017. A recent review of biomass burning (biomass burning is not entirely representative of bonfire night but there are some notable similarities i.e. wood burning) plumes suggests a possible correlation between biomass burning plumes where the aerosol has been aged for less than 5 hours (which would include all our measurements) and a PM mass increase; however, it is not clear if this correlation is real due to a low number of data points (Hodshire et al., 2019). The same review showed a distinct positive correlation between oxidation (based on organic aerosol composition markers) and aging. As INPs are not necessarily related to bulk particle properties, it remains unclear how any of these factors may affect the ice-nucleating ability of the combustion aerosol we sampled.

4.2.2 Aerosol sampling

Aerosol was sampled onto 0.4 µm pore size track-etched membrane polycarbonate filters (Nuclepore, Whatman) using an omnidirectional ambient air particulate sampler (BGI PQ100, Mesa Laboratories Inc.) designed to US Environmental Protection Agency (EPA) regulations (designation no. RFPS-1298-124). The PQ100 had a PM_{10} cut-off and sampled at a volumetric flow rate of 16.7 L min^{-1} (i.e. 1 m^3 h^{-1}). Despite the pore size in the filters being 0.4 µm, the filters retain a high collection efficiency for particles much smaller than this through a variety of mechanisms, as shown in various studies (Lindsley, 2014; Soo, Monaghan, Lee, Kashon, & Harper, 2016). Based on data from these studies the minimum collection efficiency of the filters occurs at 30 nm, with the efficiency being 85%. The collection efficiency was much higher over the rest of the aerosol size distribution (approaching 100%). The filter samples in this study were collected approximately hourly in order to provide sufficient temporal resolution to track the evolution of the combustion events, and also to collect enough aerosol to obtain detectable INP signals. Sampling times were chosen in order to encompass the conditions before and after the celebrations started, and the corresponding rise and fall in aerosol concentrations. Table 3 shows the sampling time and the volume of collected air of each filter.

4.2.3 INP analysis

After sampling, each filter was washed with 5 mL of purified water (18.2 MΩ cm at 25 °C, 0.22 µm filtered) for 1 h on a rotary mixer (Clifton RM-1, Nickel-Electro Ltd.) operated at 0.5 Hz, similar to previously described methods (Thomas C J Hill et al., 2014; O'Sullivan et al., 2018), in order to generate a suspension of the collected aerosol particles. The suspensions were then subjected to immersion mode freezing analysis using three different but complementary cold stage techniques to quantify ambient INP concentrations over more than six orders of magnitude (~10^{-3} to 10^3 L^{-1} of air), covering a key range of atmospheric relevance. Each cold stage instrument uses a different droplet volume during the freezing experiment, and the size of the droplet is directly proportional to the freezing temperature when measuring the same species of INP. Simply, the greater the droplet volume, the more likely that more active (in terms of freezing temperature) INPs will be present (Vali, 1971).

The InfraRed Nucleation by Immersed Particles Instrument (IR-NIPI) is a large volume drop freeze assay employs a 96 multiwell plate containing 50 µL aliquots of sample, which is placed upon a cold plate. The operation of the IR-NIPI is described in Harrison et al. (2018), wherein

the multiwell plate containing the droplet array is cooled at 1 °C min^{-1} until all of the droplets are frozen. This cooling process is monitored by an infrared camera and a time lapse of thermal images is taken. When a droplet freezes, it releases heat energy that is detected by the IR camera, which is used to determine the temperature at which the droplet froze. The microlitre Nucleation by Immersed Particle Instrument (µL-NIPI) (Whale et al., 2015) involves pipetting ~50 droplets of 1 µL volume onto a hydrophobic glass slide that is positioned on a cold stage. The droplets are frozen upon cooling the stage to −40 °C at 1 °C min^{-1}, with the freezing temperature for each droplet recorded via a digital camera. Finally, a microfluidic platform was employed to generate 278 ± 66 pL droplets of aqueous sample for analysis using a Peltier element-based version of the picolitre Nucleation by Immersed Particle Instrument (pL-NIPI) technique (Tarn et al., 2018), which had previously comprised of a nebuliser for droplet production and a liquid nitrogen-based cold stage for cooling (O'Sullivan et al., 2014). Water-in-oil droplets were generated on-chip and collected off-chip, then cooled to −40 °C at 1 °C min^{-1} on the Peltier element-based cold stage, with freezing events recorded using a digital camera. The fabrication and operation of the microfluidic chip and cold stage are described by Tarn et al. (2018). Briefly, the microfluidic chip featured a flow-focussing droplet generation structure that was fabricated in polydimethylsiloxane (PDMS) using standard soft lithography procedures, allowing water-in-oil droplets to be produced using a fluorinated oil phase (3M™ Novec™ 7500 oil containing 2 % w/w Pico-Surf™ 1 surfactant, Sphere Fluidics, UK). All collected aerosol samples were analysed using the µL-NIPI, but only selected samples were further analysed using the IR-NIPI and the microfluidic pL-NIPI. Control experiments were performed using handling blanks by putting a filter through the entire experimental process apart from having air sampled through it.

The number of INPs per unit volume of sampled air, $[\mathrm{INP}]_T$, were calculated from the immersion mode freezing analysis using equation 33, adapted from Vali (1971):

$$[\mathrm{INP}]_T = \frac{-\ln(1-f_{\mathrm{ice}}(T))}{V_{\mathrm{d}}} \cdot \frac{V_{\mathrm{w}}}{V_{\mathrm{a}}} \qquad (33)$$

where $f_{ice}(T)$ is the fraction of droplets frozen at temperature T, V_d is the droplet volume, V_w is the volume of water used to wash particles off the filter (i.e. 5 mL), and V_a is the volume of air sampled through the filter. V_d varies between different NIPI instruments as described above, and the details of V_a for each sample are provided in Table 3. In order to estimate the uncertainty in the INP concentrations we used a method that accounts for the randomness of the distribution of ice-nucleation active sites across the droplets in the experiment, and also accounts for the counting uncertainty associated with detecting ice-nucleation active sites within a population (Harrison et al., 2016).

4.2.4 Online aerosol monitoring

Aerosol size distributions and BC mass loading were measured throughout the event, allowing for the comparison of INP concentrations with varying aerosol and BC loadings. In order to measure particle size distributions an aerodynamic particle sizer (APS; Model 3321, TSI Inc.) was used during all three sampling periods, while a scanning mobility particle sizer (SMPS; Model 3936, TSI Inc.) was used in 2016 only. Unfortunately, the SMPS system was not operational in 2017. The APS was sensitive to a particle diameter distribution in the range of 0.542-19.81 µm (aerodynamic), whereas the SMPS had an effective range of 17.5-552.3 nm

(electrical mobility). A BC aethalometer (microAeth AE51, Aethlabs) was used to measure BC mass concentrations (ng m^{-3}) with a specific attenuation of 12.5 m^2 g^{-1} applied to convert optical attenuation into mass. Comparisons of the AE51 (single wavelength, 880 nm) to the widely used AE31 (multi-wavelength) aethalometer can be found in the literature, and showed that the measured BC mass concentrations agreed to within 14 % (Cheng & Lin, 2013). PM_{10} concentration data was also obtained from a Department for Environment, Food and Rural Affairs (DEFRA) station based in Leeds city centre (approximately 1 km away from the sampling site).

4.2.5 Scanning electron microscopy

Further to the aerosol instrumentation, several filter samples were taken in parallel to those collected for INP measurements so that scanning electron microscopy (SEM) could then be employed to obtain chemical composition and size distributions of the aerosol particles trapped on the filters using the technique described by (Sanchez-Marroquin et al., 2019). The filters collected for SEM analysis had similar time resolutions to those used for INP analysis, but were not measured at exactly the same time. In brief, the SEM analysis was performed using a Tescan Vega3 XM scanning electron microscope fitted with an X-max 150 SDD energy-dispersive X-ray spectroscopy (EDS) system, and controlled by AZtec 3.3 software with a particle analysis expansion (AZtecFeature). Filter samples were coated with 30 nm of iridium prior to analysis, and the microscope was operated at 20 keV and a working distance of 15 mm using the secondary electron detector. The particles were scanned in different areas across the filter, using two different magnifications: approximately ×5,000 for particles with a diameter greater than 0.3 µm and approximately ×1,500 for particles greater than 1 µm in diameter. The particle identification was performed based on the relative brightness with respect to the background. The equivalent circular diameter of each particle (defined as $(4A_p/\pi)^{0.5}$, where A_p is the cross-sectional area of the particle) was extracted from each image of the filter to obtain a size distribution. In addition, EDS was performed in the centre of some of the particles of each image (50,000 counts per particle), from which the measured spectra were used to calculate elemental weight percentages using the AZtec software. In total, more than 4,000 particles per filter were analysed. Using these elemental weight percentages, particles were then categorised according to their composition using a sequential algorithm in the AZtecFeature software. The scanning electron microscopy with energy-dispersive X-ray spectroscopy (SEM-EDS) classification of particles into different categories was achieved using the same methodology as described in Sanchez-Marroquin et al., (2019), with some slight changes: 'Na rich' and 'S rich' particles have been combined into one category, along with unclassified particles (labelled as 'Others'). Particles in the categories of 'Si only', 'Si rich', 'Al-Si rich' ad 'Ca rich' have been considered as being mineral dust or ash. In this work, typically <5 % of particles in each sample were not classified by the scheme and are labelled as 'Others' in the results.

4.3 Results and discussion

4.3.1 Atmospheric INP measurements

The atmospheric INP concentrations as a function of temperature ($[INP]_T$) for the three nights are presented in Figure 45a, with the $[INP]_T$ spectra colour coded for BC concentration. Measurements were made over six orders of magnitude, from 1.5×10^{-3} to 4×10^3 INP L^{-1}, using the three different cold stage devices (Figure 45a). The maximum variation in INP

concentration at a given temperature throughout the $[INP]_T$ spectra in Figure 45a was approximately 1.5 orders of magnitude. The spectra on each day were similar to one another during the three sampling periods over the two years, as shown in Figure 45b.

Figure 45a also shows the range of INP concentrations reported for locations across the terrestrial northern hemisphere mid-latitudes based on the INP content of precipitation samples (Petters & Wright, 2015). The majority of the measured INP concentrations fell within the range defined by Petters & Wright, (2015), with a small fraction being slightly above this range between temperatures of −15 and −22 °C. This showed that, during the majority of the measurement periods, INP concentrations fell within a typical range for the terrestrial mid-latitudes.

The colour coded $[INP]_T$ spectra in Figure 45a indicate that there was no correlation of BC with INP concentration in the measured temperature regime. To further demonstrate the lack of $[INP]_T$ dependence on BC (a tracer for combustion aerosol), Figure 45c shows a correlation plot comparing the change in $[INP]_T$ at −20 °C (chosen as we have the greatest number of data points at this temperature) with the change in mean BC mass concentration throughout the sampling duration for different samples. The relatively low R^2 values on each day indicate that the concentrations of INP and BC were not correlated. Fraction frozen curves for all of the spectra, from which the INP concentration plots were derived, are shown in the Figure 46 alongside those of the handling blanks.

4.3.2 Time evolution of aerosol and INP concentrations

In Figure 47, we compare the time evolution of $[INP]_T$ with a measure of aerosol loading and BC mass during the three distinct combustion events.
Relatively low aerosol concentrations (measured with an APS; ~0.5-20 µm particle diameter range) were observed until around 18:00 on all three sampling days, before the majority of Bonfire Night celebrations began (Figure 47a). At around this time on each day, aerosol concentrations began to rise, and increased by over one order of magnitude in 2016 and two orders of magnitude over both days in 2017.

During the 05/11/2016 sampling event, the SMPS (~18-550 nm particle diameter range) also measured an increase in total aerosol number concentration of approximately an order of magnitude (Figure 48). The full size distribution for a selection of times is shown for 05/11/2016 in Figure 49a-b, with APS size distributions only for both 2017 events shown in Figure 10b-f. In Figure 49f (05/11/2017) a large increase in coarse mode aerosol surface can be seen in the 00:00 size distribution, which may correspond to the increase in number concentration seen during that evet after 22:00. These number and surface area distributions demonstrate that the aerosol concentration increased across the fine and coarse modes over the course of the combustion event. On 05/11/2016, aerosol concentrations returned to relatively low levels once the main celebrations had concluded (approximately 22:00). However, for the sampling periods on 04/11/2017 and 05/11/2017, the high concentrations persisted until the earlier hours of the following morning, with the 05/11/2017 aerosol concentrations remaining well above background levels until measurements were stopped shortly after 02:00 on 06/11/2017. This is consistent with the greater wind speeds on the evening of the 05/11/2016, which resulted in the polluted air being swept away and replaced with cleaner air. A plot of PM_{10} concentrations from a Leeds city centre air monitoring station

for each sampling day is also shown in Figure 50. The trends show qualitative agreement between the APS data from the measurement site and the PM_{10} monitoring station, indicating that the increases in aerosol concentration during the combustion events were representative of a wider area across the city.

The variation in BC concentrations throughout the three events is shown in Figure 47b. On each of the sampling days, BC began to substantially increase at approximately 18:00, peaking at 5-30 μg m^{-3} and remaining elevated for several hours. During 05/11/2016, BC concentrations peaked between 19:00-20:00 and then decreased throughout the remainder of the sampling period. On 04/11/2017, BC concentrations peaked at approximately 21:30 and again at 22:45, reaching concentrations of 15 μg m^{-3}, which mirrored the corresponding aerosol concentration shown in Figure 47a. Thereafter, the BC concentrations began to subside, but remained significantly elevated when compared to pre-event concentrations. The sampling event on 05/11/2017 saw an extreme peak at 19:30, with BC concentrations measured at 31 μg m^{-3}, before subsiding to similar levels to those observed on 04/11/2017. Similarly, to the aerosol concentrations, the 04/11/2017 BC concentrations remained elevated into the early hours of the next day.

The INP concentrations at a series of temperatures for each combustion event are shown in Figures 8c-e on the same time scale as the aerosol and BC measurements. As can be seen, despite large increases in aerosol concentration and BC from 18:00 onwards (Figures 8a-b), no corresponding increases in INP concentrations were observed outside of the random run-to-run variability, i.e. about a factor of two (based on the standard deviation of $[INP]_T$; see Table 4). The low variability in $[INP]_T$ is consistent with the back trajectory analyses (Figures 2-5), which revealed fortuitous sampling conditions in which the air mass origins exhibited very little variability within each sampling period. Hence, these air masses were exposed to similar INP sources during their transport within each sampling period. This was fortunate, because it allowed us to make a direct comparison of $[INP]_T$ spectra between peak pollution times and prior to the events. The lack of dependency of INP concentration on aerosol loading is particularly striking between about 19:00 and 21:00 on 05/11/2016, 21:00 and 22:00 on 04/11/2017, and 19:00 and 20:00 on 05/11/2017, as these time periods showed a peak in terms of aerosol and BC concentrations. This suggests that the aerosol emitted during these combustion events did not substantially contribute to the atmospheric INP population. As discussed above, the INP concentrations observed in Leeds were typical of mid-latitude INP concentrations (see the Petters & Wright (2015) data in Figure 45), and thus the concentrations of ambient INPs were not unusually high, hence an increase in activity due to the presence of a new source of INPs would likely have been noticeable. It would be interesting to conduct a similar series of experiments in a very low INP environment, such as a location influenced directly by remote marine air (Paul J DeMott et al., 2016; Christina S. McCluskey et al., 2018), where any ice-nucleating ability of combustion aerosol might become apparent.

4.3.3 Aerosol particle characterisation by SEM-EDS

SEM-EDS was used to measure the chemical composition of two filter samples collected on 05/11/2017 (16:05-17:25, referred to as ‘early’; 00:00-00:45, referred to as ‘peak loading’) using the methodology defined previously (Sanchez-Marroquin et al., 2019). Figure 51 shows the size distribution in terms of particle number concentration and particle surface area

concentration for both filters, broken down into groups based on their chemical composition. For both filters, the aerosol samples were dominated by carbonaceous particles, which are consistent with organic aerosol, primary biogenic particles or BC. In addition, there were significant contributions of mineral dust and/or ash (particles in the categories "Si only", "Si rich", "Al-Si rich" and "Ca rich"), and particles dominated by metal signals, mainly Fe and Al ("Metal rich"), which could have a crustal or anthropogenic origin. In addition, there was also a significant fraction of "Cl rich" particles. Particles in this category were dominated by the presence of Cl (and sometimes K) but not Na, so they were not compatible with sea spray aerosol (which appear in the "Na rich" category) (Sanchez-Marroquin et al., 2019). These Cl-rich particles may originate from fireworks set off during the festivities, which often contain metal chlorides and some potassium compounds in the form of perchlorates or chlorates, among many other components (Don-Yuan Liu, Dan Rutherford, Matt Kinsey, & Prather, 1997; Li et al., 2017; Lin, 2016). Crespo et al. (2012), for example, reported strong increases in Cl and K concentrations in the fine aerosol fraction, as well as a significant increase in the coarse fraction, during a pyrotechnic event. Further, a study of forty-one wildfires in the United States showed that increased concentrations of Cl and K are also associated with wildfires (Schlosser et al., 2017), suggesting that the observed increase in Cl and K rich particles during the sampling event may also be due to the burning of wood and other biomass on bonfires.

In terms of changes between the early and peak event filters, a clear increase can be seen in the concentration of carbonaceous particles, particularly those above 1 µm diameter that most likely resulted from incomplete combustion. A clear increase in Cl-containing aerosol was observed that was probably associated with pyrotechnics, although it could potentially be attributed to biomass burning. An increase in mineral dust/ash particles was also observed across all sizes, which may be related to emissions of combustion ash particles; this is discussed further below. However, the measured surface areas for each filter in the mineral dust/ash category were within error of each other (6 ± 4 µm^2 cm^{-3} for the peak filter and 1.3 ± 0.7 µm^2 cm^{-3} for the early filter). Overall, the chemistry of the aerosol particle population changed in a manner consistent with what we would qualitatively expect over Bonfire Night. Figure 52 shows images of a filter before and after sampling to give an example of the aerosol loading.

4.3.4 Contribution of atmospheric INP by combustion ash and mineral dust

The difference measured between the early and peak filters in the mineral dust/ash category from the SEM-EDS analysis is potentially explained by an increase in ash lofted from bonfires as part of the celebration. In order to quantify the potential contribution of ash to the atmospheric INP concentration, the SEM-EDS measurement for the surface area concentration of mineral dust/ash in the atmosphere from the 'peak' filter (6 ± 4 µm^2 cm^{-3}) was taken as an upper limit to the ash surface area contributed by the combustion event. We used this surface area measurement with the ice nucleation activity parameterisation for wood bottom ash from Umo et al. (2015) to calculate an upper limit to the potential contribution of ash to the atmospheric INP concentration. Coal fly ash was found to be more active than bottom ashes (Grawe et al., 2018;Umo et al., 2015), but is probably not relevant for Bonfire Night emissions. Umo et al. (2015) derived their n_s parameterisation using a surface area derived from gas adsorption measurements, which generally produce a larger surface area than the geometric surface area. Hence, this may produce an estimate of INP

concentration which is biased low, but he bias is most likely not large enough to change the conclusions below. It should also be noted that bottom ash samples are not necessarily an ideal proxy for combustion ash aerosol produced on Bonfire Night, but the activity of the ash component of combustion aerosol has not been measured. The ice nucleating activity of combustion ash is thought to be related to the mineral components of this material (Grawe et al., 2018;Umo et al., 2015).

Across the entire temperature range that the Umo et al. (2015) parameterisation is valid for (−11 to −34 °C), the upper limit to the contribution of atmospheric INPs is well below the measured $[INP]_T$ (Figure 53). Thus, we conclude that any combustion ash emitted as part of the combustion events would have been a minor component in the overall atmospheric INP burden; this is consistent with the lack of variation of the $[INP]_T$ spectra throughout each event. However, we do not rule out combustion ashes being important in other situations due to the caveats with this analysis (described above).

Based on the SEM-EDS measurements, inferences can be made to the composition of the background INP population. While it was not the focus of this study, it is interesting to question what the INP species were in the atmosphere at this time. O'Sullivan et al. (2018) carried out a detailed study on INP concentrations and species in a location ~19 km from the Bonfire Night sampling site at the same time of year to the measurements made in this study. As such, we refer to the detailed discussion of that paper with regards to the interpretation of what INP species may have contributed to the local INP population. In brief, that study found that background INP concentrations were dominated by mineral dust at T < −18 °C, and above this temperature bio-INPs played an important but highly variable role.

In order to understand the contribution of mineral dust to the INP spectra we report, we used two parameterisations for calculating $[INP]_T$ based on mineral/desert dust surface area, in conjunction with the SEM-EDS mineral dust/ash surface area from section 3.3. We used two different mineral dust parameterisations, one based on the ice-active K-feldspar content of desert dust (H19) and one based on measurements of freshly dispersed desert dust (N12) (Harrison et al., 2019; Niemand et al., 2012). For the H19 parameterisation, a 1 wt. % concentration of K-feldspar has been assumed. The predictions are shown in Figure 54. The shaded area for each parameterisation shows the range of INP concentrations predicted by the surface area concentrations from both the "early" and "peak" filters analysed using SEM-EDS, including uncertainties. Figure 54 shows that both parameterisations capture some of the data below –20 °C, with INP concentrations above –20 °C sometimes being above the ranges predicted by both N12 and H19. The N12 parameterisation predicts a higher INP concentration than H19 above about -20 °C, which is a better fit to the data, however INP measurements in desert dust plumes indicate that N12 produces too high an ice nucleation activity in transported dust, especially above about -20 °C (Price et al., 2018). No heat tests were performed in this study, so it is not possible to distinguish between heat sensitive biological INPs and non-heat sensitive INP like mineral dust. Nevertheless, the results in Figure 54 are consistent with those of O'Sullivan et al. (2018).

4.3.5 Limiting ice-active site surface density, ns(T), for black carbon

The datasets produced during this study provided an opportunity to estimate a limiting value for the ice-nucleating ability of atmospheric BC associated with bonfires and fireworks.

Previous estimates of the ice-nucleating ability of BC were based on experiments of laboratory-generated soot samples, whereas in this study we have based our estimate on atmospheric BC that has undergone some degree of processing in the atmosphere and is produced by a range of fuels and combustion conditions. We determined an upper limit to the ice-active site surface density, $n_s(T)$, for BC using the mass concentration of BC shown in Figure 47b, together with INP concentrations measured throughout the combustion events. To estimate an upper limit for the ice-nucleating efficiency of BC, it was assumed that all ice nucleation in the samples was due to BC, which is certainly an overestimate but is consistent with the notion of an upper limit. Estimating a surface area of BC allowed $n_s(T)$ values to be calculated using equation 2 (Connolly et al., 2009):

$$n_s(T) = \frac{-\ln(1 - f_{ice}(T))}{A} \quad (34)$$

where $f_{ice}(T)$ is the cumulative fraction of droplets frozen on cooling to temperature T during the cold stage experiments, and A is the surface area of BC per droplet. The estimation of A was determined by assuming that each BC particle was a sphere of 140 nm diameter and had a density of 1.2 g cm^{-3}, based on literature data for BC produced from combustion aerosol (Bond et al., 2013; Gong et al., 2016; Zhang et al., 2016). These assumptions most likely lead to an underestimate in A, which is also consistent with the notion of an upper limit of $n_s(T)$.

We show the limiting $n_s(T)$ values from each sample in Figure 55, colour-coded to indicate the mean BC mass concentration during the sampling period (as in Figure 45a). The sampling periods with highest BC concentrations defined the lowest of the limiting values of $n_s(T)$. We fit a polynomial curve to the lowest $n_s(T)$ values, which correspond to the most constrained upper limits we can define (shown by the magenta curve in Figure 56). The equation for the fit is $n_s(T) = \exp(-3.76336674 \times 10^{-4}\ T^4 - 3.25873608 \times 10^{-2}\ T^3 - 9.92600404 \times 10^{-1}\ T^2 - 1.29473300 \times 10^{1}\ T - 4.97896324 \times 10^{1})$.

We then compared our fit to literature parameterisations for the n_s of BC in Figure 56. The parameterisation from Murray et al. (2012) based on data from DeMott (1990) and Diehl & Mitra (1998), is 3-4 orders of magnitude higher than the limiting value produced from this study in the overlapping temperature range (−18 - −33 °C). Using the Murray et al., (2012) parameterisation with the highest BC loading captured by a filter during the Bonfire Night festival in our study would give an $[INP]_T$ of approximately 105 L^{-1} at −20 °C, a value substantially greater than any measured during our campaign. The parameterisations from Phillips et al. (2008) and Phillips et al. (2013) are both below the Murray et al., (2012) parameterisation in terms of $n_s(T)$, but are still above our estimate for a limiting $n_s(T)$ value by more than 2 orders of magnitude for nearly the entire overlapping temperature range.

More recent studies of the ice-nucleating ability of BC have, like our Bonfire Night study, produced relatively low upper limits to the ice-nucleating ability of BC (Schill et al., 2016; Ullrich et al., 2017; Vergara-Temprado et al., 2018). These parameterisation are based on data for BC from a number of different fuel sources and combustion conditions, all where no activity was observed. Overall, in the context of the literature data, the limiting value of $n_s(T)$ for BC-based INPs in this study is similar to the values presented by the more recent studies (Schill et al., 2016; Ullrich et al., 2017; Vergara-Temprado et al., 2018)., thus contributing

further evidence to the growing perception that BC is of secondary importance as an INP in mixed-phase clouds in the terrestrial mid-latitudes. However, why the earlier work indicated that BC is an effective ice nucleating material (B. J. Murray et al., 2012; Vaughan T. J. Phillips et al., 2008, 2013), is unclear and it may be that combustion of some fuels under some conditions can produce BC that is strongly ice active. As mentioned above, elemental carbon in some forms has been shown to nucleate ice effectively (Alstadt et al., 2017; Bai et al., 2019; Whale et al., 2015), but it remains unclear if this highly ice-active form of black carbon is atmospherically important. Nevertheless, we have shown that BC generated on Bonfire Night from a range of fuels and combustion conditions has a very low ice nucleating activity and does not significantly enhance the INP population.

4.4 Conclusions

INP concentrations were monitored during three similar combustion aerosol events, alongside measurements of aerosol size distribution and BC mass concentration. We took advantage of the annual Bonfire Night celebrations, an annual major bonfire and firework event that takes place across the UK during the evenings on and around 5th November. We demonstrated that the combustion aerosol generated did not measurably enhance the atmospheric INP concentrations despite a large increase in BC and aerosol concentrations throughout the events. This indicates that BC and other combustion aerosol generated during Bonfire Night are relatively poor INPs, and are unable to compete with the background INPs already present in the atmosphere. Using these atmospheric measurements, we derived an upper limit for the ice-active site surface density, $n_s(T)$, of BC, which was consistent with several recent laboratory-derived upper limits. The fact that the BC concentrations peaked at such a high value during our sampling campaign helped to provide a robust constraint to the ice-nucleating ability of BC generated during this type of event. The BC loading during our sampling periods peaked at approximately 31 μg m^{-3}, with sustained concentrations of 10-15 μg m^{-3} being observed over the course of the combustion aerosol event on the 05/11/2017, which is of a similar magnitude to concentrations observed in some of the most polluted parts of the world (Chen et al., 2018; Chen et al., 2016; Cooke & Wilson, 1996b). Concentrations in the mid-troposphere are typically well below 0.1 μg m^{-3} (Koch et al., 2009; Wofsy, 2011). However, there are some literature studies that have found significant INP activity for BC (Paul J. DeMott, 1990; Diehl & Mitra, 1998; Levin et al., 2016; Popovicheva et al., 2008), combustion ashes (Grawe et al., 2016; Umo et al., 2015), and combustion aerosol more generally (Christina S. McCluskey et al., 2014; Markus D. Petters et al., 2009; Anthony J. Prenni, Petters, et al., 2009), hence we cannot discount the possibility that some combination of fuels and combustion conditions might produce more ice-active combustion aerosol. This may be especially true in locations where the background INP loading is relatively low, where even a relatively weak ice-nucleating activity in combustion aerosols may be locally or regionally important for mixed-phase clouds.

Acknowledgments

This work was funded by the European Research Council (H2020 ERC, grants: 648661 MarineIce and 713664 CryoProtect), the Natural Environment Research Council (NERC, grants NE/M010473/1, NE/L013479/1), the EU-BACCHUS consortium (FP7/2007-797 2013; 603445) and the Engineering and Physical Sciences Research Council (EPSRC, grant EP/M003027/1). Special thanks to Wolfgang Buermann for use of his office during sampling, and Franz Conen (University of Basel) for the loan of a Mesa Labs BGI PQ100 sampling unit. The authors declare

no conflicts of interest. The data associated with this paper are openly available from the University of Leeds Data Repository https://doi.org/10.5518/809.

4.5 Figures and tables

Figure 40: A map of the a) immediate area around the sampling site b) the wider Leeds area. The light blue line indicates the 0.5 km area surrounding sampling site that is University campus, with the dark blue line showing the 10 km surrounding suburban area.

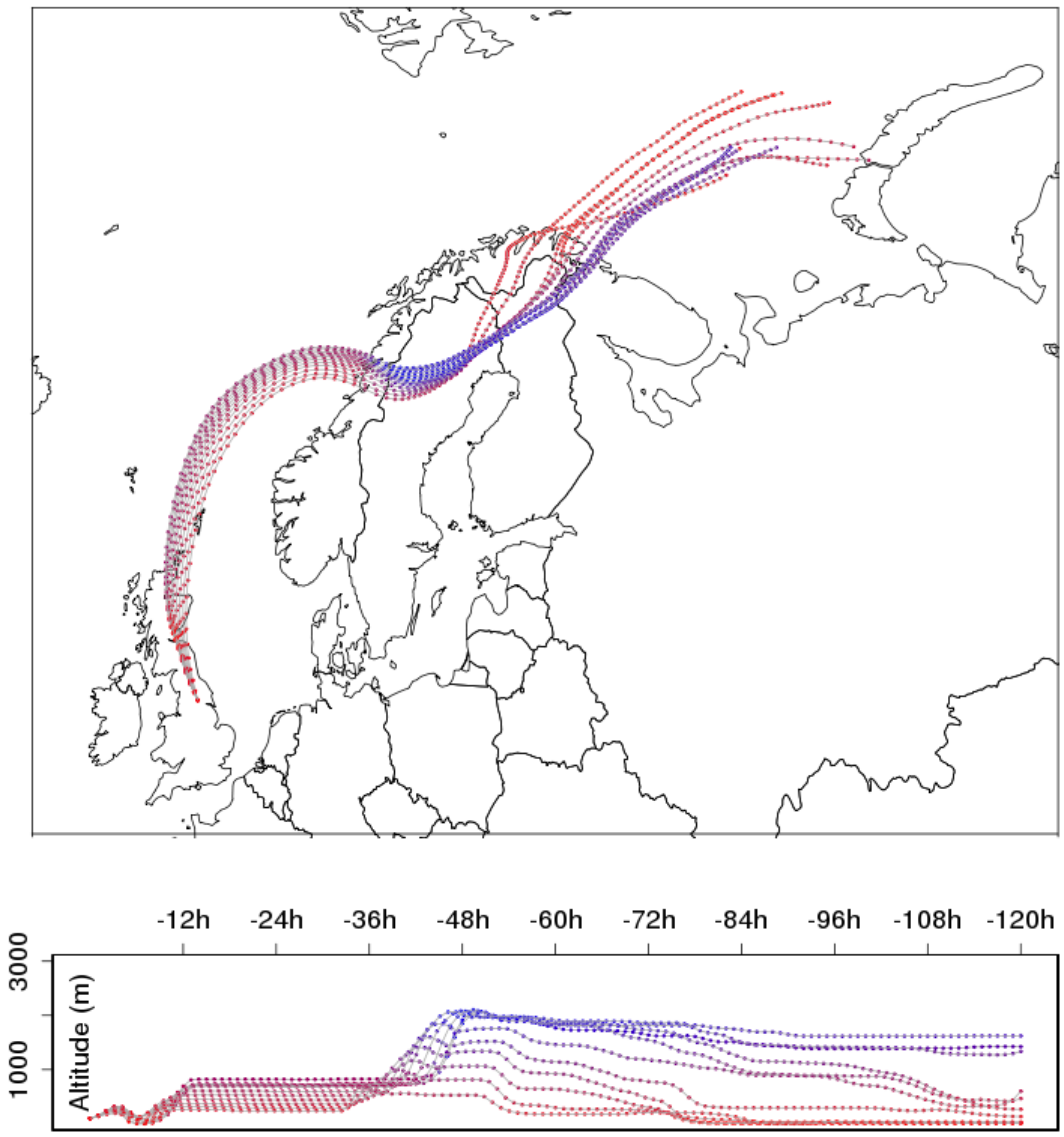

Figure 41: Backward trajectories of air masses during the sampling period on 05/11/2016 (DD/MM/YYY). The back trajectories are shown hourly, up to 120 h prior to the collection of a sample onto a filter. The colour scale shows the altitude of the air masses throughout the back trajectory, with red indicating a lower altitude and blue indicating a higher altitude. The back trajectories were generated using the NOAA HYSPLIT model (Stein et al., 2015).

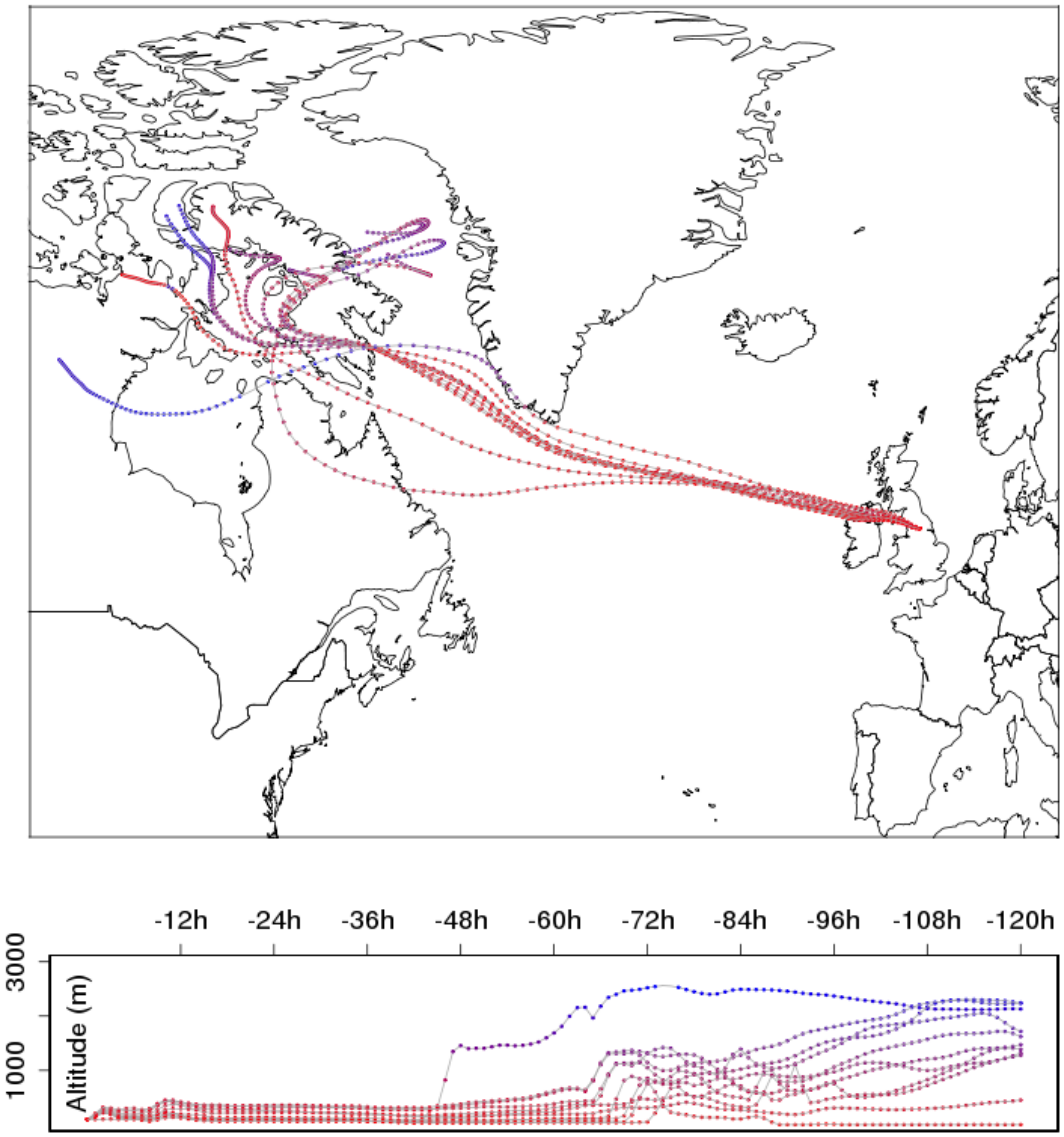

Figure 42: Backward trajectories of air masses during the sampling period on 04/11/2017 (DD/MM/YYY). The back trajectories are shown hourly, up to 120 h prior to the collection of a sample onto a filter. The colour scale shows the altitude of the air masses throughout the back trajectory, with red indicating a lower altitude and blue indicating a higher altitude. The back trajectories were generated using the NOAA HYSPLIT model (Stein et al., 2015).

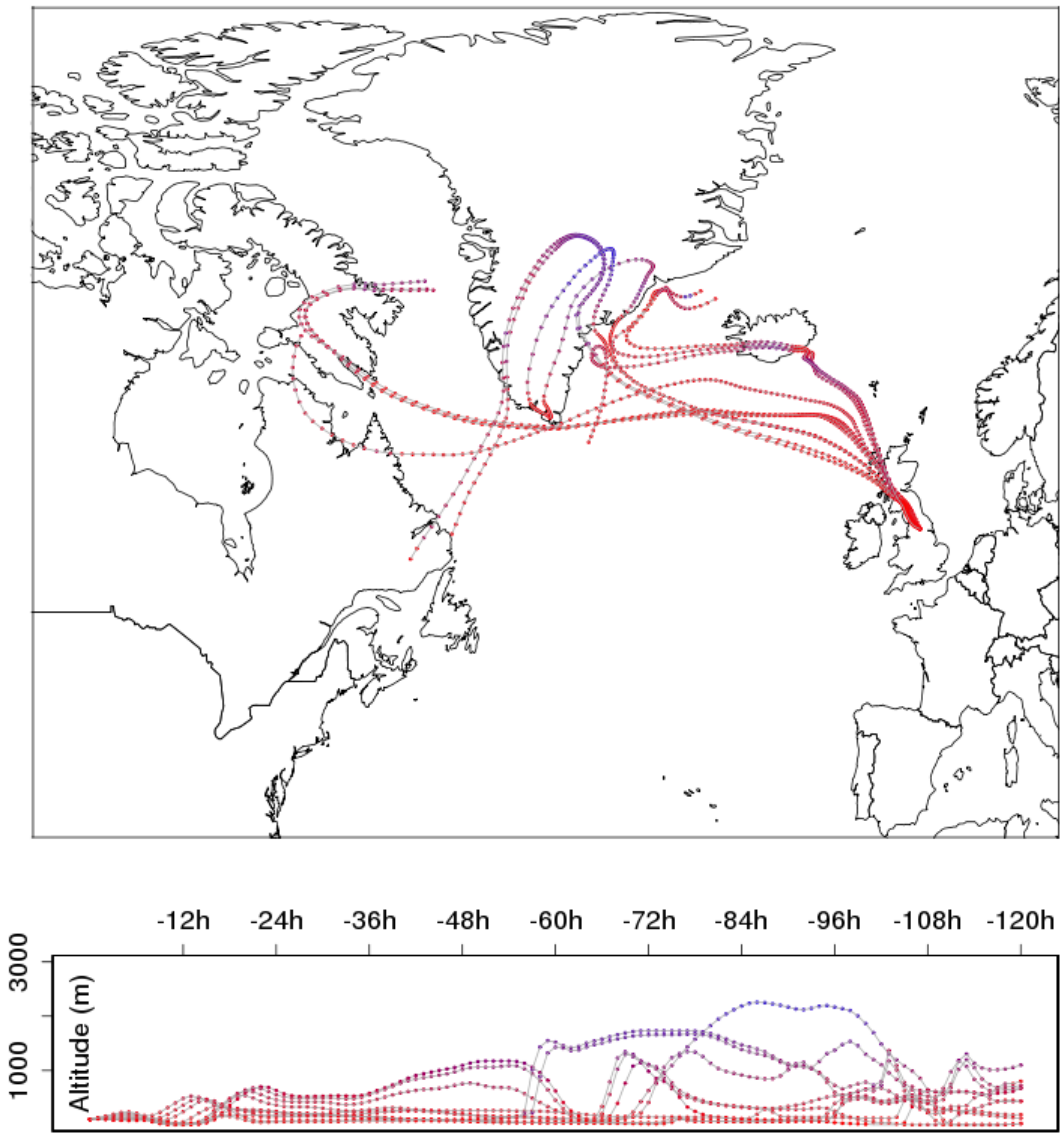

Figure 43: Backward trajectories of air masses during the sampling period on 05/11/2017 (DD/MM/YYY). The back trajectories are shown hourly, up to 120 h prior to the collection of a sample onto a filter. The colour scale shows the altitude of the air masses throughout the back trajectory, with red indicating a lower altitude and blue indicating a higher altitude. The back trajectories were generated using the NOAA HYSPLIT model (Stein et al., 2015).

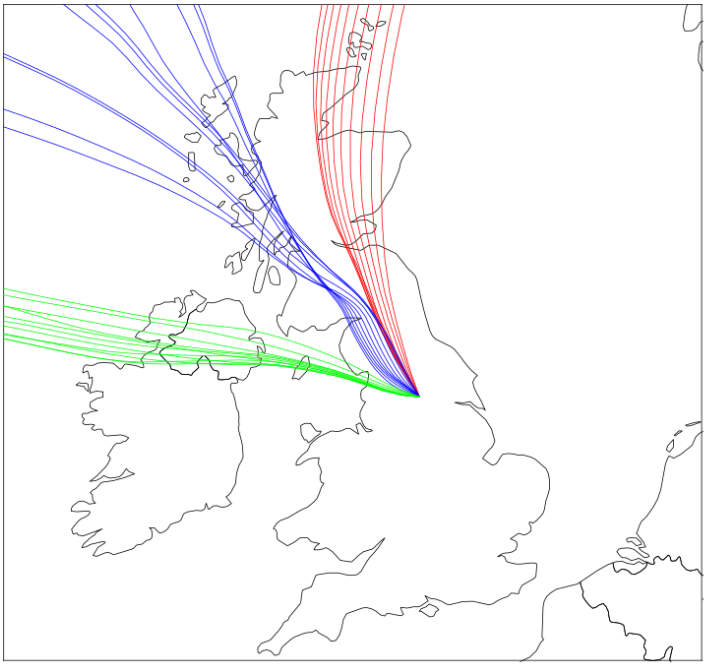

Figure 44: HYSPLIT back trajectories for all three days, zoomed in on the U.K. Red indicates 05/11/2016, green 04/11/2017, blue 05/11/2017.

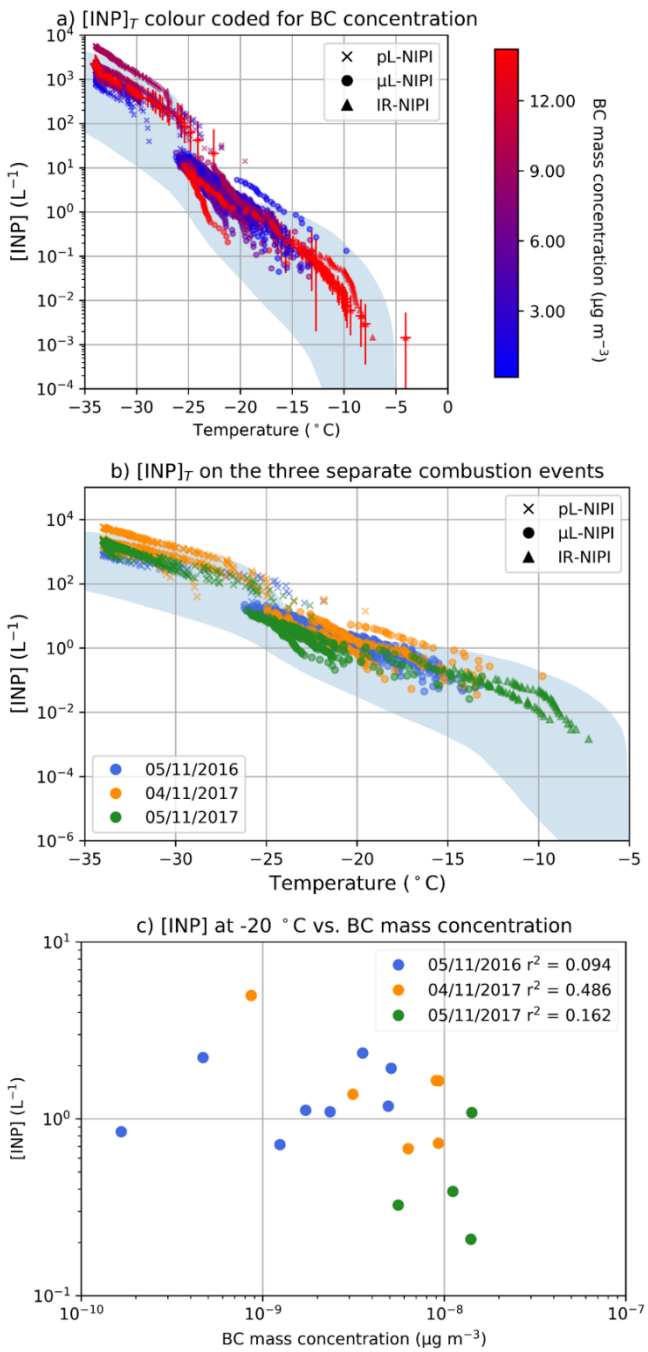

Figure 45: Atmospheric INP concentrations measured during the three sampling periods and their relationship to black carbon (BC). (a) Atmospheric $[INP]_T$ spectra corresponding to each filter sample collected during three combustion aerosol events. The IR-NIPI obtained measurements from about −8 to −15 °C (for a small number of samples), the µL-NIPI in the range −15 to −25 °C (for all samples), and the pL-NIPI in the range −25 to −34 °C (for a selection of samples). The blue envelope is based upon the range of observed INP concentrations in mid-latitude terrestrial environments (Petters & Wright, 2015). The $[INP]_T$ spectra are colour coded according to the mean BC mass concentration during the run sample time, as measured by the aethalometer. The first sample taken on 05/11/2017 is not included as the aethalometer was only operating for part of the sampling time. (b) The same plot as in a) but in which the $[INP]_T$ are colour coded by day. (c) A correlation plot

showing [INP] at −20 °C versus BC mass concentration, colour coded by day. Error bars are shown on a selection of spectra on each cold stage device.

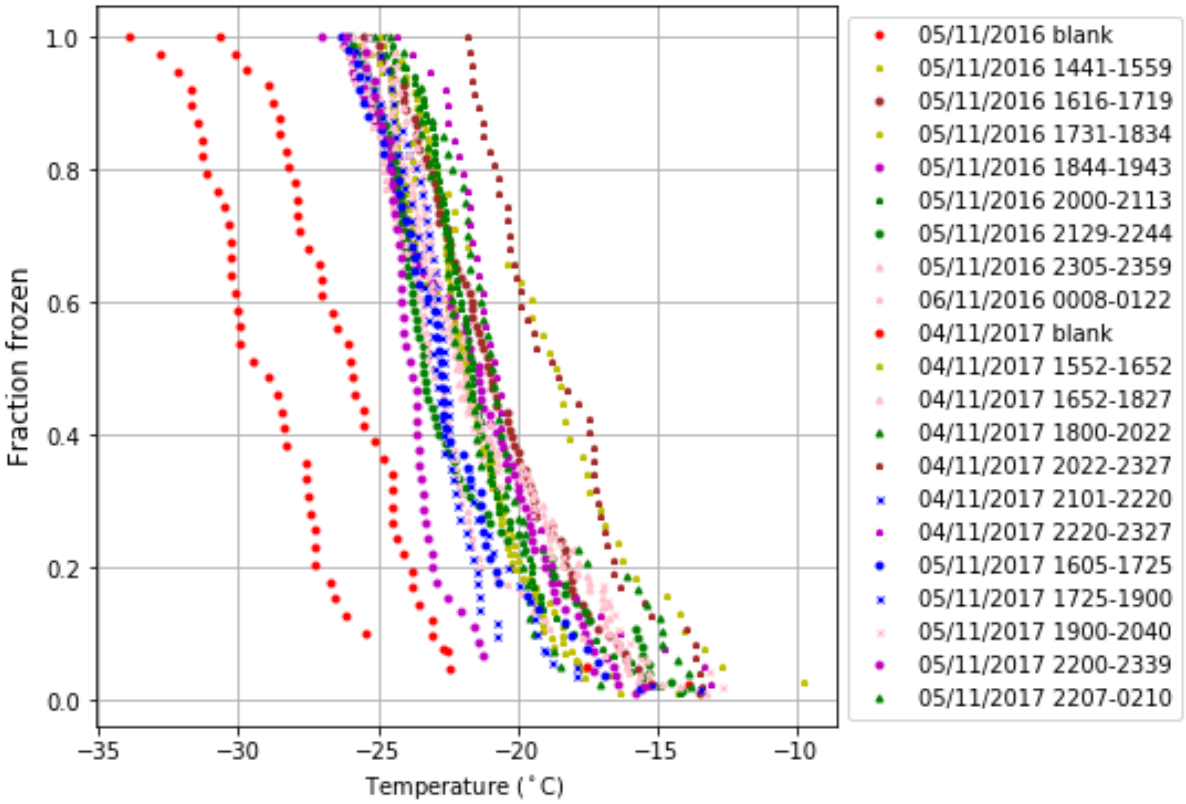

Figure 46: Fraction frozen curves for each sample collected and analysed via the microlitre Nucleation by Immersed Particle Instrument (µL-NIPI) technique during the Bonfire Night festivals over two years. A handling blank was also run each year prior to sampling.

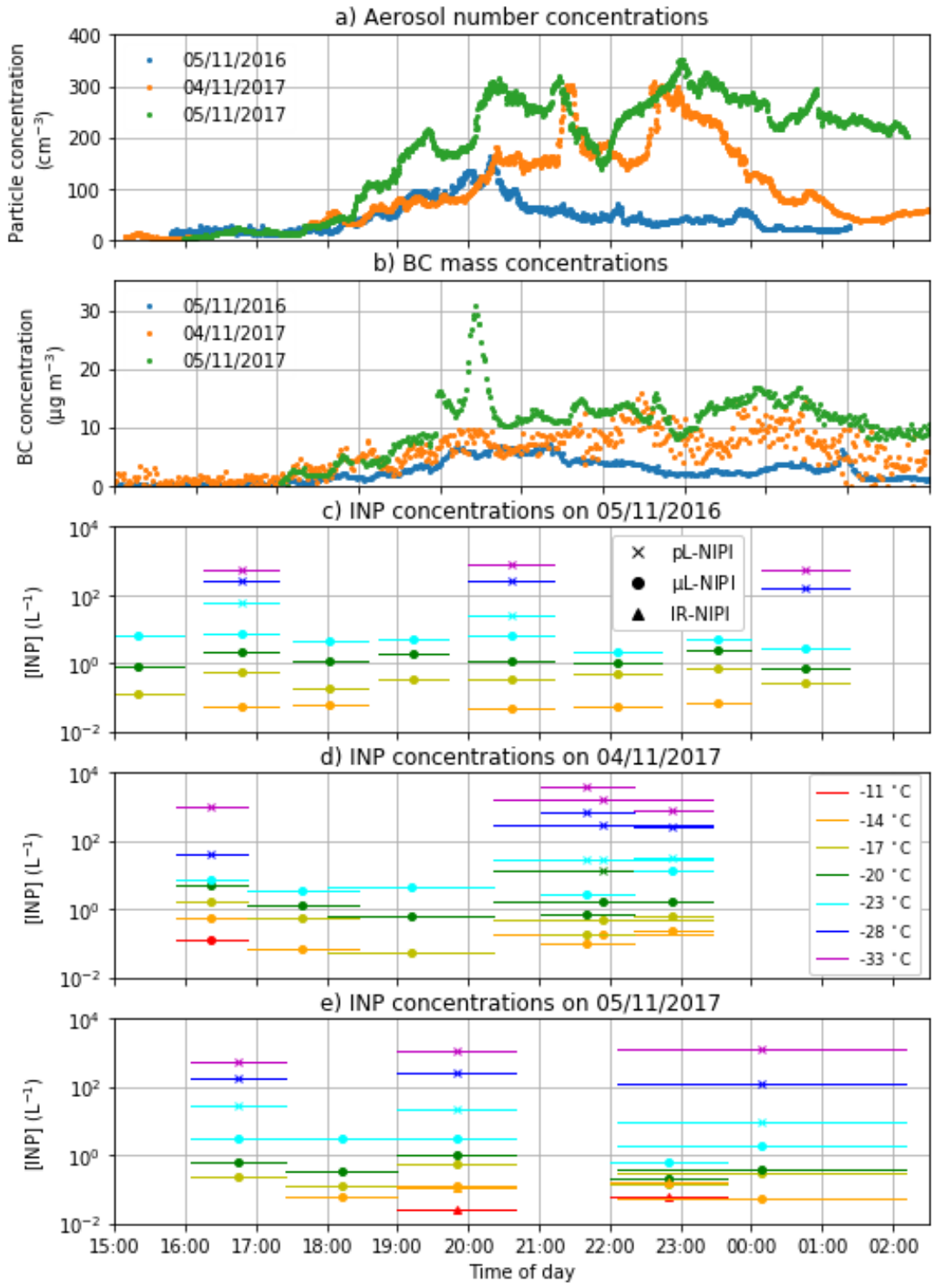

Figure 47: Aerosol number concentration, black carbon (BC) mass concentration, and INP concentrations as a function of time throughout each of the three combustion events. (a) The concentration of aerosol particles measured using an APS (0.542 - 19.81 µm aerodynamic diameter). (b) The BC concentration measured using a BC aethalometer. (c,d,e) INP concentrations at different temperatures for 05/11/2016, 04/11/2017, and 05/11/2017, respectively. Points are plotted on the x-axis at the mid-point of the sampling time. Shape markers indicate the midpoint of a run, with horizontal lines either side showing the entire sampling period

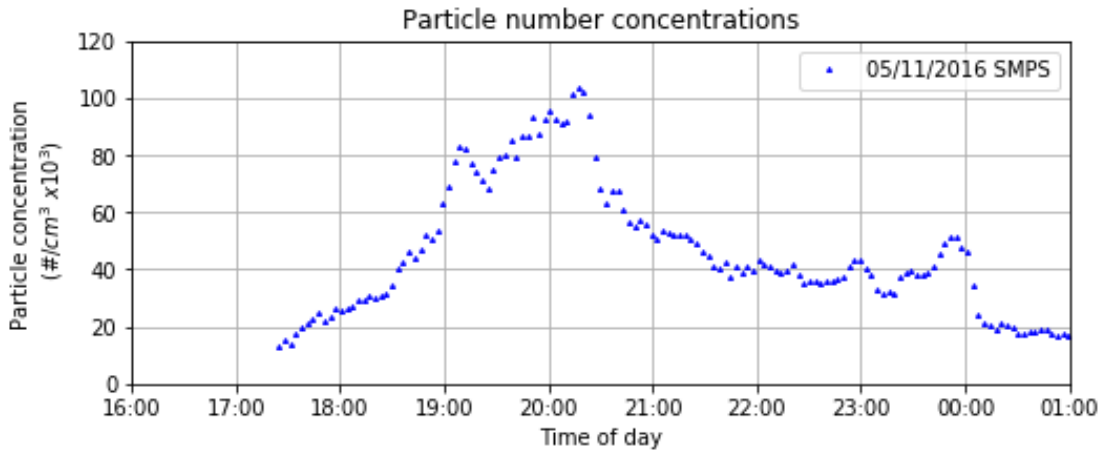

Figure 48: Aerosol number concentrations as measured by the scanning mobility particle sizer (SMPS) on 05/11/2016 (17.5 - 552.3 nm particle diameter range).

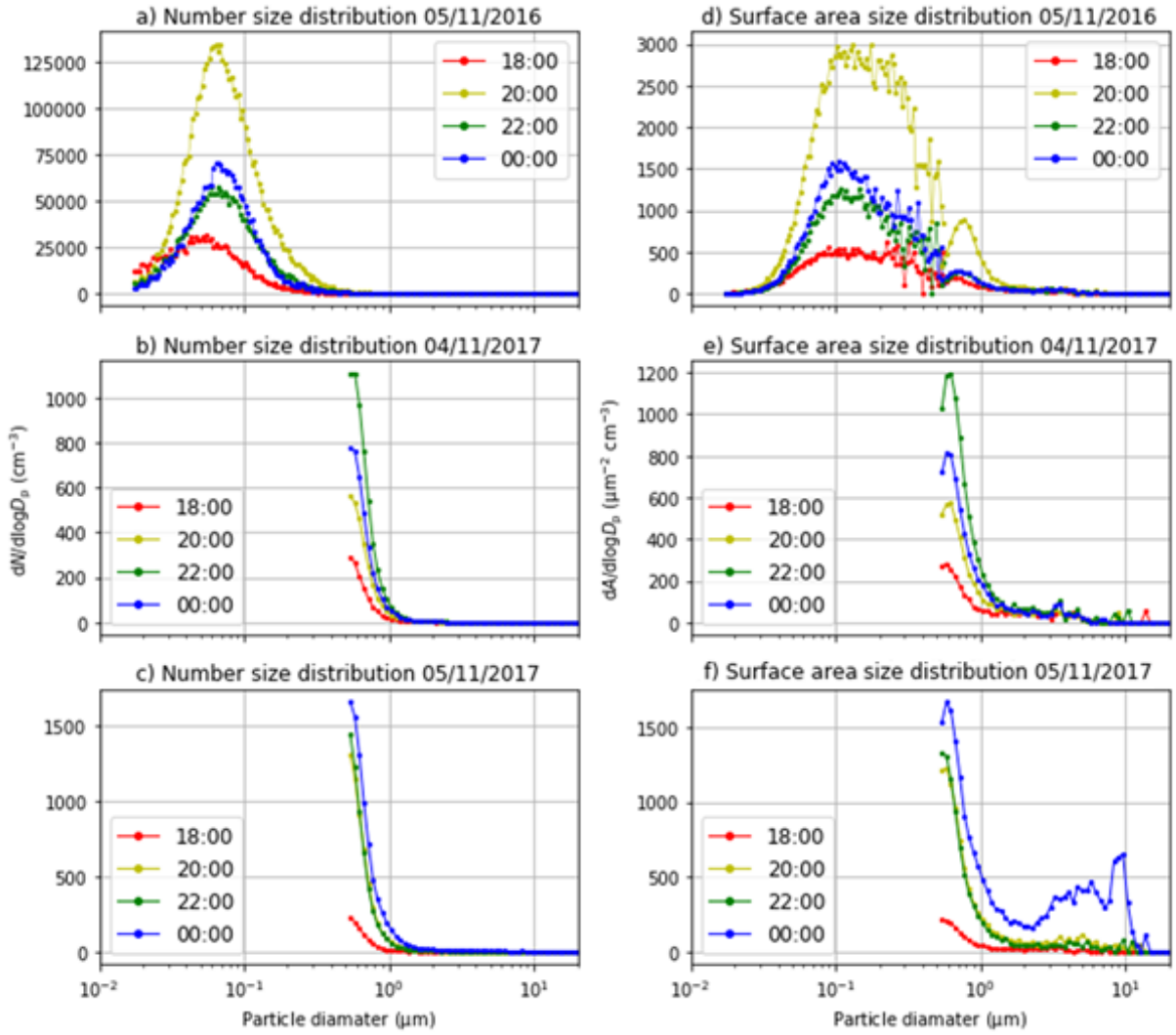

Figure 49: All available particle size distribution data from each sampling event. The SMPS was only available in 2016, and thus panels b, c, e, f have size distributions only above 0.5 microns. The distributions are not corrected to volume equivalent diameter.

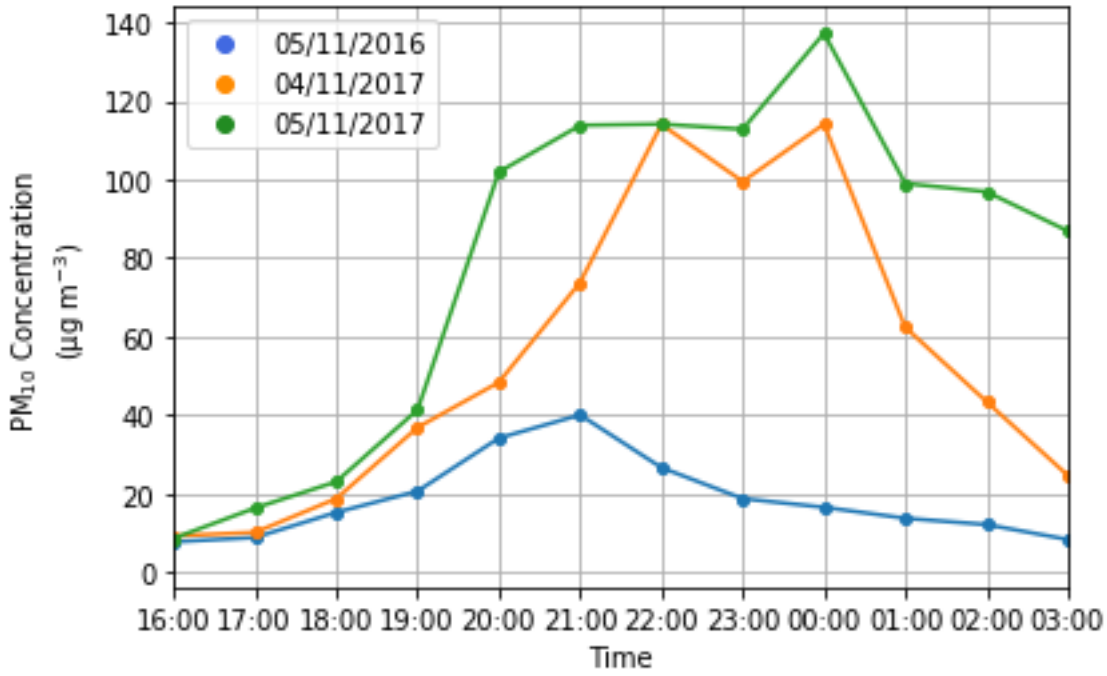

Figure 50: Concentration of particulate matter of 10 □m in diameter or below (PM_{10}) during the evenings over which aerosol sampling took place. The data was collected at a Department of Environment, Food and Rural Affairs (DEFRA) site in Leeds city centre (https://uk-air.defra.gov.uk/networks/site-info?site_id=LEED). This site is approximately 1 km from our sampling site.

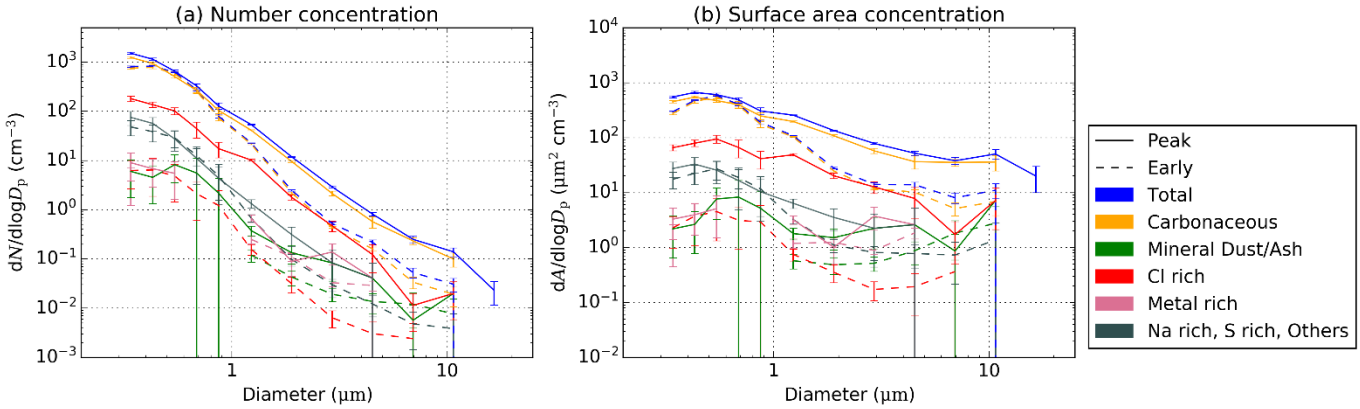

Figure 51: Composition of particles collected on the early (05/11/2017 16:05-17:25) and peak (05/11/2017 00:00-00:45) filters in terms of (a) number concentration and (b) surface area. The errors were calculated using Poisson counting statistics. These plots were generated using SEM-EDS analysis.

Figure 52: Filters before (a) and after sampling (b). The dark colour of the filter after ~1 hour sampling during the combustion event is clear. Filter sampling in Leeds during normal conditions does not yield dark filters.

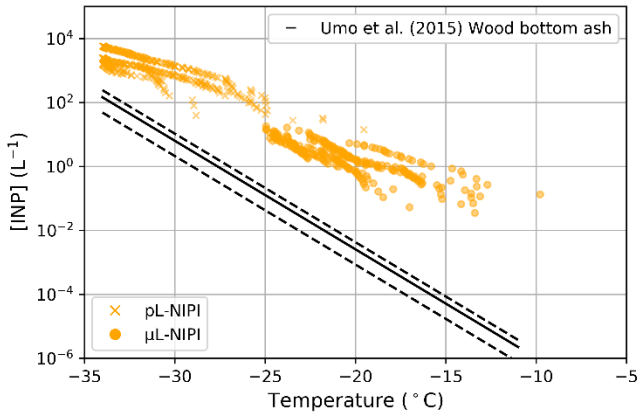

Figure 53: Comparison of a predicted upper limit [INP]T spectrum for combustion ash compared with measured $[INP]_T$ spectra. The $[INP]_T$ spectrum for ash was based on the measured surface area of mineral dust/ash from the SEM-EDS analysis, assuming all this material was ash, and the parameterisation for wood bottom ash (Umo et al., 2015). The dashed lines represent uncertainties in $[INP]_T$ based upon the uncertainties in the SEM derived surface area of mineral dust/ash. The $[INP]_T$ measurements and the SEM filters were collected on 04/11/2017.

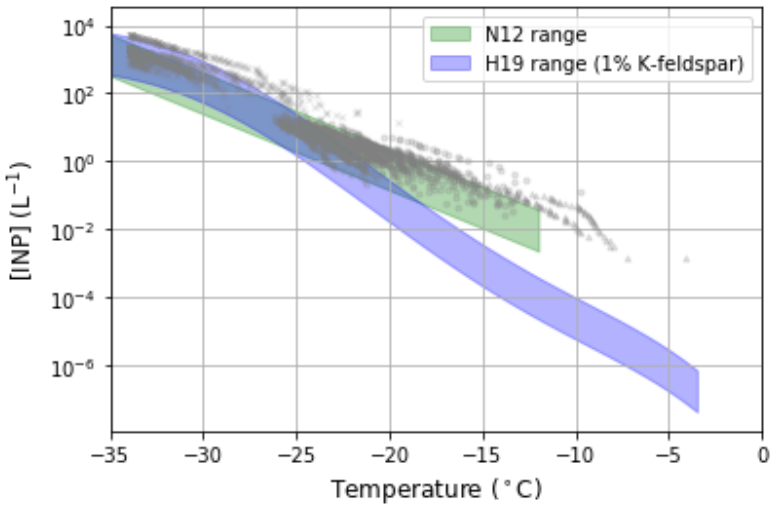

Figure 54: A plot showing $[INP]_T$ values measured during the sampling events, overlaid with [INP] predictions based on the Niemand 2012 (N12) and Harrison 2019 (H19) parametrisation and surface area concentration obtained from SEM-EDS analysis.

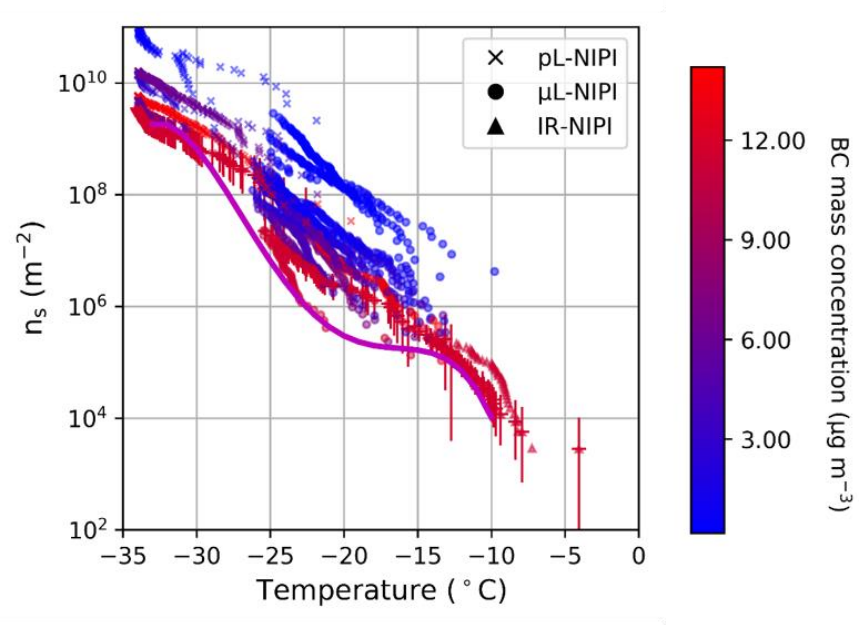

Figure 55: Estimate of the upper limit to the ice-active site surface density, $n_s(T)$, values for BC. Limiting values are estimated from the INP concentration in combination with the BC mass concentration. Triangles, circles and crosses denote data from the IR-NIPI, µL-NIPI and microfluidic pL-NIPI assays, respectively. The lower limit of the data was fitted with a polynomial between −10 °C - −33 °C, which is shown as a magenta line and used as an upper limit of $n_s(T)$ for BC during Bonfire Night. Error bars are shown on a selection of spectra across the 3 cold stages.

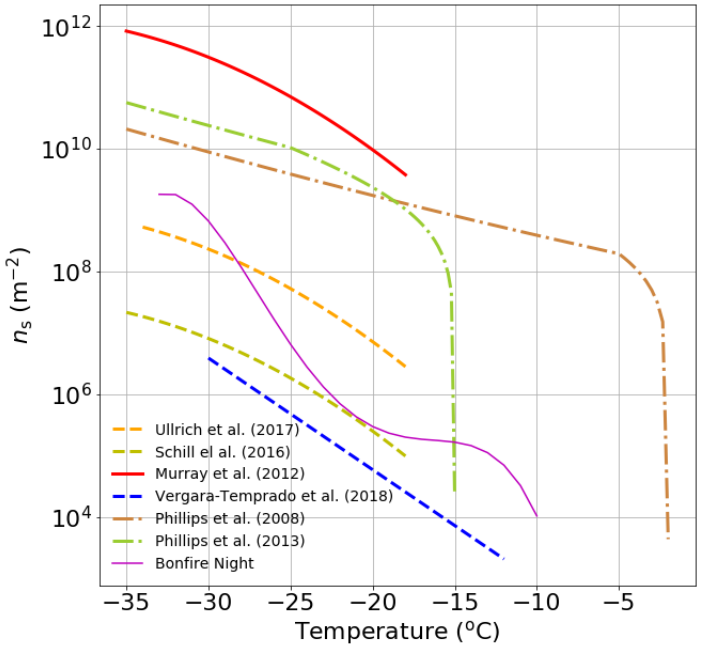

Figure 56: A plot of different BC parameterisations from the literature along with the upper limit to n_s derived in this study of Bonfire Night emissions. The parameterisations from Schill et al., (2016), Ullrich et al., (2017) and Vergara-Temprado et al., (2018) are also upper limits to the activity of BC and were based on laboratory measurements.

Table 3: Sampling times and volumes of air sampled (at 16.7 L min^{-1}) for each filter collected for ice-nucleating particle (INP) analysis during the Bonfire Night festival.

Filter no.	Start time	Midpoint of sampling	End time	Sampling duration (min)	Volume of air sampled (L)
1	05/11/2016 14:41	05/11/2016 15:20	05/11/2016 15:59	78	1300
2	05/11/2016 16:16	05/11/2016 16:48	05/11/2016 17:19	63	1050
3	05/11/2016 17:31	05/11/2016 18:03	05/11/2016 18:34	63	1050
4	05/11/2016 18:44	05/11/2016 19:14	05/11/2016 19:43	59	983
5	05/11/2016 20:00	05/11/2016 20:37	05/11/2016 21:13	73	1216
6	05/11/2016 21:29	05/11/2016 22:07	05/11/2016 22:44	75	1250
7	05/11/2016 23:05	05/11/2016 23:32	05/11/2016 23:59	54	900
8	06/11/2016 00:08	06/11/2016 00:45	06/11/2016 01:22	74	1233
9	04/11/2017 15:52	04/11/2017 16:22	04/11/2017 16:52	60	1000
10	04/11/2017 16:52	04/11/2017 17:40	04/11/2017 18:27	95	1583
11	04/11/2017 18:00	04/11/2017 19:11	04/11/2017 20:22	142	2367
12	04/11/2017 20:22	04/11/2017 21:55	04/11/2017 23:27	185	3083
13	04/11/2017 21:01	04/11/2017 21:41	04/11/2017 22:20	79	1316
14	04/11/2017 22:20	04/11/2017 22:54	04/11/2017 23:27	67	1116
15	05/11/2017 16:05	05/11/2017 16:45	05/11/2017 17:25	80	1333
16	05/11/2017 17:25	05/11/2017 18:13	05/11/2017 19:00	95	1583
17	05/11/2017 19:00	05/11/2017 19:50	05/11/2017 20:40	100	1667
18	05/11/2017 22:00	05/11/2017 22:50	05/11/2017 23:39	99	1650
19	05/11/2017 22:07	06/11/2017 00:09	06/11/2017 02:10	243	4050

Table 4: Mean INP concentrations at selected temperatures for pre-event measurements (defined as measurements taken prior to 18:00) and during event measurements (post 18:00). Also included are standard deviations for all event measurements.

05/11/2016			
Temperature (°C)	Pre-event INP (INP L^{-1})	Event mean INP (INP L^{-1})	Event standard deviation (INP L^{-1})
-17.00	0.34	0.40	0.21
-18.00	0.52	0.62	0.31
-19.00	0.93	0.98	0.46
-20.00	1.53	1.40	0.61
-21.00	2.51	1.92	0.81
-22.00	3.89	3.06	1.25
-23.00	6.86	4.39	1.73
04/11/2017			
Temperature (°C)	Pre-event INP (INP L^{-1})	Event mean INP (INP L^{-1})	Event standard deviation (INP L^{-1})
-17.00	1.71	0.39	0.25
-18.00	2.51	0.57	0.39
-19.00	4.01	0.76	0.49
-20.00	4.98	1.21	0.48
-21.00	5.35	2.11	1.02
-22.00	5.75	3.45	2.51
-23.00	7.19	5.94	4.94
05/11/2017			
Temperature (°C)	Pre-event INP (INP L^{-1})	Event mean INP (INP L^{-1})	Event standard deviation (INP L^{-1})
-17	0.23	0.28	0.21
-18	0.39	0.31	0.25
-19	0.55	0.41	0.34
-20	0.64	0.50	0.40
-21	0.91	0.60	0.47
-22	1.74	1.09	0.70
-23	3.32	2.26	1.22

4.6 References

Adachi, K., & Buseck, P. R. (2011). Atmospheric tar balls from biomass burning in Mexico. Journal of Geophysical Research, 116(D5), D05204. https://doi.org/10.1029/2010JD015102

Alstadt, V. J., Dawson, J. N., Losey, D. J., Sihvonen, S. K., & Freedman, M. A. (2017). Heterogeneous Freezing of Carbon Nanotubes: A Model System for Pore Condensation and Freezing in the Atmosphere. Journal of Physical Chemistry A, 121(42), 8166–8175. https://doi.org/10.1021/acs.jpca.7b06359

Ansmann, A., Tesche, M., Seifert, P., Althausen, D., Engelmann, R., Fruntke, J., et al. (2009). Evolution of the ice phase in tropical altocumulus: SAMUM lidar observations over Cape Verde. Journal of Geophysical Research Atmospheres, 114(17). https://doi.org/10.1029/2008JD011659

Ardon-Dryer, K., & Levin, Z. (2014). Ground-based measurements of immersion freezing in the eastern Mediterranean. Atmos. Chem. Phys, 14, 5217–5231. https://doi.org/10.5194/acp-14-5217-2014

Bai, G., Gao, D., Liu, Z., Zhou, X., & Wang, J. (2019). Probing the critical nucleus size for ice formation with graphene oxide nanosheets. Nature, 576(7787), 437–441. https://doi.org/10.1038/s41586-019-1827-6

Baustian, K. J., Cziczo, D. J., Wise, M. E., Pratt, K. A., Kulkarni, G., Hallar, A. G., & Tolbert, M. A. (2012). Importance of aerosol composition, mixing state, and morphology for heterogeneous ice nucleation: A combined field and laboratory approach. Journal of Geophysical Research: Atmospheres, 117(D6), n/a-n/a. https://doi.org/10.1029/2011JD016784

Bi, K., McMeeking, G. R., Ding, D. P., Levin, E. J. T., DeMott, P. J., Zhao, D. L., et al. (2019). Measurements of Ice Nucleating Particles in Beijing, China. Journal of Geophysical Research: Atmospheres, 124(14), 8065–8075. https://doi.org/10.1029/2019JD030609

de Boer, G., Morrison, H., Shupe, M. D., & Hildner, R. (2011). Evidence of liquid dependent ice nucleation in high-latitude stratiform clouds from surface remote sensors. Geophysical Research Letters, 38(1), n/a-n/a. https://doi.org/10.1029/2010GL046016

Bond, T. C., Doherty, S. J., Fahey, D. W., Forster, P. M., Berntsen, T., DeAngelo, B. J., et al. (2013). Bounding the role of black carbon in the climate system: A scientific assessment. Journal of Geophysical Research: Atmospheres, 118(11), 5380–5552. https://doi.org/10.1002/jgrd.50171

Chen, Wu, Z., Augustin-Bauditz, S., Grawe, S., Hartmann, M., Pei, X., et al. (2018). Ice-nucleating particle concentrations unaffected by urban air pollution in Beijing, China. Atmospheric Chemistry and Physics, 18(5), 3523–3539. https://doi.org/10.5194/acp-18-3523-2018

Chen, Y., Schleicher, N., Fricker, M., Cen, K., Liu, X., Kaminski, U., et al. (2016). Long-term variation of black carbon and PM 2.5 in Beijing, China with respect to meteorological conditions and governmental measures. Environmental Pollution, 212, 269–278. https://doi.org/10.1016/j.envpol.2016.01.008

Cheng, Y.-H., & Lin, M.-H. (2013). Real-Time Performance of the microAeth ® AE51 and the Effects of Aerosol Loading on Its Measurement Results at a Traffic Site. Aerosol and Air Quality Research, 13, 1853–1863. https://doi.org/10.4209/aaqr.2012.12.0371

Connolly, P. J., Möhler, O., Field, P. R., Saathoff, H., Burgess, R., Choularton, T., & Gallagher, M. (2009). Studies of heterogeneous freezing by three different desert dust samples. Atmos. Chem. Phys. Atmospheric Chemistry and Physics, 9, 2805–2824. Retrieved from www.atmos-chem-phys.net/9/2805/2009/

Cooke, W. F., & Wilson, J. J. N. (1996). A global black carbon aerosol model. Journal of Geophysical Research: Atmospheres, 101(D14), 19395–19409. https://doi.org/10.1029/96JD00671

Cozic, J., Mertes, S., Verheggen, B., Cziczo, D. J., Gallavardin, S. J., Walter, S., et al. (2008). Black carbon enrichment in atmospheric ice particle residuals observed in lower tropospheric mixed phase clouds. Journal of Geophysical Research, 113(D15), D15209. https://doi.org/10.1029/2007JD009266

Crespo, J., Yubero, E., Nicolás, J. F., Lucarelli, F., Nava, S., Chiari, M., & Calzolai, G. (2012). High-time resolution and size-segregated elemental composition in high-intensity pyrotechnic exposures. Journal of Hazardous Materials, 241–242, 82–91. https://doi.org/10.1016/j.jhazmat.2012.09.017

Cziczo, D. J., Froyd, K. D., Hoose, C., Jensen, E. J., Diao, M., Zondlo, M. A., et al. (2013). Clarifying the dominant sources and mechanisms of cirrus cloud formation. Science, 340(6138), 1320–1324. https://doi.org/10.1126/science.1234145

DeMott, Cziczo, D. J., Prenni, A. J., Murphy, D. M., Kreidenweis, S. M., Thomson, D. S., et al. (2003). Measurements of the concentration and composition of nuclei for cirrus formation. Proceedings of the National Academy of Sciences of the United States of America, 100(25), 14655–14660. https://doi.org/10.1073/pnas.2532677100

DeMott, P. J. (1990). An Exploratory Study of Ice Nucleation by Soot Aerosols. Journal of Applied Meteorology, 29(10), 1072–1079. https://doi.org/10.1175/1520-0450(1990)029<1072:AESOIN>2.0.CO;2

DeMott, P. J., Sassen, K., Poellot, M. R., Baumgardner, D., Rogers, D. C., Brooks, S. D., et al. (2003). African dust aerosols as atmospheric ice nuclei. Geophysical Research Letters, 30(14). https://doi.org/10.1029/2003GL017410

DeMott, P. J., Hill, T. C. J., McCluskey, C. S., Prather, K. A., Collins, D. B., Sullivan, R. C., et al. (2016). Sea spray aerosol as a unique source of ice nucleating particles. Proceedings of the National Academy of Sciences of the United States of America, 113(21), 5797–803. https://doi.org/10.1073/pnas.1514034112

Diehl, K., & Mitra, S. K. (1998). A laboratory study of the effects of a kerosene-burner exhaust on ice nucleation and the evaporation rate of ice crystals. Atmospheric Environment, 32(18), 3145–3151. https://doi.org/10.1016/S1352-2310(97)00467-6

Don-Yuan Liu, Dan Rutherford, Matt Kinsey, and, & Prather*, K. A. (1997). Real-Time Monitoring of Pyrotechnically Derived Aerosol Particles in the Troposphere. https://doi.org/10.1021/AC9612988

Elsasser, M., Busch, C., Orasche, J., Schön, C., Hartmann, H., Schnelle-Kreis, J., & Zimmermann, R. (2013). Dynamic Changes of the Aerosol Composition and Concentration during Different Burning Phases of Wood Combustion. Energy & Fuels, 27(8), 4959–4968. https://doi.org/10.1021/ef400684f

Fornea, A. P., Brooks, S. D., Dooley, J. B., & Saha, A. (2009). Heterogeneous freezing of ice on atmospheric aerosols containing ash, soot, and soil. Journal of Geophysical Research, 114(D13), D13201. https://doi.org/10.1029/2009JD011958

Gong, X., Zhang, C., Chen, H., Nizkorodov, S. A., Chen, J., & Yang, X. (2016). Size distribution and mixing state of black carbon particles during a heavy air pollution episode in Shanghai. Atmospheric Chemistry and Physics, 16(8), 5399–5411. https://doi.org/10.5194/acp-16-5399-2016

Gorbunov, B., Baklanov, A., Kakutkina, N., Windsor, H. ., & Toumi, R. (2001). Ice nucleation on soot particles. Journal of Aerosol Science, 32(2), 199–215. https://doi.org/10.1016/S0021-8502(00)00077-X

Grawe, S., Augustin-Bauditz, S., Hartmann, S., Hellner, L., Pettersson, J. B. C., Prager, A., et al. (2016). The immersion freezing behavior of ash particles from wood and brown coal burning. Atmospheric Chemistry and Physics, 16(21), 13911–13928. https://doi.org/10.5194/acp-16-13911-2016

Grawe, S., Augustin-Bauditz, S., Clemen, H.-C., Ebert, M., Eriksen Hammer, S., Lubitz, J., et al. (2018). Coal fly ash: linking immersion freezing behavior and physicochemical particle properties. Atmospheric Chemistry and Physics, 18(19), 13903–13923. https://doi.org/10.5194/acp-18-13903-2018

Harrison, A. D., Whale, T. F., Carpenter, M. A., Holden, M. A., Neve, L., O'Sullivan, D., et al. (2016). Not all feldspars are equal: a survey of ice nucleating properties across the feldspar group of minerals. Atmospheric Chemistry and Physics, 16(17), 10927–10940. https://doi.org/10.5194/acp-16-10927-2016

Harrison, A. D., Whale, T. F., Rutledge, R., Lamb, S., Tarn, M. D., Porter, G. C. E., et al. (2018). An instrument for quantifying heterogeneous ice nucleation in multiwell plates using infrared emissions to detect freezing. Atmospheric Measurement Techniques, 11(10), 5629–5641. https://doi.org/10.5194/amt-11-5629-2018

Harrison, A. D., Lever, K., Sanchez-Marroquin, A., Holden, M. A., Whale, T. F., Tarn, M. D., et al. (2019). The ice-nucleating ability of quartz immersed in water and its atmospheric importance compared to K-feldspar. Atmospheric Chemistry and Physics, 19(17), 11343–11361. https://doi.org/10.5194/acp-19-11343-2019

Hartmann, M., Blunier, T., Brügger, S. O., Schmale, J., Schwikowski, M., Vogel, A., et al. (2019). Variation of Ice Nucleating Particles in the European Arctic Over the Last Centuries. Geophysical Research Letters, 46(7), 4007–4016. https://doi.org/10.1029/2019GL082311

Herbert, R. J., Murray, B. J., Dobbie, S. J., & Koop, T. (2015). Sensitivity of liquid clouds to homogenous freezing parameterizations. Geophysical Research Letters, 42(5), 1599–1605. https://doi.org/10.1002/2014GL062729

Hill, T. C. J., Moffett, B. F., Demott, P. J., Georgakopoulos, D. G., Stump, W. L., & Franc, G. D. (2014). Measurement of ice nucleation-active bacteria on plants and in precipitation by quantitative PCR. Applied and Environmental Microbiology, 80(4), 1256–67. https://doi.org/10.1128/AEM.02967-13

Hobbs, P. V., & Locatelli, J. D. (1969). Ice Nuclei from a Natural Forest Fire. Journal of Applied Meteorology, 8(5), 833.

Holden, M. A., Whale, T. F., Tarn, M. D., O'Sullivan, D., Walshaw, R. D., Murray, B. J., et al. (2019). High-speed imaging of ice nucleation in water proves the existence of active sites. Science Advances, 5(2). https://doi.org/10.1126/sciadv.aav4316

Hoose, C., & Möhler, O. (2012). Heterogeneous ice nucleation on atmospheric aerosols: a review of results from laboratory experiments. Atmospheric Chemistry and Physics, 12(20), 9817–9854. https://doi.org/10.5194/acp-12-9817-2012

Jiang, Q., Sun, Y. L., Wang, Z., & Yin, Y. (2015). Aerosol composition and sources during the Chinese Spring Festival: fireworks, secondary aerosol, and holiday effects. Atmospheric Chemistry and Physics, 15(11), 6023–6034. https://doi.org/10.5194/acp-15-6023-2015

Kamphus, M., Ettner-Mahl, M., Klimach, T., Drewnick, F., Keller, L., Cziczo, D. J., et al. (2010). Chemical composition of ambient aerosol, ice residues and cloud droplet residues in mixed-phase clouds: single particle analysis during the Cloud and Aerosol Characterization

Experiment (CLACE 6). Atmospheric Chemistry and Physics, 10, 8077–8095. https://doi.org/10.5194/acp-10-8077-2010

Kanji, Z. A., Ladino, L. A., Wex, H., Boose, Y., Burkert-Kohn, M., Cziczo, D. J., et al. (2017). Overview of Ice Nucleating Particles. Meteorological Monographs, 58, 1.1-1.33. https://doi.org/10.1175/AMSMONOGRAPHS-D-16-0006.1

Kanji, Z. A., Welti, A., Corbin, J. C., & Mensah, A. A. (2020). Black Carbon Particles Do Not Matter for Immersion Mode Ice Nucleation. Geophysical Research Letters. https://doi.org/10.1029/2019gl086764

Kireeva, E. D., Popovicheva, O. B., Persiantseva, N. M., Khokhlova, T. D., & Shonija, N. K. (2009). Effect of black carbon particles on the efficiency of water droplet freezing. Colloid Journal, 71(3), 353–359. https://doi.org/10.1134/S1061933X09030090

Koch, D., Schulz, M., Kinne, S., Mcnaughton, C., Spackman, J. R., Balkanski, Y., et al. (2009). Evaluation of black carbon estimations in global aerosol models. Atmos. Chem. Phys. Atmospheric Chemistry and Physics, 9, 9001–9026. Retrieved from www.atmos-chem-phys.net/9/9001/2009/

Kumai, M. (1961). SNOW CRYSTALS AND THE IDENTIFICATION OF THE NUCLEI IN THE NORTHERN UNITED STATES OF AMERICA. Http://Dx.Doi.Org/10.1175/1520-0469(1961)018<0139:SCATIO>2.0.CO;2. https://doi.org/10.1175/1520-0469(1961)018<0139:SCATIO>2.0.CO;2

Lavanchy, V. M. H., Gäggeler, H. W., Schotterer, U., Schwikowski, M., & Baltensperger, U. (1999). Historical record of carbonaceous particle concentrations from a European high-alpine glacier (Colle Gnifetti, Switzerland). Journal of Geophysical Research: Atmospheres, 104(D17), 21227–21236. https://doi.org/10.1029/1999JD900408

Levin, E. J. T., McMeeking, G. R., DeMott, P. J., McCluskey, C. S., Carrico, C. M., Nakao, S., et al. (2016). Ice-nucleating particle emissions from biomass combustion and the potential importance of soot aerosol. Journal of Geophysical Research: Atmospheres, 121(10), 5888–5903. https://doi.org/10.1002/2016JD024879

Li, J., Xu, T., Lu, X., Chen, H., Nizkorodov, S. A., Chen, J., et al. (2017). Online single particle measurement of fireworks pollution during Chinese New Year in Nanning. Journal of Environmental Sciences, 53, 184–195. https://doi.org/10.1016/j.jes.2016.04.021

Lighty, J. A. S., Veranth, J. M., & Sarofim, A. F. (2000). Combustion aerosols: Factors governing their size and composition and implications to human health. Journal of the Air and Waste Management Association, 50(9), 1565–1618. https://doi.org/10.1080/10473289.2000.10464197

Lin, C.-C. (2016). Journal of the Air & Waste Management Association A review of the impact of fireworks on particulate matter in ambient air. Journal of the Air & Waste Management Association, 66, 1171–1182. https://doi.org/10.1080/10962247.2016.1219280

Lindsley, W. G. (n.d.). NIOSH Manual of Analytical Methods (NMAM), 5th Edition Filter Pore Size and Aerosol Sample Collection. Retrieved from https://www.cdc.gov/niosh/docs/2014-151/pdfs/chapters/chapter-fp.pdf

Lohmann, U., Diehl, K., Lohmann, U., & Diehl, K. (2006). Sensitivity Studies of the Importance of Dust Ice Nuclei for the Indirect Aerosol Effect on Stratiform Mixed-Phase Clouds. Journal of the Atmospheric Sciences, 63(3), 968–982. https://doi.org/10.1175/JAS3662.1

Mahrt, F., Marcolli, C., David, R. O., Grönquist, P., Meier, E. J. B., Lohmann, U., & Kanji, Z. A. (2018). Ice nucleation abilities of soot particles determined with the Horizontal Ice Nucleation Chamber. Atmos. Chem. Phys, 18, 13363–13392. https://doi.org/10.5194/acp-18-13363-2018

McCluskey, C. S., DeMott, P. J., Prenni, A. J., Levin, E. J. T., McMeeking, G. R., Sullivan, A. P., et al. (2014). Characteristics of atmospheric ice nucleating particles associated with biomass burning in the US: Prescribed burns and wildfires. Journal of Geophysical Research: Atmospheres, 119(17), 10458–10470. https://doi.org/10.1002/2014JD021980

McCluskey, C. S., Ovadnevaite, J., Rinaldi, M., Atkinson, J., Belosi, F., Ceburnis, D., et al. (2018). Marine and Terrestrial Organic Ice-Nucleating Particles in Pristine Marine to Continentally Influenced Northeast Atlantic Air Masses. Journal of Geophysical Research: Atmospheres, 123(11), 6196–6212. https://doi.org/10.1029/2017JD028033

Moreno, T., Querol, X., Alastuey, A., Cruz Minguillón, M., Pey, J., Rodriguez, S., et al. (2007). Recreational atmospheric pollution episodes: Inhalable metalliferous particles from firework displays. Atmospheric Environment, 41(5), 913–922. https://doi.org/10.1016/j.atmosenv.2006.09.019

Murray, B. J., O'Sullivan, D., Atkinson, J. D., & Webb, M. E. (2012). Ice nucleation by particles immersed in supercooled cloud droplets. Chemical Society Reviews, 41(19), 6519. https://doi.org/10.1039/c2cs35200a

Niemand, M., Möhler, O., Vogel, B., Vogel, H., Hoose, C., Connolly, P., et al. (2012). A Particle-Surface-Area-Based Parameterization of Immersion Freezing on Desert Dust Particles. Journal of the Atmospheric Sciences, 69(10), 3077–3092. https://doi.org/10.1175/JAS-D-11-0249.1

O'Sullivan, D., Murray, B. J., Malkin, T. L., Whale, T. F., Umo, N. S., Atkinson, J. D., et al. (2014). Ice nucleation by fertile soil dusts: relative importance of mineral and biogenic components. Atmospheric Chemistry and Physics, 14(4), 1853–1867. https://doi.org/10.5194/acp-14-1853-2014

O'Sullivan, D., Adams, M. P., Tarn, M. D., Harrison, A. D., Vergara-Temprado, J., Porter, G. C. E., et al. (2018). Contributions of biogenic material to the atmospheric ice-nucleating particle population in North Western Europe. Scientific Reports, 8(1), 13821. https://doi.org/10.1038/s41598-018-31981-7

Petters, M. D., & Wright, T. P. (2015). Revisiting ice nucleation from precipitation samples. Geophysical Research Letters, 42(20), 8758–8766. https://doi.org/10.1002/2015GL065733

Petters, Markus D., Parsons, M. T., Prenni, A. J., DeMott, P. J., Kreidenweis, S. M., Carrico, C. M., et al. (2009). Ice nuclei emissions from biomass burning. Journal of Geophysical Research, 114(D7), D07209. https://doi.org/10.1029/2008JD011532

Petzold, A., Ogren, J. A., Fiebig, M., Laj, P., Li, S.-M., Baltensperger, U., et al. (2013). Geoscientific Instrumentation Methods and Data Systems Recommendations for reporting " black carbon " measurements. Atmos. Chem. Phys, 13, 8365–8379. https://doi.org/10.5194/acp-13-8365-2013

Phillips, V. T. J., DeMott, P. J., Andronache, C., Phillips, V. T. J., DeMott, P. J., & Andronache, C. (2008). An Empirical Parameterization of Heterogeneous Ice Nucleation for Multiple Chemical Species of Aerosol. Journal of the Atmospheric Sciences, 65(9), 2757–2783. https://doi.org/10.1175/2007JAS2546.1

Phillips, V. T. J., Demott, P. J., Andronache, C., Pratt, K. A., Prather, K. A., Subramanian, R., et al. (2013). Improvements to an Empirical Parameterization of Heterogeneous Ice Nucleation and Its Comparison with Observations. Journal of the Atmospheric Sciences, 70(2), 378–409. https://doi.org/10.1175/JAS-D-12-080.1

Pope, R. J., Marshall, A. M., & O'Kane, B. O. (2016). Observing UK Bonfire Night pollution from space: analysis of atmospheric aerosol. Weather, 71(11), 288–291. https://doi.org/10.1002/wea.2914

Popovicheva, O., Kireeva, E., Persiantseva, N., Khokhlova, T., Shonija, N., Tishkova, V., & Demirdjian, B. (2008). Effect of soot on immersion freezing of water and possible atmospheric implications. Atmospheric Research, 90(2–4), 326–337. https://doi.org/10.1016/j.atmosres.2008.08.004

Pósfai, M., Gelencsér, A., Simonics, R., Arató, K., Li, J., Hobbs, P. V., & Buseck, P. R. (2004). Atmospheric tar balls: Particles from biomass and biofuel burning. Journal of Geophysical Research D: Atmospheres, 109(6). https://doi.org/10.1029/2003jd004169

Pratt, K. A., Demott, P. J., French, J. R., Wang, Z., Westphal, D. L., Heymsfield, A. J., et al. (2009). In situ detection of biological particles in cloud ice-crystals. Nature Geoscience, 2(6), 398–401. https://doi.org/10.1038/NGEO521

Prenni, A. J., Petters, M. D., Kreidenweis, S. M., Heald, C. L., Martin, S. T., Artaxo, P., et al. (2009). Relative roles of biogenic emissions and saharan dust as ice nuclei in the amazon basin. Nature Geoscience, 2(6), 402–405. https://doi.org/10.1038/ngeo517

Prenni, A. J., Demott, P. J., Sullivan, A. P., Sullivan, R. C., Kreidenweis, S. M., & Rogers, D. C. (2012). Biomass burning as a potential source for atmospheric ice nuclei: Western wildfires and prescribed burns. Geophysical Research Letters, 39(11). https://doi.org/10.1029/2012GL051915

Price, H. C., Baustian, K. J., Mcquaid, J. B., Blyth, A., Bower, K. N., Choularton, T., et al. (2018). Atmospheric Ice-Nucleating Particles in the Dusty Tropical Atlantic. https://doi.org/10.1002/2017JD027560

Reyes-Villegas, E., Priestley, M., Ting, Y.-C., Haslett, S., Bannan, T., Le Breton, M., et al. (2018). Simultaneous aerosol mass spectrometry and chemical ionisation mass spectrometry measurements during a biomass burning event in the UK: insights into nitrate chemistry. Atmos. Chem. Phys, 18, 4093–4111. https://doi.org/10.5194/acp-18-4093-2018

Rosenfeld, D., Yu, X., Liu, G., Xu, X., Zhu, Y., Yue, Z., et al. (2011). Glaciation temperatures of convective clouds ingesting desert dust, air pollution and smoke from forest fires. Geophysical Research Letters, 38(21), n/a-n/a. https://doi.org/10.1029/2011GL049423

Sanchez-Marroquin, A., Hedges, D. H. P., Hiscock, M., Parker, S. T., Rosenberg, P. D., Trembath, J., et al. (2019b). Characterisation of the filter inlet system on the FAAM BAe-146 research aircraft and its use for size-resolved aerosol composition measurements. Atmospheric Measurement Techniques, 12(11), 5741–5763. https://doi.org/10.5194/amt-12-5741-2019

Šantl-Temkiv, T., Sahyoun, M., Finster, K., Hartmann, S., Augustin-Bauditz, S., Stratmann, F., et al. (2015). Characterization of airborne ice-nucleation-active bacteria and bacterial fragments. Atmospheric Environment, 109, 105–117. https://doi.org/10.1016/j.atmosenv.2015.02.060

Schill, G. P., Jathar, S. H., Kodros, J. K., Levin, E. J. T., Galang, A. M., Friedman, B., et al. (2016). Ice-nucleating particle emissions from photochemically aged diesel and biodiesel exhaust. Geophysical Research Letters, 43(10), 5524–5531. https://doi.org/10.1002/2016GL069529

Schlosser, J. S., Braun, R. A., Bradley, T., Dadashazar, H., MacDonald, A. B., Aldhaif, A. A., et al. (2017). Analysis of aerosol composition data for western United States wildfires between 2005 and 2015: Dust emissions, chloride depletion, and most enhanced aerosol constituents. Journal of Geophysical Research: Atmospheres, 122(16), 8951–8966. https://doi.org/10.1002/2017JD026547

Schnell, R. C., Pueschel, R. F., Weickmann, H. K., & Wellman, D. L. (1980). Ice nucleus and aerosol measurements in the plume of the Johnstown, PA., steel mill. Geophysical Research Letters, 7(5), 397–400. https://doi.org/10.1029/GL007i005p00397

Singh, A., Bloss, W. J., & Pope, F. D. (2015). Remember, remember the 5th of November; gunpowder, particles and smog. Weather, 70(11), 320–324. https://doi.org/10.1002/wea.2587

Soo, J.-C., Monaghan, K., Lee, T., Kashon, M., & Harper, M. (2016). Air sampling filtration media: Collection efficiency for respirable size-selective sampling. Aerosol Science and Technology : The Journal of the American Association for Aerosol Research, 50(1), 76–87. Retrieved from http://www.ncbi.nlm.nih.gov/pubmed/26834310

Spracklen, D. V., Carslaw, K. S., Pöschl, U., Rap, A., & Forster, P. M. (2011). Global cloud condensation nuclei influenced by carbonaceous combustion aerosol. Atmospheric Chemistry and Physics, 11(17), 9067–9087. https://doi.org/10.5194/acp-11-9067-2011

Stein, A. F., Draxler, R. R., Rolph, G. D., Stunder, B. J. B., Cohen, M. D., & Ngan, F. (2015). Noaa's hysplit atmospheric transport and dispersion modeling system. Bulletin of the American Meteorological Society. https://doi.org/10.1175/BAMS-D-14-00110.1

Storelvmo, T. (2017). Aerosol Effects on Climate via Mixed-Phase and Ice Clouds. Annual Review of Earth and Planetary Sciences, 45(1), 199–222. https://doi.org/10.1146/annurev-earth-060115-012240

Tan, I., Storelvmo, T., & Zelinka, M. D. (2016). Observational constraints on mixed-phase clouds imply higher climate sensitivity. Science (New York, N.Y.), 352(6282), 224–7. https://doi.org/10.1126/science.aad5300

Tarn, M. D., Sikora, S. N. F., Grace, ·, Porter, C. E., O 'sullivan, D., Adams, M., et al. (2018). The study of atmospheric ice-nucleating particles via microfluidically generated droplets. Microfluidics and Nanofluidics, 22(22). https://doi.org/10.1007/s10404-018-2069-x

Twohy, C. H., DeMott, P. J., Pratt, K. A., Subramanian, R., Kok, G. L., Murphy, S. M., et al. (2010). Relationships of Biomass-Burning Aerosols to Ice in Orographic Wave Clouds. Journal of the Atmospheric Sciences, 67(8), 2437–2450. https://doi.org/10.1175/2010JAS3310.1

Ullrich, R., Hoose, C., Möhler, O., Niemand, M., Wagner, R., Höhler, K., et al. (2017). A New Ice Nucleation Active Site Parameterization for Desert Dust and Soot. Journal of the Atmospheric Sciences, 74(3), 699–717. https://doi.org/10.1175/JAS-D-16-0074.1

Umo, Murray, B. J., Baeza-Romero, M. T., Jones, J. M., Lea-Langton, A. R., Malkin, T. L., et al. (2015). Ice nucleation by combustion ash particles at conditions relevant to mixed-phase clouds. Atmospheric Chemistry and Physics, 15(9), 5195–5210. https://doi.org/10.5194/acp-15-5195-2015

Umo, Wagner, R., Ullrich, R., Kiselev, A., Saathoff, H., Weidler, P. G., et al. (2019). Enhanced ice nucleation activity of coal fly ash aerosol particles initiated by ice-filled pores. Atmospheric Chemistry and Physics, 19(13), 8783–8800. https://doi.org/10.5194/acp-19-8783-2019

Vali, G., DeMott, P. J., Möhler, O., & Whale, T. F. (2015). Technical Note: A proposal for ice nucleation terminology. Atmospheric Chemistry and Physics, 15(18). https://doi.org/10.5194/acp-15-10263-2015

Vali, Gabor. (1971). Quantitative Evaluation of Experimental Results an the Heterogeneous Freezing Nucleation of Supercooled Liquids. Journal of the Atmospheric Sciences, 28(3), 402–409. https://doi.org/10.1175/1520-0469(1971)028<0402:QEOERA>2.0.CO;2

Vergara-Temprado, J., Holden, M. A., Orton, T. R., O'Sullivan, D., Umo, N. S., Browse, J., et al. (2018). Is Black Carbon an Unimportant Ice-Nucleating Particle in Mixed-Phase Clouds? Journal of Geophysical Research: Atmospheres, 123(8), 4273–4283. https://doi.org/10.1002/2017JD027831

Westbrook, C. D., & Illingworth, A. J. (2011). Evidence that ice forms primarily in supercooled liquid clouds at temperatures > −27°C. Geophysical Research Letters, 38(14), n/a-n/a. https://doi.org/10.1029/2011GL048021

Whale, T. F., Murray, B. J., O'Sullivan, D., Wilson, T. W., Umo, N. S., Baustian, K. J., et al. (2015). A technique for quantifying heterogeneous ice nucleation in microlitre supercooled water droplets. Atmospheric Measurement Techniques, 8(6), 2437–2447. https://doi.org/10.5194/amt-8-2437-2015

Whale, Thomas F., Rosillo-Lopez, M., Murray, B. J., & Salzmann, C. G. (2015). Ice Nucleation Properties of Oxidized Carbon Nanomaterials. Journal of Physical Chemistry Letters, 6(15), 3012–3016. https://doi.org/10.1021/acs.jpclett.5b01096

Wofsy, S. C. (2011). HIAPER Pole-to-Pole Observations (HIPPO): fine-grained, global-scale measurements of climatically important atmospheric gases and aerosols. Phil. Trans. R. Soc. A, 369, 2073–2086. https://doi.org/10.1098/rsta.2010.0313

Wright, T. P., Petters, M. D., Hader, J. D., Morton, T., & Holder, A. L. (2013). Minimal cooling rate dependence of ice nuclei activity in the immersion mode. Journal of Geophysical Research: Atmospheres, 118(18), 10,535-10,543. https://doi.org/10.1002/jgrd.50810

Zhang, Y., Zhang, Q., Cheng, Y., Su, H., Kecorius, S., Wang, Z., et al. (2016). Measuring the morphology and density of internally mixed black carbon with SP2 and VTDMA: new insight into the absorption enhancement of black carbon in the atmosphere. Atmospheric Measurement Techniques, 9(4), 1833–1843. https://doi.org/10.5194/amt-9-1833-2016

Zhao, B., Wang, Y., Gu, Y., Liou, K. N., Jiang, J. H., Fan, J., et al. (2019). Ice nucleation by aerosols from anthropogenic pollution. Nature Geoscience, 12(8), 602–607. https://doi.org/10.1038/s41561-019-0389-4

Chapter 5

Ice nucleation by viruses and their potential for cloud glaciation

Michael P. Adams[1, #], Nina S. Atanasova[2, 3, #], Svetlana Sofieva[2, 3], Janne Ravantti[3], Aino Heikkinen[2 +], Zoé Brasseur[4], Jonathan Duplissy[4], Dennis H. Bamford[3] & Benjamin J. Murray[1]

Author affiliations

1 - Institute for Climate and Atmospheric Science, School of Earth and Environment, University of Leeds, Leeds, UK

2 - Finnish Meteorological Institute, Helsinki, Finland

3 - Molecular and Integrative Biosciences Research Programme, Faculty of Biological and Environmental Sciences, University of Helsinki, Finland

4 - Institute for Atmospheric and Earth System Research / Physics, Faculty of Science, University of Helsinki, Finland

[#] Authors contributed equally to the work

+ Institute for Molecular Medicine Finland, HiLIFE, University of Helsinki, Helsinki, Finland

Chapter 5 is based upon a paper currently under review in *Biogeosciences* entitled *Viruses and their potential for cloud glaciation*. I am lead author of the study, with Dr Atanasova being a joint first author. I conceptualised the study along with NA, JD, DHB and BJM. MA, NA, SS, AH and ZB carried out ice nucleation experiments. All virus purification was carried out by NA, SS and AH. SS and JR lead the genomic sequencing work. All authors contributed to the writing of the paper, with NA explicitly writing the sections of virus purification methods and SS and JR writing the section of genomic sequencing.

Whilst I am lead author on the paper this chapter is based upon, it was an extremely collaborative piece of work bringing together expertise from two different fields. The main examples of this are in section 5.2 (Materials and methods; specifically sub-section 5.2.1, 5.2.2, 5.2.3 and 5.2.5) and 5.3 (Results; specifically 5.3.2) which were written by co-authors from the University of Helsinki using their expert virology and genomics knowledge. Figures 57a-d, 60, 62a and 67 were also made by co-authors from the University of Helsinki. I made all other Figures.

Abstract

In order to effectively predict the formation of ice in clouds we need to know which subsets of aerosol particles are effective at nucleating ice, how they are distributed and where they are from. A large proportion of ice-nucleating particles (INPs) in many locations are likely of biological origin, and some INPs are extremely small being just tens of nanometers in size. The identity and sources of such INPs are not well characterized. Here, we show that several different types of virus particles can nucleate ice, with up to about one in twenty million virus particles able to nucleate ice at -20°C. In addition, we conclude that virus architecture is not the sole driver of viral ice nucleation. In terms of the impact on cloud glaciation, the ice-nucleating ability (the fraction which are ice nucleation active as a function of temperature) taken together with typical virus particle concentrations in the atmosphere lead to the conclusion that virus particles make a minor contribution to the atmospheric ice-nucleating particle population in the terrestrial influenced atmosphere. However, they cannot be ruled out as being important in the remote marine atmosphere. It is striking that virus particles have an ice-nucleating activity and further work should be done to explore other types of

viruses for both their ice-nucleating potential and to understand the mechanism by which viruses nucleate ice.

5.1 Introduction

The formation of ice in clouds is critically important for the planet's radiative balance and our prediction of future changes in climate with increased greenhouse gas concentrations (Tan et al., 2016; Vergara-Temprado et al., 2018). Ice-nucleating particles (INPs) have the potential to cause supercooled liquid cloud droplets, present in mixed-phase clouds, to freeze at temperatures greater than homogenous freezing, which can drastically alter cloud properties such as albedo, composition and lifetime (Hoose & Möhler, 2012; Kanji et al., 2017b; B. J. Murray et al., 2012). Despite the potential importance of INPs, there is still a lack of knowledge regarding their characteristics, sources, and ultimately their temporal and spatial distribution around the globe.

Our current knowledge of atmospheric INPs (under mixed-phase cloud conditions) suggests a number of potentially important aerosol types, including mineral dust, marine organics and terrestrial bioaerosols (DeMott et al., 2010; Kanji et al., 2017). The characteristics and source regions for mineral dust are relatively better understood than other potentially important INPs, and mineral dust from both high (A. Sanchez-Marroquin et al., 2020; Tobo et al., 2019) and low latitude sources (Boose, Welti, et al., 2016; Paul J. DeMott et al., 2003; Price et al., 2018) is thought to be the dominant INP around much of the globe at temperatures < − 20 °C. Marine organics and terrestrial bioaerosols have both been demonstrated to play a major role in the global INP burden, but the nature of these INPs are less well understood than that of mineral dust. Marine organics are of particular importance in remote marine regions where there is little mineral dust (Burrows et al., 2013; T. W. Wilson et al., 2015). Terrestrial bioaerosols are thought to outcompete mineral dust in the terrestrial mid-latitudes at temperatures > − 20 °C, however their source(s) and nature are at present poorly understood (Conen et al., 2016; McCluskey et al., 2018; O'Sullivan et al., 2018; Vergara-Temprado et al., 2017).

Known INPs of biological origin include bacteria, fungi, pollen and marine organics amongst others (Kanji et al., 2017b). Bacteria and fungi exhibit ice nucleation due to the presence of ice-nucleating proteins (Green & Warren, 1985; Lindow' et al., 1982; Pouleur, Richard, Martin, & Antoun, 1992), whilst the ice-nucleating ability of pollen has been linked to polysaccharides (Dreischmeier, Budke, Wiehemeier, Kottke, & Koop, 2017; Pummer, Bauer, Bernardi, Bleicher, & Grothe, 2012). Marine organic INPs, associated with sea spray, are thought to be biogenic and are often smaller than 0.22 µm, but it is currently not clear exactly what these ice-nucleating particles are and there may be multiple marine INP types (Creamean et al., 2019; DeMott et al., 2016; Irish et al., 2017, 2019; Schnell et al., 1975; Wang et al., 2015; Wilson et al., 2015). Compared to non-biological INPs, some microorganisms such as specific bacteria or fungi nucleate ice at relatively high temperatures; for example, the best-studied ice nucleating bacterium, *Pseudomonas syringae*, can nucleate ice at temperatures up to −2 °C (Morris et al., 2004; Morris et al., 2013). Despite the ice nucleation potential of primary biological aerosol particles, recognized since 1970s (Schnell, Vali, Schnell, & Vali, 1976), the global distribution and sources of biological INPs remain poorly understood (Kanji et al., 2017b; B. J. Murray et al., 2012). Hence characterizing the ice nucleating ability of the various categories of biological aerosol particles is important.

In bacteria, membrane proteins are thought to interact with water and impose order in supercooled water in such a way as to promote nucleation of ice. Pandey et al. (2016) demonstrated that in the case of *P. syringae* patterned hydrophilic-hydrophobic regions due to the interactions of amino acids belonging to the membrane protein led to the increased ordering of water molecules coupled with efficient removal of thermal energy from the

surrounding water molecules into the bacterial cell. This mechanism could potentially protect microorganisms at sub-zero temperatures and preserve their viability and infectivity in the atmosphere (Wilson, Grogan, and Walker 2012; Morris, Monteil, and Berge 2013). Whether or not a bacterium has the potential to produce ice-nucleating proteins is dependent on the presence of an ice nucleation gene. At present, eight ice-nucleating proteins are known and reviewed in the protein database UniProt, each with an associated gene (protein IDs: O33479, P06620, Q47879, P16239, O30611, P09815, P20469, P18127). It is thought that a single functional ice nucleation protein gene in bacteria is both necessary and sufficient for ice nucleation activity. The INA of a bacterium that has a gene for the ice-nucleating protein in its genome depends on the expression of the gene (i.e., if the protein coded by the gene is actually produced by the bacterium), the integration of the protein into the outer membrane of the bacterial cell and stabilization of the protein complex by the surrounding membrane constituents.

Viruses are a presently under-studied source with respect to their potential as atmospheric biological INPs. Very little is known about viruses in the atmosphere in general, and even less about their potential to influence cloud properties through cloud glaciation. The only studies we are aware of in which the ice-nucleating ability of a virus was examined was that of Junge & Swanson (2008) (who studied the polar *Colwellia* phage virus) and Cascajo-Castresana et al. (2020) who studied a series of common proteins and a single virus. The former found that these virus particles did not nucleate ice in their experimental system. The latter observed ice nucleation activity in the Tobacco mosaic virus (TMV), a plant virus that infects the family of Solanaceae such us tobacco, tomato, or pepper. TMV was shown to be above the baseline of the buffer solution it was suspended in, and it was noted in the study that whilst TMV had a lower onset freezing temperature of other samples in the study (a range of proteins), when normalized to cumulative active site density it was more active.
Compared to bacteria and other micron-sized, single-celled microorganisms, viruses are considerably smaller (from ~25 nm in diameter; except for the nucleocytoplasmic large DNA viruses that are cellular size). The small size of virus particles means that their atmospheric lifetime has the potential to be on the order of many days to weeks in the atmosphere, although this will depend on the size of the particles that they are internally mixed with. This relatively long lifetime means that viruses can persist in the atmosphere long enough to reach locations that other aerosol particles wouldn't (i.e. remote marine/polar regions where INP concentrations are typically low), but also can still be present once more active INP have been preferentially processed via freezing and precipitation. This is considerably longer than the lifetime of larger biological particles, especially those larger than ~10 µm, which have lifetimes of only hours (Grythe, Ström, Krejci, Quinn, & Stohl, 2014; Reche, D'Orta, Mladenov, Winget, & Suttle, 2018) and therefore have atmospheric abundances which decrease rapidly during transport (Hoose et al., 2010).

In addition to supermicron entities such as bacteria, submicron sized biological particles have also been shown to be effective ice nucleating particles (O'Sullivan et al., 2015). For example, it has been shown that there are biological INPs belonging to fungal and pollen samples at sizes below 200 nm (Fröhlich-Nowoisky et al., 2015; Pummer et al., 2012). Fertile soil samples when dispersed in water and filtered, have also been shown to have a significant number of ice-nucleating particles below 200 nm (Tom C J Hill et al., 2016; O'Sullivan et al., 2015). O'Sullivan et al. (2015) showed that some ice nucleation persisted in fertile soil samples

filtered to 1000 kDa, however ice nucleation above −10 °C was removed by these filtrations. Decayed plant litter was shown to have comparable INP concentrations before and after filtration through 200 nm filter pores, and retained a fraction of these INPs when further filtered through 20 nm filter pores (G. Vali et al., 1976). Ice-nucleating particles below 200 nm were measured in North American Arctic snow samples and in precipitation from North China temperate grassland (Du et al., 2017; Rangel-Alvarado, Nazarenko, & Ariya, 2015). The snow samples were shown to be of biological origin and subsequently tested for virus-like structures, of which none was observed. Despite this, the authors stated they could not preclude viruses as a potential explanation for the observed ice-nucleating activity, based on the size of the INPs and their likely origin. Measurements of INPs in the Arctic sea surface microlayer showed that most of the observed ice nucleation (in the immersion mode) was caused by particles between 0.02 and 0.2 µm in size and were heat labile; viruses were suggested as a potential explanation (Irish et al. 2017; Wilson et al. 2015). Atmospheric measurements made in the Arctic showed the presence of atmospheric INPs in the size range 150 - 340 nm (Creamean et al., 2019; Creamean et al., 2018). Size resolved measurements made in a boreal forest in Hyytiälä, Finland showed an instance in which INPs in the size range 250 - 500 nm dominated the atmospheric INP burden at temperatures > −22 °C, whilst measurements made at near surface level locations in the U.K showed INPs present at sizes below 250 nm (Porter et al., 2020). There is a growing body of evidence that suggests there is a reservoir of currently unidentified biological particles in the fine mode (<250 nm) present in soil/plant life, the oceans and the atmosphere. In this study, we test the hypothesis that viruses are a potential candidate for the source of these fine mode INPs.

It has been estimated that there are ~10^{31} virus particles in the biosphere (Whitman, Coleman, & Wiebe, 1998), with approximately 10^7 virus particles per ml of seawater, 10^8-10^9 per ml in marine surface sediments (Suttle, 2005, 2007) and 10^8-10^9 per gram of soil in different types of terrestrial environments (Srinivasiah et al., 2008). Numerous studies indicate that there are approximately 10-100 times more viruses compared to their host cells in any given environment (Cai et al., 2019; Srinivasiah et al., 2008). With respect to viral abundance in the atmosphere, there is at present a dearth of knowledge. Rastelli et al. (2017) measured the viral abundance in both the seawater microlayer and the aerosol phase directly above using a bubble generator system designed to mimic wave breaking in open seawater. Virus concentrations for seawater and sampled air were 5×10^{11} virus particles m^{-3} and $0.3–3.5 \times 10^5$ virus particles m^{-3}, respectively. Virus particles were measured from outdoor air samples using a filter based technique taken at a University campus, with the atmospheric virus particle concentration being measured as $1.2 \pm 0.7 \times 10^6$ virus particles m^{-3} (Prussin, Garcia, & Marr, 2015). The spatial and temporal variability of airborne viruses were investigated in a series of different locations (residential district, forest and an industrial complex), with concentrations of 1.7×10^6 to 4.0×10^7 virus particles m^{-3} being measured (Whon et al., 2012). Overall, the range of outdoor virus concentrations recorded in the literature range between 0.3×10^5 to 4.0×10^7 virus particles m^{-3}. It is likely that these numbers do not represent the full variability of virus particle concentration due to the scarcity of measurements.

Despite the large number of virus particles measured in various environments there are a relatively small number of different particle structures a virion (an infective virus particle) can have. This is due to physical constrains of protein fold space that make up the virus particle

architecture (Abrescia, Bamford, Grimes, & Stuart, 2012). Structurally similar viruses can have different host organisms and different geographical source locations (Atanasova, Roine, Oren, Bamford, & Oksanen, 2012; Bamford, 2003; Saren et al., 2005) . There are several observations of virus isolates with high genome identity originating from spatially distant environments (Atanasova, Demina, Buivydas, Bamford, & Oksanen, 2015; Pietila et al., 2012; Saren et al., 2005; Tschitschko et al., 2015).We have chosen virus particles for this study that represent several different symmetric or asymmetric virus architecture types, icosahedral, icosahedral with internal lipid membrane, icosahedral enveloped and lemon-shaped. As it would be beyond the realms of feasibility to test even a tiny fraction of the 10^{31} different viruses in the biosphere, we took the approach that we believe allows us to investigate the maximum parameter space and test the hypothesis that virus architecture/structure controls its ice-nucleating ability. In this study we present the ice-nucleating ability of viruses with these different architecture types, demonstrate the potential of different structural components in viruses to nucleate ice, and attempt to estimate the potential of viruses as a class of atmospheric ice-nucleating particles.

5.2 Materials and Methods

5.2.1 Growth media and strains

Bacterial and archaeal strains and viruses used in this study are listed in Table 5. Bacterial host strains were aerobically grown in Luria-Berthani broth at 28 °C for *Pseudomonas syringae* pathovar *phaseolicola* HB10Y, and *P. syringae* LM2489, and at 37 °C for *Escherichia coli* HMS174 and *E. coli* C122 strains. Archaeal host strains were aerobically grown in 23 % Modified Growth Medium (MGM) at 37 °C (Nuttall & Smith, 1993).

5.2.2 Virus purification and production of Phi6 subviral particles

Here, 1× signifies once purified particles and 2× twice purified, concentrated virus sample. Bacteriophages PRD1 and Phi6 were 1× purified as described in Bamford et al. (1995). The 2× purification of PRD1 was performed (Bamford et al., 1995; Lampi et al., 2018). The PRD1 particles devoid of DNA (procapsids) were collected after 1× purification, during which the DNA containing particles sediment further along the sucrose gradient compared to the empty procapsids. The 1× purified Phi6 was further purified to 2× by density gradient ultracentrifugation in 20-70 % sucrose in 20 mM K-phosphate buffer pH 7.2 with 1 mM $MgCl_2$ (designated here as K-phosphate buffer) followed by concentration as described in Bamford et al. (1995). Viruses Phi8, Phi12, Phi13 and, Phi2954 were produced and precipitated according to Qiao et al. (2010), and the 1× purification was performed by rate-zonal ultracentrifugation in 5-20 % sucrose gradients in K-phosphate buffer, Sorvall AH629 rotor, 24 000 rpm, 50 min, 15 °C, followed by concentration using differential ultracentrifugation, Sorvall T865 rotor, 34 000 rpm, 3 h, 10 °C. All other viruses were purified to 1× preparations according to protocols described in Eskelin et al. (2019) (for PhiX174), Pietilä et al. (2009) (for HRPV-1), Pietila et al. (2012) (for HRPV-6), Demina et al. (2016) (for HCIV-1) and Bath et al. (2006) (for His1).

Phi6 subviral particles were prepared according to Bamford et al. (1995), modified by Eskelin & Poranen (2018) (for butylated hydroxytoluene treated particles). Phi6 NC were prepared by adding 1 % final concentration of Triton X100 to 1× purified Phi6 particles in K-phosphate buffer and incubating 30 min at 22 °C. The treated particles were collected by ultracentrifuge,

Ti1270 rotor, 30 000 rpm, 4 h, 15 °C. Particles were flushed three times with and resuspended in 0.5 ml K-phosphate buffer overnight at 5 °C.

5.2.3 SDS-gel electrophoresis

The protein concentration of viral and subviral particles was measured by the Bradford assay using bovine serum albumin as a standard (Bradford, 1976). Virus samples were analyzed by sodium dodecyl sulfate- 16% polyacrylamide gel electrophoresis (SDS-PAGE) (Olkkonen & Bamford, 1989) to visualize viral protein profiles.

5.2.4 Ice nucleation sample preparation

Samples for µl-NIPI (T. F. Whale et al., 2015) experiments were prepared by diluting 1× or 2× purified virus particles to specific buffer solutions (Table 5) so that the final concentration of pfu/ml was 10^{10}-10^{12}. Subviral particles were used without dilution. Virus host strains were collected by centrifugation (Eppendorf, 13 000 rpm, 5 min, 22 °C), diluted into the same buffer as the virus (Table 5), centrifuged (Eppendorf, 13 000 rpm, 5 min, 22 °C) and resuspended into buffer according to Table 5.

5.2.5 Search for ice nucleation motifs

Currently, there are eight referenced ice nucleation proteins identified from bacterial cells according to the public protein database (UniProt, https://www.uniprot.org/). The ice nucleation motifs (INMs) predicted based on these genes are short protein sequences conserved in this protein family. They are abundant for the ice nucleation proteins (IN proteins), but scarce in the rest of the bacterial genomes. The group of motifs specific for a protein family can serve as a functional fingerprint indicating similarities in structure and function. It was previously determined that INM3 corresponds to the clathrate structure part of the protein responsible for ice nucleation activity in bacterial IN proteins (Gurian-Sherman & Lindow, 1993; Kajava & Lindow, 1993).

The INMs were acquired from SPRINT, an interface for PRINTS data bank of protein family fingerprints. SPRINT is a public domain database currently maintained at the University of Manchester (http://130.88.97.239/dbbrowser/sprint/). The INMs can be found in SPRINT by identifier ICENUCLEATN. All known ice nucleation motifs in IUPAC (International Union of Pure and Applied Chemistry) nomenclature are listed in Table 6. Since some of the putative viral proteins are not fully characterized, we used protein INMs from SPRINT to build generalized nucleotide motifs. The annotated viral genomes were acquired from the National Centre for Biotechnology Information (NCBI) genome database (Table 7).
Ice nucleation motifs were searched for in the viral genomes using MEME (Multiple Em for Motif Elicitation) Suite 5.1.0. (Bailey et al., 2009). The search was performed using MCAST (Motif Cluster Alignment Search Tool) and FIMO (Find Individual Motif Occurrences)-tools (Grant et al., 2011; Bailey & Noble, 2003). MCAST searches for input motifs in the query sequence for statistically significant clusters of non-overlapping occurrences. FIMO, in turn, searches for individual motif occurrences in the sequences, each motif independently. Each found occurrence was scored with p-value. The p-score thresholds for significant findings were set to 0.0001.

Putative IN-proteins were determined in the viral genomes based on the repetitiveness of IN motif occurrences in the sequences, as well as the total INM coverage. The INM coverage is calculated from the total length of the protein sequence matching the INM sequences

compared to the total length of the protein. The INMs were annotated to the sequences using Artemis 17.0.1 and the protein alignments were performed using Muscle 3.8.425 and visualized using Geneious Prime 2020.1.1. All the potential IN proteins are listed in Table 9. http://130.88.97.239/cgibin/dbbrowser/sprint/searchprintss.cgi?display_opts=Prints&category=None&queryform=false&prints_accn=PR00327

5.2.6 Ice nucleation experiments

Viral samples were prepared as described previously, and were vortexed for 30 seconds prior to being used. Ice nucleation experiments were carried out using the µL-NIPI (T. F. Whale et al., 2015). In brief, 1 µL droplets (in which sample material was suspended) were pipetted onto an aluminium cold stage, and ramped down in temperature. Droplet freezing was recorded using an optical sensor, with the droplet temperature being recorded at the freezing point.

Fraction frozen curves were calculated using equation 35

$$FF(T) = \frac{Number\ of\ droplets\ frozen(T)}{Number\ of\ droplet total} \quad (35)$$

$N_n(T)$ curves were calculated according to equation 36

$$n_n(T) = \frac{-ln(1-FF(T))}{VN} \quad (36)$$

Where FF(T) is the fraction frozen as shown in equation 1 and VN is the number of virus particles

5.2.7 Freezing point depression of pure water due to NaCl correction

The freezing point depression of pure water due to NaCl (i.e. in the buffer solutions) was calculated using Blagden's law:

$$\Delta TF = K_F \cdot b \cdot i \quad (37)$$

where ΔT_F is the freezing depression, K_F is the cryoscopic constant (1.853 K kg mol^{-1} for water), b molality and i is the Van't Hoff factor (2 for NaCl).

5.3Results

5.3.1 Ice nucleating ability of virus particles

We studied virus ice nucleation from a virus structural perspective using the nucleation by immersed particle instrument (µl-NIPI) technique (T. F. Whale et al., 2015). We examined the ice nucleation activity (INA) of 11 viruses with different particle architectures, in an effort to probe the hypothesis that virus architecture/structure influences the ice-nucleating ability of virus particles. (Figure 57). These viruses included five enveloped Cystoviruses of *P. syringae* hosts with particle diameters of ~85 nm (Phi8, 6, 12, 12 and 2954; Figure 57a), two icosahedral viruses with an internal lipid membrane and particle diameters of ~70 nm (Figure 57a, PRD1 and HCIV-1), one of the icosahedral viruses without the DNA (Figure 57 1b, PRD1 no DNA), one 30 nm icosahedral virus without lipids (Figure 57b, PhiX174), two enveloped pleomorphic viruses with particle diameter of ~50 nm (Figure 57c), and one lemon-shaped virus (Figure 57d). Phi6-like viruses are commonly used as models for viruses that cause respiratory illnesses like SARS-CoV-2, the causative agent of COVID-19, due to structure similarity. Of the

eleven viruses tested, nine showed an INA distinct from the INA of the buffer solution they were suspended in (Figure *58*).

Phi12, an enveloped virus infecting *Pseudomonas syringae*, was found to be the most ice nucleation active virus in our study (in terms of the number of INPs per virus particle, n_n). Phi12 was observed to trigger freezing from −15°C to −21°C, with n_n values between 5×10^{-10} to 5×10^{-8} particles^{-1}, meaning that approximately 1 in every 20 million Phi12 particle could nucleate ice at –20 °C which is in stark contrast to the more readily quoted 1 in every 100,000 for more common atmospheric INPs such as mineral dust or marine organics. The other structurally similar cystoviruses of *P. syringae* were all ice nucleation active, although less so compared to Phi12 (Figure 57e). At this point we address the question of if the host bacterial cells might introduce ice nucleating entities which might be confused with the virus particles. In particular, several ice nucleation active *P. syringae* strains have been described in previous studies (de Araujo, Rodrigues, Gonçalves, & Galante, 2019). However, none of the *P. syringae* host strains of the viruses used in this study exhibited an INA distinguishable from that of the buffer solution (Table 5, Figure 59). Also, none of the strains contain a functional ina-gene, only partial pseudogenes. This indicates that the INA observed here is solely due to the virus particles. In addition (and more importantly), the virus samples used in the µl-NIPI test were purified according to established virus purification protocols (See Methods and Meterials) and the purity was verified on sodium dodecyl sulfate-polyacrylamid gel electrophoresis (SDS-PAGE; Figure 60). Furthermore, a well-established model virus, Phi6, was purified twice and the results of both purifications were examined on the µl-NIPI assay strongly implying that the virus particles are responsible for the observed INA (Figure 61) rather than contamination from the process or host bacteria.

The source of the INA was further studied using two of the best-characterized model viruses, Phi6 of *P. syringae*, and PRD1 of *E. coli*. Regarding Phi6, we used biochemical dissociation to disassemble the virus particles into sub-viral particles (Figure 62). First, the virus spike proteins were removed using butylated hydroxy toluene (BHT), with the resulting particle referred to as Phi6 BHT and the separate spike proteins referred to as Phi6 P3. Secondly, the lipid envelope and the associated proteins were removed using the anionic detergent Triton X100, exposing the nucleocapsid (NC) structure of Phi6 virion (Figure 62a). Each of the sub-viral particles was shown to have an INA distinguishable from the K-phosphate buffer (Figure 62b). Each of the sub-viral components, along with Phi6, was normalized to the mass of particles per volume of sample (n_m). When normalized in this manner, each component spanned approximately the same range in n_m space, $10^2 – 10^4$ (mg^{-1}) across a range of temperatures. The freezing spectrum of each component was similar, with the Phi6 BHT sub-viral components having slightly warmer freezing temperatures than Phi6 at equivalent n_m values, whereas spike proteins (P3 in Figure 62b) had a slightly lower freezing temperature than Phi6. NC was found to be the most IN active sub-viral particle of Phi6 (Figure 62c), freezing approximately 4 °C warmer across the measured n_m range when compared to Phi6. INA is in part related to size (Pummer et al., 2015), hence since the spike proteins are only ~20 nm in diameter, whereas the BHT and NC particles are close to 80 nm. Hence, the difference in activity may be related to size. It is not clear how virus particles behave in the atmosphere, but several environmental stressors can disrupt virus particles exposing their internal parts. The other Phi6 sub-viral particles were also IN active (Figure 62) indicating, that the virus has broad IN potential, either being active as a whole or in a disrupted form. PRD1

was measured for its INA both with and without DNA. The n_n values for PRD1 with and without DNA are shown in Figure 63, and are similar to one another. This result suggests that the presence of PRD1's DNA is not related to the INA of the particles.

To further our understanding of the influence of virus structure on IN activity, we tested six other viruses, four archaeal and two bacterial. Of these six viruses, two archaeal viruses (HRPV1 and HRPV6) were enveloped like Phi6, but lack particle symmetry and an NC structure (Figure 57c). HRPV1 (Figure 58b) was not distinguishable from the Saline buffer (Table 5) it was suspended in, whilst HRPV6 (Figure 58) was distinguishable from the buffer, but was not distinguishable from its host, and as such are shown as limiting values (Figure 64). Viruses with icosahedral symmetry that contain an internal lipid membrane (PRD1 and HCIV-1, Figure 57b) were also tested to further probe the dependency of viral INA on structure. PRD1, a well-known model virus (Bamford et al., 1995) was shown to be INA with a signal distinguishable from both the K-phosphate buffer and its host (Figure 65), and n_n values comparable to that of the majority of the P. syringae viruses (excluding Phi12) (Figure 57e). HCIV-1 did not have an INA distinguishable from the Saline buffer it was suspended in and is thus shown as a limiting value (Figure 57b). Another icosahedral virus, PhiX174, this time without a lipid membrane (Figure 1B) was tested and had n_n values similar to that of PRD1 and the majority of the P. syringae viruses. We further studied the INA dependency on virus architecture by studying an asymmetrical lemon-shaped archaeal virus, His1 (Bath et al., 2006). Interestingly, the virus had a higher INA than all the tested viruses, except for Phi12 (Figure 57d-e), indicating that structurally different viruses, symmetric or asymmetric, can be IN active. His1 was shown to be distinguishable from the saline buffer solution (Figure 58) and its host (Figure 66).

5.3.2 Genetic analysis of ice active virus particles

The genomes of the 11 viruses included in this study were explored by bioinformatic analysis to further examine the source of IN activity. The ice nucleation activity observed in bacteria is due to protein structures which mimic ice crystal clathrate structure on the cell surface thus facilitating ice crystal formation around the cell (Kajava & Lindow, 1993). In viruses, the source of INA might also be manifested due to proteinaceous origin. The possibility of the capsid or membrane proteins in virus particles possessing similar structure and function as explanation for their ice nucleation capacity was explored in this study. This hypothesis was approached using ice nucleation motifs, specific and conserved short sequences in IN proteins, to search for the proteins potentially capable of nucleating ice.

Viral proteins with significant INM coverage and presence of INM3 in their sequence were predicted in eight of the viruses (Figure 67; Table 10). According to the results, only Phi13 and PhiX174 did not have potential IN proteins, with His1 having coverage below 15% and so is not shown in the table. Other viruses contained at least one potential protein with INM coverage of 15-50% and obligatory INM3 presence. However, the INA of Phi13 and PhiX174 is similar to the majority of the tested viruses such as Phi6. Similarly, HRPV1 and HCIV1 contain potential IN proteins, but these viruses had the weakest INA of the tested virus particles. Therefore, the presence of INMs in the sequence does not correlate to the capacity to nucleate ice.

5.3.3 Implications for the atmospheric ice nucleating particle population

In order to estimate the INP concentrations associated with virus particles in the atmosphere we have combined the n_n values shown in Figure 57e and the upper limit of the concentration of viruses in the atmosphere from literature data (taken as 4×10^7 particles m^{-3}; see discussion in the introduction). It is important to note that we based these virus INP concentrations on the INA of the specific samples which we studied and it may be possible that other virus particles have greater INA. However, since there are a limited number of virus architectures and we test a range of these architectures, we tentatively suggest that that we capture the typical range of INA of virus particles. Also shown on Figure 68 are envelopes showing the range of data from field campaigns in terrestrial (orange) and remote marine/polar environments (green) (see Table 8 for a list of representative measurements included in these envelopes).

As discussed in the introduction, in terrestrial environments, mineral dust is thought to be a very important INP type, with marine organics playing a secondary role (Vergara-Temprado 2017). In addition, there is evidence that biological INP play an important role in the terrestrial mid-latitudes (Franz Conen et al., 2016; Tom C J Hill et al., 2016; O'Sullivan et al., 2018; Pratt et al., 2009; Šantl-Temkiv et al., 2019). Figure 68 shows that across the entire temperature spectra relevant for mixed-phase clouds, the concentration of virus INPs are lower than the lowest typical INP concentrations in terrestrial influenced areas. The closest the terrestrial envelope and the virus data points come to overlapping is between −18 °C to −22 °C, at which temperatures the difference in INP concentration is approximately one order of magnitude, i.e. at most they might contribute about 10% of the INP population at around -20 °C. Furthermore, one might expect that in environments where there is a strong source of virus particles, there is also a strong source of other biological materials, hence the influence of virus INP may be overestimated in our simple analysis. Overall, these results suggest that virus INPs generally play a minor role in regions influenced by terrestrial INPs.

Remote marine locations are less influenced by active terrestrial sources and thus the INP populations there are different from those of the terrestrial atmosphere (Creamean et al., 2019; DeMott et al., 2016; McCluskey et al., 2018a; McCluskey et al., 2018b). Marine organics and sea spray aerosol have been shown to be INP sources of first order importance in such environments (DeMott et al., 2016; Vergara-Temprado et al., 2017; Wilson et al., 2015). There have been field measurements made in remote marine environments, which have reported remarkably low INP concentrations. McCluskey et al. (2018b) measured INP concentrations in a pristine marine environment at the Mace Head research station in 2015, with INP concentrations as low as 10^{-3} L^{-1} at −20 °C. In a separate field campaign, measurements were made in the Southern Ocean, INP concentrations range between 3.8×10^{-4} to 4.6×10^{-3} at −20 °C (McCluskey et al., 2018a). Figure 68 shows overlap between the virus INP data points and the marine envelope in the temperature range −15 °C to −27 °C, with the most active of the virus INPs being approximately 15× higher than the lower limit of the marine envelope at −20 °C. Whilst this by no means proves that virus INPs are important in remote marine environment, it indicates they may contribute to the atmospheric INP burden in such regions. However, the lowest INP concentrations in the remote marine environment are most likely associated with periods when the aerosol concentrations were lowest, as a result of the combined effect of precipitation and weak sources. Under these conditions, virus particles would also presumably be depleted.

5.4 Discussion

In this study we show a range of viruses can nucleate ice heterogeneously when immersed in supercooled solution droplets. A selection of virus types with diverse architectures are shown to have ice-nucleating abilities spanning three orders of magnitude at −20 °C, when normalized to particle number. We probed the virus ice-nucleating ability dependence on virus particle structure/architecture, showing that for our selected viruses there was not a dependency on virus architecture. Bioinformatic analysis shows that our current knowledge of ice nucleation due to *ina* genes/proteins exhibited by bacterial ice nucleators is likely insufficient to understand why viruses nucleate ice, which can be due to e.g. the overall arrangement of structural proteins making up the virus particles.

Our results are based on a small subsample of virus types but include several of the most prominent viral architectures, in an effort to maximize our coverage of this parameter space. Nine out of 11 tested viruses were ice nucleation active indicating that several structurally different viruses can have IN potential. In addition, it has been shown previously that a tobacco mosaic virus can also nucleate ice (Cascajo-Castresana et al., 2020). While we have selected virus particles with a range of architectures that are relatively common in nature, it is possible that other virus particles nucleate ice more or less effectively. In particular, the specific virus types we have studied here are from the terrestrial or aquatic environment; the isolation and testing of a range of marine viruses presents an important next step in quantifying the importance of viral ice nucleators. More work needs to be done to understand what drives viral ice nucleation, whether it would be dependent on virus structure/morphology, host, or some other factor.

This study shows the potential role viruses play as atmospheric INPs in certain environments. The ubiquity of viruses in the atmosphere implies they could serve as a baseline of INPs in situations where other, better-known atmospheric INPs are absent in any meaningful quantity. However, our estimates for the upper limit of virus INPs suggest they do not play a meaningful role in terrestrial environment, but may contribute to the INP population in marine environments. More work needs to be done to understand both why viruses nucleate ice and what role they play in both regional and global atmospheric ice nucleation.

5.5 Acknowledgements

Helin Veskiväli and Emeline Vidal are thanked for technical assistance. We thank Dr. Leonard Mindich for providing bacteriophages Phi12, Phi13, Phi2954 and *P. syringae* bacterial strain. Professor Ben Fane is thanked for providing PhiX174 bacteriophage. The use of the facilities and expertise of the Instruct-HiLIFE Biocomplex unit, member of Biocenter Finland and Instruct-FI, is gratefully acknowledged. N.S.A. wants to acknowledge the Academy of Finland Postdoctoral Grant 309570 and the Scientific Advisory Board for Defense grant VN/627/2020-PLM-9. We thank the European Research Council (648661 MarineIce, and 713664 CryoProtect) and the Natural Environment Research Council (NE/T00648X/1, M-Phase) for funding. The data associated with this paper are openly available from the University of Leeds Data Repository https://doi.org/XXXXX.

5.6 Figures and Tables

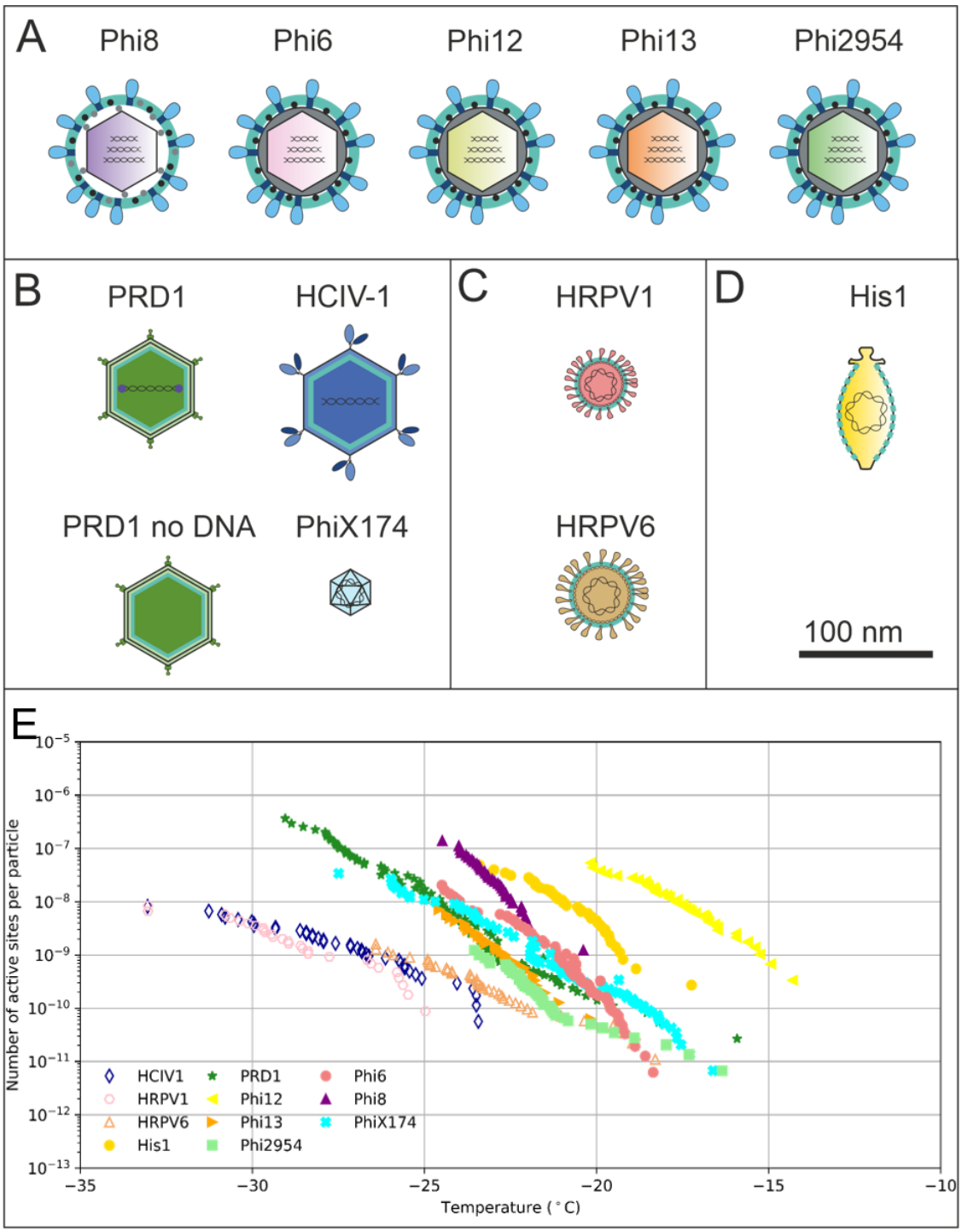

Figure 57: Graphical representation of the virus particles used in the ice nucleation study and their ice nucleating ability. A. Enveloped icosahedral viruses. B. Icosahedral viruses. C. Pleomorphic viruses. D. Lemon-shaped virus. E. Ice nucleation activity plots, where hollow marker indicate limit of detection (LoD) measurements in which the freezing temperatures were consistent with the virus free saline buffer control. Virus particles are to scale according to the 100 nm scale bar. Temperature values have been corrected for freezing point depression of NaCl.

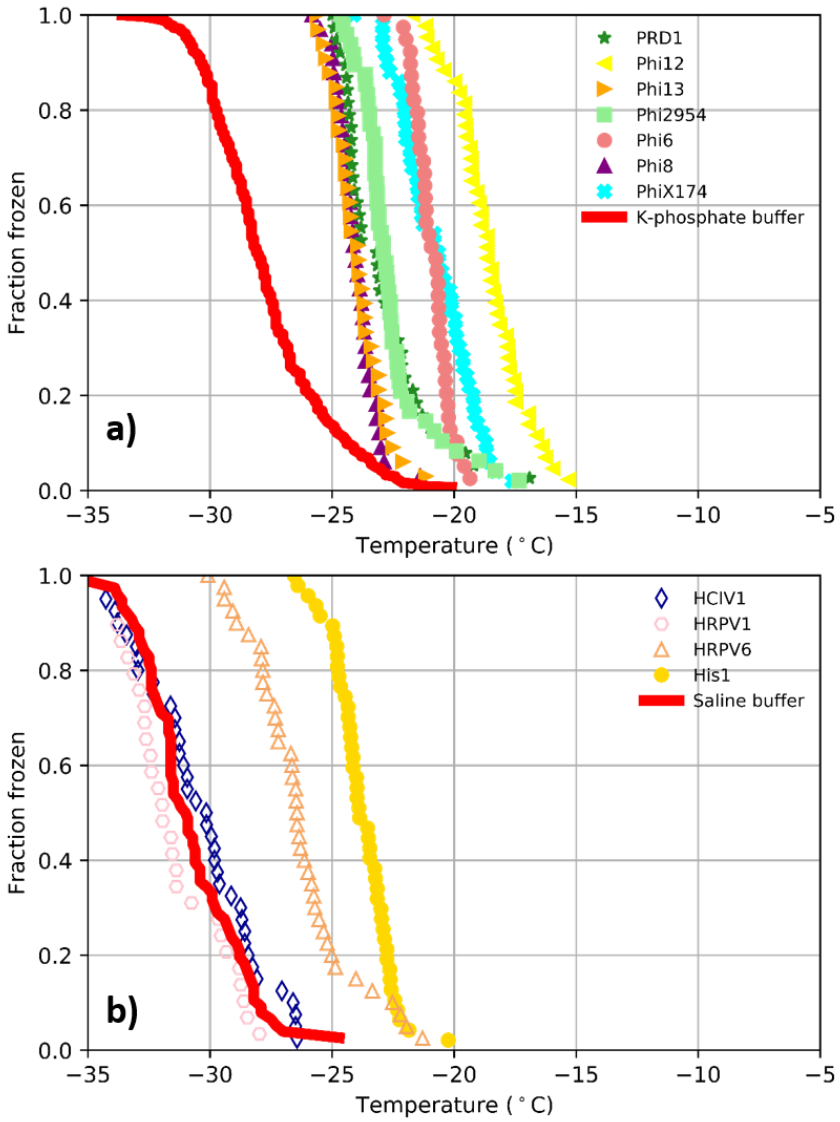

Figure 58: Fraction from curves for virus samples compared to the buffer solutions they were suspended in. A. Viruses suspended in K-phosphate buffer. B. Viruses suspended in Saline buffer. These fraction frozen curves are not adjusted for salt concentrations in the buffer solution, but both samples were suspended in the same buffer solution and would have experienced the same freezing point depression due to NaCl.

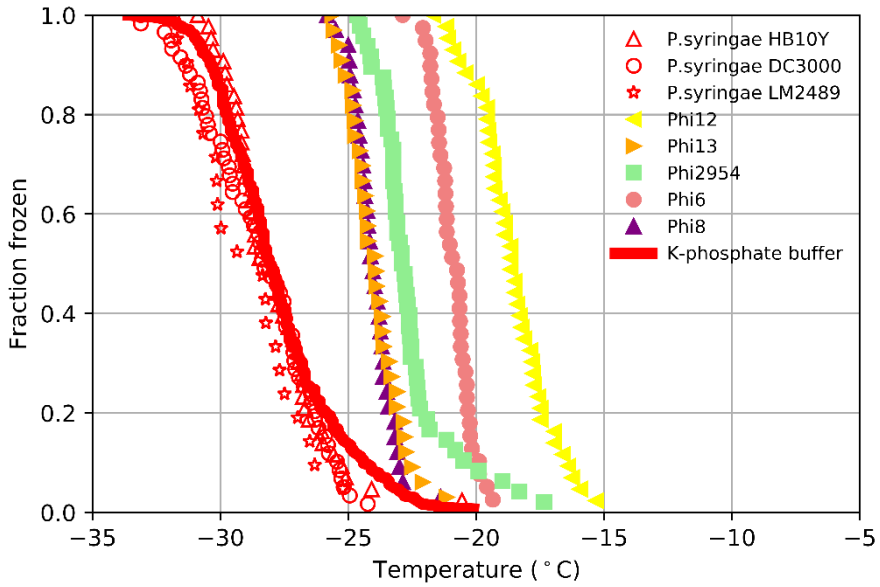

Figure 59: Fraction frozen curves of the bacterial viruses of P.syringae, the P.syringae strains used as hosts, and the K-phosphate buffer they were suspended in. The host bacteria did not give an INA signal distinguishable from the K-phosphate buffer. These fraction frozen curves are not adjusted for salt concentrations in the buffer solution, but both samples were suspended in the same buffer solution and would have experienced the same freezing point depression due to NaCl.

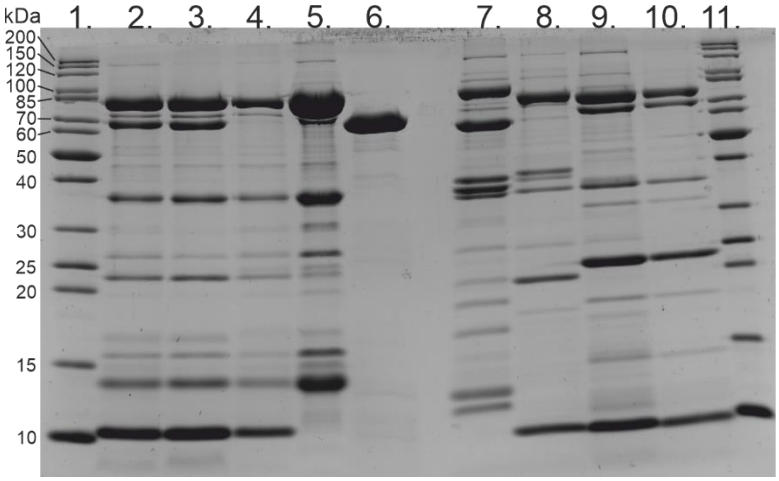

Figure 60: Subviral particles of Phi6 and protein profiles of Cystoviruses. 1. Protein standard, sizes marked on the left side in kilodaltons (kDa). 2. 1× purified Phi6 virus. 3. 2× purified Phi6 virus. 4. BHT treated Phi6. 5. NC of Phi6. 6. P3 protein of Phi6. 7. Phi8 virus. 8. Phi12 virus. 9. Phi13 virus. 10. Phi2954 virus. 11. Protein standard.

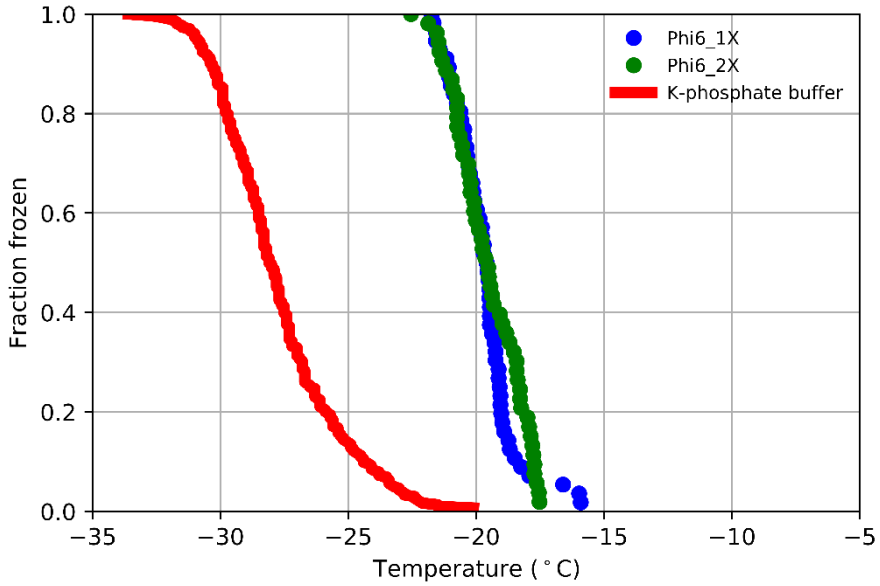

Figure 61: Fraction frozen curves showing the INA of Phi6 when purified using the 1X and 2X methods. The lack of reduction in INA when the sample is purified further implies that the INA is driven by the virus particles, not any contaminants.

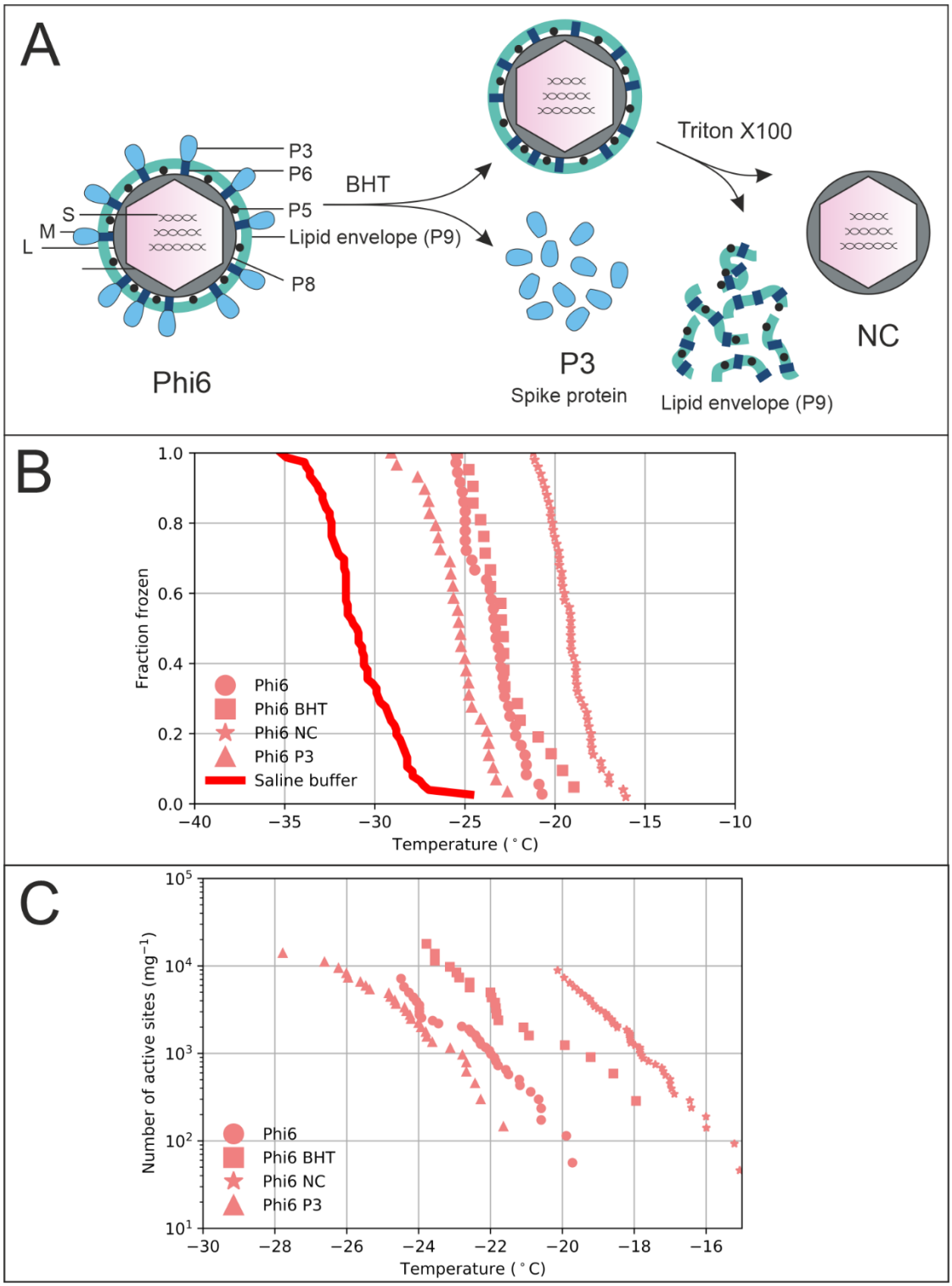

Figure 62: Ice nucleation activity of the subviral particles of Phi6 virus. A. Biochemical dissociation of Phi6 virion. Small genome fragment is marked as S, medium genome fragment as M and large genome frgment as L; P3 is spike protein, P5 is lytic enzyme, P6 is membrane fusion protein, P8 is outer capsid lattice protein and P9 is major envelope protein; BHT means butylated hydroxyl toluene; NC is nucleocapsid. B. Fraction frozen curves for Phi6 and its sub-viral components. These values have not been correct for freezing point depression due to NaCl. C. The INA of Phi6 and its sub-viral components

normalized to the mass of particle per volume of suspension. Phi6 BHT in graphs B and C refers to spikeless enveloped icosahedral structure. Temperature values have been corrected for freezing point depression of NaCl.

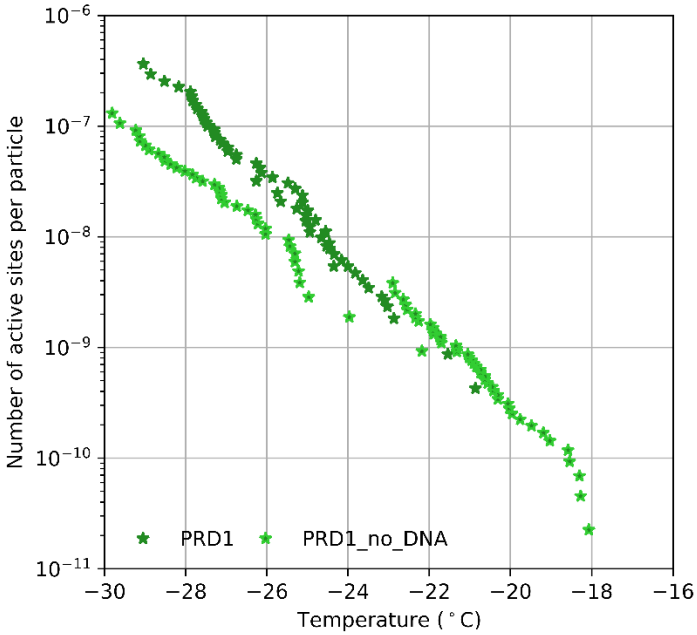

Figure 63: The number of active sites per particle for PRD1 with and without DNA. Temperature values have been corrected for freezing point depression of NaCl.

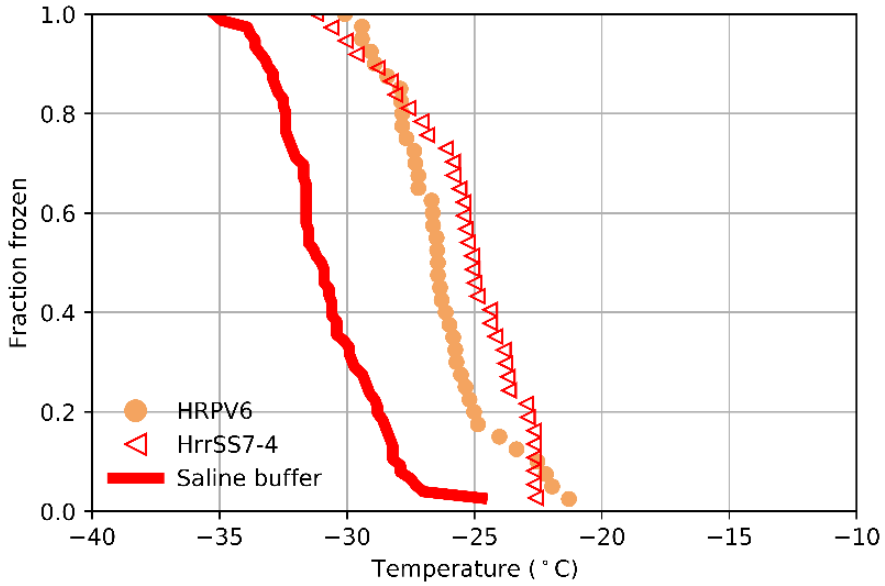

Figure 64: Fraction frozen curves of the archael virus HRPV6, its host, HrrSS7-4, and the saline buffer they were suspended in. HRPV6 did not give an INA signal distinguishable from its host. These fraction frozen curves are not adjusted for salt concentrations in the buffer solution, but both samples were suspended in the same buffer solution and would have experienced the same freezing point depression due to NaCl.

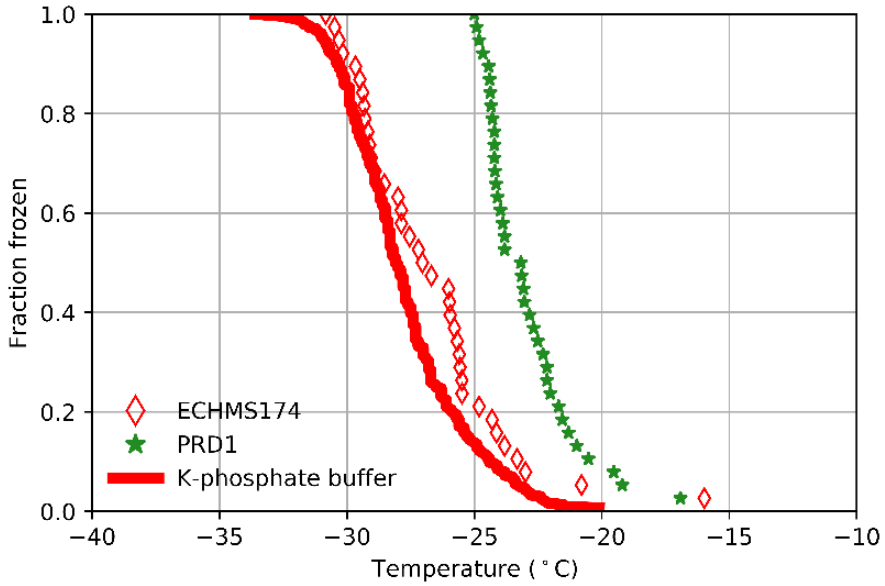

Figure 65: Fraction frozen curves of the bacterial virus PRD1, its host, ECHMS174, and the K-phosphate buffer in which they were suspended. PRD1 gave an INA distinguishable from both the K-phosphate buffer and its host. These fraction frozen curves are not adjusted for salt concentrations in the buffer solution, but both samples were suspended in the same buffer solution and would have experienced the same freezing point depression due to NaCl.

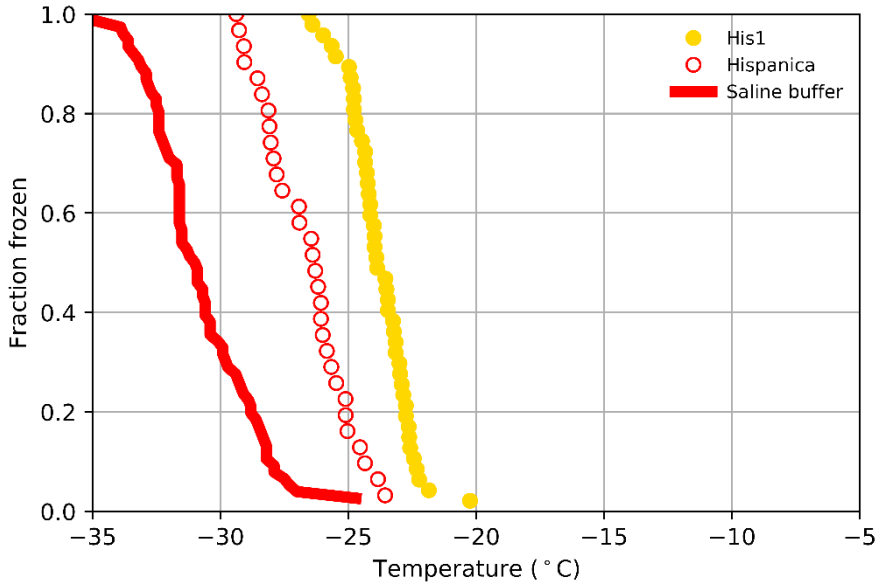

Figure 66: Fraction frozen curves of the bacterial virus His1, its host, Haloarcula hispanica, and the K-phosphate buffer they were suspended in. PRD1 gave an INA distinguishable from both the Saline buffer and its host. These fraction frozen curves are not adjusted for salt concentrations in the buffer solution, but both samples were suspended in the same buffer solution and would have experienced the same freezing point depression due to NaCl.

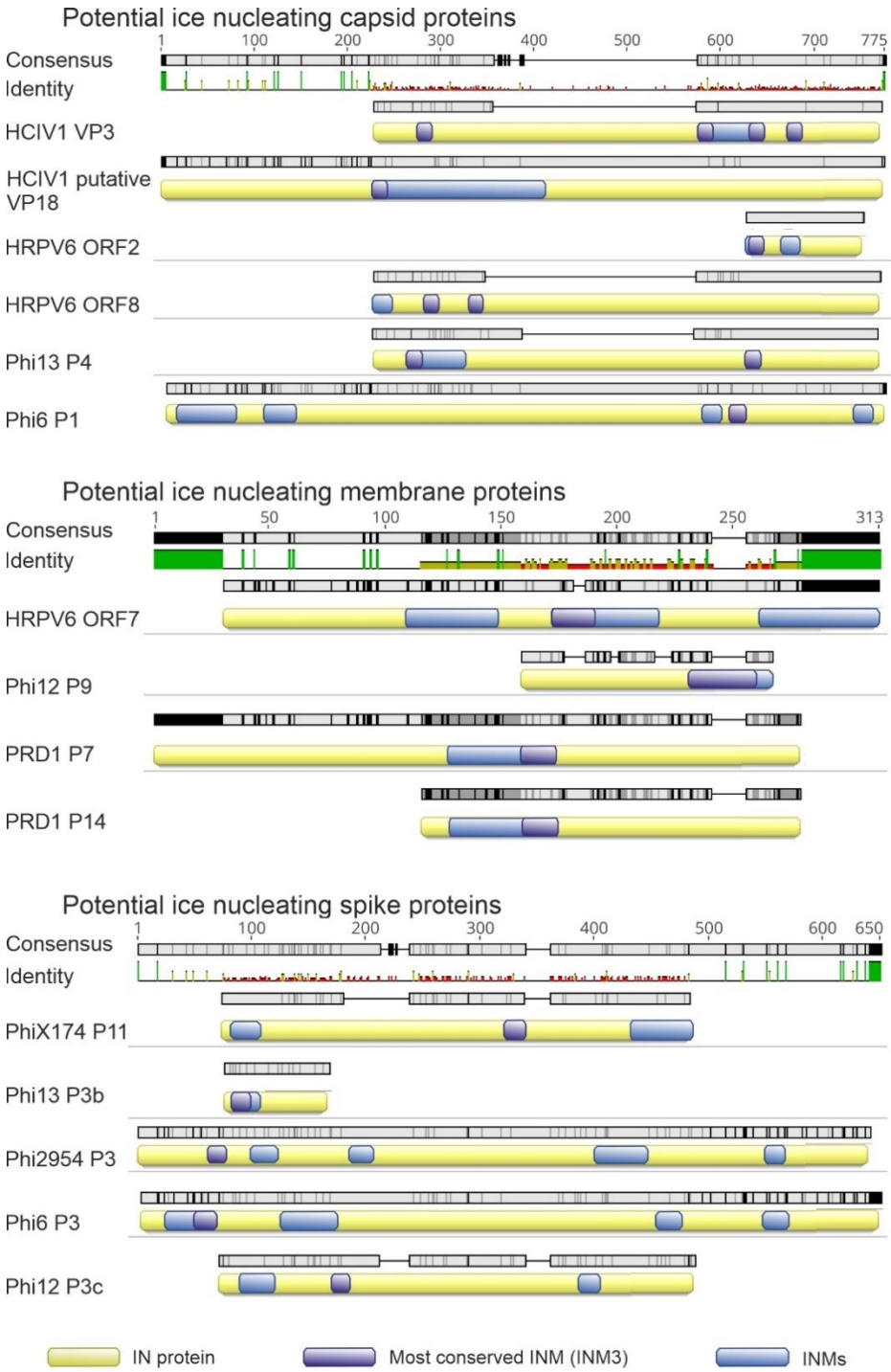

Figure 67: Multiple sequence alignment of potential IN proteins in the tested INA viruses. The predicted INMs shown in blue and the most conserved motif marked in violet. Multiple sequence alignment was done using Muscle program in Geneious Prime.

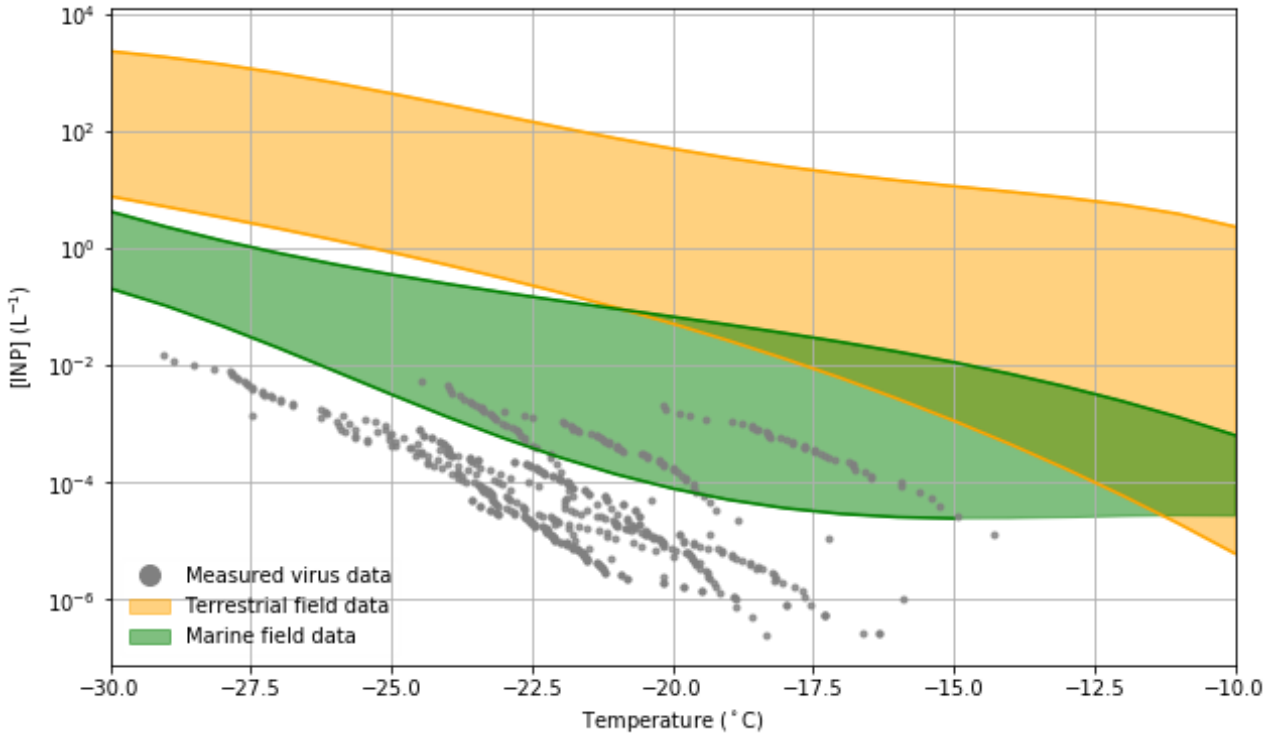

Figure 68: Estimated viral INP concentration based on measured ice-nucleating ability of virus particles and upper limit literature values of viral particles in the atmosphere compared to measured INP concentrations in both terrestrial (orange) and marine/polar (green) environments. Table 4 shows a list of the studies from which the data to create the field measurement envelopes were obtained. Temperature values have been corrected for freezing point depression of NaCl.

Table 5: Viruses and virus hosts used in this study.

Virus	Virus morphology	Virus host	Host domain	Virus origin	Virus buffer	Reference
Phi6	Enveloped; icosahedral	Pseudomonas syringae[d] HB10Y	Bacteria	Bacteria-infected bean, USA	K-phosphate buffer[a]	Vidaver et al., 1973
Phi6		P. syringae DC3000	Bacteria			
Phi8	Enveloped; icosahedral	P. syringae[d] LM2489	Bacteria	Bacteria-infected pea, USA	K-phosphate buffer	Mindich et al., 1999
Phi12	Enveloped; icosahedral	P. syringae[d] LM2489	Bacteria	Bacteria-infected bacil, USA	K-phosphate buffer	Mindich et al., 1999
Phi13	Enveloped; icosahedral	P. syringae[d] LM2489	Bacteria	Bacteria-infected radish, USA	K-phosphate buffer	Mindich et al., 1999
Phi2954	Enveloped; icosahedral	P. syringae[d] HB10Y	Bacteria	Bacteria-infected radish, USA	K-phosphate buffer	Qiao et al., 2010.
PRD1	Icosahedral with inner membrane	Salmonella enterica DS88	Bacteria	Sewage water, USA	K-phosphate buffer	Caldentey et al., 1990.
PRD1		Escherichia coli HMS174	Bacteria			
PhiX174	Icosahedral	E. coli C122	Bacteria	Human samples, Paris, France	Tris-HCl buffer[b]	McKenna et al., 1992
His1	Lemon-shaped	Haloarcula hispanica	Archaea	Salt lake water, Australia	Saline buffer[c]	Bath et al., 2006; Pietilä et al., 2013
HRPV-1	Pleomorphic	Halorubrum sp. PV6	Archaea	Saltern water, Italy	Saline buffer	Pietilä et al., 2009
HRPV-6	Pleomorphic	Halorubrum sp. SS7-4	Archaea	Salt crystals, Thailand	Saline buffer	Pietilä et al., 2012
HClV-1	Icosahedral with inner membrane	Haloarcula californiae	Archaea	Saltern water, Italy	Saline buffer	Demina et al., 2016

[a] K-phosphate buffer contains: 20 mM K-phosphate pH 7.2, 1 mM $MgCl_2$

[b] Tris-HCl buffer contains: 50 mM Tris-HCl pH 7.2, 100 mM NaCl

[c] Saline buffer contains: 20 mM K-phosphate pH 7.2, 500 mM NaCl, 1 mM $MgCl_2$

[d] The classification was updated, also known as *Pseudomonas savastanoi*

Table 6: A list of known INMs as generalized nucleotide sequences from SPRINT database in IUPAC codes used for MEME searches.

INM	Sequence
Motif 1	GAYCAYKGNGGNHTNRTHTGGCCNNYNNBNGGNHYNGTNGARWSNMRNTWYTGG
Motif 2	YTNWSNNYNMAYGCNGAYGCNMRNHGNRWNGTNKSNGARGTNRMNRYNGVNGANHKNHTN
Motif 3	YTNACNRCNGGNTAYGGNWSNACNHSNACNGCNGGNGCNGAYWSN
Motif 4	TAYYTNACNGCNGGNGAYMGNWSNAARYTNACNGCNGGNVAYGAYWSNRYNYTNATGGCNGGNGAY
Motif 5	YTNATHTTYMGNYKNTGGGAYGGNRARMGNTAYMSNMANBTNGTNGYNMRNACNGGN
Motif 6	GRNRTHGARDSNGAYRTNCCNTAYYANRTNRAYGANGANDVNRAYNTNBTNRWNAARSCN

Table 7: Genbank IDs of the analyzed viral genomes. For Cystoviruses, DNA fragments are specified in brackets (S/M/L).

Virus	Genbank ID
PhiX174	NC_001422.1
HRPV6	NC_017089.1
HRPV1	NC_012558.1
His1	NC_013758.1
PRD1	NC_001421.2
Phi2954	NC_012091.2 (L), NC_012092.1 (M), NC_012093.1 (S)
Phi13	NC_004172.1 (L), NC_004171.1 (M), NC_004170.1 (S)
Phi12	NC_004173.1 (L), NC_004175.1 (M), NC_004174.1 (S)
Phi8	NC_003299.1 (L), NC_003300.1 (M), NC_003301.1 (S)
Phi6	NC_003715.1 (L), NC_003716.1 (M), NC_003714.1 (S)
HCIV1	NC_030848.1

Table 8: A list of studies from which data used in the creation of the field measurement envelopes for Figure 4 was obtained.

Study	Environment	Location
Price et al., 2018	Terrestrial influenced	Eastern tropical Atlantic in African dust plumes
O'Sullivan et al., 2018	Terrestrial	UK (rural site)
Ardon-dyer, Levin., 2014	Terrestrial	Israel
Petters and Wright, 2015	Terrestrial	Terrestrial mid-latitudes
McCluskey et al., 2018	Marine	Ireland (Macehead)
McCluskey et al., 2018	Marine	Southern Ocean

Table 9: Ice nucleation proteins, coding genes and references.

Protein name	Gene name	Organism	Length (aa)	Reference
Ice nucleation protein	inaV	Pseudomonas syringae	1196	Schmid, Daniel, Pridmore, David, Capitani, Guido, Battistutta, Roberto, Neeser, Jean-Richard and Jann, Alfred(1997), Molecular organisation of the ice nucleation protein InaV from Pseudomonas syringae , FEBS Letters, 414, doi: 10.1016/S0014-5793(97)01079-X
Ice nucleation protein	inaZ	Pseudomonas syringae pv. syringae	1200	Green, R., Warren, G. Physical and functional repetition in a bacterial ice nucleation gene. Nature 317, 645–648 (1985). https://doi.org/10.1038/317645a0
Ice nucleation protein InaU	inaU	Pantoea ananas (Erwinia uredovora)	1034	Yasuyuki Michigami, Satoshi Watabe, Keiko Abe, Hitoshi Obata & Soichi Arai (1994) Cloning and Sequencing of an Ice Nucleation Active Gene of Erwinia uredovora, Bioscience, Biotechnology, and Biochemistry, 58:4, 762-764, DOI: 10.1271/bbb.58.762
Ice nucleation protein	iceE	Enterobacter agglomerans (Erwinia herbicola) (Pantoea agglomerans)	1258	Gareth Warren, Loren Corotto. The consensus sequence of ice nucleation proteins from Erwinia herbicola, Pseudomonas fluorescens and Pseudomonas syringae, Gene, Volume 85, Issue 1, 1989, Pages 239-242, ISSN 0378-1119, https://doi.org/10.1016/0378-1119(89)90488-5.
Ice nucleation protein	inaK	Pseudomonas syringae	1148	Directly submitted to the EMBL/GenBank/DDBJ databases July 1997; UniProtKB: locus ICEK_PSESX, accession O30611.
Ice nucleation protein	inaW	Pseudomonas fluorescens	1210	Warren G, Corotto L, Wolber P. Conserved repeats in diverged ice nucleation structural genes from two species of Pseudomonas. Nucleic Acids Res. 1986 Oct 24;14(20):8047-60. doi: 10.1093/nar/14.20.8047. PMID: 3774551; PMCID: PMC311833.
Ice nucleation protein InaA	inaA	Pantoea ananas (Erwinia uredovora)	1322	Abe, Keiko, Watabe, Satoshi, Emori, Yasufumi, Watanabe, Michiko and Arai, Soichi (1989), An ice nucleation active gene of Erwinia ananas , FEBS Letters, 258, doi: 10.1016/0014-5793(89)81678-3
Ice nucleation protein	inaX	Xanthomonas campestris pv. translucens	1567	Zhao, J., Orser, C.S. Conserved repetition in the ice nucleation gene inaX from Xanthomonas campestris pv. translucens . Mol Gen Genet 223, 163–166 (1990). https://doi.org/10.1007/BF00315811

Table 10: Potential IN proteins, their location, function and INM-coverage.

Virus name	IN-protein candidates	Protein function	Location in virus	IN-motif coverage (%)	Protein ID number
Phi6	P3	Adsorption to host cells, attachment to type IV pilus	spikes	18	NP_620351.1
	P1	Major inner capsid protein, RNA binding, replication and transcription	capsid	20	NP_620348.1
Phi12	P3c	Putative host attachment protein	spikes	16	NP_690834.1
	P9	Membrane protein	external lipid membrane	28	NP_690828.1
Phi13	P3b	Putative host attachment protein	spikes	31	NP_690814.1
	P4	Hexameric packaging NTPase	5-fold vertices of the procapsid	21	NP_690818.1
Phi2954	P3	Host attachment protein	spikes	18	YP_002600769.1
PhiX174	P11	Minor spike protein	spikes	29	NP_040713.1
HCIV1	Putative protein VP18	Putative minor capsid protein	unknown hypothetically capsid	24	YP_009272867.1
	VP3	Capsid protein	capsid	31	YP_009272848.1
HRPV6	ORF2	Unknown	unknown hypothetically capsid	33	YP_005454286.1
	ORF7	Integral component of the membrane	external lipid membrane	47	YP_005454291.1
	ORF8	ATP-binding, AAA-type ATPase	unknown hypothetically capsid	16	YP_005454292.1
PRD1	P7	Transclycosylase	lipid membrane	18	YP_009639979.1
	P14	DNA delivery	lipid membrane	31	YP_009639980.1

5.7 References

Abrescia, Nicola G.A., Dennis H. Bamford, Jonathan M. Grimes, and David I. Stuart. 2012. "Structure Unifies the Viral Universe." Annual Review of Biochemistry 81 (1): 795–822. https://doi.org/10.1146/annurev-biochem-060910-095130.

Araujo, Gabriel Guarany de, Fabio Rodrigues, Fabio Luiz Teixeira Gonçalves, and Douglas Galante. 2019. "Survival and Ice Nucleation Activity of Pseudomonas Syringae Strains Exposed to Simulated High-Altitude Atmospheric Conditions." Scientific Reports 9 (1): 1–11. https://doi.org/10.1038/s41598-019-44283-3.

Atanasova, Nina S., Tatiana A. Demina, Andrius Buivydas, Dennis H. Bamford, and Hanna M. Oksanen. 2015. "Archaeal Viruses Multiply: Temporal Screening in a Solar Saltern." Viruses 7 (4): 1902–26. https://doi.org/10.3390/v7041902.

Atanasova, Nina S., Elina Roine, Aharon Oren, Dennis H. Bamford, and Hanna M. Oksanen. 2012. "Global Network of Specific Virus-Host Interactions in Hypersaline Environments." Environmental Microbiology 14 (2): 426–40. https://doi.org/10.1111/j.1462-2920.2011.02603.x.

Bailey, Timothy L., Mikael Bodén, Fabian A. Buske, Martin Frith, Charles E. Grant, Luca Clementi, Jingyuan Ren, Wilfred W. Li, and William S. Noble. 2009. "MEME SUITE: Tools for Motif Discovery and Searching." Nucleic Acids Research. https://doi.org/10.1093/nar/gkp335.

Bamford, Dennis H. 2003. "Do Viruses Form Lineages across Different Domains of Life?" Research in Microbiology. Elsevier Masson SAS. https://doi.org/10.1016/S0923-2508(03)00065-2.

Bamford, Dennis H., Päivi M. Ojala, Mikko Frilander, Laura Walin, and Jaana K.H. Bamford. 1995. "Isolation, Purification, and Function of Assembly Intermediates and Subviral Particles of Bacteriophages PRD1 and Σ6." Methods in Molecular Genetics 6 (C): 455–74. https://doi.org/10.1016/S1067-2389(06)80028-2.

Bath, Carolyn, Tania Cukalac, Kate Porter, and Michael L. Dyall-Smith. 2006. "His1 and His2 Are Distantly Related, Spindle-Shaped Haloviruses Belonging to the Novel Virus Group, Salterprovirus." Virology 350 (1): 228–39. https://doi.org/10.1016/j.virol.2006.02.005.

Boose, Yvonne, André Welti, James Atkinson, Fabiola Ramelli, Anja Danielczok, Heinz G. Bingemer, Michael Plötze, Berko Sierau, Zamin A. Kanji, and Ulrike Lohmann. 2016. "Heterogeneous Ice Nucleation on Dust Particles Sourced from Nine Deserts Worldwide – Part 1: Immersion Freezing." Atmospheric Chemistry and Physics 16 (23): 15075–95. https://doi.org/10.5194/acp-16-15075-2016.

Bradford, Marion M. 1976. "A Rapid and Sensitive Method for the Quantitation of Microgram Quantities of Protein Utilizing the Principle of Protein-Dye Binding." Analytical Biochemistry 72 (1–2): 248–54. https://doi.org/10.1016/0003-2697(76)90527-3.

Burrows, S. M., C. Hoose, U. Pöschl, and M. G. Lawrence. 2013. "Ice Nuclei in Marine Air: Biogenic Particles or Dust?" Atmospheric Chemistry and Physics 13 (1): 245–67. https://doi.org/10.5194/acp-13-245-2013.

Cai, Lanlan, Bo B. Jørgensen, Curtis A. Suttle, Maoqiu He, Barry A. Cragg, Nianzhi Jiao, and Rui Zhang. 2019. "Active and Diverse Viruses Persist in the Deep Sub-Seafloor Sediments over Thousands of Years." ISME Journal 13 (7): 1857–64. https://doi.org/10.1038/s41396-019-0397-9.

Cascajo-Castresana, María, Robert O. David, Maiara A. Iriarte-Alonso, Alexander M. Bittner, and Claudia Marcolli. 2020. "Protein Aggregates Nucleate Ice: The Example of Apoferritin."

Atmospheric Chemistry and Physics 20 (6): 3291–3315. https://doi.org/10.5194/acp-20-3291-2020.
Charles E. Grant, Timothy L. Bailey, and William Stafford. 2011. “FIMO: Scanning for Occurrences of a given Motif.” Bioinformatics 27 (7): 1017–18. https://doi.org/10.1093/bioinformatics/btr064.
Conen, Franz, Emiliano Stopelli, and Lukas Zimmermann. 2016. “Clues That Decaying Leaves Enrich Arctic Air with Ice Nucleating Particles.” Atmospheric Environment 129 (March): 91–94. https://doi.org/10.1016/j.atmosenv.2016.01.027.
Creamean, J. M., J. N. Cross, R. Pickart, L. McRaven, P. Lin, A. Pacini, R. Hanlon, et al. 2019. “Ice Nucleating Particles Carried From Below a Phytoplankton Bloom to the Arctic Atmosphere.” Geophysical Research Letters 46 (14): 8572–81. https://doi.org/10.1029/2019GL083039.
Creamean, Jessie M, Rachel M Kirpes, Kerri A Pratt, Nicholas J Spada, Maximilian Maahn, Gijs De Boer, Russell C Schnell, and Swarup China. 2018. “Marine and Terrestrial Influences on Ice Nucleating Particles during Continuous Springtime Measurements in an Arctic Oilfield Location.” Atmos. Chem. Phys 18: 18023–42. https://doi.org/10.5194/acp-18-18023-2018.
Demina, Tatiana A., Maija K. Pietilä, Julija Svirskaitė, Janne J. Ravantti, Nina S. Atanasova, Dennis H. Bamford, and Hanna M. Oksanen. 2016. “Archaeal Haloarcula Californiae Icosahedral Virus 1 Highlights Conserved Elements in Icosahedral Membrane-Containing DNA Viruses from Extreme Environments.” MBio 7 (4). https://doi.org/10.1128/mBio.00699-16.
DeMott, P. J., A. J. Prenni, X. Liu, S. M. Kreidenweis, M. D. Petters, C. H. Twohy, M. S. Richardson, T. Eidhammer, and D. C. Rogers. 2010. “Predicting Global Atmospheric Ice Nuclei Distributions and Their Impacts on Climate.” Proceedings of the National Academy of Sciences of the United States of America 107 (25): 11217–22. https://doi.org/10.1073/pnas.0910818107.
DeMott, Paul J., Kenneth Sassen, Michael R. Poellot, Darrel Baumgardner, David C. Rogers, Sarah D. Brooks, Anthony J. Prenni, and Sonia M. Kreidenweis. 2003. “African Dust Aerosols as Atmospheric Ice Nuclei.” Geophysical Research Letters 30 (14). https://doi.org/10.1029/2003GL017410.
DeMott, Paul J, Thomas C J Hill, Christina S McCluskey, Kimberly A Prather, Douglas B Collins, Ryan C Sullivan, Matthew J Ruppel, et al. 2016. “Sea Spray Aerosol as a Unique Source of Ice Nucleating Particles.” Proceedings of the National Academy of Sciences of the United States of America 113 (21): 5797–5803. https://doi.org/10.1073/pnas.1514034112.
Dreischmeier, Katharina, Carsten Budke, Lars Wiehemeier, Tilman Kottke, and Thomas Koop. 2017. “Boreal Pollen Contain Ice-Nucleating as Well as Ice-Binding ‘antifreeze’ Polysaccharides.” Scientific Reports 7 (1): 1–13. https://doi.org/10.1038/srep41890.
Du, Rui, Pengrui Du, Zedong Lu, Weishan Ren, Zongmin Liang, Saisai Qin, Ziming Li, Yaling Wang, and Pingqing Fu. 2017. “Evidence for a Missing Source of Efficient Ice Nuclei.” Scientific Reports 7 (1): 1–8. https://doi.org/10.1038/srep39673.
Eskelin, Katri, and Minna M. Poranen. 2018. “Controlled Disassembly and Purification of Functional Viral Subassemblies Using Asymmetrical Flow Field-Flow Fractionation (AF4).” Viruses 10 (11). https://doi.org/10.3390/v10110579.
Eskelin, Katri, Minna M. Poranen, and Hanna M. Oksanen. 2019. “Asymmetrical Flow Field-Flow Fractionation on Virus and Virus-like Particle Applications.” Microorganisms. MDPI AG. https://doi.org/10.3390/microorganisms7110555.

Fröhlich-Nowoisky, J., T. C. J. Hill, B. G. Pummer, P. Yordanova, G. D. Franc, and U. Pöschl. 2015. “Ice Nucleation Activity in the Widespread Soil Fungus Mortierella Alpina.” Biogeosciences 12 (4): 1057–71. https://doi.org/10.5194/bg-12-1057-2015.

Green, Robert L., and Gareth J. Warren. 1985. “Physical and Functional Repetition in a Bacterial Ice Nucleation Gene.” Nature 317 (6038): 645–48. https://doi.org/10.1038/317645a0.

Grythe, H, J Ström, R Krejci, P Quinn, and A Stohl. 2014. “Atmospheric Chemistry and Physics A Review of Sea-Spray Aerosol Source Functions Using a Large Global Set of Sea Salt Aerosol Concentration Measurements.” Atmos. Chem. Phys 14: 1277–97. https://doi.org/10.5194/acp-14-1277-2014.

Gurian-Sherman, Douglas, and Steven E. Lindow. 1993. “Bacterial Ice Nucleation: Significance and Molecular Basis.” The FASEB Journal 7 (14): 1338–43. https://doi.org/10.1096/fasebj.7.14.8224607.

Hill, Tom C J, Paul J Demott, Yutaka Tobo, Janine Fröhlich-Nowoisky, Bruce F Moffett, Gary D Franc, and Sonia M Kreidenweis. 2016. “Sources of Organic Ice Nucleating Particles in Soils.” Atmos. Chem. Phys 16: 7195–7211. https://doi.org/10.5194/acp-16-7195-2016.

Hoose, C., J. E. Kristjánsson, and S. M. Burrows. 2010. “How Important Is Biological Ice Nucleation in Clouds on a Global Scale?” Environmental Research Letters 5 (2). https://doi.org/10.1088/1748-9326/5/2/024009.

Hoose, C., and O. Möhler. 2012. “Heterogeneous Ice Nucleation on Atmospheric Aerosols: A Review of Results from Laboratory Experiments.” Atmospheric Chemistry and Physics 12 (20): 9817–54. https://doi.org/10.5194/acp-12-9817-2012.

Irish, Victoria E., Pablo Elizondo, Jessie Chen, Cédric Chou, Joannie Charette, Martine Lizotte, Luis A. Ladino, et al. 2017. “Ice-Nucleating Particles in Canadian Arctic Sea-Surface Microlayer and Bulk Seawater.” Atmospheric Chemistry and Physics 17 (17): 10583–95. https://doi.org/10.5194/acp-17-10583-2017.

Irish, Victoria E., Sarah J. Hanna, Yu Xi, Matthew Boyer, Elena Polishchuk, Mohamed Ahmed, Jessie Chen, et al. 2019. “Revisiting Properties and Concentrations of Ice-Nucleating Particles in the Sea Surface Microlayer and Bulk Seawater in the Canadian Arctic during Summer.” Atmospheric Chemistry and Physics 19 (11): 7775–87. https://doi.org/10.5194/acp-19-7775-2019.

Junge, K, and B D Swanson. 2008. “High-Resolution Ice Nucleation Spectra of Sea-Ice Bacteria: Implications for Cloud Formation and Life in Frozen Environments.” Biogeosciences. Vol. 5. www.biogeosciences.net/5/865/2008/.

Kajava, Andrey V., and Steven E. Lindow. 1993. “A Model of the Three-Dimensional Structure of Ice Nucleation Proteins.” Journal of Molecular Biology. https://doi.org/10.1006/jmbi.1993.1424.

Kanji, Zamin A., Luis A. Ladino, Heike Wex, Yvonne Boose, Monika Burkert-Kohn, Daniel J. Cziczo, Martina Krämer, et al. 2017. “Overview of Ice Nucleating Particles.” Meteorological Monographs 58 (January): 1.1-1.33. https://doi.org/10.1175/AMSMONOGRAPHS-D-16-0006.1.

Lampi, Mirka, Hanna M. Oksanen, Florian Meier, Evelin Moldenhauer, Minna M. Poranen, Dennis H. Bamford, and Katri Eskelin. 2018. “Asymmetrical Flow Field-Flow Fractionation in Purification of an Enveloped Bacteriophage Φ6.” Journal of Chromatography B: Analytical Technologies in the Biomedical and Life Sciences 1095 (September): 251–57. https://doi.org/10.1016/j.jchromb.2018.07.008.

Lindow', Steven E, Deane C Arny, and Christen D Upper. 1982. "Bacterial Ice Nucleation: A Factor in Frost Injury to Plants'." Plant Physiol. Vol. 70. www.plantphysiol.org.

McCluskey, C. S., T. C. J. Hill, R. S. Humphries, A. M. Rauker, S. Moreau, P. G. Strutton, S. D. Chambers, et al. 2018. "Observations of Ice Nucleating Particles Over Southern Ocean Waters." Geophysical Research Letters 45 (21): 11,989-11,997. https://doi.org/10.1029/2018GL079981.

McCluskey, Christina S., Jurgita Ovadnevaite, Matteo Rinaldi, James Atkinson, Franco Belosi, Darius Ceburnis, Salvatore Marullo, et al. 2018. "Marine and Terrestrial Organic Ice-Nucleating Particles in Pristine Marine to Continentally Influenced Northeast Atlantic Air Masses." Journal of Geophysical Research: Atmospheres 123 (11): 6196–6212. https://doi.org/10.1029/2017JD028033.

Morris, C. E., D. G. Georgakopoulos, and D. C. Sands. 2004. "Ice Nucleation Active Bacteria and Their Potential Role in Precipitation." Journal de Physique IV (Proceedings) 121 (December): 87–103. https://doi.org/10.1051/jp4:2004121004.

Morris, Cindy E., Caroline L. Monteil, and Odile Berge. 2013a. "The Life History of Pseudomonas Syringae: Linking Agriculture to Earth System Processes." Annual Review of Phytopathology 51 (August): 85–104. https://doi.org/10.1146/annurev-phyto-082712-102402.

———. 2013b. " The Life History of Pseudomonas Syringae : Linking Agriculture to Earth System Processes ." Annual Review of Phytopathology 51 (1): 85–104. https://doi.org/10.1146/annurev-phyto-082712-102402.

Murray, B. J., D. O'Sullivan, J. D. Atkinson, and M. E. Webb. 2012. "Ice Nucleation by Particles Immersed in Supercooled Cloud Droplets." Chemical Society Reviews 41 (19): 6519. https://doi.org/10.1039/c2cs35200a.

Nuttall, Stewart D., and Michael L.Dyall Smith. 1993. "HF1 and HF2: Novel Bacteriophages of Halophilic Archaea." Virology 197 (2): 678–84. https://doi.org/10.1006/viro.1993.1643.

O'Sullivan, D., M. P. Adams, M. D. Tarn, A. D. Harrison, J. Vergara-Temprado, G. C. E. Porter, M. A. Holden, et al. 2018. "Contributions of Biogenic Material to the Atmospheric Ice-Nucleating Particle Population in North Western Europe." Scientific Reports 8 (1): 13821. https://doi.org/10.1038/s41598-018-31981-7.

O'Sullivan, D., B. J. Murray, J. F. Ross, T. F. Whale, H. C. Price, J. D. Atkinson, N. S. Umo, and M. E. Webb. 2015. "The Relevance of Nanoscale Biological Fragments for Ice Nucleation in Clouds." Scientific Reports 5 (January): 8082. https://doi.org/10.1038/srep08082.

Olkkonen, Vesa M., and Dennis H. Bamford. 1989. "Quantitation of the Adsorption and Penetration Stages of Bacteriophage Φ6 Infection." Virology 171 (1): 229–38. https://doi.org/10.1016/0042-6822(89)90530-8.

Pandey, Ravindra, Kota Usui, Ruth A. Livingstone, Sean A. Fischer, Jim Pfaendtner, Ellen H.G. Backus, Yuki Nagata, et al. 2016. "Ice-Nucleating Bacteria Control the Order and Dynamics of Interfacial Water." Science Advances 2 (4): e1501630. https://doi.org/10.1126/sciadv.1501630.

Pietila, M. K., N. S. Atanasova, V. Manole, L. Liljeroos, S. J. Butcher, H. M. Oksanen, and D. H. Bamford. 2012. "Virion Architecture Unifies Globally Distributed Pleolipoviruses Infecting Halophilic Archaea." Journal of Virology 86 (9): 5067–79. https://doi.org/10.1128/jvi.06915-11.

Pietilä, Maija K., Elina Roine, Lars Paulin, Nisse Kalkkinen, and Dennis H. Bamford. 2009. "An SsDNA Virus Infecting Archaea: A New Lineage of Viruses with a Membrane Envelope." Molecular Microbiology 72 (2): 307–19. https://doi.org/10.1111/j.1365-2958.2009.06642.x.

Porter, Grace C. E., Sebastien N. F. Sikora, Michael P. Adams, Ulrike Proske, Alexander D. Harrison, Mark D. Tarn, Ian M. Brooks, and Benjamin J. Murray. 2020. “Resolving the Size of Ice-Nucleating Particles with a Balloon Deployable Aerosol Sampler: The SHARK.” Atmospheric Measurement Techniques 13 (6): 2905–21. https://doi.org/10.5194/amt-13-2905-2020.

Pouleur, Stephan, Claude Richard, Jean-guy Martin, and Hani Antoun. 1992. Ice Nucleation Activity in Fusarium Acuminatum and Fusarium Avenaceumt. Vol. 58. American Society for Microbiology. https://doi.org/10.1128/aem.58.9.2960-2964.1992.

Pratt, Kerri A., Paul J. Demott, Jeffrey R. French, Zhien Wang, Douglas L. Westphal, Andrew J. Heymsfield, Cynthia H. Twohy, Anthony J. Prenni, and Kimberly A. Prather. 2009. “In Situ Detection of Biological Particles in Cloud Ice-Crystals.” Nature Geoscience 2 (6): 398–401. https://doi.org/10.1038/NGEO521.

Price, H C, K J Baustian, J B Mcquaid, A Blyth, K N Bower, T Choularton, R J Cotton, et al. 2018. “Atmospheric Ice-Nucleating Particles in the Dusty Tropical Atlantic.” https://doi.org/10.1002/2017JD027560.

Prussin, Aaron J., Ellen B. Garcia, and Linsey C. Marr. 2015. “Total Concentrations of Virus and Bacteria in Indoor and Outdoor Air.” Environmental Science and Technology Letters 2 (4): 84–88. https://doi.org/10.1021/acs.estlett.5b00050.

Pummer, B. G., C. Budke, S. Augustin-Bauditz, D. Niedermeier, L. Felgitsch, C. J. Kampf, R. G. Huber, et al. 2015. “Ice Nucleation by Water-Soluble Macromolecules.” Atmospheric Chemistry and Physics 15 (8): 4077–91. https://doi.org/10.5194/acp-15-4077-2015.

Pummer, B G, H Bauer, J Bernardi, S Bleicher, and H Grothe. 2012. “Suspendable Macromolecules Are Responsible for Ice Nucleation Activity of Birch and Conifer Pollen.” Atmos. Chem. Phys 12. https://doi.org/10.5194/acp-12-2541-2012.

Qiao, Xueying, Yang Sun, Jian Qiao, Fabiana Di Sanzo, and Leonard Mindich. 2010. “Characterization of Φ2954, a Newly Isolated Bacteriophage Containing Three DsRNA Genomic Segments.” BMC Microbiology 10. https://doi.org/10.1186/1471-2180-10-55.

Rangel-Alvarado, Rodrigo Benjamin, Yevgen Nazarenko, and Parisa A. Ariya. 2015. “Snow-Borne Nanosized Particles: Abundance, Distribution, Composition, and Significance in Ice Nucleation Processes.” Journal of Geophysical Research: Atmospheres 120 (22): 11,760-11,774. https://doi.org/10.1002/2015JD023773.

Rastelli, Eugenio, Cinzia Corinaldesi, Antonio Dell’Anno, Marco Lo Martire, Silvestro Greco, Maria Cristina Facchini, Matteo Rinaldi, Colin O’Dowd, Darius Ceburnis, and Roberto Danovaro. 2017. “Transfer of Labile Organic Matter and Microbes from the Ocean Surface to the Marine Aerosol: An Experimental Approach.” Scientific Reports 7 (1): 11475. https://doi.org/10.1038/s41598-017-10563-z.

Reche, Isabel, Gaetano D’Orta, Natalie Mladenov, Danielle M. Winget, and Curtis A. Suttle. 2018. “Deposition Rates of Viruses and Bacteria above the Atmospheric Boundary Layer.” The ISME Journal 12 (4): 1154–62. https://doi.org/10.1038/s41396-017-0042-4.

Sanchez-Marroquin, A., O. Arnalds, K. J. Baustian-Dorsi, J. Browse, P. Dagsson-Waldhauserova, A. D. Harrison, E. C. Maters, et al. 2020. “Iceland Is an Episodic Source of Atmospheric Ice-Nucleating Particles Relevant for Mixed-Phase Clouds.” Science Advances 6 (26): eaba8137. https://doi.org/10.1126/sciadv.aba8137.

Šantl-Temkiv, Tina, Branko Sikoparija, Teruya Maki, Federico Carotenuto, Pierre Amato, Maosheng Yao, Cindy E. Morris, et al. 2019. “Bioaerosol Field Measurements: Challenges and Perspectives in Outdoor Studies.” Aerosol Science and Technology. Taylor and Francis Inc. https://doi.org/10.1080/02786826.2019.1676395.

Saren, Ari Matti, Janne J. Ravantti, Stacy D. Benson, Roger M. Burnett, Lars Paulin, Dennis H. Bamford, and Jaana K.H. Bamford. 2005. “A Snapshot of Viral Evolution from Genome Analysis of the Tectiviridae Family.” Journal of Molecular Biology 350 (3): 427–40. https://doi.org/10.1016/j.jmb.2005.04.059.

Schnell, R. C., Gabor Vali, R. C. Schnell, and Gabor Vali. 1976. “Biogenic Ice Nuclei: Part I. Terrestrial and Marine Sources.” Http://Dx.Doi.Org/10.1175/1520-0469(1976)033<1554:BINPIT>2.0.CO;2, August. https://doi.org/10.1175/1520-0469(1976)033<1554:BINPIT>2.0.CO;2.

Schnell, R C, G Vali, and R C Schnell’. 1975. “Freezing Nuclei in Marine Waters.” https://doi.org/10.3402/tellusa.v27i3.9911.

Srinivasiah, Sharath, Jaysheel Bhavsar, Kanika Thapar, Mark Liles, Tom Schoenfeld, and K. Eric Wommack. 2008. “Phages across the Biosphere: Contrasts of Viruses in Soil and Aquatic Environments.” Research in Microbiology 159 (5): 349–57. https://doi.org/10.1016/j.resmic.2008.04.010.

Suttle, Curtis A. 2005. “Viruses in the Sea.” Nature. Nature Publishing Group. https://doi.org/10.1038/nature04160.

———. 2007. “Marine Viruses - Major Players in the Global Ecosystem.” Nature Reviews Microbiology 5 (10): 801–12. https://doi.org/10.1038/nrmicro1750.

Tan, Ivy, Trude Storelvmo, and Mark D Zelinka. 2016. “Observational Constraints on Mixed-Phase Clouds Imply Higher Climate Sensitivity.” Science (New York, N.Y.) 352 (6282): 224–27. https://doi.org/10.1126/science.aad5300.

Timothy L. Bailey, and William Stafford Noble. 2003. “Searching for Statistically Significant Regulatory Modules.” Bioinformatics 19 (2): 16–25. https://doi.org/10.1093/bioinformatics/btg1054.

Tobo, Yutaka, Kouji Adachi, Paul J. DeMott, Thomas C.J. Hill, Douglas S. Hamilton, Natalie M. Mahowald, Naoko Nagatsuka, et al. 2019. “Glacially Sourced Dust as a Potentially Significant Source of Ice Nucleating Particles.” Nature Geoscience 12 (April). https://doi.org/10.1038/s41561-019-0314-x.

Tschitschko, Bernhard, Timothy J. Williams, Michelle A. Allen, David Páez-Espino, Nikos Kyrpides, Ling Zhong, Mark J. Raftery, and Ricardo Cavicchioli. 2015. “Antarctic Archaea-Virus Interactions: Metaproteome-Led Analysis of Invasion, Evasion and Adaptation.” ISME Journal 9 (9): 2094–2107. https://doi.org/10.1038/ismej.2015.110.

Vali, G., M. Christensen, R. W. Fresh, E. L. Galyan, L. R. Maki, R. C. Schnell, G. Vali, et al. 1976. “Biogenic Ice Nuclei. Part II: Bacterial Sources.” Http://Dx.Doi.Org/10.1175/1520-0469(1976)033<1565:BINPIB>2.0.CO;2, August. https://doi.org/10.1175/1520-0469(1976)033<1565:BINPIB>2.0.CO;2.

Vergara-Temprado, Jesús, Annette K Miltenberger, Kalli Furtado, Daniel P Grosvenor, Ben J Shipway, Adrian A Hill, Jonathan M Wilkinson, Paul R Field, Benjamin J Murray, and Ken S Carslaw. 2018. “Strong Control of Southern Ocean Cloud Reflectivity by Ice-Nucleating Particles.” Proceedings of the National Academy of Sciences of the United States of America 115 (11): 2687–92. https://doi.org/10.1073/pnas.1721627115.

Vergara-Temprado, Jesús, Benjamin J. Murray, Theodore W. Wilson, Daniel O’sullivan, Jo Browse, Kirsty J. Pringle, Karin Ardon-Dryer, et al. 2017. “Contribution of Feldspar and Marine Organic Aerosols to Global Ice Nucleating Particle Concentrations.” Atmospheric Chemistry and Physics 17 (5): 3637–58. https://doi.org/10.5194/acp-17-3637-2017.

Wang, Xiaofei, Camille M. Sultana, Jonathan Trueblood, Thomas C.J. Hill, Francesca Malfatti, Christopher Lee, Olga Laskina, et al. 2015. “Microbial Control of Sea Spray Aerosol

Composition: A Tale of Two Blooms." ACS Central Science 1 (3): 124–31. https://doi.org/10.1021/acscentsci.5b00148.
Whale, T. F., B. J. Murray, D. O'Sullivan, T. W. Wilson, N. S. Umo, K. J. Baustian, J. D. Atkinson, D. A. Workneh, and G. J. Morris. 2015. "A Technique for Quantifying Heterogeneous Ice Nucleation in Microlitre Supercooled Water Droplets." Atmospheric Measurement Techniques 8 (6): 2437–47. https://doi.org/10.5194/amt-8-2437-2015.
Whitman, William B., David C. Coleman, and William J. Wiebe. 1998. "Prokaryotes: The Unseen Majority." Proceedings of the National Academy of Sciences of the United States of America. https://doi.org/10.1073/pnas.95.12.6578.
Whon, Tae Woong, Min-Soo Kim, Seong Woon Roh, Na-Ri Shin, Hae-Won Lee, and Jin-Woo Bae. 2012. "Metagenomic Characterization of Airborne Viral DNA Diversity in the Near-Surface Atmosphere." Journal of Virology 86 (15): 8221–31. https://doi.org/10.1128/JVI.00293-12.
Wilson, Sandra L., Paul Grogan, and Virginia K. Walker. 2012. "Prospecting for Ice Association: Characterization of Freeze-Thaw Selected Enrichment Cultures from Latitudinally Distant Soils." Canadian Journal of Microbiology 58 (4): 402–12. https://doi.org/10.1139/W2012-010.
Wilson, Theodore W., Luis A. Ladino, Peter A. Alpert, Mark N. Breckels, Ian M. Brooks, Jo Browse, Susannah M. Burrows, et al. 2015. "A Marine Biogenic Source of Atmospheric Ice-Nucleating Particles." Nature 525 (7568): 234–38. https://doi.org/10.1038/nature14986.

Chapter 6

Characteristics of ice-nucleating particles in a boreal forest environment

M.P. Adams[1], J.U. Proske[1], G.C.E Porter[1], A.D. Harrison[1], M. Daily[1], S. Sikora, Z. Brasseur[2], J. Duplissy[2], T. Petäjä[2], K.S. Carslaw[1] and B.J. Murray[1]

1 - School of Earth and Environment, University of Leeds, Leeds, United Kingdom

2 - Institute for Atmospheric and Earth System Research/Physics, Faculty of Science, University of Helsinki, Helsinki, Finland

Chapter 6 is based around an in preparation paper entitled *characteristics of ice-nucleating particles in a boreal forest environment*, on which I am the lead author. I planned the Leeds part of the HyICE field campaign, with assistance from BJM and JD. MPA, GCEP, ADH, MID, BJM, JUP and ZB made up the field work team in Hyytiälä. JUP led the modelling simulations, with MPA, KSC and BJM supervising. SS gave technical assistance. All authors contributed to writing the manuscript.

JUP carried out the model simulations using GLOMAP that appear within this chapter under the supervision of myself, BJM and KC. JUP produced Figures 77 and 78. I created all other Figures and wrote all sections of this chapter.

Abstract

The formation of ice in clouds plays a key role in determining cloud properties which influence cloud radiative effects, lifetime and precipitation. Ice-nucleating particles (INPs) catalyse the freezing of meta-stable supercooled liquid droplets in clouds at temperatures above which they freeze homogeneously. Shallow clouds in the mixed-phase regime are found in the low to mid-troposphere, and are very sensitive to the presence of INPs. In this study we measured and characterized the INPs in a boreal forest environment (at the Hyytiälä forestry research station, Finland), which is known for the presence of primary bioaerosol particles, and compared the results with simulations of INP concentrations in the same space and time, using a model that does not consider terrestrial bioaerosol as a source of INPs. Contrasting our results with a global model of INP (GLOMAP) from desert dust and marine organics reveal that the model under-predicts the INPs present at Hyytiälä. Experiments revealed that in nearly all instances the INP sampled were heat-labile, and the majority of INPs were found in in the size range 2.5 – 10 μm. This indicates that these INP are biological in nature and are probably derived from fungus and bacteria which produce heat sensitive ice-nucleating proteins. Furthermore, whilst the model could not predict the INP concentrations measured, upon heating the samples showed a decrease in activity, bringing the concentrations in line with the model predictions. As the INP activity of mineral dust has been shown to be resistant to heat, this suggests that once the more active, potentially biogenic INPs have been deactivated by heating, the INPs present in mineral dust, or another heat insensitive INP, may be the next most important INP type.

6.1 Introduction

Our limited knowledge about cloud radiative processes is a major weakness in our understanding of climate change and an obstacle for the improvement of climate projections. Cloud feedbacks represent one of the largest uncertainties in climate models (U. Lohmann & Feichter, 2005; B J Murray et al., 2020; Storelvmo, 2017; Tan et al., 2016). In mixed-phase clouds, a rare subset of aerosol particles called ice-nucleating particles (INPs) catalyze droplet freezing above −33 °C and thereby alter cloud properties. Contaminant-free micrometer-sized water droplets freeze homogeneously below −33 °C (Herbert et al, 2015). For heterogeneous freezing, INPs are required (DeMott et al., 2010; Hoose & Möhler, 2012; Kanji et al., 2017; Murray et al., 2012). Therefore, even though INPs account only for a small fraction of atmospheric aerosol particles, they exert a disproportionate effect on cloud properties. The current understanding of the spatial and temporal variation of INPs is poor, stemming from a lack of field measurements of INP concentrations and a lack of understanding of which aerosol species are driving atmospheric ice nucleation in different environments.

Mineral dust has been demonstrated to be an effective INP in laboratory studies, typically being more active at temperatures below −15 °C due to a steep slope through [INP_T] space (Atkinson et al., 2013; Boose, Welti, et al., 2016; Connolly et al., 2009; Harrison et al., 2019; Niemand et al., 2012). Desert dust from low-latitude arid regions such as the Sahara and Gobi deserts tends to dominate the atmospheric INP population in the low-mid latitudes, especially at temperatures below −15 °C (DeMott et al. 2003; Price et al. 2018; Boose, Sierau, et al. 2016). Additionally, more recent works have shown high-latitude dust sources to emit INPs capable of influencing the atmospheric INP concentrations in their region (A. Sanchez-Marroquin et al., 2020; Tobo et al., 2019). As concentrations of low-latitude desert dust are much lower in the high-latitudes (compared to in the lower-latitudes), other sources such as the aforementioned high-latitude dusts or marine organics become more important. Marine organics have been shown to be effective INPs, and have clear aerosolization mechanisms (Wilson et al. 2015; Irish et al. 2017; 2019; DeMott et al. 2016; Ickes et al. 2020), with Vergara-Temprado et al., (2017) using modelling simulations to demonstrate the importance of marine organics in remote marine environments.

Biological particles, such as bacteria, fungi, viruses, pollen and others, have been demonstrated to be extremely effective ice nucleators in lab studies (O'Sullivan et al. 2015; 2016; Morris, Georgakopoulos, and Sands 2004; Morris, Monteil, and Berge 2013; Pummer et al. 2015; Kieft and Ruscettit 1990; Pouleur et al. 1992), with field observations being made of bioaerosols acting as INPs (Hill et al., 2016; Joly et al., 2014; O'Sullivan et al., 2018; Petters & Wright, 2015; Pratt et al., 2009; Tobo et al., 2013).

Tobo et al., (2013) made measurements during the North American monsoon season at the Manitou Experimental Forest Observatory (MEFO) in Colorado, USA, in a mid-latitude ponderosa pine forest environment. They found evidence of INPs they determined to be from primary biological aerosol particles (PBAPs) and measured INP concentrations in the temperature range −34 - −9 °C, and specifically noted the rapid increase of INPs active at warmer temperatures in response to the concentration of PBAPs. They went on to modify an existing parameterization for predicting INP concentrations based on the number of aerosol particles > 0.5 µm (DeMott *et al*, 2010) to include the number of fluorescent biological aerosol

particles (FBAPs). The study concluded that INPs from PBAPs could play an important role in determining atmospheric INP concentrations, especially at warmer temperatures.

O'Sullivan et al., (2018) measured INP concentrations at a rural environment in the UK. Measurements were compared to model predications made by a global aerosol transport model (GLOMAP; Mann et al., 2010) for the measurement area in the year 2001 (Vergara-Temprado *et al.*, 2017). GLOMAP includes mineral dust (represented by the K-feldspar parameterization given in Atkinson et al., (2013) and marine organics (based on Wilson et al., (2015)). This study found that all samples with INPs active at −18 °C in concentrations > 0.1 L^{-1} saw this activity reduced upon heating of the sample in boiling water for 30 minutes. Furthermore, the study showed that GLOMAP under predicted the atmospheric INP concentration at the measurement site when such thermally-labile INPs were present, but was consistent with the measurements when they were not. The study went on to state that these heat-labile INPs were likely biogenic in nature, and had potentially undergone long-range transport, implying this may have an influence on cloud glaciation on a global scale at temperatures > −18 °C.

A number of other campaigns have measured and characterized terrestrial biological INPs in the field environment, using a number of different methodologies: Hill et al., (2016) showing soil organic matter has the capacity to nucleate ice at temperatures warmer than −15 °C and the ice-nucleating activity is thermally-labile, Joly et al., (2014) measured biological INPs in cloud water collected from the summit from Puy de Dôme (1465 m a.s.l., France), and Pratt et al., (2009) used a combination of online INP measurements and aerosol time-of-flight spectroscopy to quantify INP concentration and the chemistry of individual ice crystal residues from clouds, providing the first direct evidence for the involvement of bioaerosols in ice processes.

Despite growing evidence from field campaigns of the presence of bioaerosols acting as INPs in the atmosphere, there is an ongoing debate as to whether bioaerosols make a significant contribution to the atmospheric INP burden (Burrows et al., 2013; Hoose et al., 2010; Phillips et al., 2009; Spracklen & Heald, 2014). Hoose et al., (2010) used a subset of known INP bioaerosols to simulate global INP averages on an annual basis, finding the fraction of atmospheric ice nucleation caused by bioaerosols to be below 1%. Spracklen and Heald (2014) conducted a similar study which considered the influence of bacteria and fungi on atmospheric ice nucleation, reaching a similar conclusion to Hoose et al., (2010), stating that fungal spores and bacteria contribute < 0.01 % of all immersion freezing events in the atmosphere. They also noted that at altitudes between 400 – 600 hPa, where the local temperature is warmer (> −15 °C) and less conducive to nucleation by soot or dust, biological aerosol particles dominate as INPs. However, both Hoose et al., (2010) and Spracklen & Heald, (2014) did not consider nanoscale biological INPs which might be far more numerous in the atmosphere than whole intact biological particles (O'Sullivan et al., 2016, 2015; Pummer et al., 2012, 2015). Conversly, Phillips et al., (2009) utilized a cloud-system resolving model to investigate the relationship between insoluble organic aerosol (a potential candidate for which they stated as bioaerosols from a land surface) and the number of ice crystals in deep convective clouds (amongst other relationships), finding a positive correlation between the two variables. It is at present unclear if bioaerosols play an important role in atmospheric ice nucleation, however if they do, it seems likely that they will do so at warmer temperatures

(i.e. lower altitudes) and in regions where desert dust is not present in abundance, or only sporadically dominant (i.e. higher latitudes).

In this study our motivation was to quantify and characterize INPs in a high-latitude, boreal forest environment towards determining the role of terrestrial bioaerosol in the atmospheric INP burden. Boreal forest is found between 50°N to 70°N, accounts for 10% of the global land area, and 30% of the world's forested area, and has been shown to be a source of aerosol particles and CCN (Kerminen, Lihavainen, Komppula, Viisanen, & Kulmala, 2005; Kuusela, 1990; Tunved et al., 2006). Spracklen et al., (2008) used a global atmospheric model to show boreal forest emissions double regional cloud condensation nuclei, and further went on to state that the resulting change in cloud albedo causes a radiative forcing of between −1.8 and $-6.7\,W\,m^{-2}$ of forest. In Northern Europe, the Hyytiälä forestry research station (61°N 24°E; Southern Finland) has been the site of a number of studies investigating the aerosol emissions from boreal forest (Markku Kulmala, Toivonen, Mäkelä, & Laaksonen, 1998; Schumacher et al., 2013; Tunved et al., 2006). Despite evidence showing that boreal forest could be an important factor in aerosol-cloud interactions, no INP measurements from Hyytiälä had been published prior to the HyICE campaign of 2018 (of which this study was a component). During this study we aimed to test the hypothesis that boreal forest acts as a source of biological ice-nucleating particles, and that these particles dominate the atmospheric INP population at temperatures > −20 °C through the characterization of the measured INP population's heat stability and size.

6.2 Methods

Measurements shown in this study were made between March – April, 2018 at the Hyytiälä forest station. Aerosol concentration and size distribution measurements were made in an aerosol cottage (a small wooden building situated in the forest where most of the permanent aerosol instrumentation is housed, shown in Figure 21; Junninen et al., 2009). Measurements were made using an Aerodynamic Particle Sizer (APS, TSI model 3321) and Scanning Mobility Particle Sizer (SMPS, constructed from a differential mobility analyser (DMA) and a TSI model 3772 CPC). Data from the SMPS and APS was merged according to the method described in Möhler et al., (2008).

INP measurements were made using a filter collection system and a cold stage instrument. Omnidirectional ambient air particulate samplers, herein referred to as 'Mesa samplers', (BGI PQ100, Mesa Laboratories Inc.) were used to sample PM_{10} and $PM_{2.5}$ (through use of a cyclone impactor) aerosol particle onto 0.4 µm pore size track-etched membrane polycarbonate filters (Nuclepore, Whatman) at a rate of 16.7 L min^{-1}. The Mesa samplers were situated approximately 10 m from the aerosol cottage (Figure 21). Aerosol particles captured on these filters were then washed off into ultrapure water via a rotary mixer for 1 hour (Clifton RM-1, Nickel-Electro Ltd.) operated at 0.5 Hz, similar to previously described methods (Hill et al., 2014; O'Sullivan et al., 2018). This aqueous suspension was then pipetted onto a hydrophobic glass slide (approx. 50 droplets per filter sample) that was positioned on the cold plate of the µL-NIPI cold stage (T. F. Whale et al., 2015). The droplets are frozen upon cooling the stage to −40°C at 1 °C min^{-1}, with the freezing temperature for each droplet recorded via a digital camera. The number of INPs per unit volume of sampled air, $[INP]_T$, were calculated via immersion mode freezing analysis as shown in equation 1, adapted from Vali (1971):

$$[\mathrm{INP}]_T = \frac{-ln(1 - f_{\mathrm{ice}}(T))}{V_{\mathrm{d}}} \cdot \frac{V_{\mathrm{w}}}{V_{\mathrm{a}}} \quad (8)$$

where $f_{ice}(T)$ is the fraction of droplets frozen at temperature T, V_d is the droplet volume, V_w is the volume of water used to wash particles off the filter (5 mL), and V_a is the total volume of air sampled through the filter. Uncertainty in the INP concentrations are estimated using a method that accounts for the randomness of the distribution of ice-nucleation active sites across the droplets in the experiment, and also accounts for the counting uncertainty associated with detecting ice-nucleation active sites within a population (Harrison et al., 2016). To infer whether sampled INPs were biological or not, a heat test was used. The heat test consisted of immersing the vessel holding the ultrapure water containing the particles washed off from the filter in boiling water (100 °C) for 30 minutes (Hill et al., 2016; O'Sullivan et al., 2018). This heated sample was then tested on the µL-NIPI as described above and compared to the original, unheated sample to see if any reduction in INP activity was observed. If a reduction in activity did occur, this was taken as an inference that the INPs were bioaerosols.

To determine whether or not the INP concentrations measured in Hyytiälä were consistent with transported desert dust and sea spray INP, or if there might be other sources which need to be taken into account in this region, we compared our measurements with a global model of INP - GLOMAP (Mann et al., 2010; O'Sullivan et al., 2018; Vergara-Temprado et al., 2017). GLOMAP was run for the time period corresponding to the measurements period (March – April 2018) and data was output on an hourly basis. This involved using the ECMWF reanalysis meteorology fields which allow us to make a direct comparison with the data (in previous studies GLOMAP has been run for one year and the output viewed on a monthly average basis, e.g. O'Sullivan et al., (2018)) As GLOMAP only considers K-feldspar and marine organics as INP types, any significant contribution to the INP population made by bioaerosols would not be predicted and we would anticipate an low model bias (Atkinson et al., 2013; Vergara-Temprado et al., 2017; T. W. Wilson et al., 2015).

6.3 Results and discussion

6.3.1 INP measurements

INP measurements were made during March - April 2018 in a boreal forest environment. Figure 70 shows an INP_T spectra for all the PM_{10} measurements made during the campaign, overlaid with the upper and lower bounds (P&W envelope) for INP concentrations measured in the terrestrial mid-latitudes (M. D. Petters & Wright, 2015). Measurements spanned 4 orders of magnitude over 18 °C, with the temperature at which 1 INP L^{-1} was reached varying by 8 °C. Whilst the majority of the measurements lie within the P&W envelope (i.e. they are typical for the terrestrial mid-latitudes), a significant fraction lies above the upper bound between −17.5 to −23 °C. This implies that in this temperature range, INP concentrations are above what is typical for the terrestrial mid-latitudes. Shown in Figure 71 is a time series spanning the measurement campaign, indicating the temperature at which different INP concentrations were reached. The time series shows high variability in the INP concentration reached at a given temperature (at least 2 orders of magnitude variability for each of the shown temperatures). It is plausible that this variation in INP concentration is due to a comparable variation in aerosol surface area concentration, if the INP concentration is

dependent on aerosol surface area concentration, which may be expected as ice nucleation is a surface driven process. The correlation between aerosol surface area concentration and INP concentration was explicitly tested, with resultant Pearson correlation coefficients of −0.11, −0.10 and −0.14 for INP concentrations of – 19 °C, – 21 °C and – 23 °C respectively. This result implies that INP concentrations are decoupled from aerosol surface concentrations in the temperature regime investigated. This hypothesis is further tested through the calculation of the number of active sites per aerosol particle (n_s; Figure 72) comparable variation to INP concentration is observed in n_s values at – 19 °C. If total aerosol surface area concentration was the primary driver of the observed ice nucleation, then the n_s values measured would be expected to collapse to a straight line.

Given the location of the campaign, bioaerosols had the potential to dominate the INP population. In order to determine whether or not the measured INPs were bioaerosols, a heat test (O'Sullivan et al, 2018) was performed on a subset of the measurements. A comparison of unheated vs. heated INP_T spectra is shown in Figure 73. The bulk of the heated data (red) is shifted toward colder temperatures from the bulk of the unheated data (blue), demonstrating that after the sample is heated, INP activity decreases. To further demonstrate and quantify the decrease in INP activity with heat, a time series of INP concentrations at −19 °C is shown for each of the unheated/heated samples in Figure 74. In each instance but one, the heated data is deactivated compared to the unheated equivalent, where the exception is within uncertainties. On average, heated samples were a factor of 12 lower in INP concentration than unheated samples at −19 °C (unheated average 0.79 INP L^{-1}; heated average 0.065 INP L^{-1}). Since the heat-lability of INPs is used as an indication of the INPs being biogenic in nature (Hill et al., 2016; O'Sullivan et al., 2018), this data indicates that the dominant INPs measured at -19 °C in the boreal forest were bioaerosols.

Size-resolved INP measurements were made by taking samples from co-located Mesa samplers at concurrent times. One Mesa sampler sampled PM_{10} aerosol, whilst the other sampled $PM_{2.5}$ aerosol. Sampling of this manner was carried out 7 times, giving some insight into the size dependence of the INPs in the boreal forest. Figure 75 shows an INP_T spectra for each of the size resolved samples. The $PM_{2.5}$ data (red) is generally shifted towards the colder temperatures when compared to the PM_{10} data (blue), but this is not as obvious as in the previous example of the heat test. The time series is shown in Figure 76, and it can be seen that in all cases but one the PM_{10} INP concentration (blue) was greater than the $PM_{2.5}$ INP concentration, where the single outlier was within experimental uncertainty. On average, INP concentrations from PM_{10} aerosol were approximately a factor of 6.7 greater than those from $PM_{2.5}$ aerosol (PM_{10} average 1.23 INP L^{-1}; $PM_{2.5}$ average 0.184 INP L^{-1}). Whilst this data shows aerosol particles greater than 2.5 µm dominated the INP population in Hyytiälä, it is worth noting that the concentration of only $PM_{2.5}$ aerosol particles active as INPs would be considered typical of a terrestrial mid-latitude environment. These smaller INPs may be more important as their lifetime is longer and they are therefore more likely to be lofted to altitudes relevant for mixed-phase clouds (Grythe et al., 2014). Porter et al., (2020) made a single, size resolved measurement of INP concentration during the HyICE18 campaign, as part of the instrument development of the SHARK. The results show INPs active at above the limit of detection of the µL-NIPI in each of the sample size bins (0.25- 0.5 µm, 0.5 - 1 µm, 1.0 – 2.5 µm, 2.5 – 10.0 µm). This single measurement provides only a snapshot of the size-resolved INP concentrations in Hyytiälä but demonstrates that a wide range of aerosol sizes (0.25 – 10 µm) were acting as INPs. It is not clear whether the particles in these different size ranges

were of different aerosol species, and the answer to this will hopefully be illuminated through future studies.

In summary, the measurements made and discussed thus far show that INP concentrations measured in a boreal forest environment were greater than typically expected for the terrestrial mid-latitudes, with the measured INPs shown to be likely biogenic in nature and in the coarse mode. Throughout the measurement period, the INP population was therefore likely dominated by a terrestrial biological source which is currently not well parameterised, despite the prevalence of boreal forest in high-latitude environments around the globe. The characteristics of the INPs measured in Hyytiälä (active a temperatures warmer than –20 °C, biological and in the coarse mode) suggest possible candidates for their nature. Aerosolised bacteria are known to be effective ice nucleators, and are often observed in super-micron sizes (Morris et al., 2004; Morris et al., 2013), whilst fungal spores and lichen particles could also explain the presence of large, bioaerosols acting as INPs.

6.3.2 Comparisons of measured to simlulated INP concentrations

GLOMAP was used to simulate the INP concentrations during the measurement campaign on an hourly basis, allowing for an accurate comparison between simulated and measured INP concentrations. GLOMAP considers only K-feldspar and marine organics as sources of INPs, meaning any INPs from other sources (such as terrestrial bioaerosols) will not be predicted by the model, leading to under-predection of the INP concentrations if such INPs are present (Vergara-Temprado et al., 2017). Figure 77 shows a 1:1 plot comparing the number of simulated INPs to the number of measured INPs, with a colour bar indicating the temperature at which concentrations were reached. The majority of the data points fall below the 1:1 line, being biased toward the measured INP axis, showing that the measured INP concentrations exceeded their simulated counterparts and thus the model underpredcited the INP concentrations for the majority of the measurements, but especially so for the warmer temperatures. This is consistent with the hypothesis that bioaerosol were acting as INPs in the boreal forest environemnt.

Once biogeinc INP have been destroyed via the heat test, the remaining INP in a sample would most likely be mineral dust, which has been shown to be resistant to the heat test (Conen et al, 2011; Zolles et al, 2015). As GLOMAP considers K-feldspar a source of INPs, simulated concentrations for this campaign should agree more closely with samples that have undergone the heat test. Shown in Figure 78 is an INP_T spectra for unheated and heated sample respectively. Overlaid on both are solid lines representing GLOMAP predictions for K-feldspar (red) and marine organics (blue). Figure 78 shows that across all measured temperatures, GLOMAP underpredicted the INP concentration in the boreal forest, however it also shows shows good agreement between GLOMAP's prediction for K-feldspar and the heated samples. This implies that once the biogenic INPs are removed the remaining INPs are likely due to K-feldspar.

6.4 Conclusion

In this study we present the results of a two month INP measurement campaign in a boreal forest environment during 2018. We quantify and characterise the INP population in the atmosphere in the time period March – April 2018, showing that INP concentrations sometimes exceeded what is typically expected in the terrestrial mid-latitudes (M. D. Petters

& Wright, 2015) and also exceeded simulated concentrations by a global aerosol transport model, GLOMAP (Vergara-Temprado et al., 2017). In addition, we conclude that INP concentrations in the measured regime is decoupled from total aerosol concentration. In conjunction with heat tests and size resolved measurements, these measurements imply that that there is a source of INPs present in the boreal forest that is biological in nature and predominately in the coarse mode (although measurements of INPs < $PM_{2.5}$ still showed values that would be considered typical in the terrestrial mid-latitudes), which is not currently accounted for in global transport models. This source may have a regional importance as an INP in areas where desert dust concentrations are lower than those measured in the lower latitudes due to the distance from emission (arid, desert regions in the low latitudes). Futher work needs to be done to fully characterise the source of these INPs and to determine how they vary spacially and temporally in order to improve the predictive capacity of model simulations of INPs in this region (Vergara-Temprado et al., 2017). Furthermore, an understanding of what makes up the current INP population is important for understanding how this may change in a warming world and predicting any feedbacks that may arise (Tan et al., 2016).

6.5 Figures and tables

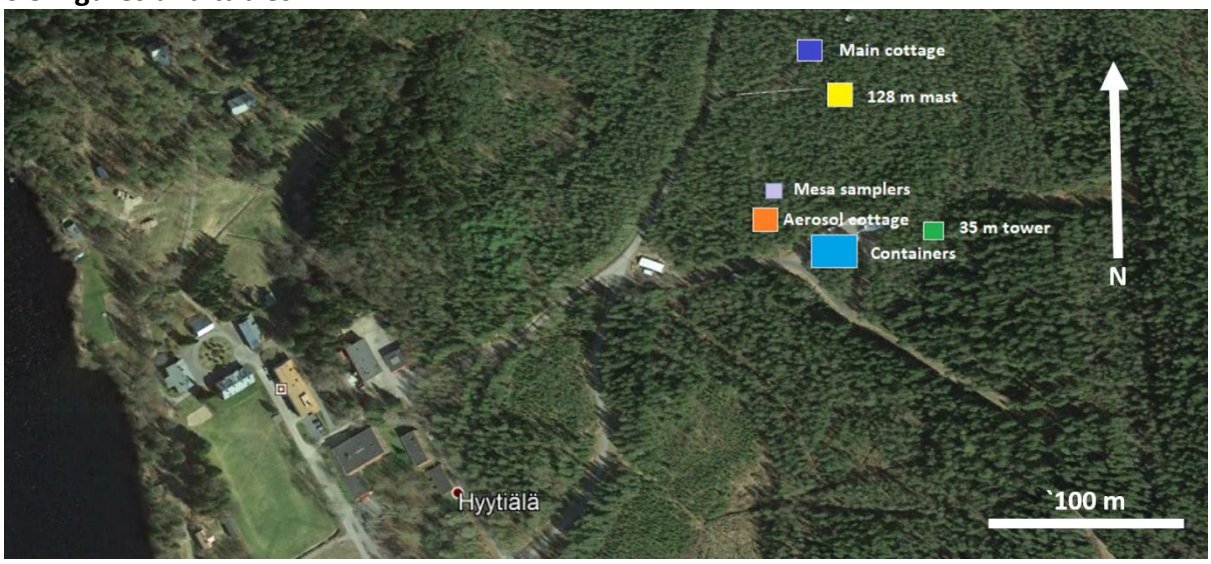

Figure 69: A map of the Hyytiälä forestry research station. Key points are noted on the map to aid in understanding the sampling location and instrument location.

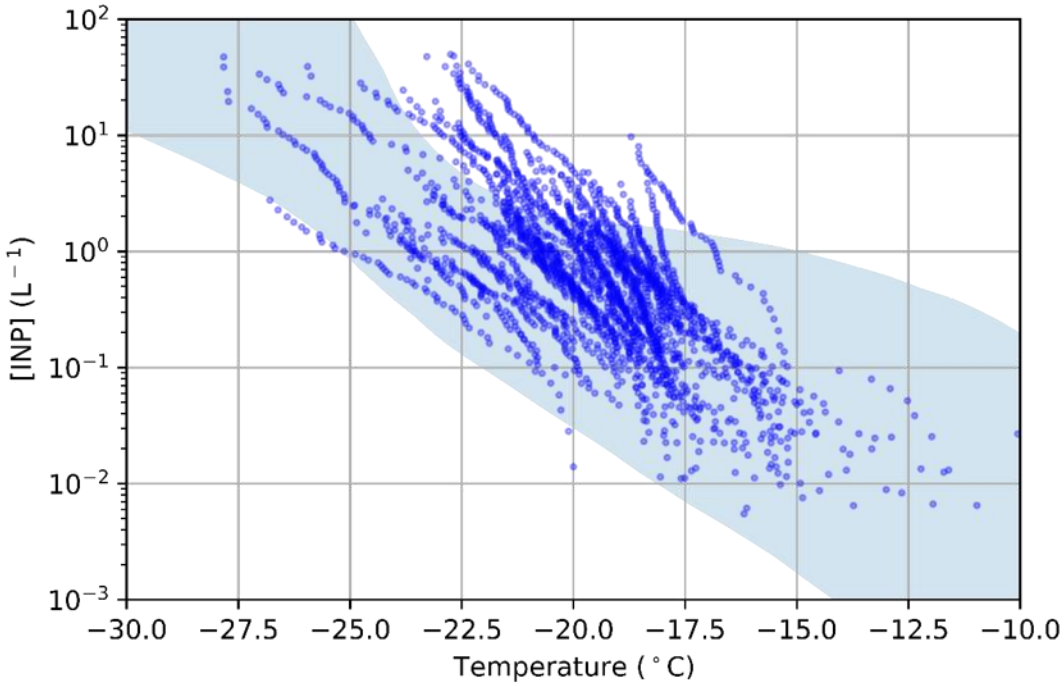

Figure 70: An INP_T spectra for all PM_{10} samples measured during March and April 2018. The overlaid envelope indicates typical INP concentrations in the terrestrial mid-latitudes (M. D. Petters & Wright, 2015)**.**

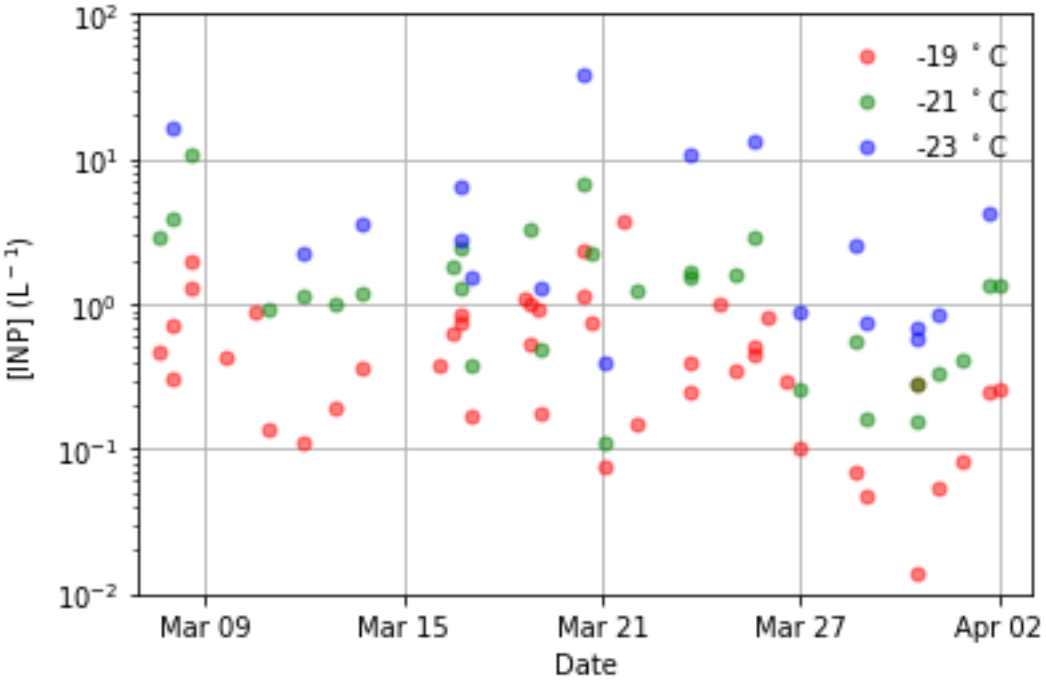

Figure 71: A time series showing INP concentration at a series of temperatures throughout the measurement period.

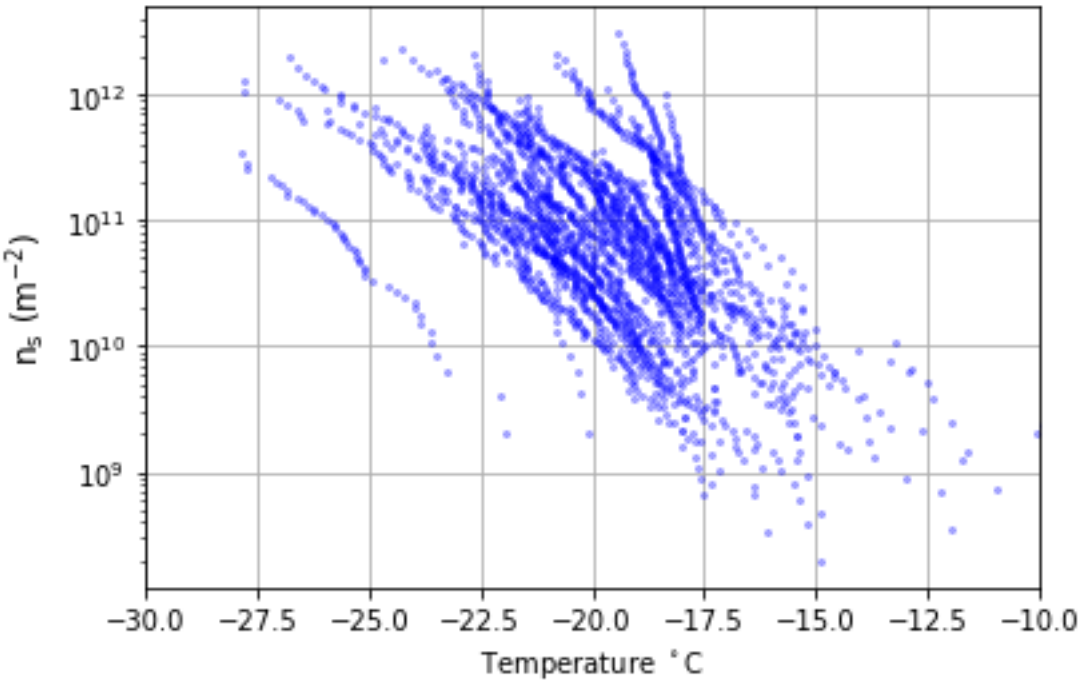

Figure 72: The number of active sites per unit surface area, n_s as a function of temperature for the samples taken during the measurement period.

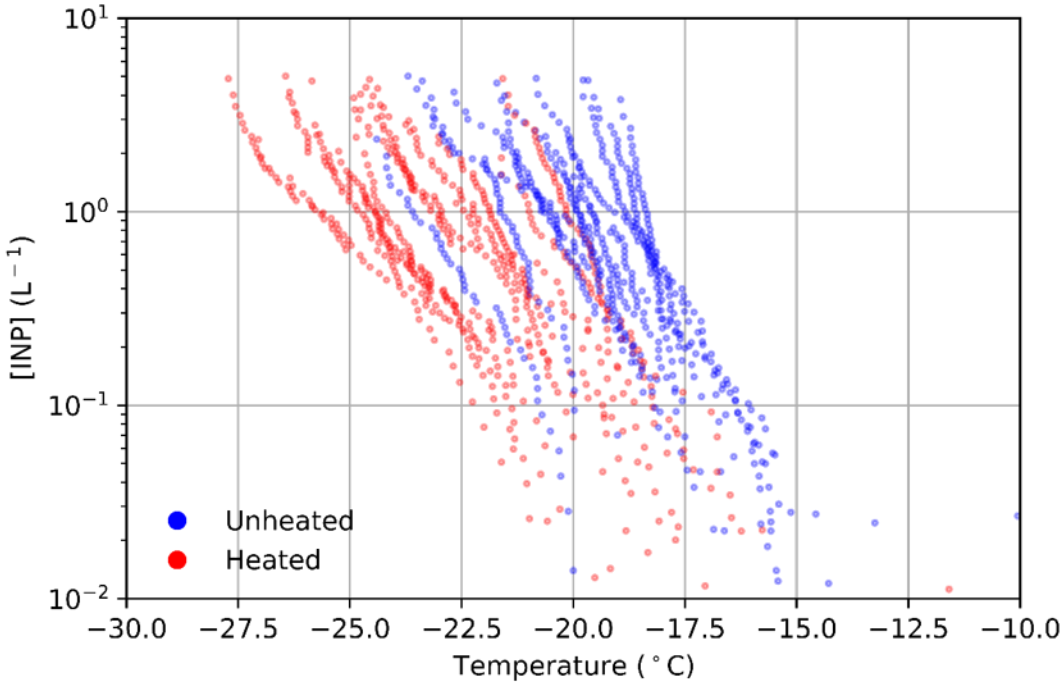

Figure 73: An INP_T spectra for all PM_{10} unheated (blue) and heated (red) data taken during the measurement period. Unheated data is only shown where there is corresponding heated data.

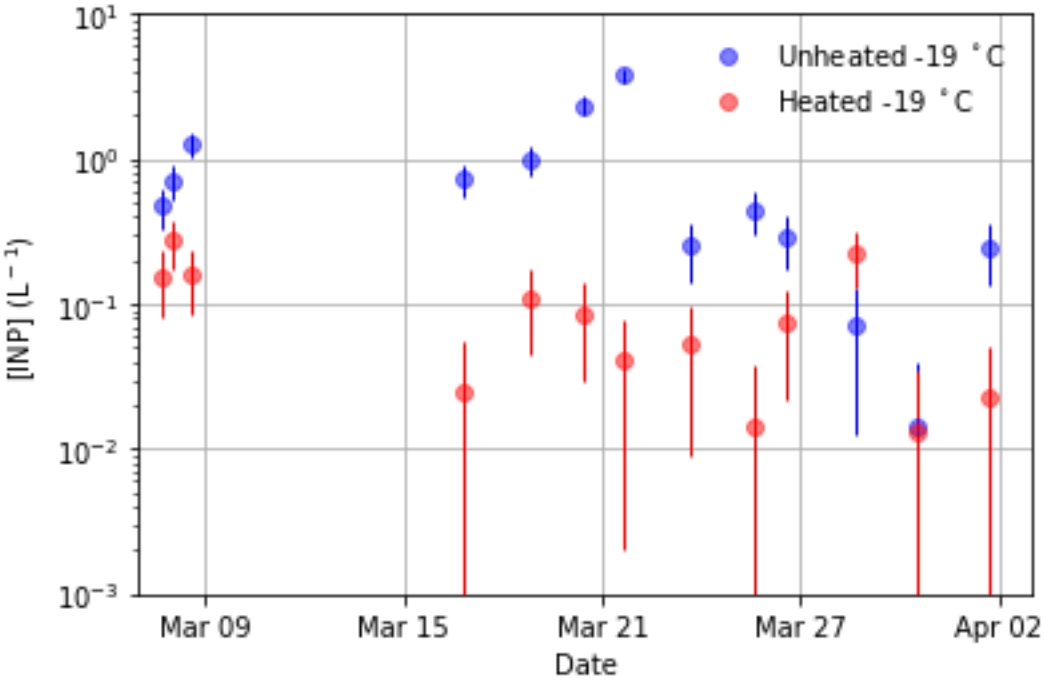

Figure 74: A time series of PM_{10} unheated (blue) and heated (red) INP concentrations at −19 °C taken during the measurement period. Unheated data is only shown where there is corresponding heated data.

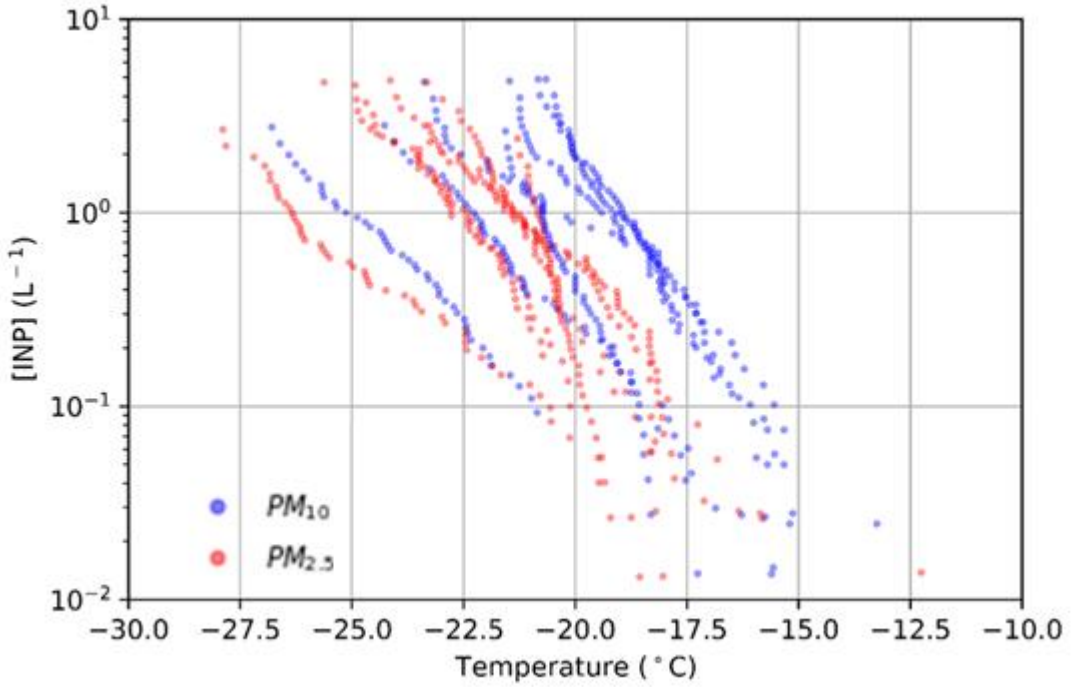

Figure 75: An INP_T spectra for all PM_{10} (blue) and $PM_{2.5}$ (red) data taken during the measurement period. PM_{10} data is only shown where there is corresponding $PM_{2.5}$ data.

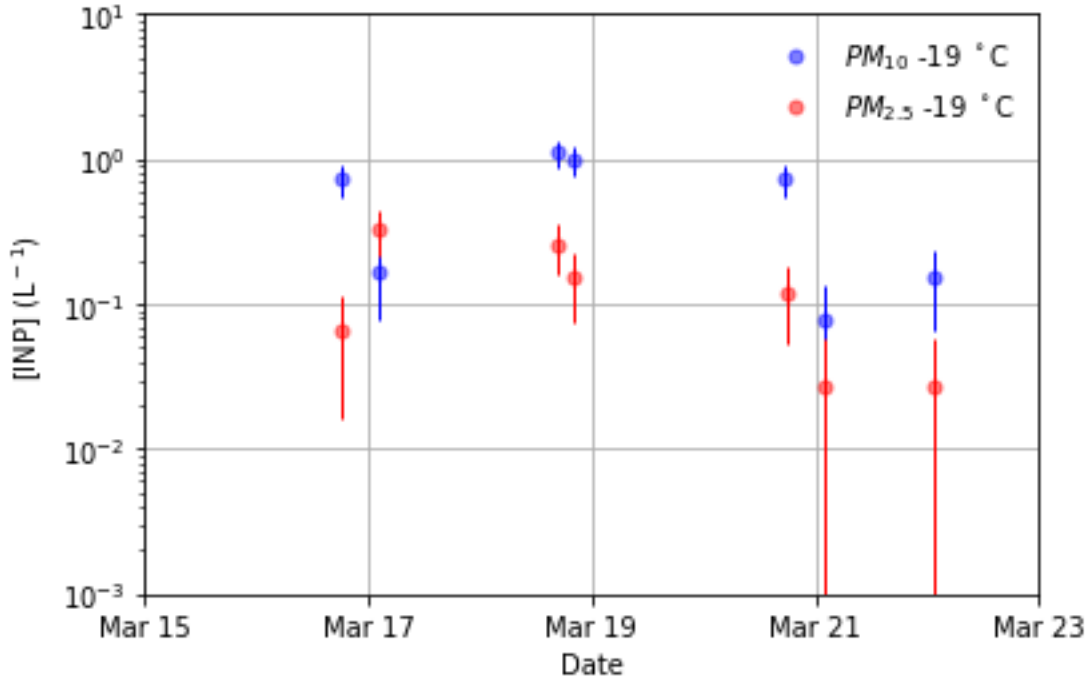

Figure 76: A time series of PM_{10} (blue) and $PM_{2.5}$ (red) INP concentrations at −19 °C taken during the measurement period. PM_{10} data is only shown where there is corresponding $PM_{2.5}$ data.

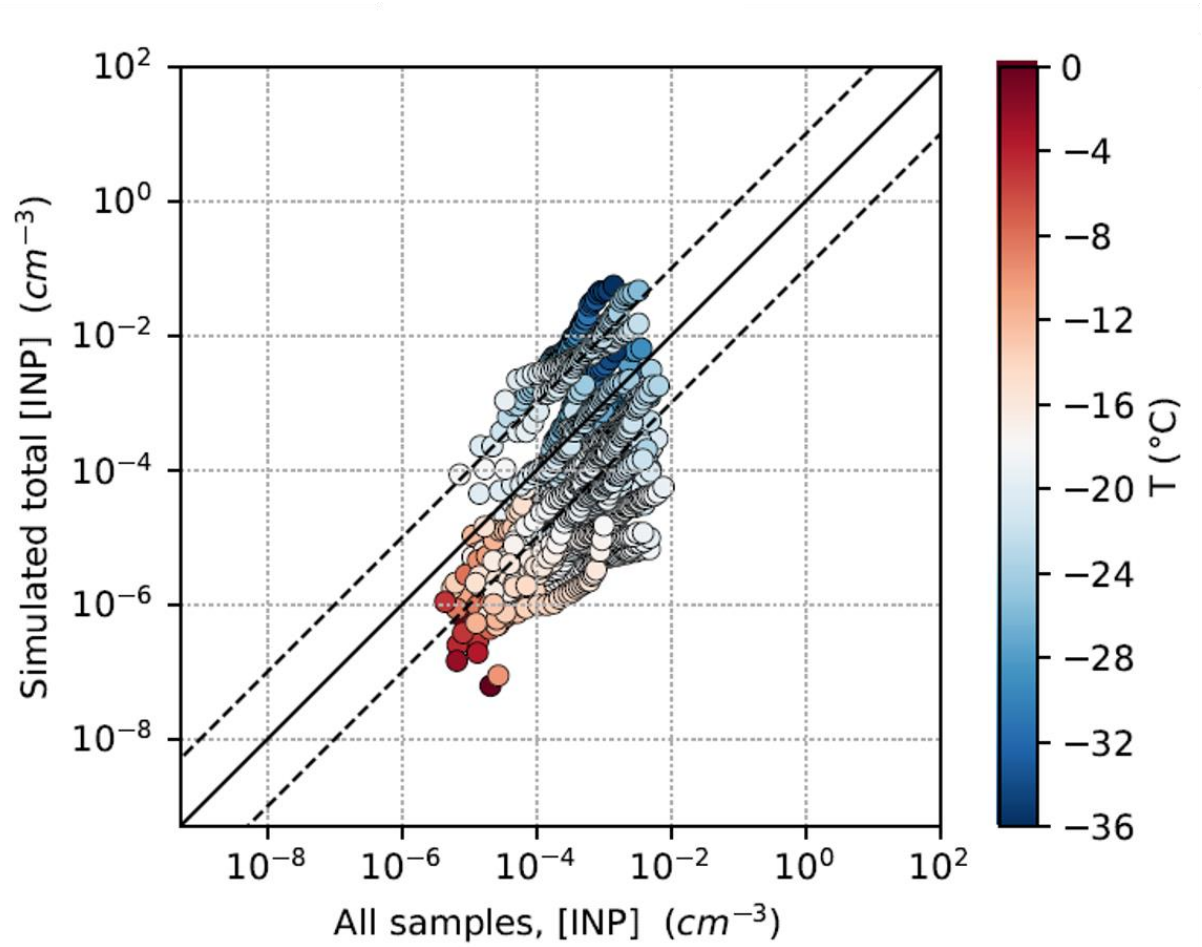

Figure 77: A 1:1 plot of simulated INP concentrations vs. measured INP concentrations. The colour scale indicates the temperature at which a concentration was measured.

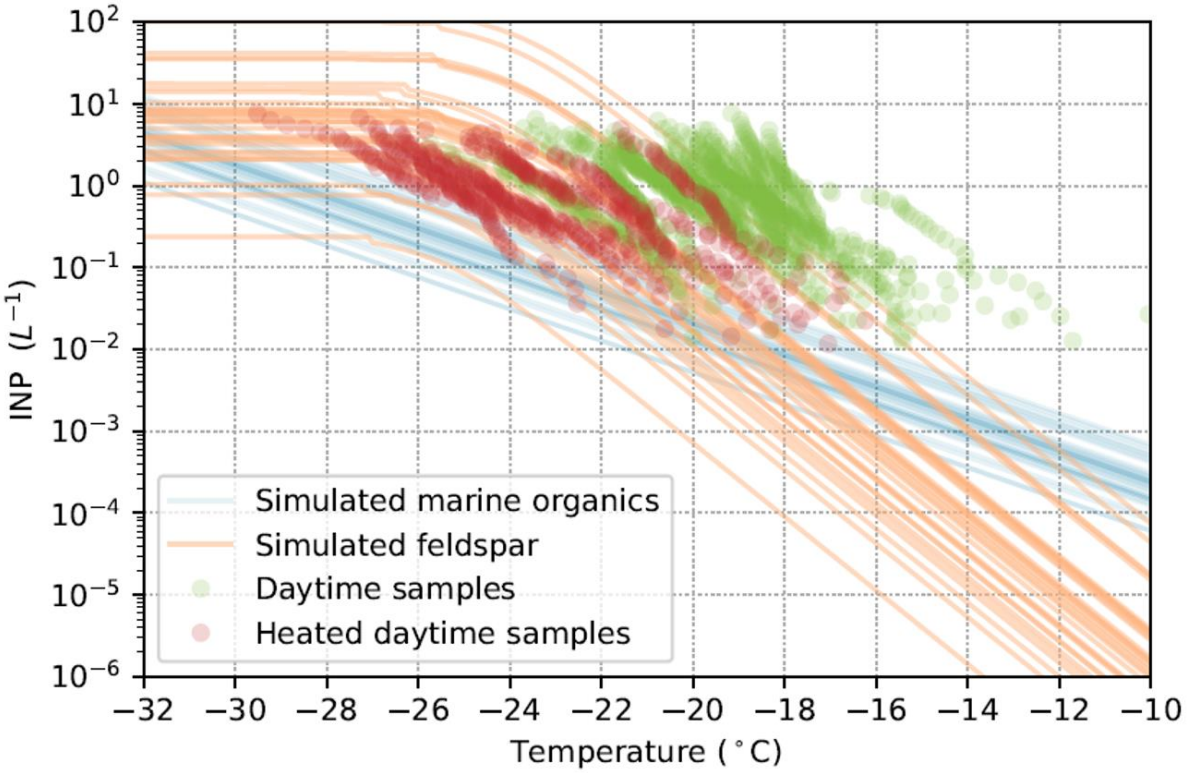

Figure 78: INP_T spectra for each of the unheated (green dots) and heated (red dots) day time sample made during the campaign. Day time samples were chosen as this is when nearly all of the heated samples were run. Solid lines indicate simulated INP concentrations due to marine organics (blue) and K-feldspar (red) according to GLOMAP.

6.6 References

Atkinson, J. D., Murray, B. J., Woodhouse, M. T., Whale, T. F., Baustian, K. J., Carslaw, K. S., et al. (2013). The importance of feldspar for ice nucleation by mineral dust in mixed-phase clouds. Nature, 498(7454), 355–358. https://doi.org/10.1038/nature12278

Boose, Y., Welti, A., Atkinson, J., Ramelli, F., Danielczok, A., Bingemer, H. G., et al. (2016). Heterogeneous ice nucleation on dust particles sourced from nine deserts worldwide - Part 1: Immersion freezing. Atmospheric Chemistry and Physics, 16(23), 15075–15095. https://doi.org/10.5194/acp-16-15075-2016

Boose, Y., Sierau, B., García, M. I., Rodríguez, S., Alastuey, A., Linke, C., et al. (2016). Ice nucleating particles in the Saharan Air Layer. Atmospheric Chemistry and Physics, 16(14), 9067–9087. https://doi.org/10.5194/acp-16-9067-2016

Burrows, S. M., Hoose, C., Pöschl, U., & Lawrence, M. G. (2013). Ice nuclei in marine air: Biogenic particles or dust? Atmospheric Chemistry and Physics, 13(1), 245–267. https://doi.org/10.5194/acp-13-245-2013

Conen, F., Morris, C. E., Leifeld, J., Yakutin, M. V., & Alewell, C. (2011). Biological residues define the ice nucleation properties of soil dust. Atmospheric Chemistry and Physics, 11(18), 9643–9648. https://doi.org/10.5194/acp-11-9643-2011

Connolly, P. J., Möhler, O., Field, P. R., Saathoff, H., Burgess, R., Choularton, T., & Gallagher, M. (2009). Studies of heterogeneous freezing by three different desert dust samples. Atmos. Chem. Phys. Atmospheric Chemistry and Physics, 9, 2805–2824. Retrieved from www.atmos-chem-phys.net/9/2805/2009/

DeMott, P. J., Prenni, A. J., Liu, X., Kreidenweis, S. M., Petters, M. D., Twohy, C. H., et al. (2010). Predicting global atmospheric ice nuclei distributions and their impacts on climate. Proceedings of the National Academy of Sciences of the United States of America, 107(25), 11217–11222. https://doi.org/10.1073/pnas.0910818107

DeMott, Paul J., Sassen, K., Poellot, M. R., Baumgardner, D., Rogers, D. C., Brooks, S. D., et al. (2003). African dust aerosols as atmospheric ice nuclei. Geophysical Research Letters, 30(14). https://doi.org/10.1029/2003GL017410

DeMott, Paul J, Hill, T. C. J., McCluskey, C. S., Prather, K. A., Collins, D. B., Sullivan, R. C., et al. (2016). Sea spray aerosol as a unique source of ice nucleating particles. Proceedings of the National Academy of Sciences of the United States of America, 113(21), 5797–803. https://doi.org/10.1073/pnas.1514034112

Grythe, H., Ström, J., Krejci, R., Quinn, P., & Stohl, A. (2014). Atmospheric Chemistry and Physics A review of sea-spray aerosol source functions using a large global set of sea salt aerosol concentration measurements. Atmos. Chem. Phys, 14, 1277–1297. https://doi.org/10.5194/acp-14-1277-2014

Harrison, A. D., Whale, T. F., Carpenter, M. A., Holden, M. A., Neve, L., O'Sullivan, D., et al. (2016). Not all feldspars are equal: a survey of ice nucleating properties across the feldspar group of minerals. Atmospheric Chemistry and Physics, 16(17), 10927–10940. https://doi.org/10.5194/acp-16-10927-2016

Harrison, A. D., Lever, K., Sanchez-Marroquin, A., Holden, M. A., Whale, T. F., Tarn, M. D., et al. (2019). The ice-nucleating ability of quartz immersed in water and its atmospheric importance compared to K-feldspar. Atmospheric Chemistry and Physics, 19(17), 11343–11361. https://doi.org/10.5194/acp-19-11343-2019

Herbert, R. J., Murray, B. J., Dobbie, S. J., & Koop, T. (2015). Sensitivity of liquid clouds to homogenous freezing parameterizations. Geophysical Research Letters, 42(5), 1599–1605. https://doi.org/10.1002/2014GL062729

Hill, Thomas C J, Moffett, B. F., Demott, P. J., Georgakopoulos, D. G., Stump, W. L., & Franc, G. D. (2014). Measurement of ice nucleation-active bacteria on plants and in precipitation by quantitative PCR. Applied and Environmental Microbiology, 80(4), 1256–67. https://doi.org/10.1128/AEM.02967-13

Hill, Tom C J, Demott, P. J., Tobo, Y., Fröhlich-Nowoisky, J., Moffett, B. F., Franc, G. D., & Kreidenweis, S. M. (2016). Sources of organic ice nucleating particles in soils. Atmos. Chem. Phys, 16, 7195–7211. https://doi.org/10.5194/acp-16-7195-2016

Hoose, C., & Möhler, O. (2012). Heterogeneous ice nucleation on atmospheric aerosols: a review of results from laboratory experiments. Atmospheric Chemistry and Physics, 12(20), 9817–9854. https://doi.org/10.5194/acp-12-9817-2012

Hoose, C., Kristjánsson, J. E., & Burrows, S. M. (2010). How important is biological ice nucleation in clouds on a global scale? Environmental Research Letters, 5(2). https://doi.org/10.1088/1748-9326/5/2/024009

Ickes, L., Porter, G. C. E., Wagner, R., Adams, M. P., Bierbauer, S., Bertram, A. K., et al. (2020). The ice-nucleating activity of Arctic sea surface microlayer samples and marine algal cultures. Atmospheric Chemistry and Physics, 20(18), 11089–11117. https://doi.org/10.5194/acp-20-11089-2020

Irish, V. E., Elizondo, P., Chen, J., Chou, C., Charette, J., Lizotte, M., et al. (2017). Ice-nucleating particles in Canadian Arctic sea-surface microlayer and bulk seawater. Atmospheric Chemistry and Physics, 17(17), 10583–10595. https://doi.org/10.5194/acp-17-10583-2017

Irish, V. E., Hanna, S. J., Xi, Y., Boyer, M., Polishchuk, E., Ahmed, M., et al. (2019). Revisiting properties and concentrations of ice-nucleating particles in the sea surface microlayer and bulk seawater in the Canadian Arctic during summer. Atmospheric Chemistry and Physics, 19(11), 7775–7787. https://doi.org/10.5194/acp-19-7775-2019

Joly, M., Amato, P., Deguillaume, L., Monier, M., Hoose, C., & Delort, A.-M. (2014). Quantification of ice nuclei active at near 0 °C temperatures in low-altitude clouds at the Puy de Dôme atmospheric station. Atmospheric Chemistry and Physics, 14(15), 8185–8195. https://doi.org/10.5194/acp-14-8185-2014

Junninen, H., Lauri, A., Keronen, P., Aalto, P., Hiltunen, V., Hari, P., & Kulmala, M. (2009). Smart-SMEAR: On-line data exploration and visualization tool for SMEAR stations. Boreal Environment Research, 14(4), 447–457.

Kanji, Z. A., Ladino, L. A., Wex, H., Boose, Y., Burkert-Kohn, M., Cziczo, D. J., et al. (2017). Overview of Ice Nucleating Particles. Meteorological Monographs, 58, 1.1-1.33. https://doi.org/10.1175/amsmonographs-d-16-0006.1

Kerminen, V. M., Lihavainen, H., Komppula, M., Viisanen, Y., & Kulmala, M. (2005). Direct observational evidence linking atmospheric aerosol formation and cloud droplet activation. Geophysical Research Letters, 32(14), 1–4. https://doi.org/10.1029/2005GL023130

Kieft, T. L., & Ruscettit, T. (1990). Characterization of Biological Ice Nuclei from a Lichen. JOURNAL OF BACTERIOLOGY, 172(6), 3519–3523. Retrieved from http://jb.asm.org/content/172/6/3519.full.pdf

Kulmala, M., Toivonen, A., Mäkelä, J. M., & Laaksonen, A. (1998). Analysis of the growth of nucleation mode particles observed in Boreal forest. Tellus, Series B: Chemical and Physical Meteorology, 50(5), 449–462. https://doi.org/10.3402/tellusb.v50i5.16229

Kuusela, K. (1990). The dynamics of boreal coniferous forests.

Lohmann, U., & Feichter, J. (2005). Global indirect aerosol effects: a review. Atmospheric Chemistry and Physics, 5(3), 715–737. https://doi.org/10.5194/acp-5-715-2005

Mann, G. W., Carslaw, K. S., Spracklen, D. V, Ridley, D. A., Manktelow, P. T., Chipperfield, M. P., et al. (2010). Geoscientific Model Development Description and evaluation of GLOMAP-mode: a modal global aerosol microphysics model for the UKCA composition-climate model. Geosci. Model Dev, 3, 519–551. https://doi.org/10.5194/gmd-3-519-2010

Möhler, O., Benz, S., Saathoff, H., Schnaiter, M., Wagner, R., Schneider, J., et al. (2008). The effect of organic coating on the heterogeneous ice nucleation efficiency of mineral dust aerosols. Environmental Research Letters, 3(2), 025007. https://doi.org/10.1088/1748-9326/3/2/025007

Morris, C. E., Georgakopoulos, D. G., & Sands, D. C. (2004). Ice nucleation active bacteria and their potential role in precipitation. Journal de Physique IV (Proceedings), 121, 87–103. https://doi.org/10.1051/jp4:2004121004

Morris, Cindy E., Monteil, C. L., & Berge, O. (2013). The life history of pseudomonas syringae: Linking agriculture to earth system processes. Annual Review of Phytopathology, 51, 85–104. https://doi.org/10.1146/annurev-phyto-082712-102402

Murray, B. J., O'Sullivan, D., Atkinson, J. D., & Webb, M. E. (2012). Ice nucleation by particles immersed in supercooled cloud droplets. Chemical Society Reviews, 41(19), 6519. https://doi.org/10.1039/c2cs35200a

Murray, B. J., Carslaw, K. S., & Field, P. R. (2020). Opinion: Cloud-phase climate feedback and the importance of ice-nucleating particles. Atmospheric Chemistry and Physics. https://doi.org/10.5194/acp-2020-852

Niemand, M., Möhler, O., Vogel, B., Vogel, H., Hoose, C., Connolly, P., et al. (2012). A Particle-Surface-Area-Based Parameterization of Immersion Freezing on Desert Dust Particles. Journal of the Atmospheric Sciences, 69(10), 3077–3092. https://doi.org/10.1175/JAS-D-11-0249.1

O'Sullivan, D., Murray, B. J., Ross, J. F., Whale, T. F., Price, H. C., Atkinson, J. D., et al. (2015). The relevance of nanoscale biological fragments for ice nucleation in clouds. Scientific Reports, 5, 8082. https://doi.org/10.1038/srep08082

O'Sullivan, D., Murray, B. J., Ross, J. F., & Webb, M. E. (2016). The adsorption of fungal ice-nucleating proteins on mineral dusts: a terrestrial reservoir of atmospheric ice-nucleating particles. Atmospheric Chemistry and Physics, 16(12), 7879–7887. https://doi.org/10.5194/acp-16-7879-2016

O'Sullivan, D., Adams, M. P., Tarn, M. D., Harrison, A. D., Vergara-Temprado, J., Porter, G. C. E., et al. (2018). Contributions of biogenic material to the atmospheric ice-nucleating particle population in North Western Europe. Scientific Reports, 8(1), 13821. https://doi.org/10.1038/s41598-018-31981-7

Petters, M. D., & Wright, T. P. (2015). Revisiting ice nucleation from precipitation samples. Geophysical Research Letters, 42(20), 8758–8766. https://doi.org/10.1002/2015GL065733

Phillips, V. T. J., Andronache, C., Christner, B., Morris, C. E., Sands, D. C., Bansemer, A., et al. (2009). Potential impacts from biological aerosols on ensembles of continental clouds simulated numerically. Biogeosciences, 6(6), 987–1014. https://doi.org/10.5194/bg-6-987-2009

Porter, G. C. E., Sikora, S. N. F., Adams, M. P., Proske, U., Harrison, A. D., Tarn, M. D., et al. (2020). Resolving the size of ice-nucleating particles with a balloon deployable aerosol sampler: the SHARK. Atmospheric Measurement Techniques, 13(6), 2905–2921. https://doi.org/10.5194/amt-13-2905-2020

Pouleur, S., Richard, C., Martin, J., & Antoun, H. Ice Nucleation Activity in Fusarium acuminatum and Fusarium avenaceumt, 58 § (1992). American Society for Microbiology. https://doi.org/10.1128/aem.58.9.2960-2964.1992

Pratt, K. A., Demott, P. J., French, J. R., Wang, Z., Westphal, D. L., Heymsfield, A. J., et al. (2009). In situ detection of biological particles in cloud ice-crystals. Nature Geoscience, 2(6), 398–401. https://doi.org/10.1038/NGEO521

Price, H. C., Baustian, K. J., Mcquaid, J. B., Blyth, A., Bower, K. N., Choularton, T., et al. (2018). Atmospheric Ice-Nucleating Particles in the Dusty Tropical Atlantic. https://doi.org/10.1002/2017JD027560

Pummer, B. G., Bauer, H., Bernardi, J., Bleicher, S., & Grothe, H. (2012). Suspendable macromolecules are responsible for ice nucleation activity of birch and conifer pollen. Atmos. Chem. Phys, 12. https://doi.org/10.5194/acp-12-2541-2012

Pummer, B. G., Budke, C., Augustin-Bauditz, S., Niedermeier, D., Felgitsch, L., Kampf, C. J., et al. (2015). Ice nucleation by water-soluble macromolecules. Atmospheric Chemistry and Physics, 15(8), 4077–4091. https://doi.org/10.5194/acp-15-4077-2015

Sanchez-Marroquin, A., Arnalds, O., Baustian-Dorsi, K. J., Browse, J., Dagsson-Waldhauserova, P., Harrison, A. D., et al. (2020). Iceland is an episodic source of atmospheric ice-nucleating particles relevant for mixed-phase clouds. Science Advances, 6(26), eaba8137. https://doi.org/10.1126/sciadv.aba8137

Schumacher, C. J., Pöhlker, C., Aalto, P., Hiltunen, V., Petäjä, T., Kulmala, M., et al. (2013). Seasonal cycles of fluorescent biological aerosol particles in boreal and semi-arid forests of Finland and Colorado. Atmospheric Chemistry and Physics, 13(23), 11987–12001. https://doi.org/10.5194/acp-13-11987-2013

Spracklen, D. V., & Heald, C. L. (2014). The contribution of fungal spores and bacteria to regional and global aerosol number and ice nucleation immersion freezing rates. Atmospheric Chemistry and Physics, 14(17), 9051–9059. https://doi.org/10.5194/acp-14-9051-2014

Spracklen, Dominick V., Bonn, B., & Carslaw, K. S. (2008). Boreal forests, aerosols and the impacts on clouds and climate. Philosophical Transactions of the Royal Society A: Mathematical, Physical and Engineering Sciences, 366(1885), 4613–4626. https://doi.org/10.1098/rsta.2008.0201

Storelvmo, T. (2017). Aerosol Effects on Climate via Mixed-Phase and Ice Clouds. Annual Review of Earth and Planetary Sciences, 45(1), 199–222. https://doi.org/10.1146/annurev-earth-060115-012240

Tan, I., Storelvmo, T., & Zelinka, M. D. (2016). Observational constraints on mixed-phase clouds imply higher climate sensitivity. Science (New York, N.Y.), 352(6282), 224–7. https://doi.org/10.1126/science.aad5300

Tobo, Y., Prenni, A. J., Demott, P. J., Huffman, J. A., McCluskey, C. S., Tian, G., et al. (2013). Biological aerosol particles as a key determinant of ice nuclei populations in a forest ecosystem. Journal of Geophysical Research Atmospheres, 118(17), 10100–10110. https://doi.org/10.1002/jgrd.50801

Tobo, Y., Adachi, K., DeMott, P. J., Hill, T. C. J., Hamilton, D. S., Mahowald, N. M., et al. (2019). Glacially sourced dust as a potentially significant source of ice nucleating particles. Nature Geoscience, 12(April). https://doi.org/10.1038/s41561-019-0314-x

Tunved, P., Hansson, H. C., Kerminen, V. M., Ström, J., Dal Maso, M., Lihavainen, H., et al. (2006). High natural aerosol loading over boreal forests. Science, 312(5771), 261–263. https://doi.org/10.1126/science.1123052

Vali, G. (1971). Quantitative Evaluation of Experimental Results an the Heterogeneous Freezing Nucleation of Supercooled Liquids. Journal of the Atmospheric Sciences, 28(3), 402–409. https://doi.org/10.1175/1520-0469(1971)028<0402:QEOERA>2.0.CO;2

Vergara-Temprado, J., Murray, B. J., Wilson, T. W., O'sullivan, D., Browse, J., Pringle, K. J., et al. (2017). Contribution of feldspar and marine organic aerosols to global ice nucleating particle concentrations. Atmospheric Chemistry and Physics, 17(5), 3637–3658. https://doi.org/10.5194/acp-17-3637-2017

Whale, T. F., Murray, B. J., O'Sullivan, D., Wilson, T. W., Umo, N. S., Baustian, K. J., et al. (2015). A technique for quantifying heterogeneous ice nucleation in microlitre supercooled water droplets. Atmospheric Measurement Techniques, 8(6), 2437–2447. https://doi.org/10.5194/amt-8-2437-2015

Wilson, T. W., Ladino, L. A., Alpert, P. A., Breckels, M. N., Brooks, I. M., Browse, J., et al. (2015). A marine biogenic source of atmospheric ice-nucleating particles. Nature, 525(7568), 234–238. https://doi.org/10.1038/nature14986

Zolles, T., Burkart, J., Häusler, T., Pummer, B., Hitzenberger, R., & Grothe, H. (2015). Identification of ice nucleation active sites on feldspar dust particles. Journal of Physical Chemistry A, 119(11), 2692–2700. https://doi.org/10.1021/jp509839x

7 Overview, conclusions and outlook

Being able to accurately predict and model the phase of mixed-phase clouds is a critical step in understanding the Earth's radiative budget and being able to correctly forecast climate change (Boucher et al., 2013; Matus & L'Ecuyer, 2017; Storelvmo, 2017; Tan et al., 2016). Ice-nucleating particles are of first order importance for determining the phase of mixed-phase clouds, however sources, concentrations and characteristics of ice-nucleating particles are poorly resolved both spatially and temporally (Hoose & Möhler, 2012; Kanji et al., 2017a; B. J. Murray et al., 2012). One of the primary reasons for this is a lack of effective instrumentation for the ongoing monitoring of atmospheric ice-nucleating particle concentrations. The focus of this research project was to develop instrumentation suitable for the ongoing measurement of atmospheric INP concentrations, and to further the understanding of what aerosol particles act as effective ice-nucleating particles. The first goal was met through the development of the PINE chamber (described in Chapter 2) and the deployment of PINE to a field environment (described in chapter 3). The second goal was met through investigating the ice-nucleating ability of combustion aerosol (described in chapter 4), measuring and quantifying the ice-nucleating ability of viruses for the first time (described in chapter 5) and through the quantifying and characterising of INPs in a boreal forest environment (described in Chapter 6).

7.1 Objective 1: Developing the PINE chamber

The PINE chamber was conceptualised in January 2016, with the project beginning in earnest in August 2016. Development was completed in March 2018 upon which time PINE was deployed on its first field campaign. The first publication describing PINE is now available, and details the working principles of PINE whilst also showing some first validating results (Möhler et al. 2020). Chapter 2 is based upon my contributions to Möhler et al., 2020. The aim of the PINE project was to develop instrumentation capable of measuring INPs in a field environment throughout the temperature spectrum, with high time resolution, in an autonomous way.

A key consideration in the development of PINE chamber was the desire to make it portable, make automated and continuous online measurements, have high time resolution and have it be able to measure across the full temperature spectra. It was important at the conception stage to consider if there was already an instrument in existence that delivered in all these areas or could be modified/upgraded to do so. Ultimately it was decided this was not the case, and to achieve all the desired criteria listed above a new instrument would have to be developed. The rationale behind this was that whilst CFDCs are capable of making online measurements at high time resolutions and have been available in a portable capacity for a number of years, there are still limitations with regards to making measurements at warmer temperatures and on a continuous basis (Boose et al., 2016; Demott et al., 2017; Lacher et al., 2017; Rogers et al., 2001). Cold stages on the other hand are extremely portable, able to make measurements across the entire immersion freezing temperature spectrum and can make field measurements at high time resolution, although only via offline analysis (Harrison et al., 2018; O'Sullivan et al., 2018; Tarn et al., 2018; Whale et al., 2015). Other instrumentation used to measure INPs in the field are detailed in Chapter 1.3.1, but none meet the criteria stated above. It was thus decided that we should develop an instrument that can, and as detailed in chapters 2 and 3 PINE was the result of this decision, able to meet each of the stated criteria.

In terms of technical development, I lead the project on a day-today basis in the 2 year development span, with conceptual and technical guidance from my supervisors Möhler and Murray, and support from the wider PINE team. PINE started out as small cloud chamber within the much larger AIDA chamber, with an OPC and pump attached. This allowed for first experiments using the concept that would become the PINE chamber, without having a fully developed inlet or cooling system. PINE was at this stage referred to as the 'mini-AIDA', and was attached at the base of the AIDA chamber in order to sample aerosol directly from it, removing the requirement for any drying or cooling. PINE would run a series of expansions in this configuration prior to an AIDA expansion, with the results being compared and guiding future iterations of the chamber.

I had a leading role in developing each of the 5 major parts of the PINE chamber (described in detail in Chapter 2) and ensuring they were operational before PINE's first deployment in March 2018. This development culminated in the EXTRA18 campaign in January 2018, a laboratory campaign held at the AIDA lab in KIT in which the PINE chamber, now a standalone instrument, was compared directly to the AIDA chamber for a selection of aerosol particles. The results from this campaign gave us confidence that PINE was ready for its first field deployment, and form figures 8-11 of Möhler et al., 2020. A lasting, if not so time consuming, contribution I had to the project was also the naming of PINE.

To summarise, this objective was the main focus of the first half of my research project, and resulted in PINE not only becoming a powerful instrument for measuring INPs in the field, but also led to the commercialisation of PINE. PINE provides the community with a portable instrument capable of working autonomously for extended periods of time and probing the ice-nucleating ability of sample aerosol throughout the enitre temperature spectrum. It is a unique, new instrument that will enable measurements to be made that can further our understanding of the temporal and spatial variation of INPs that previous instrumentation could not.

7.2 Objective 2: Deploying and validating PINE in the field

The second objective of this research project was to deploy to a field environment and validate against existing field instruments the now developed PINE chamber. It was decided that PINE would be deployed to the Hyytiälä forestry research station in Finland as part of the HyICE18 campaign. Hyytiälä is situated in a boreal forest environment and has no published INP measurements from there at the time of the campaign.

My role in this campaign was partly to lead the Leeds contingent to make filter based INP measurements (described in Chapter 5 Chapter 1.7.5), but also to assist in the setup and operation of the PINE chamber, which would be the day-to-day responsibility of Franziska Vogel (then a Masters student, now a PhD student working with PINE). I was also responsible for the data analysis post-campaign. Chapter 3 goes into details about the technical considerations of working with PINE in the field, with particular attention being paid to background measurement and limits of detection. One of the major strengths of PINE is that it can be operated with zero background counts, which allows the instrument limit of detection to be increased as a function of measurement time. Demonstrating this in a field

environment, outside the clean and well-maintained setting of a laboratory was a key aim of this campaign, and is demonstrated in chapter 3.

During the HyICE18 campaign PINE was operated at a number of different measurement temperatures in order to test its capabilities in the field. The volume of data generated by the chamber was in excess of 100 Gb of plain text files. As part of this data analysis, I had to rewrite the analysis code that we had previously used in laboratory experiments and optimise it for working with such a large volume of data. I then had to integrate the PINE data set with other data sets such as meteorological variables and aerosol measurements. The output of this is in Figures 14-20 of Chapter 3, which show a time series of INP measurements throughout the whole campaign, and a series of case studies during the campaign. PINE was also validated against two established field instruments, the µL-NIPI and PINC. PINE is shown to agree well with both instruments during comparable measurement periods. In this chapter I highlight the strength of PINE to make measurements of varying INP concentrations on short time scales. This is important as INP concentration in Hyytiälä varied by over an order of magnitude on the scale of hours (Figure 36), and this variation may be more pronounced in other environments and in different conditions. In environments where bioaerosls are suspected to play an important role, the diurnal cycle of flora with the sun may control the emission of such particle that dominate the INP concentration at specific times of the day, potentially on short time scale. The same can be true for discrete pollution events or air mass changes when measuring atmospheric dust particle in low latitude deserts. Without the capability to make these high-time resolution measurements we would not know when we need to make them and how important they may be.

In summary, the second objective of this research project was meet by deploying PINE to the Hyytiälä forestry research station as part of the HyICE18 campaign, during which time it proved to be capable of autonomous measurements and was validated against other field instruments. The manuscript Chapter 3 is based on will serve as a reference point for all future PINE field campaigns and demonstrate that measurements made by PINE are validated.

7.3 Objective 3: Quantifying the importance of combustion aerosol as an atmospheric ice-nucleating particle

Objectives 3-5 of this research project was motivated by the need for an improved understanding of what aerosol species serve as atmospheric ice-nucleating particles. The first of these objectives was aimed at improving our understanding of the ice-nucleating ability of combustion aerosol. Chapter 4 describes measurements made during Bonfire Night, a celebration in the U.K. that involves the lighting of bonfires and setting off fireworks.

On November 5th 2016, myself and a team which I led took hourly filter samples from a PM10 sampling unit to measure the change in ice-nucleating activity over the course of Bonfire night, also measuring aerosol concentration and size distribution and black carbon concentration. The aerosol captured in these filters were analysed in close to real time, with a small number analysed the next day. The results showed no change in INP concentrations throughout the event, despite aerosol and black carbon concentrations increasing by a factor of 10 and 100 respectively. This was striking, and despite being initially viewed as a negative result, motivated me to further analyse the data. Using the mass concentration of black

carbon measured throughout the combustion event, a limiting value for the number of ice nucleation active sites, n_s was calculated.

This first successful attempt to quantify the ice-nucleating ability motivated us to carry out an expanded study the following year. In November 2017, measurements were made over two days, November 4th and 5th. Bonfire night in 2017 was held on a Sunday, meaning there were a large number of celebrations on the day prior also. In addition to increasing the number of measurement days, we also took filter measurements for SEM analysis (shown in Chapter 4) and analysed the filter samples on three different cold stages in order to characterize as much of the INP_T spectrum as possible (Harrison et al., 2018; Tarn et al., 2018; T. F. Whale et al., 2015). Our results in 2017 matched those of 2016 in terms of the underlying conclusion that combustion aerosol produced on Bonfire night is a poor ice nucleator, but also allowed us to further constrain our limiting value for the n_s of black carbon as pollution levels were much higher during the 2017 measurement days.
In summary, we used the natural laboratory created by the combustion aerosol emitted during 3 measurements days on and around bonfire night 2016/2017 to show that despite aerosol concertation increasing by over a factor of 100, combustion aerosol could still not compete with ambient INPs present. We also presented a limiting value for the n_s of black carbon, which was in line with recent literature based on laboratory studies (Schill et al., 2016; Ullrich et al., 2017; Vergara-Temprado et al., 2018). This study furthered our understanding of what is, and more precisely what isn't, and important source of atmospheric ice-nucleating particles.

7.4 Objective 4: Investigating the potential for viruses to nucleate ice

The fourth objective of this research project was again in line with the stated goal of furthering the understanding of what aerosol particles act as effective ice-nucleating particles. Predicting the phase of clouds in the marine atmospheric boundary layer is critical for constraining estimates of climate feedback in a warming world (Vergara-Temprado et al. 2018; Murray, Carslaw, and Field, 2020). Sea spray aerosol containing biogenic organic material, virus particles and other marine biological materials has been shown to nucleate ice (Irish et al., 2017, 2019; T. W. Wilson et al., 2015), but the specific components which cause nucleation are unclear. There are estimated to be 10^7 virus particles per ml of seawater, 10^8-10^9 per ml in marine surface sediments (Suttle, 2005, 2007), and there is a clear mechanism by which organic matter from the sea surface microlayer can be aerosolized into the marine atmospheric boundary layer. Thus, the hypothesis was made that viruses could be a source of atmospheric INPs in marine environments.

Chapter 5 is based upon a paper currently in submission entitled *Viruses and their potential for cloud glaciation*, led by myself as first author with Dr Nina Atanasova as joint-first author. Estimates of the number of virus particles in the biosphere are around 10^{31} (Whitman et al., 1998),, with an unknown number of different viruses making up this number. It would be impossible to even test a small fraction of these different viruses using existing techniques. Despite the huge number of different viruses known, there are a relatively small number of architectures that these viruses can hold (Abrescia et al., 2012). As ice nucleation is a surface driven process, experiments were carried out on some of the most common virion architectures in order to cut through the parameter space. The first order question we were then asking was '*Can viruses nucleate ice? If so, does their architecture matter?'.* The answer

to the first question was answered clearly, as shown throughout Chapter 5, that viruses can nucleate ice. Whilst there was a clear signal in the ice nucleation experiments, it is worth noting that viruses are quite poor ice nucleators, showing extremely low active site density when normalised to their particle concentration. By testing a range of the most common virus architectures, we reached the conclusion that virion architecture is not the primary factor in determining whether a virus species will be an effective INP type.

In line with our overall aim of improving the understanding of understanding of what aerosol particles act as effective ice-nucleating particles, we attempted to quantify the importance of virus INPs in the atmosphere. We did this by estimating the number of virus INPs in the atmosphere based upon our measurements and estimates of atmospheric virus particles (Prussin et al., 2015; Rastelli et al., 2017; Whon et al., 2012). We then used literature data to estimate the range of INP concentrations in the atmosphere in both terrestrial and marine environments. Whilst no means an exact calculation, this allowed us to determine whether virus INPs could contribute to the INP burden in either marine or terrestrial environments. We ultimately concluded that virus INPs are likely unimportant in terrestrial environments, but may play a minor role in marine environments.

7.5 Objective 5: Measuring the concentrations and characteristics of ice-nucleating particles in a boreal forest

Objective 5, similar to objectives 3 and 4, sought to further our understanding of what aerosol species serve as atmospheric ice-nucleating particles. After taking part in the field campaign of O'Sullivan et al., (2018), I found myself interested in the potential roles of bioaerosols as ice-nucleating particles. Thus, when the opportunity came up to take part in the HyICE18 campaign with PINE, I devised a plan to also make filter based measurements in order to quantify and characterise INPs in a boreal environment.

Measurements were made in Hyytiälä over a 6 week period, with INP concentrations being measured and also the nature of the INPs present in the atmosphere probed. Sampled INPs were tested for proteinaceous activity associated with ice nucleation by bioaerosols (Tom C J Hill et al., 2016; O'Sullivan et al., 2018), and also size-resolved. These measurements illustrated that INP concentrations in Hyytiälä were above those typical of the terrestrial mid-latitudes, that the INP responsible were biological and in the coarse mode (however a notable concentration of INPs was also present in the fine mode).

Model simulations of INP concentrations in Hyytiälä for the time period we were there were made using a global aerosol transport model - GLOMAP (Mann et al., 2010; Vergara-Temprado et al., 2017). These simulations only considered K-feldspar and marine organics as sources of INPs, having no capacity to predict INP contributions from terrestrial bioaerosols. When comparing measured INP concentrations to simulations, there was a clear low bias in the model output, thus the INPs present in Hyytiälä were not predicted by GLOMAP, and may dominated the atmospheric INP burden in the region.
Given the characteristics of the INPs measured (their activity at temperatures above –20 °C, their size and their likely biological origin), several candidates come to mind as to their identity. Aerosolised bacteria or fungi spores, or potentially aerosolised lichen particles (lichens were observed on the trees in Hyytiälä and have a known ice-nucleating ability (Kieft and Ruscettit (1990)) may present the answer as to what aerosol particles are driving INP

concentrations in boreal environments. Future work will seek to test this hypothesis through the sampling and culturing of bioaerosols in Hyytiälä and through wind tunnel experiments involving lichens growing on trees in the forest.

7.6 Future work

Throughout the course of this research project, several objectives have been met and questions answered. Some of these objectives were self-contained and had a degree of finality (i.e. develop and deploy the PINE chamber), however some areas of research presented within this thesis have led to more questions than they originally sought to answer, and hopefully either I or someone else will be able to do so in the future.

The first area of future work I would like to discuss is the role of boreal forests as a source of ice-nucleating particles in a warming world. As described in detail in chapters 3 and 6, INP concentrations in a boreal forest can vary by orders of magnitude at a fixed temperature, and have a distinctly non-linear INP_T spectra, whilst there is also evidence they evolve with time. The field campaign that chapters 3 and 6 are based one spanned just two seasons in a single year, meaning the data obtained does not tell us how the boreal forest environment may produce INPs in Summer or Autumn, or what year on year variations in weather patterns may cause. On a longer time scale, climate change will cause our world to warm in the coming decades, which will have a profound effect on the biome, which holds true for boreal forests also. As demonstrated in chapter 6, the INPs present in a boreal forest may be important in the high-latitude environments they a predominant in, but we do not yet understand the source of or mechanism by which these INPs are emitted into the atmosphere. If bioaerosols from the boreal forest are driving the INP population, then it is possible that these will change as the planet warms, influencing clouds further and potentially inducing unforeseen feedbacks. An aspiration for future research would be to return to Hyytiälä for an extend period and thoroughly measure the INP population in the atmosphere, and then use the measurements made there to infer the source and mechanism by which they are emitted, and to then explicitly demonstrate these sources and mechanisms through focused studies.

The second area of aspirational work I would highlight is the potential for viruses to be an important source of INPs in remote marine/polar environments. Given the opportunity I would like to return to Helsinki to work further will my collaborators there to isolate and purify viruses that are specific to these environments and then have had their presence demonstrated. Through the more focused targeting of atmospherically relevant viruses (a field which is currently growing at pace) we could remove some of the uncertainty presented in Chapter 5 about the atmospheric relevance of viral INPs.

7.7 Conclusions and outlook

This research project has furthered the knowledge of INP concentrations in the atmosphere, and shed light on the aerosol particles driving ice nucleation in different environments and at different temperatures. The world we live in is a changing one; climate change is causing global temperature to increase and will affect all factors of our lives in the future. Some of these effects are known and can be quantified, some are known and cannot be quantified, and then some of these effects will reveal themselves only through their manifestation in the environment. Feedback processes may occur, where the increase in mean global temperature

results in a further increase in global mean temperature (positive feedback) or in a decrease (negative feedback). This holds true for atmospheric ice nucleation.

Shallow clouds that cover much of the mid and high-latitude regions of the globe serve to dampen the global temperature rise associated with CO_2 in the atmosphere. These clouds will transition to a state wherein they are comprised of more liquid water than ice, as the Earth warms, in turn increasing the scattering of incoming solar radiation and dampening the warming effect. Murray et al., (2020) argues that the magnitude of this mitigation is overestimated in current climate models, and a better representation of INPs in these models, along with the predictive capacity to understand atmospheric INP concentrations, is required to properly quantify this feedback effect. Chapters 3-5 help us understand what some of these feedbacks may be.

Chapter 3 investigates the potential for anthropogenic combustion aerosol to act as atmospheric INPs. Humanity has long been polluting the atmosphere, with the effects well documented in terms of the rise in global CO_2 and other greenhouse gases, along with the degradation of the ozone layer. In Chapter 3 we demonstrate that at least combustion aerosol emitted through anthropogenic means similar to those observed on the U.K's Bonfire Night is not having a significant influence on the population of ice nucleating particles, and is unlikely to do so as the atmosphere continues to warm, as it cannot compete with current ambient INPs.

Chapters 4 and 5 both focus on the potential for bioaerosols to act as atmospheric INPs, although from different perspectives. Chapter 4 proposes that viruses may play a role in atmospheric ice nucleation in remote marine locations, whilst Chapter 5 shows that INP concentrations in the boreal forest environment are higher than is typical for the terrestrial mid-latitudes and those predicted through model simulations, and the INPs responsible are likely bioaerosols of coarse mode size. These bioaerosols will be affected by the increase in global temperature, and understanding their role as atmospheric INPs is crucial to understanding their impact on cloud glaciation and feedbacks.

Finally, a base requirement for improving our understanding of the INP distribution around the world is having instrumentation capable of measuring it. Chapters 2 & 3 detail the development and validation of the PINE chamber, and demonstrate the importance of its capability to make automated, high-time resolution measurements throughout the MPC temperature regime. Through the deployment of PINE chambers at measurement stations throughout the globe, a real-time understanding of the global atmospheric INP burden could be obtained.

Ultimately, the work in this research project has sought to take steps towards improving our understanding of how many INPs there are in the atmosphere and what those INPs are. The techniques and insights in this thesis will aid in understanding the role of INPs in the atmosphere at present and in the future.

7.8 References

Abrescia, N. G. A., Bamford, D. H., Grimes, J. M., & Stuart, D. I. (2012). Structure Unifies the Viral Universe. Annual Review of Biochemistry, 81(1), 795–822. https://doi.org/10.1146/annurev-biochem-060910-095130

Boucher, O., Randall, D., Artaxo, P., Bretherton, C., Feingold, G., Forster, P., et al. (2013). Clouds and Aerosols. In: Climate Change 2013: The Physical Science Basis. Contribution of Working Group I to the Fifth Assessment Report of the Intergovernmental Panel on Climate Change Coordinating Lead Authors: Lead Authors.

Harrison, A. D., Whale, T. F., Rutledge, R., Lamb, S., Tarn, M. D., Porter, G. C. E., et al. (2018). An instrument for quantifying heterogeneous ice nucleation in multiwell plates using infrared emissions to detect freezing. Atmospheric Measurement Techniques, 11(10), 5629–5641. https://doi.org/10.5194/amt-11-5629-2018

Hill, T. C. J., Demott, P. J., Tobo, Y., Fröhlich-Nowoisky, J., Moffett, B. F., Franc, G. D., & Kreidenweis, S. M. (2016). Sources of organic ice nucleating particles in soils. Atmos. Chem. Phys, 16, 7195–7211. https://doi.org/10.5194/acp-16-7195-2016

Hoose, C., & Möhler, O. (2012). Heterogeneous ice nucleation on atmospheric aerosols: a review of results from laboratory experiments. Atmospheric Chemistry and Physics, 12(20), 9817–9854. https://doi.org/10.5194/acp-12-9817-2012

Irish, V. E., Elizondo, P., Chen, J., Chou, C., Charette, J., Lizotte, M., et al. (2017). Ice-nucleating particles in Canadian Arctic sea-surface microlayer and bulk seawater. Atmospheric Chemistry and Physics, 17(17), 10583–10595. https://doi.org/10.5194/acp-17-10583-2017

Irish, V. E., Hanna, S. J., Xi, Y., Boyer, M., Polishchuk, E., Ahmed, M., et al. (2019). Revisiting properties and concentrations of ice-nucleating particles in the sea surface microlayer and bulk seawater in the Canadian Arctic during summer. Atmospheric Chemistry and Physics, 19(11), 7775–7787. https://doi.org/10.5194/acp-19-7775-2019

Kanji, Z. A., Ladino, L. A., Wex, H., Boose, Y., Burkert-Kohn, M., Cziczo, D. J., et al. (2017). Overview of Ice Nucleating Particles. Meteorological Monographs, 58, 1.1-1.33. https://doi.org/10.1175/amsmonographs-d-16-0006.1

Kieft, T. L., & Ruscettit, T. (1990). Characterization of Biological Ice Nuclei from a Lichen. JOURNAL OF BACTERIOLOGY, 172(6), 3519–3523. Retrieved from http://jb.asm.org/content/172/6/3519.full.pdf

Mann, G. W., Carslaw, K. S., Spracklen, D. V, Ridley, D. A., Manktelow, P. T., Chipperfield, M. P., et al. (2010). Geoscientific Model Development Description and evaluation of GLOMAP-mode: a modal global aerosol microphysics model for the UKCA composition-climate model. Geosci. Model Dev, 3, 519–551. https://doi.org/10.5194/gmd-3-519-2010

Matus, A. V., & L'Ecuyer, T. S. (2017). The role of cloud phase in Earth's radiation budget. Journal of Geophysical Research: Atmospheres, 122(5), 2559–2578. https://doi.org/10.1002/2016JD025951

Murray, B. J., O'Sullivan, D., Atkinson, J. D., & Webb, M. E. (2012). Ice nucleation by particles immersed in supercooled cloud droplets. Chemical Society Reviews, 41(19), 6519. https://doi.org/10.1039/c2cs35200a

Murray, B. J., Carslaw, K. S., & Field, P. R. (2020). Opinion: Cloud-phase climate feedback and the importance of ice-nucleating particles. Atmospheric Chemistry and Physics. https://doi.org/10.5194/acp-2020-852

O'Sullivan, D., Adams, M. P., Tarn, M. D., Harrison, A. D., Vergara-Temprado, J., Porter, G. C. E., et al. (2018). Contributions of biogenic material to the atmospheric ice-nucleating particle

population in North Western Europe. Scientific Reports, 8(1), 13821. https://doi.org/10.1038/s41598-018-31981-7

Ottmar Möhler, Adams, M. P., Lacher, L., Vogel, F., Nadolny, J., Ullrich, R., et al. (2020). AMTD - The portable ice nucleation experiment PINE: a new online instrument for laboratory studies and automated long-term field observations of ice-nucleating particles. Retrieved September 8, 2020, from https://amt.copernicus.org/preprints/amt-2020-307/

Prussin, A. J., Garcia, E. B., & Marr, L. C. (2015). Total concentrations of virus and bacteria in indoor and outdoor air. Environmental Science and Technology Letters, 2(4), 84–88. https://doi.org/10.1021/acs.estlett.5b00050

Rastelli, E., Corinaldesi, C., Dell'Anno, A., Lo Martire, M., Greco, S., Cristina Facchini, M., et al. (2017). Transfer of labile organic matter and microbes from the ocean surface to the marine aerosol: an experimental approach. Scientific Reports, 7(1), 11475. https://doi.org/10.1038/s41598-017-10563-z

Schill, G. P., Jathar, S. H., Kodros, J. K., Levin, E. J. T., Galang, A. M., Friedman, B., et al. (2016). Ice-nucleating particle emissions from photochemically aged diesel and biodiesel exhaust. Geophysical Research Letters, 43(10), 5524–5531. https://doi.org/10.1002/2016GL069529

Storelvmo, T. (2017). Aerosol Effects on Climate via Mixed-Phase and Ice Clouds. Annual Review of Earth and Planetary Sciences, 45(1), 199–222. https://doi.org/10.1146/annurev-earth-060115-012240

Suttle, C. A. (2005, September 15). Viruses in the sea. Nature. Nature Publishing Group. https://doi.org/10.1038/nature04160

Suttle, C. A. (2007). Marine viruses - Major players in the global ecosystem. Nature Reviews Microbiology, 5(10), 801–812. https://doi.org/10.1038/nrmicro1750

Tan, I., Storelvmo, T., & Zelinka, M. D. (2016). Observational constraints on mixed-phase clouds imply higher climate sensitivity. Science (New York, N.Y.), 352(6282), 224–7. https://doi.org/10.1126/science.aad5300

Tarn, M. D., Sikora, S. N. F., Grace, ·, Porter, C. E., O 'sullivan, D., Adams, M., et al. (2018). The study of atmospheric ice-nucleating particles via microfluidically generated droplets. Microfluidics and Nanofluidics, 22(22). https://doi.org/10.1007/s10404-018-2069-x

Ullrich, R., Hoose, C., Möhler, O., Niemand, M., Wagner, R., Höhler, K., et al. (2017). A New Ice Nucleation Active Site Parameterization for Desert Dust and Soot. Journal of the Atmospheric Sciences, 74(3), 699–717. https://doi.org/10.1175/JAS-D-16-0074.1

Vergara-Temprado, J., Murray, B. J., Wilson, T. W., O'sullivan, D., Browse, J., Pringle, K. J., et al. (2017). Contribution of feldspar and marine organic aerosols to global ice nucleating particle concentrations. Atmospheric Chemistry and Physics, 17(5), 3637–3658. https://doi.org/10.5194/acp-17-3637-2017

Vergara-Temprado, J., Miltenberger, A. K., Furtado, K., Grosvenor, D. P., Shipway, B. J., Hill, A. A., et al. (2018). Strong control of Southern Ocean cloud reflectivity by ice-nucleating particles. Proceedings of the National Academy of Sciences of the United States of America, 115(11), 2687–2692. https://doi.org/10.1073/pnas.1721627115

Vergara-Temprado, J., Holden, M. A., Orton, T. R., O'Sullivan, D., Umo, N. S., Browse, J., et al. (2018). Is Black Carbon an Unimportant Ice-Nucleating Particle in Mixed-Phase Clouds? Journal of Geophysical Research: Atmospheres, 123(8), 4273–4283. https://doi.org/10.1002/2017JD027831

Whale, T. F., Murray, B. J., O'Sullivan, D., Wilson, T. W., Umo, N. S., Baustian, K. J., et al. (2015). A technique for quantifying heterogeneous ice nucleation in microlitre supercooled water

droplets. Atmospheric Measurement Techniques, 8(6), 2437–2447. https://doi.org/10.5194/amt-8-2437-2015

Whitman, W. B., Coleman, D. C., & Wiebe, W. J. (1998, June 9). Prokaryotes: The unseen majority. Proceedings of the National Academy of Sciences of the United States of America. https://doi.org/10.1073/pnas.95.12.6578

Whon, T. W., Kim, M.-S., Roh, S. W., Shin, N.-R., Lee, H.-W., & Bae, J.-W. (2012). Metagenomic characterization of airborne viral DNA diversity in the near-surface atmosphere. Journal of Virology, 86(15), 8221–31. https://doi.org/10.1128/JVI.00293-12

Wilson, T. W., Ladino, L. A., Alpert, P. A., Breckels, M. N., Brooks, I. M., Browse, J., et al. (2015). A marine biogenic source of atmospheric ice-nucleating particles. Nature, 525(7568), 234–238. https://doi.org/10.1038/nature14986